



Australian Government  
Geoscience Australia



Record 2012/71 | GeoCat 74811

# The 2012 Australian Earthquake Hazard Map

D. R. Burbidge (ed.)



# The 2012 Australian Earthquake Hazard Map

GEOSCIENCE AUSTRALIA  
RECORD 2012/71

D. R. Burbidge (ed.)



**Australian Government**  
**Geoscience Australia**

**Department of Resources, Energy and Tourism**

Minister for Resources and Energy: The Hon. Martin Ferguson, AM MP

Secretary: Mr Drew Clarke

**Geoscience Australia**

Chief Executive Officer: Dr Chris Pigram

This paper is published with the permission of the CEO, Geoscience Australia



© Commonwealth of Australia (Geoscience Australia) 2012

With the exception of the Commonwealth Coat of Arms and where otherwise noted, all material in this publication is provided under a Creative Commons Attribution 3.0 Australia Licence.

(<http://www.creativecommons.org/licenses/by/3.0/au/>)

Geoscience Australia has tried to make the information in this product as accurate as possible. However, it does not guarantee that the information is totally accurate or complete. Therefore, you should not solely rely on this information when making a commercial decision.

**ISSN 1448-2177**

**ISBN 978-1-922201-03-4 (Print)**

**ISBN 978-1-922201-04-1 (PDF)**

**GeoCat 74811**

**Bibliographic reference:** Burbidge, D.R. (ed.), 2012. *The 2012 Australian Earthquake Hazard Map*. Record 2012/71. Geoscience Australia: Canberra.

# Table of Contents

<b>Executive Summary .....</b>	<b>xi</b>
<b>Glossary and Abbreviations .....</b>	<b>xiii</b>
<b>1. Introduction .....</b>	<b>1</b>
<i>D. R. Burbidge</i> .....	1
1.1 The Current Earthquake Hazard Map (AS1170.4-2007).....	1
1.2 Editions .....	2
1.3 Method Overview.....	3
1.3.1 Earthquake Source Models .....	3
1.3.2 Ground Motion Prediction Equations .....	3
1.3.3 Hazard Map Computation.....	4
<b>2. Revised Australian Earthquake Catalogue.....</b>	<b>5</b>
<i>T. I. Allen, M. Leonard and C. D. N. Collins</i> .....	5
2.1 Introduction.....	5
2.2 Catalogue Sources.....	5
2.3 Revision of Local Magnitudes .....	6
2.3.1 Western and Central Australia .....	9
2.3.2 Mt Lofty and Flinders Ranges .....	10
2.3.3 Eastern Australia.....	11
2.3.4 Queensland .....	12
2.3.5 Discussion of Local Magnitude Revisions .....	13
2.4 Selection of preferred magnitude <i>m</i> .....	13
2.5 Declustering and Deblasting .....	14
2.6 Summary of Catalogue Modifications .....	16
<b>3. Source Zonation.....</b>	<b>17</b>
<i>M. Leonard, A. McPherson and D. Clark</i> .....	17
3.1 Assessment of Existing Source Zones.....	17
3.2 A New Method for defining Source zones .....	17
3.2.1 Spatial Statistical Analysis Method .....	18
3.2.2 Implications for seismic hazard assessment .....	19
3.2.3 Background Zones.....	20
3.2.4 Regional Source Zones.....	21
3.2.5 Hotspots .....	22
3.2.6 Offshore zones.....	25
3.3 Summary of Source Model Development.....	26
<b>4. Earthquake Recurrence Parameterisation.....</b>	<b>27</b>
<i>M. Leonard</i> .....	27
4.1 Parameterisation - Estimation of ‘ <i>a</i> ’ and ‘ <i>b</i> ’ .....	27
4.2 Magnitude of Completeness.....	29
4.3 Maximum magnitude .....	31
4.3.1 Curve Fitting (CF) .....	33
4.3.2 Trough and Plateau (T&P).....	37
4.3.3 Cumulative length statistics (CLS).....	38
4.3.4 Preferred value of <i>M</i> <sub>max</sub> .....	40
4.4 Summary of Recurrence Estimation.....	40

<b>5. Ground-Motion Prediction Equations.....</b>	<b>44</b>
<i>T. I. Allen.....</i>	<i>44</i>
5.1 Introduction.....	44
5.2 GMPE Comparisons with Western Australian Data.....	45
5.3 GMPE Comparisons with Eastern Australian Data.....	46
5.4 Treatment of Ground-Motion Uncertainties.....	48
5.5 Final GMPE Weightings for the 2012 Hazard Map.....	50
5.6 GMPEs for Offshore Zones.....	52
<b>6. The 2012 Australian Earthquake Hazard Maps.....</b>	<b>54</b>
<i>D. R. Burbidge, M. Leonard, D. Robinson and D. Gray.....</i>	<i>54</i>
6.1 Method.....	54
6.2 Results.....	55
6.2.1 Background Source Zones Only.....	56
6.2.2 Regional Source Zones Only.....	57
6.2.3 Hotspot Source Zones Only.....	58
6.2.4 Combined Regional and Background Zones.....	59
6.2.5 Combining the Regional, Background and Hotspot Zones.....	61
6.3 The Preferred Australian Earthquake Hazard Map.....	62
6.3.1 Effect of the Gaussian width.....	64
6.3.2 Effect of return period.....	64
6.3.3 Effect of spectral response period.....	65
6.3.4 Selected Hazard Curves.....	65
6.4 Discussion.....	67
6.4.1 Uncertainties and limitations.....	67
6.4.2 Choice of map for AS1170.4.....	68
6.4.3 Other Applications of the Seismic Hazard Maps.....	69
6.4.4 Summary.....	69
<b>Acknowledgements.....</b>	<b>70</b>
<b>References.....</b>	<b>71</b>
<b>7. Appendix A: Logic Used for the Development of the Earthquake Catalogue.....</b>	<b>76</b>
<i>T. I. Allen.....</i>	<i>76</i>
7.1 Introduction.....	76
7.2 Steps to create Master Catalogue (mdat):.....	76
7.3 Steps to revise Local magnitudes, $M_L$ .....	77
7.4 $m_b$ to $M_W$ Conversion Factors.....	80
7.5 AUSTCAT fields.....	81
7.6 References.....	81
<b>8. Appendix B: Sources of earthquake solutions in the catalogue.....</b>	<b>83</b>
<i>C. D. N. Collins.....</i>	<i>83</i>
8.1 Sources in GG-cat 2010.....	83
8.2 References.....	87
<b>9. Appendix C: Effectiveness of the catalogue declustering.....</b>	<b>88</b>
<i>M. Leonard.....</i>	<i>88</i>
9.1 Introduction.....	88
9.2 Yilgarn (zone 25).....	88
9.3 Mt Lofty and Flinders Ranges (Zone 17).....	91
9.4 Summary.....	92

<b>10. Appendix D: Summary of neotectonic domains model simplification for ground-motion modelling as part of the new Australian National Hazard Map .....</b>	<b>93</b>
<i>D. Clark and A. McPherson .....</i>	<i>93</i>
10.1 Introduction.....	93
10.2 Domain simplification.....	93
10.3 Fault length analysis.....	95
10.4 Considerations for Maximum magnitude earthquake ( <i>Mmax</i> ) for background zones .....	97
10.5 References.....	99
<b>11. Appendix E Calculation of MC and the sensitivity of recurrence rates on MC .....</b>	<b>101</b>
<i>M. Leonard .....</i>	<i>101</i>
11.1 Introduction.....	101
11.2 Method.....	102
11.3 Conclusion .....	107
<b>12. Appendix F Sensitivity and Validation Testing of EQR.....</b>	<b>108</b>
<i>D. R. Burbidge.....</i>	<i>108</i>
12.1 Introduction.....	108
12.2 Number of events .....	108
12.3 Maximum Magnitude.....	109
12.4 Minimum Magnitude .....	110
12.5 Number of Magnitude Bins.....	111
12.6 Validation Tests .....	111
12.6.1 PEER Set 1 Case 1.....	112
12.6.2 PEER Set 1 Case 11.....	112
12.7 Effect of Smoothing.....	113
12.7.1 Effect of Smoothing on a Hazard Map .....	115
12.8 Summary .....	115
12.9 References.....	116

## List of Tables

Table 1: The assumed period of use of the Richter (1958) scale for regional networks in Australia .....	8
Table 2: Period of time and distance from mainshock for an earthquake to be classified as an aftershock using Method 2 or 3 .....	15
Table 3: the number of earthquakes removed by the declustering algorithm .....	16
Table 4: Magnitude completeness models shown in Figure 24. ....	31
Table 5: Mmax estimates for the six domains using the curve fitting technique .....	37
Table 6: Mmax estimates for the six domains using the trough and plateau technique.....	38
Table 7: Maximum scarp length (km) estimates for the six domains using the length statistics technique.....	39
Table 8: Weighting applied to each cumulative percentage cut-off maximum magnitude.....	40
Table 9: Average characteristic magnitude (proxy Mmax) estimates based upon scarp length.....	40
Table 10: The Mmax values used in the hazard map calculation.....	40
Table 11: Summary table of the recurrence parameters used for the background zones.....	41
Table 12: Summary table of the recurrence parameter used for the regional zones.....	42
Table 13: Summary table of the recurrence parameter used for the Hotspots .....	43
Table 14: Candidate GMPEs considered for use in the Australian earthquake hazard map. ....	45
Table 15: Mean ( $\mu$ ) and standard deviation ( $\sigma$ ) of near source ( $R \leq 80$ km) model residuals ( $\log_{10}$ observed – $\log_{10}$ predicted) for combined periods of ground-motion against Australian ground-motion data. ....	48
Table 16: Ground-motion prediction equation weights used in the 2012 Australian Earthquake Hazard Map .....	50
Table F 1 Summary of the main parameters used in the hazard calculations .....	116

# List of Figures

Figure 1: Earthquake hazard on rock for the 500 year return period at a response spectral period of 0.0 s (PGA) shown in 3D evaluated for the geometric mean of the horizontal components.....	xii
Figure 2: The current earthquake hazard map for Australia as applied in AS 1170.4-2007 (Standards Australia 2007) .....	2
Figure 3: The spatial extent of the earthquake catalogues compiled and merged for the Australian National Earthquake Hazard Map.....	6
Figure 4: Comparison of several Australian-specific distance correction factors ( $-\log A_0$ ) minus the Richter (1935; 1958) $-\log A_0$ curve .....	7
Figure 5: Map of Australian epicentres for pre-1990 earthquakes $M_L$ 3.0 and above indicating the change in local magnitude $M_L$ .....	9
Figure 6: Histograms showing residuals of catalogue magnitudes minus revised magnitudes for (a) all of WCA region, and (b) for the WCA region for $M_L$ (Richter) $\geq 4.0$ .....	10
Figure 7: Histograms showing residuals of catalogue magnitudes minus revised magnitudes for (a) all of MLFR region, and (b) for the MLFR region for $M_L$ (Richter) $\geq 4.0$ .....	11
Figure 8: Histograms showing residuals of catalogue magnitudes minus revised magnitudes for (a) all of SEA region and (b) for the SEA region for $M_L$ (Richter) $\geq 4.0$ .....	12
Figure 9: Histograms showing residuals of catalogue magnitudes minus revised magnitudes for (a) all of Queensland region and (b) for the Queensland region for $M_L$ (Richter) $\geq 4.0$ .....	13
Figure 10: The earthquake spatial density of Australia, based on the declustered catalogue .....	19
Figure 11: The declustered catalogue of earthquakes with magnitude $M \geq 3.0$ , with the background zones indicated by the dotted magenta line. ....	21
Figure 12: The earthquake spatial density of Australia, based on the declustered catalogue with the interpreted Regional zones superimposed .....	22
Figure 13: Mt Collins hotspot, 23 km south of Cowra and 14 km west of Wyangala Dam .....	23
Figure 14: The hotspot 15 km northeast of Jindabyne, including the Jindabyne and Eucumbene lakes .....	23
Figure 15: Talbingo Lake. This hotspot appears to be a 17 year long sequence associated with the filling of the dam.....	23
Figure 16: This hotspot is centred on the 1979 Cadoux earthquake, radius 40 km.....	24
Figure 17: The Burakin sequence provides an example of a hotspot that suggests a short-lived burst of activity that is not expected to represent continued activity. ....	24
Figure 18: The spatial density distribution based on the full catalogue. Hotspots considered continuous are shown in blue circles and hotspots considered to be associated with short lived sequences are shown in magenta circles.....	25
Figure 19: The seismicity to the north of Australia and the three offshore zones used.....	26
Figure 20: Magnitude-frequency statistics of Zone 10 (Victorian North East).....	29
Figure 21: Magnitude-frequency statistics for Zone 1 (Chillagoe-Cairns).....	29
Figure 22: Magnitude-frequency statistics for Zone 13 (Western Tasmania and Bass Strait). ....	29
Figure 23: Magnitude-frequency statistics for Zone 16 (Eyre Peninsula).....	29
Figure 24: The magnitude of completeness models used.....	30
Figure 25: Neotectonic domains map of the Australian continent (Clark et al. 2011) .....	32

Figure 26: Length (km) vs. Cumulative Number data for the scarps in Domain 3 .....	34
Figure 27: Scarp length data (km) versus cumulative number and the fitted curves for Domains 1, 2, 4, 5 and 6.....	36
Figure 28: Histogram of the incremental and cumulative fault scarp length statistics for Domain 3 for 10-km bins.....	37
Figure 29: Cumulative statistics for fault length data from each of the Neotectonic domains defined by Clark et al. (2011) .....	39
Figure 30: Residuals ( $\log_{10}$ observed – $\log_{10}$ predicted) of 5% damped response spectral accelerations (in $\text{cm/s}^2$ ) recorded from $M_W \geq 4.0$ earthquakes in the Yilgarn Craton, Western Australia.....	47
Figure 31: Residuals ( $\log_{10}$ observed – $\log_{10}$ predicted) of 5% damped response spectral accelerations(in $\text{cm/s}^2$ ) recorded from earthquakes in eastern Australia .....	49
Figure 32: Comparison of the median horizontal 5% damped pseudo response spectra (PSA) for GMPEs used in the PSHA for the 2012 Australian Earthquake Hazard Map (see Table 16) for a scenario $M_W$ 5.5 earthquake plotted against $R_{rup}$ for a series of response spectral periods.....	51
Figure 33: Comparison of the median horizontal 5% damped pseudo response spectra (PSA) for GMPEs used in the PSHA for the 2012 Australian Earthquake Hazard Map (see Table 16) for a scenario $M_W$ 6.5 earthquake plotted against $R_{rup}$ for a series of response spectral periods.....	52
Figure 34: Comparison of the attenuation from subduction zone GMPEs (Youngs et al., 1997; Zhao et al., 2006) and those models used for eastern (non-cratonic) Australia .....	53
Figure 35: The 500 year return period Background zone PGA (0.0 s RSA period) hazard map smoothed with a 300 km Gaussian spatial filte .....	57
Figure 36: The 500 year return period Regional zone PGA (0.0 s RSA period) hazard map with a 60 km Gaussian spatial filter.....	58
Figure 37: The 500 year return period Hotspot zone PGA (0.0 s RSA period) hazard map with a 60 km Gaussian spatial filter.....	59
Figure 38: The 500 year return period PGA (0.0 s RSA period) hazard map for the map with regional zones surrounded by background zones combined with some offshore zones to the north of Australia.....	60
Figure 39 The 500 year return period PGA (0.0 s RSA period) hazard map for the map with regional layer weighted 0.67 and the background layer weighted 0.33.....	60
Figure 40: The 500 year return period, PGA (RSA 0.0 s period) hazard map calculated using the maximum recurrence rate for the Regional and Background layers.....	61
Figure 41: The 500 year return period PGA (0.0 s RSA period) hazard map calculated using the maximum hazard value of the combined Regional and Background hazard map (Regional_robust) and the Hotspot hazard map in (a) 2D and (b) 3D. ....	62
Figure 42: The 500 year return period PGA hazard map calculated with a 50/50 weighting in the regions where the Hotspot exceeds the combined Regional and Background layer (Regional_weight) and after smoothing with a 90km wide Gaussian filter. The map is shown in 2D in (a) and in 3D perspective in (b). ....	62
Figure 43: The 500 year return period PGA hazard map calculated with a 50/50 weighting in the regions where the hotspot exceeds the hazard shown in Figure 40 .....	63
Figure 44: The maximum hazard value for the preferred combination of layers (Figure 43) but with the spatial filter width increased to 300 km for all layers in (a) 2D and (b) 3D.....	64
Figure 45: The 0.0s hazard value for all three source zone layers for return periods of (a) 2,500 years and (b) 10,000 years .....	64

Figure 46: The 500 year hazard value for all three source zone layers for (a) 0.1s RSA period and (b) 1.0 s RSA period.....	65
Figure 47: Response spectral acceleration as a function of return period at six different spectral periods for locations in (a) Adelaide, (b) Brisbane, (c) Canberra (d) Melbourne, (e) Perth, and (f) Sydney for the preferred model shown in Figure 43 .....	66
Figure 48: The effect of changing the Mmax variable on the hazard at a single location in Zone 11 (Victoria) at a return period of 500 years. ....	67
Figure B 1 Distribution of earthquakes by Source in GG-Cat (2010). ....	87
Figure C 1 (a) The occurrence of all earthquakes M greater than or equal to 3.0 in the Yilgarn region of Western Australia between 1960 and 2010 .....	89
Figure C 2: (a) The declustered catalogue of earthquakes with a magnitude greater than or equal to 3.0 in the Yilgarn region of Western Australia between 1960 and 2010 and (b) the Poisson statistics of the earthquake catalogue. ....	90
Figure C 4 Occurrence and Poisson data for the Mt Lofty and Flinders Ranges, top row (a and b) are the full catalogue, and the bottom row (c and d) are the declustered and demined catalogue. ....	92
Figure E 1 Earthquake recurrence analysis of the Adelaide Fold Belt region .....	103
Figure E 2 Dates from which the catalogue is complete in each region for $M \geq 3.5$ and above. ....	104
Figure E 3 As per Figure E 2 but the areas have been extrapolated using Voronoi polygons based on the centroid of each zone in Figure 2. ....	104
Figure E 4 MLFR recurrence rates for (a) single (b), regional multi corner, and (c) local multi corner $M_C$ models.....	105
Figure E 5 (a) seismicity,(b) $M_C$ and (c) recurrence for northeast Western Australia. ....	106
Figure E 6 Seismicity, $M_C$ and recurrence for southeast Queensland. ....	107
Figure F 1 The minimum (blue curve) and maximum (red curve) PGA hazard at 500 years across a square target zone as a function of the number of events in the synthetic catalogue. ....	109
Figure F 2: The minimum (blue) and maximum (red) 500 year PGA hazard in the test hazard map as a function of maximum magnitude for two different earthquakes rates (a) 1 earthquake above $M_W 3.0$ per annum, and (b) 50 earthquakes above $M_W 3.0$ per annum. ....	109
Figure F 3: The effect on the minimum (blue) and maximum (red) hazard in the test area when the minimum magnitude of the earthquakes included in the synthetic catalogue is changed. ....	110
Figure F 4: The effect of the number of magnitude bins on the hazard on the minimum (blue) and maximum (red) hazard in the test area. ....	111
Figure F 5: This figure compares the ground motions predicted by EQRM (black curve) to the ground motions calculated by PEER (red curve) for seven sites surrounding a strike-slip fault (PEER Test Case 1) .....	112
Figure F 6: This figure compares the annual probability of exceedence for different Peak Ground Accelerations (PGA) predicted by EQRM (black curve) and those calculated by the PEER for a site above an earthquake source zone (PEER Test Case 11) .....	113
Figure F 7: Three cross sections through three 500yr, PGA hazard maps to show the effect of smoothing.....	114
Figure F 8: The 500 year return period PGA hazard map for (a) the Regional source zones with a 150 km Gaussian filter, and (b) the Hotspot zones and a 300 km Gaussian filter. ....	115



## Executive Summary

In July 2009 Geoscience Australia (GA) initiated a project to update the Australian earthquake hazard map using the latest available methods and data. This document summarises the work done since that time and presents a new set of earthquake hazard maps for consideration in the next revision of the earthquake loading code AS1170.4 “Structural design actions: Part 4 Earthquake actions in Australia”. The key improvements in the 2012 Australian Earthquake Hazard Map are summarised below.

The earthquake catalogues used to generate the existing earthquake hazard map found in AS1170.4-2007 were based only on events up until the late 1980s, although a later revision in the 1990s also considered earthquakes that had occurred up until then. The earthquake catalogue used here includes events up until 2011; a total of 8,000 earthquakes above magnitude 3. The catalogue is a combined version of several other regional catalogues provided by external agencies and seismologists. This combined catalogue represents the most complete known catalogue of earthquakes ever compiled for Australia.

Historically, a variety of local magnitude  $M_L$  formulae have been used to measure the size of earthquakes across Australia. Here we develop a more consistent catalogue through conversion of the various magnitude measurements of the earthquakes into a more consistent ‘pseudo  $M_L$ ’ scale. Furthermore, we introduce a systematic logic to select preferred magnitude types (e.g. moment magnitude  $M_W$ , surface-wave magnitude  $M_S$ , etc.) when the use of  $M_L$  is not appropriate.

Probable aftershocks, foreshocks and mine blasts have been identified in the catalogue using a combination of methods based on the latest thinking of how earthquakes cluster in intraplate regions. The method uses both manual event classification by an expert and an automatic classification system. While the method has probably not removed every aftershock, mine blast or earthquake swarm event, to the best of our knowledge, the declustered catalogue used here is cleaner than any previous Australian catalogue.

Earthquake source zones applied in the hazard map are developed using a unique combination of three different layers, which capture seismic characteristics at sub-national, regional and high-activity point (hotspot) scales. The zones defined balance the stability and conservatism requirements of a hazard map for the building code while still allowing it to be flexible enough to accommodate a wide range of uses. In each zone we estimate earthquake probability by fitting the catalogue data to truncated Gutenberg-Richter (Gutenberg and Richter, 1944) relations using a new automatic algorithm. The method provides robust values for the Gutenberg-Richter values,  $a$  and  $b$ , and requires little to no manual adjustment.

The maximum magnitude of earthquakes within the majority of the zones is based on the neotectonic domains work of Clark *et al.* (2011) and the work of Leonard and Clark (2011). This makes the map one of the first in the world to apply a semi-quantitative measure of  $M_{max}$  for majority of the source zones in the map rather than simply adding a constant to the observed maximum magnitude from a historic catalogue.

Ground-motion prediction equations for previous maps were based on limited intensity data and often involved applying relations developed for other countries. Here we apply recently developed equations (two of them Australia-specific), based on modern methods and data. Weightings applied to the various ground-motion equations are determined by comparing their predictions to observed Australian ground-motion data. These equations were used to calculate the ground motion at a range of response spectral accelerations, rather than just calculating the hazard for peak ground acceleration (PGA), as has been done in many previous assessments.

A suite of maps is calculated using GA’s Earthquake Risk Model (EQRM). The EQRM is open-source, allowing the results to be tested or modified independently. In addition to determining earthquake hazard (i.e. likelihood of ground-shaking), the use of EQRM also provides the capability to calculate earthquake risk (e.g. likelihood of damage) in the future, provided the necessary site classification, exposure and vulnerability models are available.

The final 2012 Australian earthquake hazard maps for a range of return periods and response spectral periods are presented herein. Figure 1 shows the 0.0 s response spectral period (or PGA) earthquake hazard in 3D for a return period of 500 years. The hazard is represented as the geometric mean of horizontal component ground-motion. This particular combination of response spectral period and return period is most comparable to those for the map used in the current building code. However, Figure 1 represents just one of many different combinations of return and response spectral period hazard calculated in this assessment.

As a result of the updates and improvements outlined above, the 2012 maps represent a significant improvement over previous national earthquake hazard maps. Accordingly, GA recommends that the 2012 maps, such as the one shown in Figure 1, be considered by Standards Australia as a basis for developing hazard factors for the next revision of the AS1170.4 earthquake loading code.

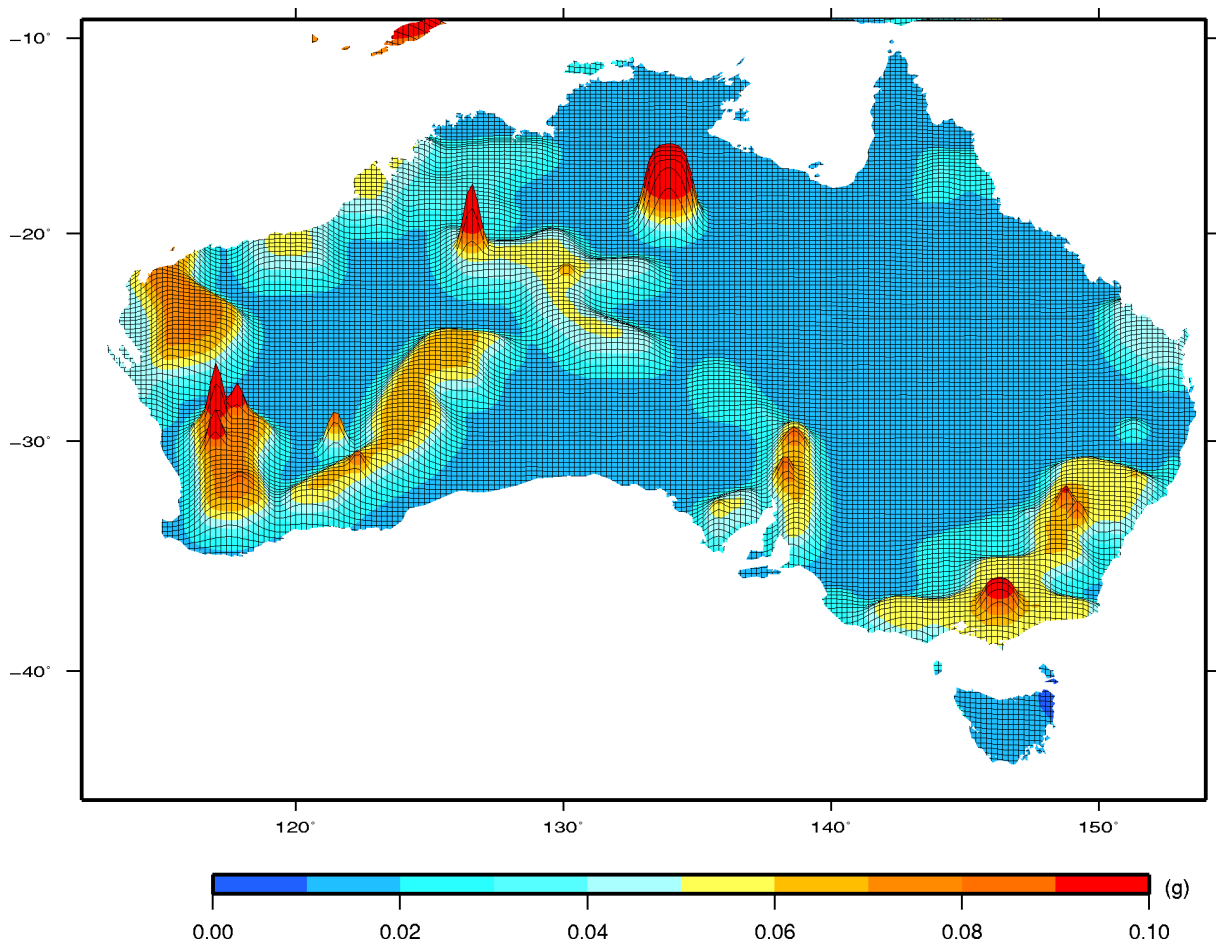


**Figure 1:** Earthquake hazard on rock for the 500 year return period at a response spectral period of 0.0 s (PGA) shown in 3D evaluated for the geometric mean of the horizontal components. This particular map is the closest in return period and response spectral period to the current hazard map in AS1170.4-2007.

## Glossary and Abbreviations

VARIABLE	DESCRIPTION OF VARIABLES USED
AS1170.4	The current earthquake loading code for Australia - "Structural design actions Part 4: Earthquake actions in Australia"
<i>a</i> -value	The Gutenberg – Richter "a" in $\log(N_M)=a - M*b$
<i>b</i> -value	The Gutenberg – Richter "b" in $\log(N_M)=a - M*b$
<i>A</i> - value	$10^a$ , where <i>a</i> is the <i>a</i> -value
D1-D7	The neotectonic domains D1 through to D7 in Clark et al (2011)
DEM	Digital Elevation Model
EA	The Eastern Australian region
EQRM	Geoscience Australia's Earthquake Risk Model
GMPE	Ground motion prediction equation
GMPM	A model incorporating a weighted suite of GMPEs used for a given geographic region
G-R	The Gutenberg – Richter Equation, $\log(N_M)=a - M*b$
$-\log A_0$	Local magnitude distance correction factors
$m_b$	Body-wave magnitude
$M_D$	Duration magnitude
$M_L$	Local magnitude determined from instrumental data
$M_{L,Richter}$	Local magnitude determined from instrumental data using the traditional Richter (1935) distance corrections ( $-\log A_0$ )
$M_{LI}$	Local (Richter) magnitude determined from isoseismal intensity data
$M_{L,rev}$	Revised local magnitude
$M_S$	Surface-wave magnitude
$M_W$	Moment magnitude
<i>M</i>	Preferred magnitude of aforementioned magnitude types.
<i>Mmax</i>	Maximum magnitude expected in a particular source area
$M_C$	Magnitude of completeness
$M_0$	Seismic moment
MLFR	The Mt Lofty and Flinders Ranges region in South Australia
$N_M$	Number of earthquakes greater than magnitude, <i>M</i>
PDF	Probability Density Function
PGA	Peak ground acceleration, or response spectral acceleration at a period of 0.0 s
PSHA	Probabilistic Seismic Hazard Analysis
$R_{epi}$	Epicentral distance (km)
$R_{hyp}$	Hypocentral distance (km)
$R_{rup}$	Shortest distance between the earthquake fault rupture plane and a site (km)
RSA	Response Spectral Acceleration
SCR	Stable Continental Region
WCA	Western and Central Australia
$V_{S30}$	Average shear wave velocity in the top 30m of regolith
<i>Z</i>	The "Hazard Factor" in AS1170.4



# 1. Introduction

*D. R. Burbidge*

The Australian Earthquake Hazard Map is an essential component of the Australian Standard AS1170.4 “Structural design actions Part 4: Earthquake actions in Australia”, which outlines actions for seismic design. This Standard is prepared by Committee BD-006, General Design Requirements and Loading on Structures of Standards Australia. The objective of this Standard is to “provide designers of structures with earthquake actions” to apply in the design of certain classes of buildings. The earthquake actions that have to be considered are all based on the level of shaking indicated by the hazard map and listed in a table at the front of the Standard. The last edition of the Standard was produced in 2007 (Standards Australia, 2007).

The current earthquake hazard map upon which these seismic loading provisions are based was developed by McCue *et al.* (1993) and is shown in [Figure 2](#). The McCue *et al.* (1993) map was constructed using source zones modified after Gaull *et al.* (1990), and incorporated an additional six years of earthquake data and approximately one hundred independent site hazard estimates determined by expert judgement (K. McCue, *pers. comm.*). Subsequent to the development of those maps, thousands more earthquakes have been recorded in Australia, augmenting the catalogue to provide improved information on the likely recurrence of Australian earthquakes. In addition to almost two decades of earthquake hypocentres, researchers now have a better understanding of the attenuation of earthquake ground-shaking throughout the Australian crust. Furthermore, recent research into palaeo-earthquakes in Australia has, for the first time, permitted the development of semi-quantitative estimates of the maximum earthquake magnitude ( $M_{max}$ ) likely to occur across different tectonic regions. Consequently, simply updating the aforementioned hazard inputs could significantly improve the map and hence the Standard.

## 1.1 THE CURRENT EARTHQUAKE HAZARD MAP (AS1170.4-2007)

Any probabilistic earthquake hazard map shows the ground-shaking which has a specific probability of being equalled or exceeded in a given period of time. Currently the earthquake hazard map in AS1170.4 is a probabilistic hazard map showing the ground motion from earthquakes with a 10% probability in 50 years of being exceeded on hard rock across Australia ([Figure 2](#)). This probability has a return period of 475 years, rounded to 500 years in AS1170.4. The Hazard Factor ( $Z$ ) most closely approximates the peak ground acceleration (PGA) (McCue 1993; Standards Australia 2007b). Future hazard maps for the code may require other measures of ground-shaking, for example the acceleration at periods which are more likely to cause damage to residential structures (known as the Response Spectral Acceleration - RSA). In order to demonstrate the effect of different RSA or return periods, in this assessment we have produced a range of maps to cover different combinations of return period and RSA period (see [Chapter 6](#)).

A scenario earthquake hazard map shows the level of ground shaking from a specific earthquake. Combining one or more ground motion maps from specific scenarios is sometimes called a “deterministic” hazard map. The hazard values predicted from such maps are entirely dependent on the choice of scenario, which is often arbitrary. Such maps are not used in the current Standard; however they are sometimes used by emergency managers for planning and preparation. Many of the inputs to a scenario hazard map are the same as a probabilistic one, thus developments in one help the other. However, since the Standard does not currently include such maps, and is unlikely to do so in the future, they will not be discussed any further herein.

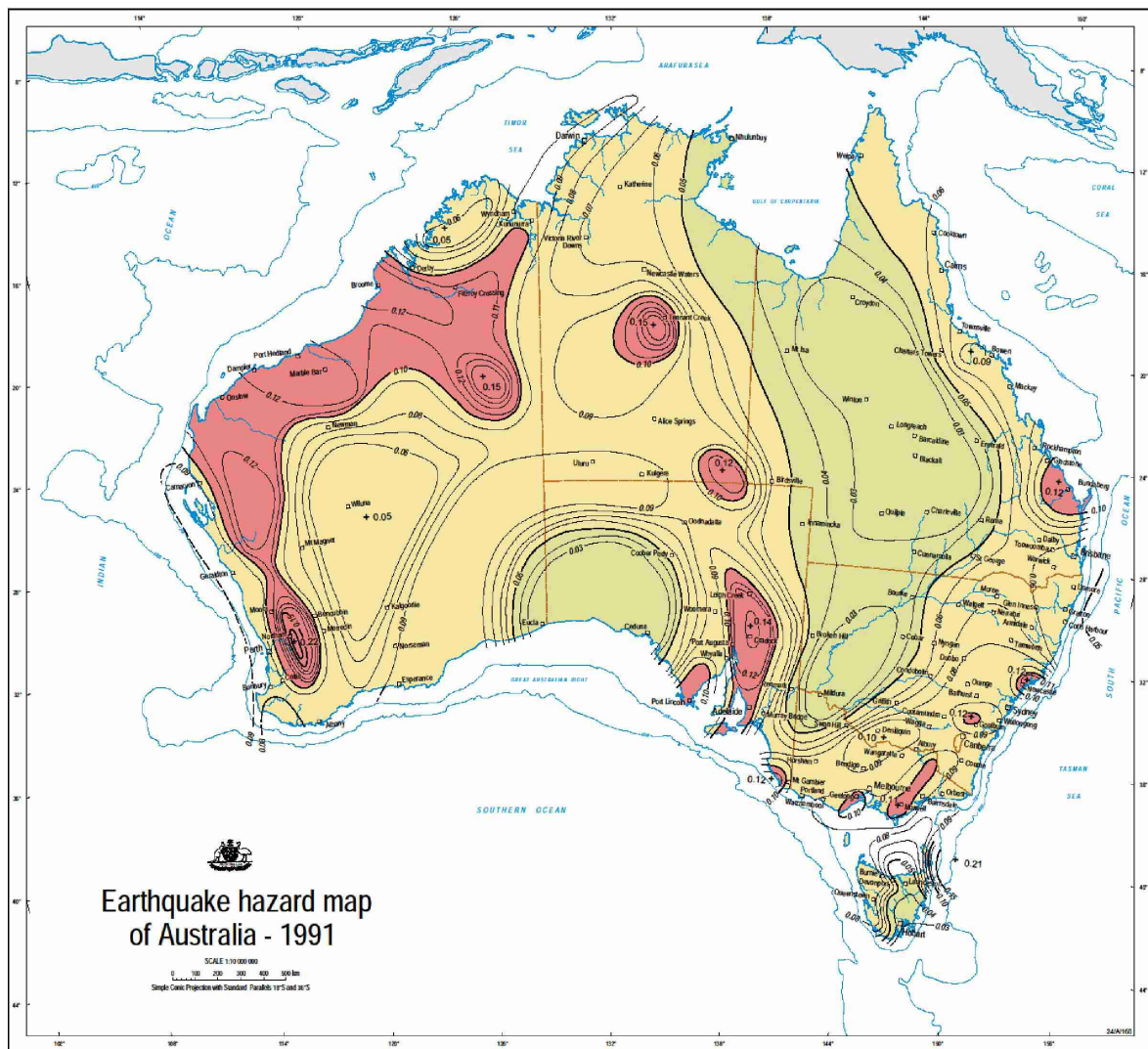


**Figure 2:** The current earthquake hazard map for Australia as applied in AS 1170.4-2007 (Standards Australia 2007). The map shows the Hazard Factor ( $Z$ ), with a 10% chance of being exceeded per annum. The Hazard Factor is approximately the same as peak ground acceleration (PGA) with an annual probability of exceedance of 1/500 (Building Seismic Safety Council, 2004, 2009).

## 1.2 EDITIONS

The Australian Earthquake Loading Standard goes through an approximately 10 year cycle of updates. Accordingly, Geoscience Australia (GA) intends to update the National Earthquake Hazard Map in a cycle tied to these updates in the standard. The current strategy is to update the map twice every update cycle of the Standard (i.e. every five years). In order to bring the current map into this cycle, GA has produced the new, updated set of maps presented in this document five years after the last major update of AS1170.4. Future updates to the map are planned to occur every five years thereafter (i.e. 2017, 2022, 2027, etc.). Given the short timeframe, the version of the map presented here has been developed primarily using existing methods, but with a larger quantity of higher quality earthquake data and input models. Details of the specific improvements are covered in [Chapters 2 to 5](#).

Maps produced beyond 2012 could involve more significant changes to the methods used and thus to the maps themselves. More detailed planning for the requirements of these future maps was discussed at a planning workshop of interested stakeholders in October 2009 and is summarised in Burbidge *et al.* (2010).

## 1.3 METHOD OVERVIEW

The general approach to estimating earthquake hazard requires:

- an earthquake source model(s) that describe the likelihood of an earthquake of a given magnitude occurring in a given location;
- one or more ground motion prediction equation(s) that define the ground-shaking experienced at a given distance from a simulated earthquake of a specific magnitude;

These two aspects are discussed briefly here, and in more detail in the following chapters.

### 1.3.1 Earthquake Source Models

Earthquake source models are often used to subdivide the target area for the hazard assessment into discrete areal zones where the seismicity is assumed to be uniform. This is also the approach used here. These regions are typically derived from an interpretation of the historical seismicity, often combined with some understanding of regional geology. However, there is no clear consensus as to how the limited historical seismicity within Australia should be interpreted.

The approach taken here was to:

1. compile the most comprehensive catalogue of Australian earthquakes possible in the time available;
2. develop a method of estimating a consistent magnitude scale for all records in the earthquake catalogue;
3. divide the continent into separate earthquake source zones. After experimenting with many different zonations, a three layered source zone model, encompassing background, regional and hot-spots, was determined to be the most appropriate;
4. calculate the Gutenberg-Richter  $a$  and  $b$  values for each zone. The  $M_{max}$  values for most of the zones are an extension of the work of Leonard and Clark (2010) and Clark *et al.* (2011).

The choice of a three layer model over the more traditional single layer approach was based on the results of testing which indicated that a single layer model could not statistically represent the observed behaviour of Australian earthquakes adequately.

The first or “background” layer is used to provide a minimum “floor” hazard value for the map. The boundaries of this layer are based primarily on geological and neotectonic data, dividing the continent into cratonic, non-cratonic and extended regions. The background layer is designed to capture the hazard from a large earthquake occurring anywhere in the continent, including areas that appear to have been relatively aseismic over the length of the current seismic catalogue (decades to a century depending on location).

The second or “regional” source zone layer attempts to capture the hazard from the regional-scale areas which have demonstrated continued activity at consistent rates over the past 50 years. These include the seismic zones, such as those defined by Leonard (2008). This layer is mostly based on the earthquake catalogue, specifically on how the density of earthquake epicentres varies across the continent.

The final “hot-spots” layer attempts to capture the very small areas of high, usually transient, seismic activity. Normally these are aftershock sequences or small swarms of earthquakes. This layer also incorporates no geological information.

### 1.3.2 Ground Motion Prediction Equations

Ground-motion prediction equations (GMPEs), also commonly referred to as attenuation equations, relate a specific measure of the expected ground shaking to earthquakes, typically based on the earthquake’s magnitude, source-to-site distance and the near-surface geology of the observation site. In active crustal regions with an abundance of recorded ground-motion data, GMPEs are typically derived from empirical

regressions of the observed data. However, in stable continental regions, like Australia, observed ground-motion datasets are not sufficient to develop reliable GMPEs based on recorded data alone. Consequently, in these regions, we often rely on ground-motion models that use source and attenuation properties derived from smaller, more abundant earthquakes, and use physical assumptions (or source scaling) to extrapolate observed ground-motions to larger earthquakes through stochastic simulation.

The limited number of high-quality ground motion recordings in Australia has restricted the development of a robust attenuation model for Australian conditions. The first attenuation models for PGA based on Australian data were developed by Gaull *et al.* 1990. The Gaull *et al.* 1990 models were developed using the attenuation of mean macroseismic intensity radii, which were converted to PGA using conversion equations developed in Papua New Guinea. This approach was necessary at the time owing to the sparse instrumental data catalogue. However, since then new Australian-specific ground motion models have become available. Somerville *et al.* (2009a,b) employ earthquake source models representative of Australian earthquakes and regional crustal velocity models to simulate broadband strong-motion records for several tectonic elements across Australia. These simulations were subsequently regressed to develop regionally specific GMPEs. The Somerville *et al.* (2009a,b) approach provides an alternative method to develop GMPEs in regions of low seismicity.

In addition, a new GMPE has been recently completed by GA for eastern Australia. This GMPE is described in detail in a forthcoming GA Record (Allen, 2012). The aforementioned Australian-specific GMPEs, in addition to GMPEs developed recently for North America, are compared with observed Australian ground motions in [Chapter 5](#). The comparison was used by Geoscience Australia, in consultation with external stakeholders, to select a weighted set of models for this hazard map for the different geological domains of Australia (cratonic and extended plus non-cratonic).

### 1.3.3 Hazard Map Computation

The information on the seismic sources and ground motion prediction equations are input to an earthquake hazard model. Here we use Geoscience Australia's Earthquake Risk Model (EQR; Robinson *et al.*, 2005, 2006) for the hazard computation, which is able to compute a suite of hazard results for different ground-motion and return periods. The EQR can be downloaded from <http://eqrm.sourceforge.net/>. The hazard maps produced using the source zones and GMPEs discussed above are presented in [Chapter 5](#).

In [Chapter 6](#) we also describe the various methods of smoothing and combining the hazard generated by different zones and models of seismicity. The final, preferred, hazard map ([Figure 1](#)) was chosen primarily to be suitable for the building code. As discussed in the chapter, other applications may well need to use different combinations of zones and/or levels of smoothing which are suitable for their needs. However, even for these applications, many of the results of this assessment will still be useful (e.g. the updated catalogues, ground motion equations and zonations) even if the final, preferred hazard map shown in [Figure 1](#) is not.

## 2. Revised Australian Earthquake Catalogue

*T. I. Allen, M. Leonard and C. D. N. Collins*

### 2.1 INTRODUCTION

One of the key inputs into a traditional probabilistic seismic hazard assessment (PSHA) is the earthquake catalogue. The catalogue must be as complete and as accurate as possible. In this chapter we discuss the earthquake catalogue developed for the update of the 2012 Australian Earthquake Hazard Map. We subsequently discuss the logic used to determine preferred magnitudes and catalogue declustering. The details of this procedure are given in [Appendices A, B and C](#).

### 2.2 CATALOGUE SOURCES

For this revision of the Australian Earthquake Hazard Map a composite earthquake catalogue was compiled. The primary data sources for this catalogue and their respective spatial extent ([Figure 3](#)) are:

1. GG-Cat: An earthquake catalogue compiled by Gary Gibson from various sources (see [Appendix B](#)).
  - Covers the extent 110°E/156°E/48°S/10°S from 1788-06-22 to 2010-05-26
2. QUAKEs: Geoscience Australia's catalogue of Australian and regional events.
  - Covers the extent 110°E /155°E /45°S /9°S from 2010-05-27 to 2010-08-26
  - Note that of the subset of ~2500 earthquakes used to derive the source parameters, 14 came from this catalogue

Supplementary data were obtained from:

3. ISC AUST: All earthquakes in the International Seismological Centre's catalogue attributed to the network AUST.
  - Covers the extent 111.9°E /155.2°E /44.9°S /10.4°S from 1967-01-31 to 2008-04-30
  - This catalogue was included to assist with the validation of catalogue magnitudes because it provides easily accessible information on the stations that recorded historical earthquakes
4. ISC Regional: Additional earthquakes beyond that captured in GG-Cat.
  - Covers the extent 108°E /160°E /50°S /4°S from 1906-06-14 to 2011-04-17
  - These data were added to allow the calculation of recurrence parameters for offshore seismic sources in the Banda Sea, Timor and PNG
5. QEDB: Queensland earthquake catalogue compiled by J. Rynn and D. Weatherly (written communication, 2011).
  - Covers QLD and adjacent regions from 1866-12-29 to 2009-12-31

All key attributes from the aforementioned catalogues were merged into a master catalogue. Catalogue attributes include hypocentre information from each data source, all magnitude types and sources, in addition to any comments for each earthquake.

GG-Cat was the primary source of data within the Australian continent, which includes offshore areas of the Australian continental crust. A complex logic was used to determine preferred location and magnitude for each event. This logic specifies a magnitude-dependent range for selecting the preferred magnitude type and is also based on the time period and the observatory to which the solution is attributed. For example, where moment magnitude  $M_W$  has been assigned, this is taken as the preferred magnitude type across the full magnitude range, whereas, local magnitudes  $M_L$  are taken below magnitude  $M$  6.0 and the larger of surface-wave magnitude  $M_S$  or body-wave magnitude  $m_b$  above  $M$  6.0 (where  $M$  is the preferred

magnitude). [Appendix A](#) provides the detailed logic for the selection of preferred hypocentral locations and earthquake magnitudes for the catalogue used as the basis for the 2012 Australian Earthquake Hazard Map.

Finally, we filter the catalogue for sources we deem to be unreliable within the Australian region, such as those that do not discriminate between natural and anthropogenic sources (e.g. the Comprehensive Nuclear-Test-Ban Treaty Organization’s International Data Centre). In our analyses, we assumed that the number of real earthquakes these sources identified that were missed by the various Australian seismic agencies were negligible. The final catalogue used for this assessment is available from the authors upon request.

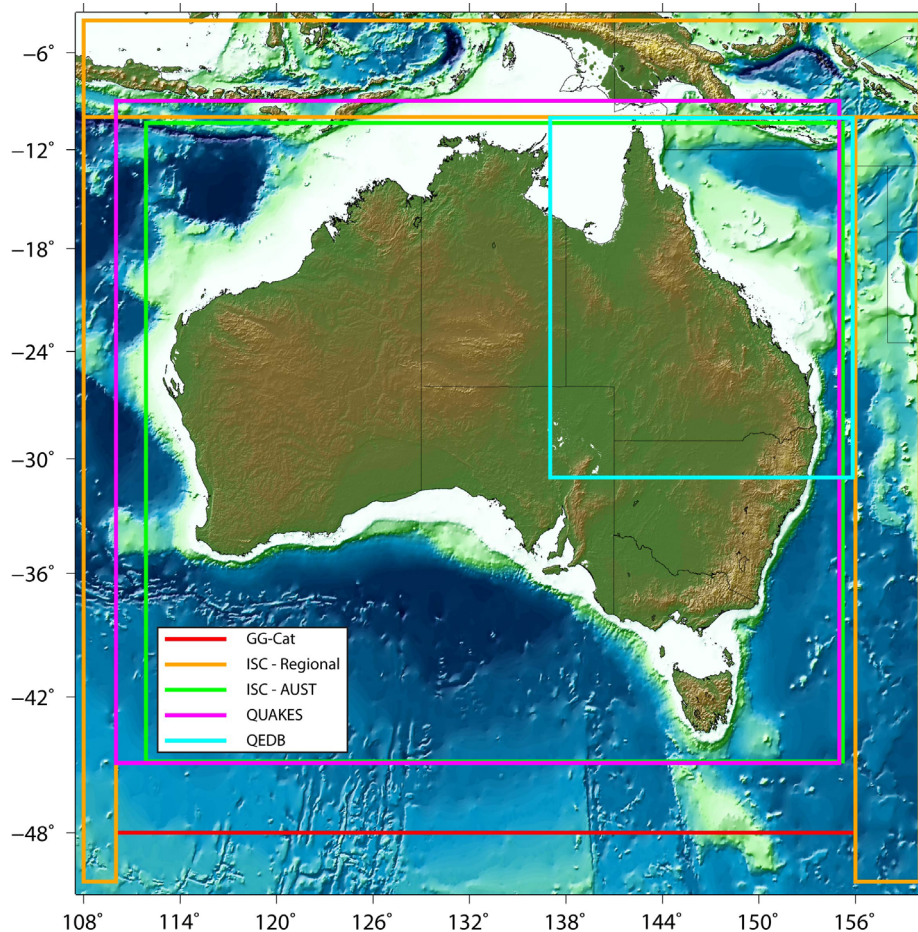


**Figure 3:** The spatial extent of the earthquake catalogues compiled and merged for the Australian National Earthquake Hazard Map. Note the full extent of GG-Cat is masked by the inner bounds of the ISC-Regional catalogue.

### 2.3 REVISION OF LOCAL MAGNITUDES

The calculation of Australian earthquake magnitudes has been the topic of several workshops and reports in the past (e.g., McGregor and Ripper, 1976; Denham, 1982), which have produced recommendations for the determination of earthquake magnitudes in Australia. The primary advances in the development of Australian-specific magnitude formulae occurred in the mid 1980’s through to the early 1990’s where much progress was made in developing Australian-specific magnitude formulae which consider the attenuation properties of the Australian crust. However, since this period of activity, little additional work has been conducted to either validate or improve these models, despite enhancements to Australia’s earthquake monitoring networks and our steadily growing database of Australian earthquake data. It is well-documented that prior to the development of Australian specific magnitude formulae, the Richter (1935; 1958) local magnitude equation – originally developed for southern California – was almost exclusively used to calculate earthquake magnitudes throughout Australia (e.g., Leonard, 2008). [Figure 4](#)

shows the relative difference of the distance correction factors ( $-\log A_0$ ) between Richter and respective Australian  $M_L$  equations presently used to calculate magnitudes. As can be seen, there are considerable differences between Richter and the Australian formulae, particularly at larger source-receiver distances. Figure 4 indicates that application of the Richter (1935; 1958)  $-\log A_0$  corrections would result in an overestimation of local magnitude at source-receiver distances greater than approximately 180 km, relative to the Australian specific  $M_L$  formulae.

Below we discuss attempts to reconcile differences in these equations in order to revise local magnitudes to be, at least, regionally consistent with current observatory practice.

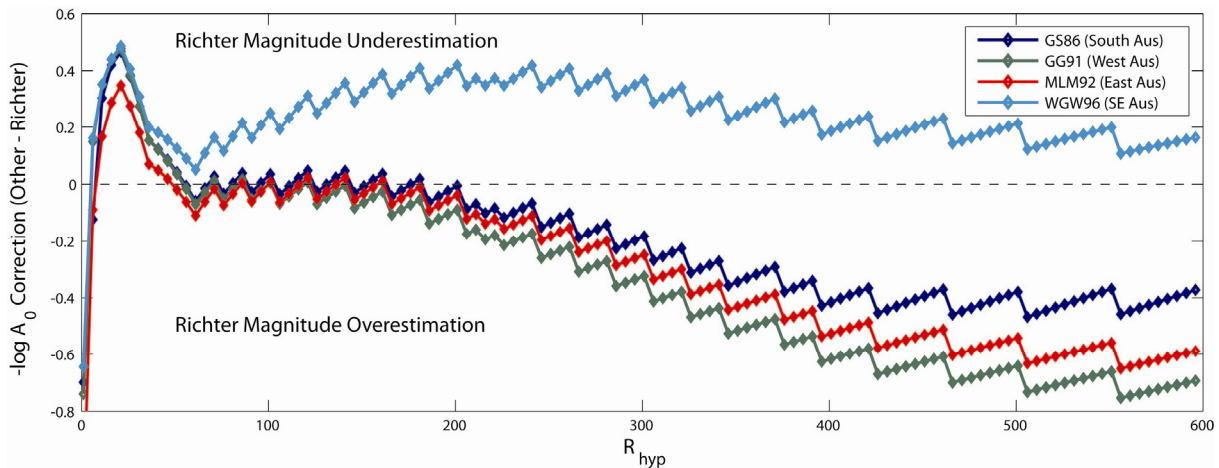


**Figure 4:** Comparison of several Australian-specific distance correction factors ( $-\log A_0$ ) minus the Richter (1935; 1958)  $-\log A_0$  curve: GS86 = Greenhalgh and Singh (1986); GG91 = Gaull and Gregson (1991); MLM92 = Michael-Leiba and Malafant (1992); and WGW94 = Wilkie et al. (1994), updated using Wilkie (1996) coefficients. Most of the Australian local magnitude  $-\log A_0$  curves are similar to the Richter coefficients between  $50 \leq R_{epi} \leq 180$  km. It is widely acknowledged that the Richter (1958) curve underestimates attenuation (and magnitude) in southern California at distances less than  $R_{epi} 30$  km (e.g., Bakun and Joyner, 1984). This finding appears consistent with the Australian  $-\log A_0$  curves presented above.

Allen (2010) first described a method to correct catalogue  $M_L$ 's to be consistent with contemporary magnitude calculations for specified regions across Australia. Ideally, recalibrating earthquake magnitude would use either recorded period and amplitude information or original station magnitudes at a single site to back-engineer measured Wood-Anderson displacement amplitudes used in the calculation of Richter  $M_L$ . However, this information is scarcely available for most Australian earthquakes and often only the final earthquake magnitude is readily available. This is particularly true prior to the 1990s – the main time-period of interest for applying the magnitude corrections. Consequently, Allen (2010) corrected magnitudes using the difference between the Richter and local magnitude curves (Figure 4) at a distance determined by the nearest recording station likely to have recorded the earthquake. This approach considered a temporally-varying network configuration based on known installation and decommission times of seismic stations. It is recognised that for earthquakes recorded on multiple distant seismographs (i.e. at epicentral distances approximately  $R_{epi} > 180$  km), this approach potentially represents a conservative re-evaluation of historical earthquake magnitudes since it only considers the difference between Richter and the local magnitude distance corrections for the closest station where the potential differences are the smallest. The Richter (1958) scale was extended to 1,500 km for these analyses following recommendations from Eiby and Muir (1961).

For those earthquakes occurring prior to approximately 1940, it is assumed that very few stations were available from which to adequately record earthquakes and calculate their magnitudes. These earthquakes are subsequently rescaled according to a regression between the original and revised magnitudes determined from post-1940 (to approximately 1990) earthquakes, where those magnitudes of uncommon magnitude types are considered to be equivalent to  $M_L$  and are modified according to the equation in Table 1.

The effect of the aforementioned magnitude corrections is discussed for western and central Australia (WCA), the Mt Lofty and Flinders Ranges (MLFR), eastern Australia (EA) and Queensland (QLD) in more detail below. The respective regions are indicated in [Figure 5](#).

**Table 1:** The assumed period of use of the Richter (1958) scale for particular regional networks in Australia. The table also indicates the Australian-specific local magnitude formula to which the magnitudes are recalibrated. In this table ADE is the South Australian state network and MEL is the network of Environmental Systems and Services (and its predecessors), Melbourne.

START TIME	STOP TIME	ASSUMED $M_L$ EQUATION USED	$M_L$ EQUATION CORRECTED TO	CRITERIA FOR CORRECTIONS
<b>CENTRAL AND WESTERN AUSTRALIA</b>				
1940	1990	Richter (1958) extended by Eiby and Muir (1961)	Gaul and Gregson (1991)	Not ADE solutions
1940	1986	Richter (1958) extended by Eiby and Muir (1961)	Gaul and Gregson (1991)	ADE solutions
<b>EASTERN AUSTRALIA</b>				
1940	Present	Richter (1958) extended by Eiby and Muir (1961)	Michael-Leiba and Malafant (1992)	For preferred magnitude of "Other" magnitude type (e.g. $M_D$ , $M_{LI}$ )
1940	1990	Richter (1958) extended by Eiby and Muir (1961)	Michael-Leiba and Malafant (1992)	Not MEL solutions
1976	1994	Richter (1958) extended by Eiby and Muir (1961)	Michael-Leiba and Malafant (1992)	MEL solutions
1994	2002	Wilkie (1996)	Michael-Leiba and Malafant (1992)	MEL solutions
2002	Post	Richter (1958) extended by Eiby and Muir (1961)	Michael-Leiba and Malafant (1992)	MEL solutions
<b>MT LOFTY AND FLINDERS RANGES</b>				
1940	1968	Richter (1958) extended by Eiby and Muir (1961)	Greenhalgh and Singh (1986)	ADE solutions
1940	1986	Richter (1958) extended by Eiby and Muir (1961)	Greenhalgh and Singh (1986)	Non-ADE solutions
<b>PRE-INSTRUMENTAL PERIOD</b>				
1788	1940	Equivalent to Richter (1958)	$M_{L,rev} = 0.93 * M_{L,Richter} + 0.02$	Not $M_L$

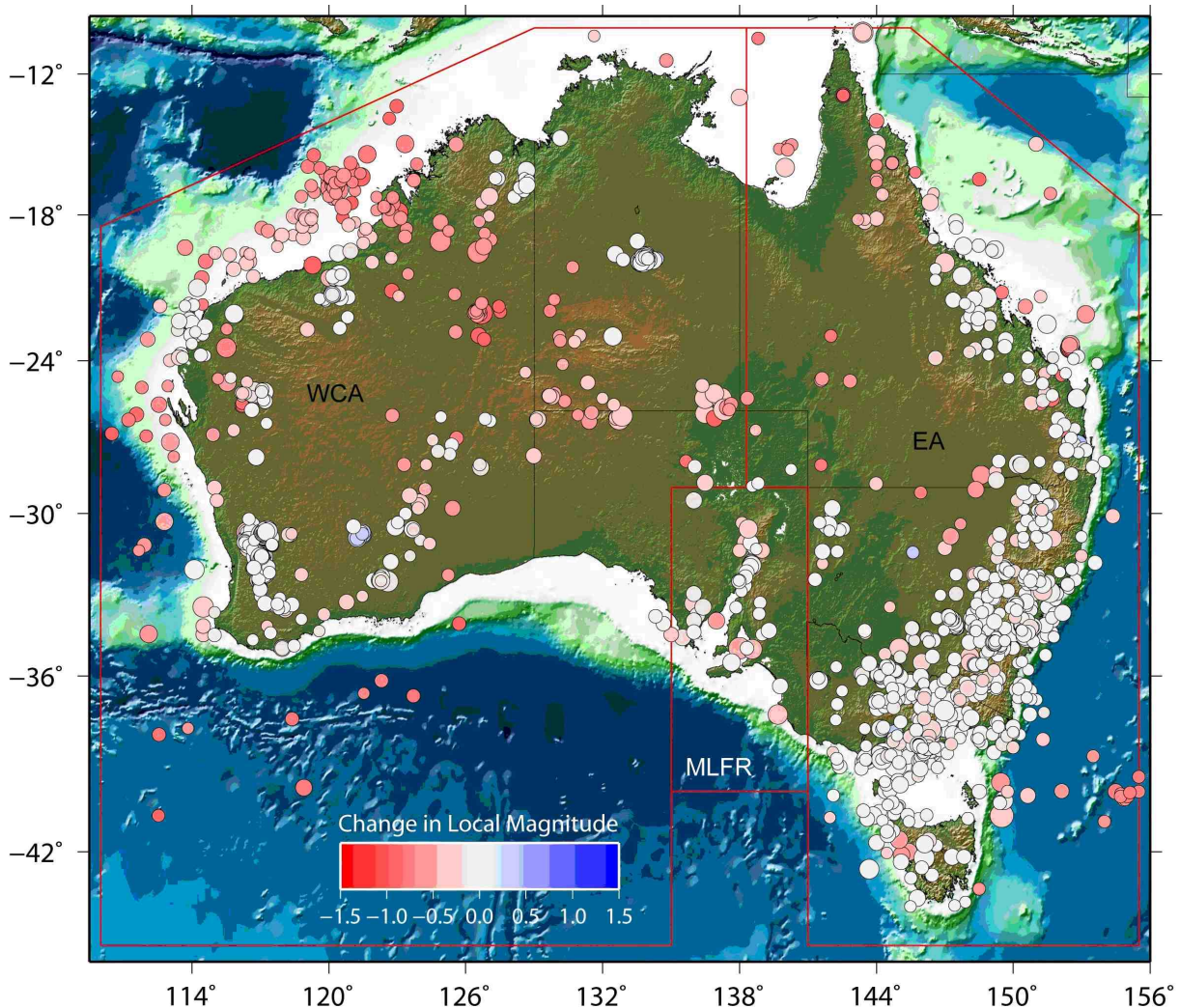


**Figure 5:** Map of Australian epicentres for pre-1990 earthquakes ML 3.0 and above indicating the change in local magnitude ML using the conversion factors described by Allen (2010). Changes most commonly translate to a decrease in magnitude. Red lines indicate the spatial bounds controlling the logic used for magnitude corrections for western and central Australia (WCA), the Mt Lofty and Flinders Ranges (MLFR), and eastern Australia (EA) regions (see Table 1).

### 2.3.1 Western and Central Australia

Earthquakes within the WCA polygon were extracted from the Australian earthquake catalogue and local magnitudes for these events were recalculated for pre-1990 earthquakes using the procedure outlined above assuming the Gaull and Gregson (1991) magnitude equation (see Table 1. Figure 6 indicates histograms of the residuals of the catalogue (Richter) ML minus the revised ML from the present study. When we consider all earthquakes within the WCA polygon, we observe a small bimodal relationship of magnitude residuals, with the largest peak at zero and a secondary peak at approximately 0.75 magnitude units (Figure 6a). Figure 6 shows that magnitudes for most earthquakes do not change significantly as a result of the present revisions. However, if we only consider earthquakes that have catalogue (i.e. Richter) magnitudes  $ML \geq 4.0$ , we observe a large secondary peak at approximately 0.75 magnitude units (Figure 6b), with some residuals up to one unit in magnitude. This figure suggests that many moderate-magnitude pre-1990 earthquakes occurred in remote locations at distances far from the nearest recording instrument. If these corrections better reflect actual magnitudes of historical earthquakes in the Australian catalogue, it will result in higher b-values (the relative rate of small-to-large earthquakes) and lower activity rates for larger earthquakes in particular regions.

Additionally, Allen (2010) considered epicentres located within the southwest seismic zone of Western Australia and noted that local magnitudes in this region generally did not change markedly from the

original magnitude. The primary reason for this is that the SWSZ had near-continuous monitoring for much of the period considered. Consequently, most epicentres in the SWSZ were located within about 180 km from the nearest seismic recorder. As previously mentioned, the Australian-specific local magnitude equations were generally similar to the original Richter (1958) equation in the distance range between  $50 \leq R_{epi} \leq 180$  km, and thus would have not been modified significantly using this method.

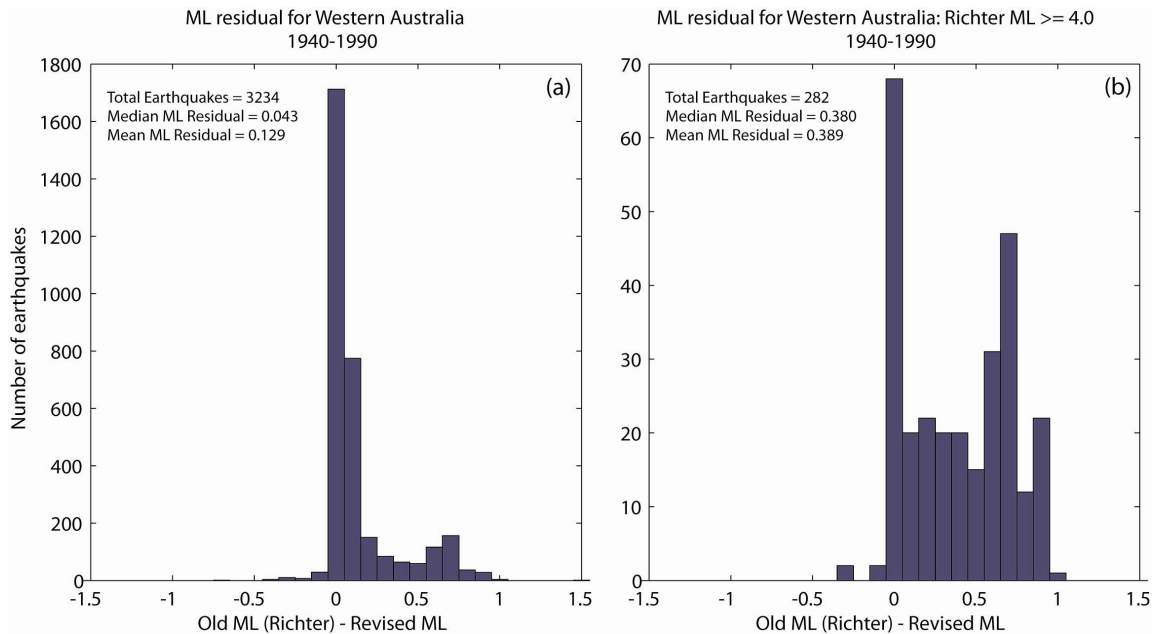


**Figure 6:** Histograms showing residuals of catalogue magnitudes minus revised magnitudes based on methodologies herein for (a) all of WCA region, and (b) for the WCA region for  $M_L$  (Richter)  $\geq 4.0$ .

### 2.3.2 Mt Lofty and Flinders Ranges

South Australia has had non-Richter magnitude formulae since White (1968) first published a region-specific local magnitude formula. This was updated with the publication of the Greenhalgh and Singh (1986) local magnitude equation. Both of these equations are considered to be mostly applicable to the zone defined within the MLFR zone in Figure 5. Using similar methods to that described above for WCA, earthquake magnitudes are revised for those periods and networks that are assumed to use non-local magnitude equations.

Figure 7 indicates a histogram of the magnitude residual between the original and revised magnitudes. As can be observed, the vast majority of earthquakes in this zone have near-zero residuals. For those earthquakes with Richter  $M_L$  4.0 and above, the trend is again towards smaller magnitudes, with a median  $M_L$  residual of less than 0.2 magnitude units. Despite the relatively high rates of seismicity observed in the MLFR zone, there are relatively few earthquakes with Richter  $M_L \geq 4.0$ .

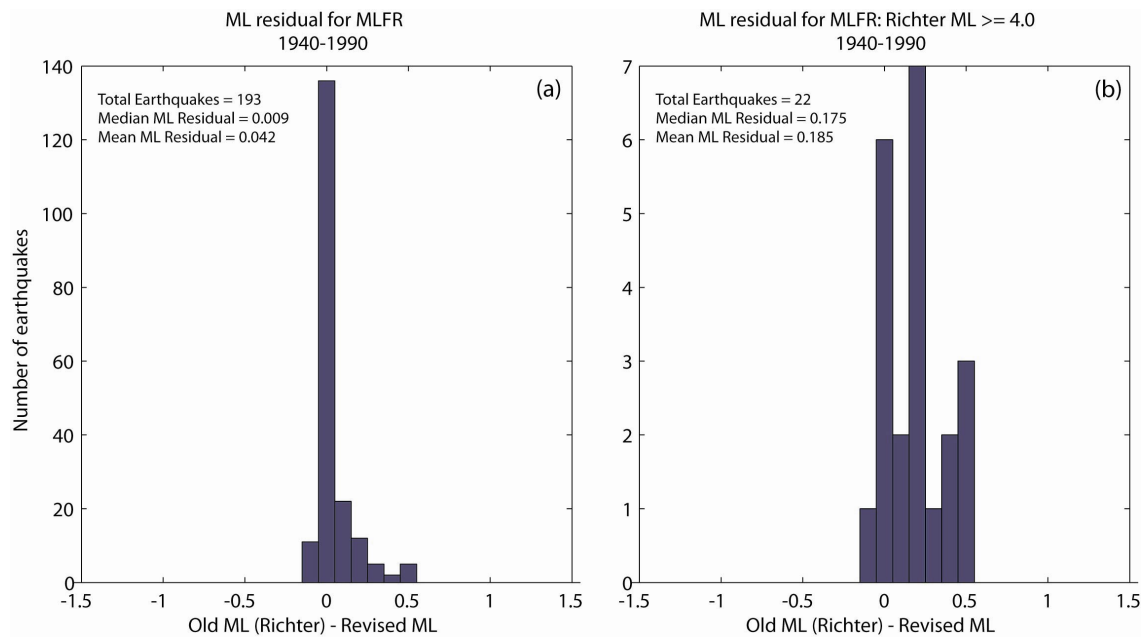


**Figure 7:** Histograms showing residuals of catalogue magnitudes minus revised magnitudes based on methodologies herein for (a) all of MLFR region, and (b) for the MLFR region for  $M_L$  (Richter)  $\geq 4.0$ .

### 2.3.3 Eastern Australia

The eastern Australian region has a rich history of seismic instrumentation due to its relatively high population density and infrastructure development. The method described above primarily rescales magnitude based on the distance to the nearest operational seismometer at the time of the earthquake. Those earthquakes with abundant nearby stations change very little because of similarities between the original Richter (1935) amplitude corrections and those corrections from Australian-specific local magnitude formulae. Earthquakes at locations far away from seismic recording stations will be revised to a larger extent because it is assumed that the use of inappropriate  $M_L$  equations leads to magnitudes that have been over-corrected for attenuation, and thus will have higher magnitudes.

Because of the relative abundance of seismic instrumentation in this region, many earthquakes occurred near a seismograph and thus earthquake magnitude would not have been significantly overestimated. Figure 8 indicates the histogram of residuals for eastern Australia. Overall, the median residual between original and revised magnitudes is very small. For the larger events (Figure 8b), there again seems to be a bi-modal relationship of residuals, only not as significant as that observed in the WCA zone above (Figure 6b). Overall, the majority of larger EA earthquake magnitudes appear to be little changed with the median magnitude residual less than 0.1 magnitude units for  $M_L \geq 4.0$  earthquakes.

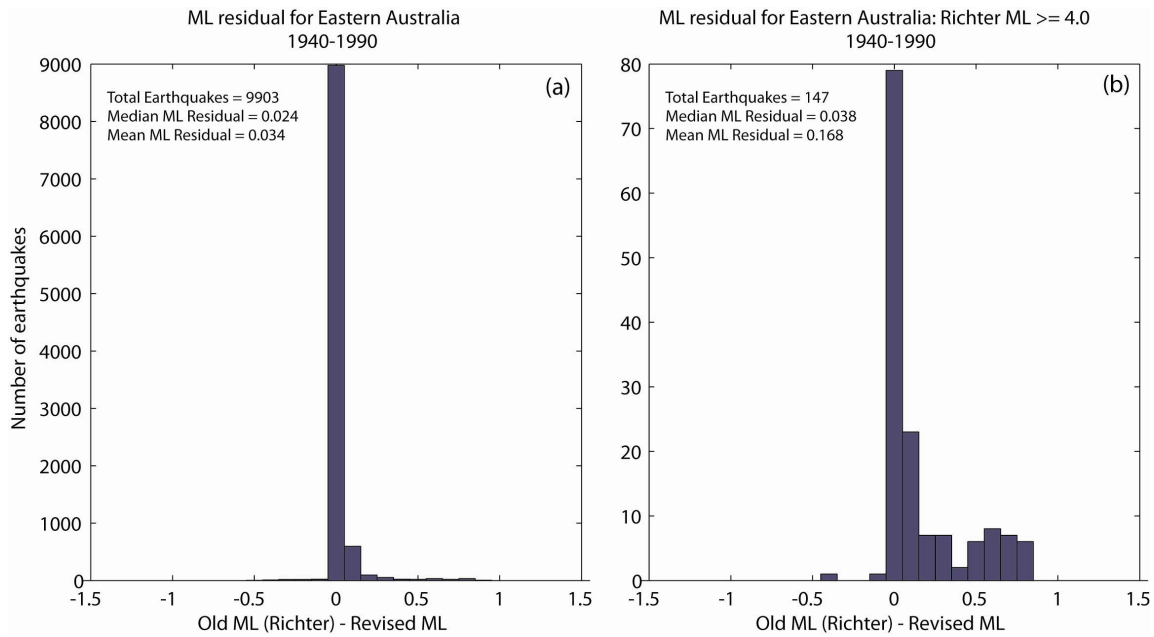


**Figure 8:** Histograms showing residuals of catalogue magnitudes minus revised magnitudes based on methodologies herein for (a) all of SEA region and (b) for the SEA region for  $M_L$  (Richter)  $\geq 4.0$ .

### 2.3.4 Queensland

At this point it is worth considering the magnitudes of earthquakes in the state of Queensland alone. Queensland has a generally lower rate of seismicity than the southeast of the continent. Because of this, in addition to its large expanse and relatively low density of urban and infrastructure development, the state has historically not been well-monitored for earthquakes. Isolating the hypocentres in the EA zone that are located in Queensland, we perform the same comparisons as those performed for EA above. While the bulk of the magnitudes still do not change in magnitude to a large degree (Figure 9a), most of the magnitudes for  $M_L \geq 4.0$  earthquakes are revised to smaller magnitudes using the methodologies described above with a median residual of 0.5 magnitude units (Figure 9b). This observation is important for two reasons: 1) there are no earthquakes of  $M_L \geq 5.0$  in Queensland in the catalogue used to derive earthquake recurrence parameters for the hazard map for the period analysed (1940-1990), and; 2) most of the large residuals for the Richter  $M_L \geq 4.0$  earthquakes in EA (Figure 8b) are located in Queensland.

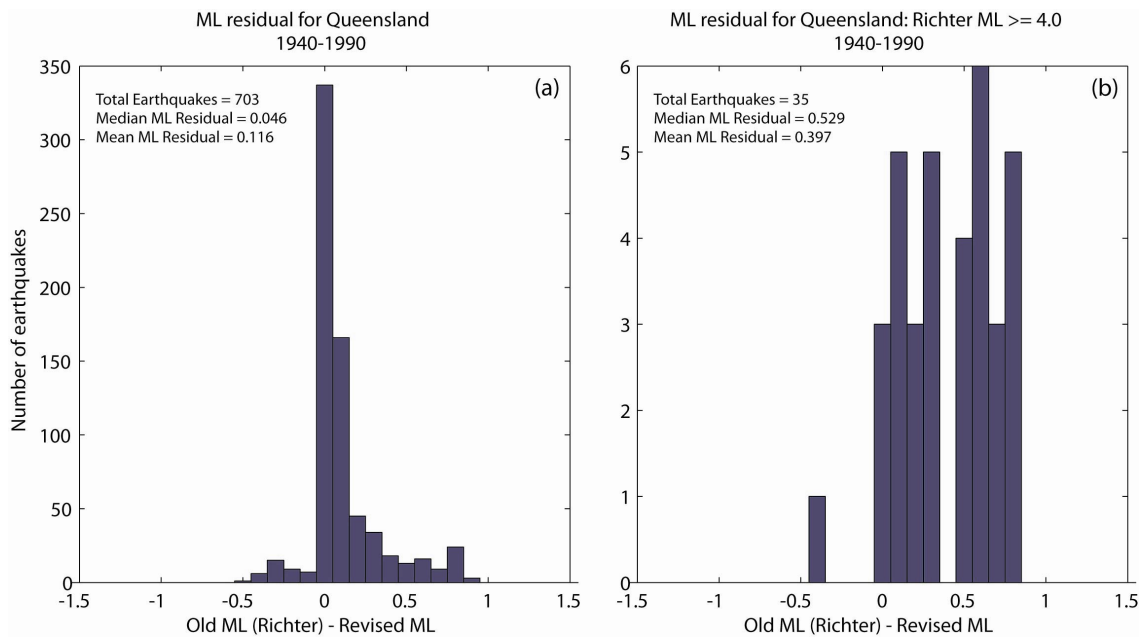


**Figure 9:** Histograms showing residuals of catalogue magnitudes minus revised magnitudes based on methodologies herein for (a) all of Queensland region and (b) for the Queensland region for  $M_L$  (Richter)  $\geq 4.0$ .

### 2.3.5 Discussion of Local Magnitude Revisions

Because we cannot access original amplitude and period data recorded at each seismic station to re-evaluate  $M_L$  with an appropriate equation, this technique must make assumptions about the magnitude equation used and the configuration of the seismic network over time. In addition, we use only the nearest hypothetical station to determine the magnitude correction. This assumption will be at a distance where the differences between the original (Richter) and new  $M_L$  attenuation corrections are smallest. Consequently, this could lead to an underestimation of the actual correction required. Figure 5 shows the change in magnitudes by spatial location, and demonstrates that earthquakes of larger Richter magnitudes occurring in remote locations (relative to seismic networks) are those earthquakes that have the most significant shift in magnitude. This is because the aforementioned method generally assumes that magnitudes determined from inappropriate attenuation formulae (e.g. Richter, 1958) and a sparse network overestimate local magnitudes relative to magnitude formulae used by modern seismic observatories. The objective in revising magnitudes is to deliver a homogeneous earthquake catalogue that provides consistent magnitudes, within a given spatial area, for the full time period being considered. Without undertaking these corrections, the catalogue would comprise earthquake magnitudes determined from disparate magnitude equations and would add significant uncertainty to the calculations of earthquake recurrence. This is particularly true for the recurrence of moderate-to-large earthquakes in the Australian earthquake catalogue which as this analysis indicates, have probably been overestimated in remote locations. To that end, the corrections undertaken herein provide more sensible local magnitudes for those earthquakes with magnitudes that may have been overestimated owing to the use of inappropriate local magnitude equations.

## 2.4 SELECTION OF PREFERRED MAGNITUDE $M$

To obtain a reliable estimate of earthquake recurrence, it is recommended that all earthquake magnitudes be converted to a single magnitude type. Moment magnitude  $M_W$ , has become the most commonly used magnitude scale in earthquake hazard assessments because it provides a physical measure of an earthquake's size. Furthermore, this scale does not saturate with magnitude. Consequently, most modern GMPEs are calibrated to  $M_W$ . The methodology above describes the harmonisation of Australian catalogue magnitudes for  $M_L$  only and does not consider  $M_W$ . Consequently, if these modern GMPEs are used, it is prudent to convert all earthquake magnitudes to a consistent  $M_W$ .

Many equations have been developed to convert other magnitude scales to  $M_W$ , most commonly from surface-wave magnitude  $M_S$  and body-wave magnitude  $m_b$  (e.g., Scordilis, 2006; CEUS-SSC, 2012). These equations can be derived relatively easily by analysing various global earthquake catalogues since the calculation technique for these magnitude types is generally consistent across global networks. However, providing a universal conversion equation from local magnitude  $M_L$  to  $M_W$  cannot be easily achieved without consideration of the local magnitude equation because of inter-equation differences in near-source  $-\log A_0$  correction factors (see Figure 4). This is because  $M_W$  is fundamentally a “source” term, and is not calibrated at a reference distance of 100 km, as is  $M_L$ .

Through the compilation of the master earthquake catalogue for Australian earthquakes used in this study, relationships between  $M_L$ ,  $M_S$ ,  $m_b$  and  $M_W$  were developed (e.g., Allen *et al.* 2011). However, the use of these conversion equations on the historical catalogue – the  $M_L$  to  $M_W$  conversion in particular – yielded atypical estimates of earthquake recurrence parameters in many regions. The net effect of these corrections was to significantly increase the relative number of small-to-large earthquakes considered for the recurrence calculations, which subsequently increases  $b$ -values. While the authors believe that these conversions are delivering a more robust representation of an earthquake’s true magnitude, the end result does violate some commonly held pre-conceptions of earthquake recurrence for small earthquakes in stable continental interiors with  $b$ -values generally assumed to be approximately near 1.0 or slightly less (CEUS-SSC, 2012).

While we do not use the catalogue converted to a consistent  $M_W$ , our present best attempt at deriving such a catalogue is an attribute within the master earthquake catalogue used in the present analyses (see Appendix A for details). The final logic for selecting preferred magnitude  $M$  is outlined below:

1. Moment magnitude  $M_W$  for all magnitudes
2. The larger of surface-wave magnitude  $M_S$  or body-wave magnitude  $m_b$  for  $M \geq 6.0$
3. Revised local magnitude for  $M_{L,rev} < 6.0$  (only present for older events)
4. Original local magnitude for  $M_L < 6.0$
5. Other magnitude types (e.g. duration magnitude  $M_D$ , etc.)

Hereafter all magnitudes are referred to as the preferred magnitude  $M$  unless otherwise specified. A table in Appendix A provides a list of the 50 largest earthquakes documented to have occurred on or adjacent to the Australian continent. The table provides the earthquake’s original and revised local magnitude estimates, in addition to the preferred magnitude used in these hazard analyses based on the logic above.

The adoption of the preferred magnitude  $M$  rather than homogenising the catalogue to a consistent magnitude type (such as  $M_W$ ) potentially represents a major limitation in the development of the Australian Earthquake Hazard Map. The primary reason for this is that the ground motions estimated by a GMPE and used in the hazard calculations will be calibrated to a magnitude type that is inconsistent with those magnitude types used to define the recurrence parameters. For example the magnitude conversion equations for stable continental regions commonly reduce an earthquake’s magnitude when converting from  $M_L$  to  $M_W$  (e.g., Johnston, 1996; Grünthal *et al.*, 2009; Allen *et al.*, 2011; Goertz-Allmann *et al.*, 2011). Consequently the recurrence parameters derived from a catalogue largely populated by  $M_L$  (such as the Australian earthquake catalogue) may lead to hazard values that are too high when combined with a GMPE calibrated to  $M_W$ .

## 2.5 DECLUSTERING AND DEBLASTING

In order to calculate the earthquake recurrence model from the catalogue, clusters of earthquakes (usually aftershocks, mining blasts and swarms) need to be removed from the catalogue. The original catalogue (GGcat\_2010-02-22) was bounded by the latitudes -10 to -45 and longitudes 110, and 160. The first step was to remove the earthquakes from the Banda Sea, Coral Sea, PNG, Tasman Sea and Indian Ocean. The polygon used included areas of extended continental crust to Australia’s NW, NE and SE.

Three declustering methods were then tested:

1. Method 1 used the expert judgement of Gary Gibson to determine whether an earthquake was a foreshock, aftershock or swarm .
2. Method 2 used a windowing method based on the declustering algorithm described in Leonard (2008), which uses a magnitude dependent time period and distance window.
3. Method 3 used a modification of the Leonard (2008) declustering algorithm to account for the long aftershock periods proposed by Stein and Liu (2009) for large continental earthquakes (e.g.  $M$  7.5, 500+ years).

Declustering algorithms classify earthquakes as being dependent events (i.e. foreshocks or aftershocks) if they occur within a specific distance and time of the mainshock. The general form of the magnitude-dependent time component of a declustering algorithm is:

$$T = 10^{(M-A)*B} + c \quad (1)$$

where  $T$  is length of the time window in days and  $M$  is the magnitude of the mainshock.

The size of the spatial window of the declustering algorithm is given by:

$$R = 10^{(M-D)*E} + f \quad (2)$$

where  $R$  is the radius of the window in kilometres.

For Method 2,  $A$ ,  $B$ , and  $c$  are 1.85, 0.69, and 0.0 respectively (Leonard, 2008). For Method 3,  $A$ ,  $B$ , and  $c$  are 2.7, 1.1, and 4.0 respectively. The Method 3 values for  $A$ ,  $B$ , and  $c$  were scaled to produce an aftershock period for a  $M$  4.0 earthquake of ~30 days and a period for a  $M$  7.5 earthquake of 500-600 years (Table 2). For both Methods 2 and 3,  $D$ ,  $E$ , and  $f$  in Equation (2) are 3.82, 0.6, 10.0, respectively.

The algorithm treats every earthquake as a potential mainshock, so aftershocks can also have aftershocks. In addition, earthquakes with a magnitude greater than 93% of the mainshock magnitude (80% of the seismic moment  $M_0$ ) were not considered as aftershocks for this Method. This prevented the removal of sequences such as the 2001-02 Burakin, WA, sequence, where there were five earthquakes of  $M_L \geq 4.7$ . In the present analyses, they are all considered to be mainshocks. Each had an aftershock sequence, but are not considered aftershocks of each other.

**Table 2:** Period of time and distance from mainshock for an earthquake to be classified as an aftershock using Method 2 or 3. Note that Method 1 does not appear in this Table because it was based purely on expert judgement.

MAGNITUDE	3.0	4.0	5.0	6.0	7.0	7.5
Method 2 (weeks)	0.9	4.3	21	104	511	1130
Method 3 (weeks)	0.9	4.4	49	610	7670	27200
Radius (km)	10.3	11.3	15.1	30.3	91	171

Method 2 was designed to be conservative and not remove an excessive number of earthquakes as aftershocks. However, the spatial and temporal analysis tools discussed in the next section, shows that Method 2 still preserves many aftershocks in the catalogue. As a result of this, we also tested the effect of using Methods 1 and 3 on the catalogue. Both these methods remove a similar number of aftershocks (see Table 3) but they are overlapping sets. In some cases Method 1 is superior. For example the aftershocks of the Simpson Desert sequence in the 1970's were often greater than 100 km from the mainshock epicentre and so were not removed by Method 3 but were removed by Method 1. Also Method 3 did not remove foreshocks unlike Method 1. In areas of higher seismicity (e.g. Southwest WA and MLFR, see Figure 5), Method 3 removed aftershocks not identified by Method 1. The likely explanation is that with many potential mainshocks and aftershocks it is very difficult to keep track of all of them if the method is based purely on expert judgement.

To overcome these problems, Method 3 was applied as a first-pass to filter aftershocks from the catalogue. Foreshocks were also removed by applying the same time and distance algorithms as Method 2 but testing backwards in time. This is referred to as Method 4 in Table 3. Method 1 was subsequently applied to the catalogue to remove any remaining foreshocks and aftershocks. Finally, the two *M* 6.3 Tennant Creek “foreshocks” were moved back into the mainshock catalogue. Table 3 shows the number of earthquakes removed by each of the methods considered individually and combined together one after the other. In Appendix C it is demonstrated that this three step process is effectively declustering the catalogue, with the declustered catalogue closely approximating a temporally Poisson process and so fulfilling the suggestion (e.g., Gardner and Knopoff, 1974) that declustered catalogues should be approximately Poisson in time.

*Table 3: the number of earthquakes removed by the declustering algorithm. The final declustered catalogue results from the successive application of Methods 3 then 4 then 1. Dependent events include foreshocks and aftershocks.*

	TOTAL	MAIN EVENT	DEPENDENT EVENTS
Full Catalogue	38106		
Method 1	35312	26186	9125
Method 3	35312	25454	9857
Method 3 then Method 4	25454	24299	1156
Method 3 then Method 4 then Method 1	24299	22901	1398

## 2.6 SUMMARY OF CATALOGUE MODIFICATIONS

Herein we have described several techniques used to generate a more complete and homogenous earthquake catalogue to be used in the update of the Australian Earthquake Hazard Map. Firstly, the catalogue takes advantage of an additional two decades of earthquake data gathered by seismic networks across the Australian continent. Relative to Gaull *et al.* (1990) which used 9,000 earthquakes, the Australian earthquake hazard map presented here considers a base dataset of over 35,000 events to assess the average recurrence of earthquakes across continental Australia and the region. The catalogue was deblasted and subsequently enhanced through the application of modern declustering techniques. These techniques remove dependent events and anthropogenic sources from the catalogue, which would otherwise bias hazard estimates.

## 3. Source Zonation

*M. Leonard, A. McPherson and D. Clark*

Fundamental to any earthquake hazard assessment is the choice of the source zones for which recurrence parameters ( $a$ ,  $b$ ,  $M_{max}$ ) are estimated. The choice of source zones, either implicitly or explicitly, implies a seismicity model. For example, a smoothed seismicity approach implies that seismicity is approximately stationary with time and so the catalogue (typically 30-50 years of instrumental data) reliably predicts future seismicity, independent of return period. Traditional zonation models define regions which are assumed to have uniform earthquake recurrence and for which the catalogue is sufficiently comprehensive to estimate the future seismicity. Their selection is usually based on historical seismicity, sometimes with contributions from geology and geophysics.

### 3.1 ASSESSMENT OF EXISTING SOURCE ZONES

An outcome of the initial hazard map stakeholder workshop in 2009 (Burbidge *et al.* 2010) was that an assessment of existing earthquake source zones for Australia should be undertaken before any decision was made to develop a new model. The two existing source zone models available for Australia – Brown and Gibson (2004) and Gaull *et al.* (1990) were considered. The zones discussed by Leonard (2008) were never intended as source zones for application in a PSHA. Even though they have been used for this purpose by some researchers, we do not consider them as a candidate model for the national hazard map.

The zones defined by Brown and Gibson (2004) are not considered appropriate for a national scale map and this assessment is endorsed by the authors (Gary Gibson, pers. comm., 2011). The large number of small zones in this model requires local catalogues, many of which are proprietary, and/or the definition of a regional  $b$ -value in order to calculate robust recurrence statistics. As such it is better suited for local seismic hazard assessments.

In developing probabilistic earthquake risk maps for Australia, Gaull *et al.* (1990) published a series of earthquake source zones based primarily on the spatial distribution of epicentres, with selective reference to geological and tectonic information. The catalogue used in their assessment was current to 1984, meaning that the product was effectively six years old upon publication. The source zones defined by Gaull *et al.* (1990) are now roughly 25 years old. Since that time the catalogue of earthquakes has not only increased in size, but it has also undergone numerous revisions/corrections, leading to the availability of a much more robust dataset for characterising contemporary seismicity. In addition, the stated  $M_{max}$  values for all background zones defined by Gaull *et al.* (1990) are inconsistent with both historical seismicity (Leonard 2008) and palaeoseismological evidence (Clark *et al.* 2011). The latter also suggests that values of  $M_{max} \geq 7.0$  are more appropriate to the continent (Clark *et al.* 2011; cf. Section 3.3) and to intraplate areas worldwide (Wheeler 2009a,b). As a result of this assessment, it was decided that the best approach would be to develop an entirely new set of source zones.

### 3.2 A NEW METHOD FOR DEFINING SOURCE ZONES

Several sources of evidence suggest that the occurrence of large earthquakes is episodic (or both spatially and temporally non-stationary). This includes models of intraplate seismicity based on results from neotectonic, geodetic and computer modelling studies of stable continental crust (e.g. Toda *et al.* 1998; Parsons 2002; Stein and Liu 2009; Li *et al.* 2009; Leonard and Clark 2011) as well as the statistical properties of Australian seismicity Leonard (2010b). Such a model of episodicity suggests that a single set of source zones will not capture the complexity of the observed seismicity. The temporal and spatial Poisson statistics of Australian seismicity suggest that a multi-layer source zonation model is required to account for the seismicity. Accordingly, we propose a three layer model, described below, consisting of: i) three large background seismicity zones covering 100% of the continent; ii) 25 regional scale source zones covering approximately 50% of the continent; and iii) 43 hotspot zones covering 2% of the continent.

The remainder of this chapter describes the methods used to define earthquake source zones for the 2012 earthquake hazard map. These, in combination with the recurrence parameters and the ground motion prediction equations, effectively shape the final hazard maps.

The selection of source zones is a subjective process, generally relying on seismology with geology providing some qualitative guidance. For the 2012 map we have attempted to make the process of deriving the zones as quantitative as possible, bearing in mind that some degree of subjectivity is inevitable.

### 3.2.1 Spatial Statistical Analysis Method

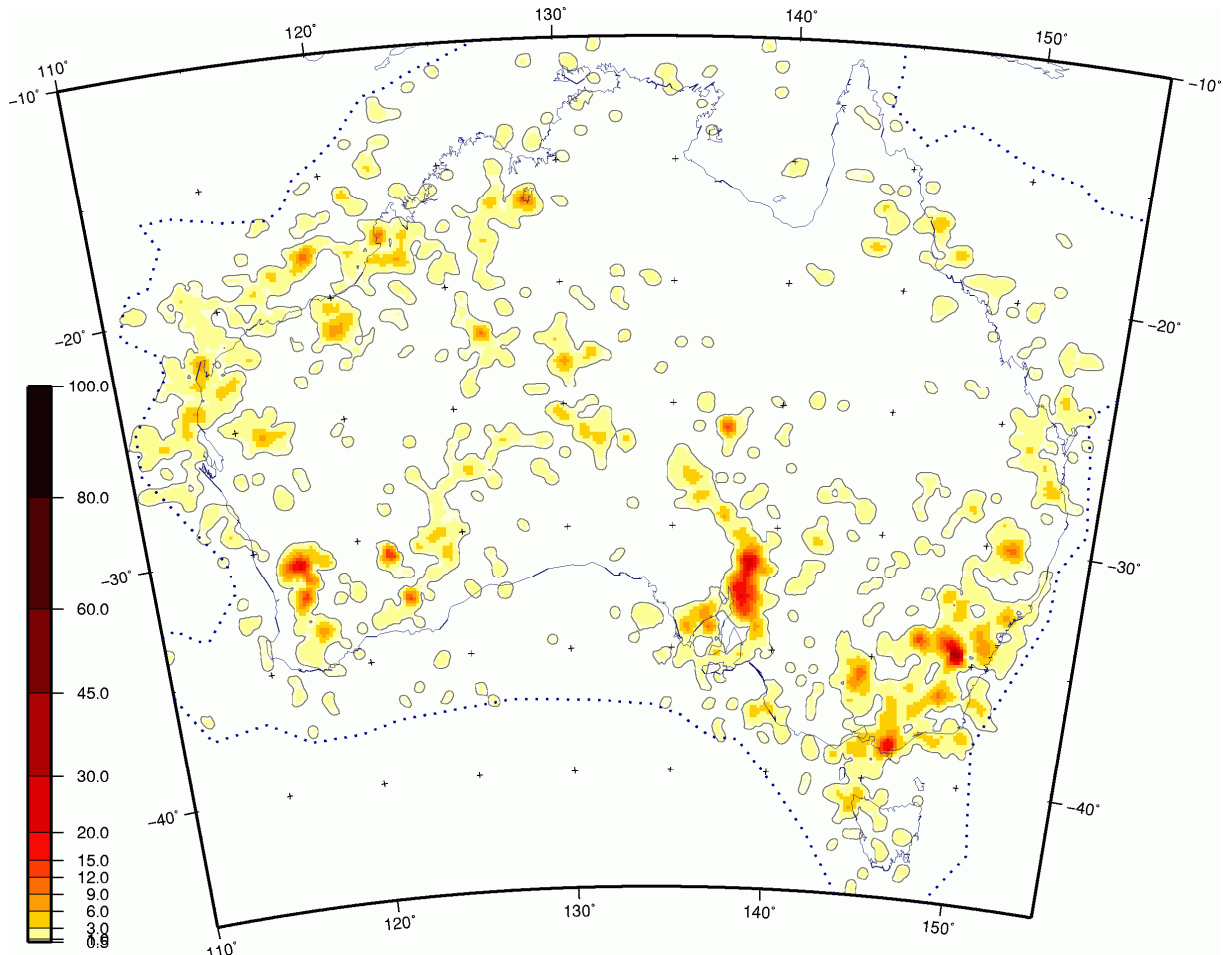
In this section we describe the basis for the seismicity model adopted and the resulting source zones. Using the spatial analysis method described by Leonard (2010b) the Australian continent was divided into 4,000  $55 \times 55$  km square cells and the number of earthquakes in each cell counted. A size of  $55 \times 55$  km square cells was found to be an appropriate balance between spatial resolution and the average number of earthquakes per cell (Leonard 2008). The process was repeated four times with the grid displaced 27.5 km to the north, to the east, and to the northeast, giving a final grid with a 27.5 km cell spacing. Approximately 2,400 earthquakes in the declustered catalogue since 1 January 1965 with  $M \geq 3.0$  are used for this purpose. These criteria were chosen to maximise the number of earthquakes under the assumption of an approximately uniform magnitude of completeness ( $M_C$ ) for the time period considered.  $M_C$  is here defined as the lowest magnitude above which all earthquakes in a space-time volume are detected (Weimer and Wyss 2000).

Figure 10 shows the spatial distribution of earthquake density, as the number of earthquakes per  $55 \times 55$  km square cell. The contour line represents a minimum value of 0.5 earthquakes per cell and the colour scale represents the number of earthquakes per cell. If the earthquakes were distributed randomly, 28% of the area would be expected to fall within the 0.5 contour, whereas the observed value is 18%. Similarly the areas with four or more earthquakes per cell should be 13 of the 4,000 cells (0.3%), whereas the actual value is 151 (3.8%), with the theoretical and actual values for five or more earthquakes per cell being 1.6 and 91, respectively. Whilst the declustering has produced a catalogue that approximates a Poisson process in time it is not spatially Poisson (Leonard 2010b). This analysis has been repeated for various sub-regions of Australia and the following is observed:

1. No area of Australia has been found that can be approximated by a single spatial Poisson model. All are clustered and are not randomly distributed. Using a declustered catalogue almost all regions require at least three Poisson models, with some requiring four, to model the spatial statistics (Leonard 2010b).
2. Using the full (not declustered catalogue) four Poisson models are required for most regions.
3. In all cases there are more cells than expected with less than one and more than four earthquakes and a deficit of cells with one or two earthquakes.
4. The larger active areas (e.g. southwest Western Australia - SW WA, the Australian Capital Territory region, Flinders Ranges, South Australia - SA) tend to contain multiple hotspots. For example, in addition to the very large sequences associated with the 1968 Meckering and 1979 Cadoux earthquakes in SW WA (Zone 25), there are several other hotspots of ongoing activity outside the source regions of the aforementioned earthquakes, and many other transient hotspots (e.g. Burakin and Katanning SW WA). Similar behaviour is seen in the Eyre Peninsula region (Zone 16) and SE Australia (Zones 7, 8, 9, 10, 12). In the Adelaide Geosyncline (Zone 17), aftershocks are less common, but a similar pattern of clustering exists.
5. Almost all hotspots indicate ongoing activity. Only a few hotspot regions appear to have commenced during the last 50 years.
6. Large dams can induce significant seismic activity, but this activity normally diminishes in less than a decade following the initial filling of the dam [e.g. Thomson Dam, Victoria; Talbingo

(Tumut 3), New South Wales]. Reservoir-triggered seismicity appears to be more prevalent during the filling of larger dams (e.g., Allen *et al.*, 2000; Gupta, 2002).

7. The presence of hotspots around several mining areas suggests that there are many blasts (or rock bursts) that have been misinterpreted as earthquakes, that mining-induced seismicity is relatively common, or both.



**Figure 10:** The earthquake spatial density of Australia, based on the declustered catalogue. The contour line represents a minimum value of 0.5 earthquakes per cell and the colour scale represents the number of earthquakes per 55 × 55 km cell.

### 3.2.2 Implications for seismic hazard assessment

As the fundamental assumption of random (or uniform) distribution of earthquakes within the source zones does not hold, a single set of source zones will not correctly reflect the seismic hazard of Australia. Using a single source zone in an area may underestimate the hazard within any hotspot and overestimate it elsewhere. Most ‘active’ areas can be better described as a regional zone with a number of embedded hotspots.

Models of episodic fault behaviour, with the area surrounding each fault undergoing its own active/quiescent cycles, possibly with subtle stress interactions between neighbouring faults, are emerging in the literature (Toda *et al.* 1998; Parsons 2002; Stein and Liu 2009; Li *et al.* 2009; Leonard and Clark 2011). The occurrence of many of Australia’s large ( $M \geq 6.0$ ) earthquakes appears to be episodic. Examples include Collier Bay, Tennant Creek, Meckering, Meeberrie, Lake Tobin and Beachport all of which had no significant seismicity in the decades prior to their occurrence. An episodic model of earthquake occurrence implies that a much larger area is involved than is observed from a short-term observation of the seismicity.

Recurrence rates, based on the last 50 years of data, suggest that the area that might be considered active for these large earthquakes is approximately 20% of the continent. However, an episodic model suggests that in the long term the “inactive” 80% is perhaps as likely to host these rare large earthquakes as the active areas. Therefore, background zones covering the non-active areas need to be included.

Combining the results of the spatial statistical analysis with models of episodic behaviour of large earthquakes suggests that at least three zonation layers are required to model the observed seismicity. The first, background, layer accounts for the large areas encompassing areas of, currently, low to very low seismicity. The second, regional, layer represents the intermediate scale zones of moderate seismic activity. The third, hotspot, layer is needed to account for the small areas of very high seismic activity.

### 3.2.3 Background Zones

The background zones were defined by aggregating the neotectonic domains of Clark *et al.* (2011, 2012) – see [Figure 25](#). These domains record the distribution and properties of palaeoearthquakes, constrained by crustal and tectonic environment using geological and geophysical data (Clark *et al.* 2011, 2012). The neotectonic domains were merged into three ‘superdomains’ - Cratonic, Non-Cratonic and Extended - on the basis of their gross crustal architecture (see [Appendix D](#)). These superdomains are approximated respectively by the Precambrian area of non-extended stable continental crust that dominates Western and central Australia, the Phanerozoic non-extended stable continental crust in Eastern Australia (plus the Proterozoic Adelaide Geosyncline), and areas of extended continental crust, primarily in the passive margin settings around the periphery of the continent. The background zones are shown in [Figure 11](#). The Non-Cratonic zone is split into the mainland section and the Tasmania section, which are separated by the extended crust of Bass Strait. For further detail on the neotectonic domains model the reader is referred to Clark *et al.* (2011, 2012).

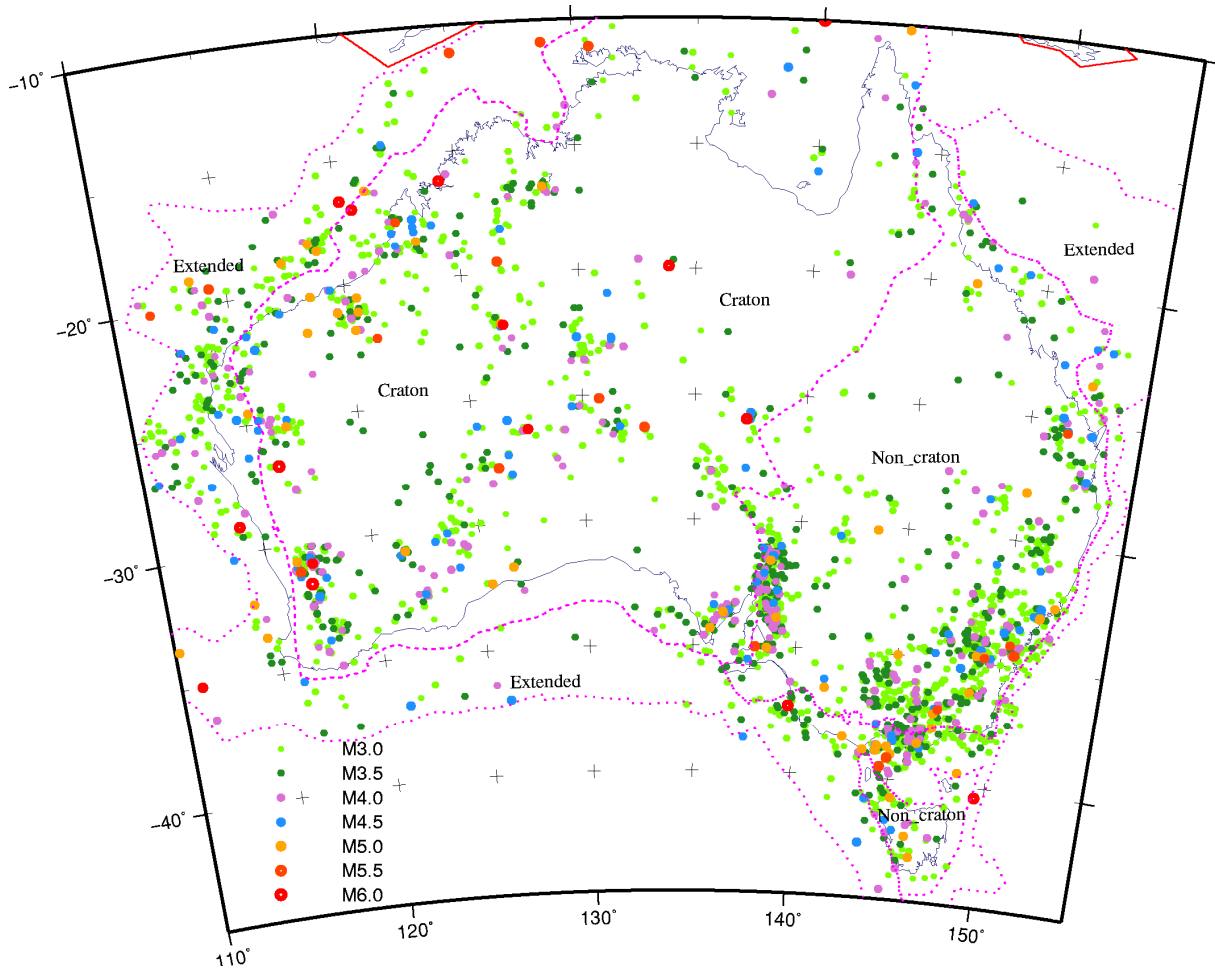


**Figure 11:** The declustered catalogue of earthquakes with magnitude  $M \geq 3.0$ , with the background zones indicated by the dotted magenta line.

### 3.2.4 Regional Source Zones

The spatial density plots were used as the basis for defining the regional source zones. The criteria, in order of importance, were that the zones should: (i) contain at least 60 earthquakes; (ii) encompass contiguous areas of approximately uniform earthquake density; (iii) include sufficient “complete” (since 1<sup>st</sup> of January 1965 with  $M \geq 3.0$ ) earthquakes to robustly calculate the recurrence parameters; (iv) be small enough area to provide meaningful differentiation between regions; (v) avoid encompassing multiple major tectonic units; and (vi) be simple rather than complicated polygon shapes.

The number of earthquakes required to robustly calculate the  $a$  and  $b$  parameters is not fixed. For example, to obtain a magnitude range of 2.0 magnitude units for  $b$ -values of 0.8, 0.9 and 1.0 the number of earthquakes required are 40, 63 and 100, respectively. Furthermore, the inclusion of  $M$  2.0-3.0 events can significantly increase the number of earthquakes, but decrease the robustness of the  $a$ - and  $b$ -value calculations. The robustness is very dependent on accurately estimating the magnitude of completeness ( $M_c$ ). We generally take a conservative approach to estimating  $M_c$ . Consequently, while fewer earthquakes are included than might be possible, we have confidence that the small earthquakes are not biasing the results.

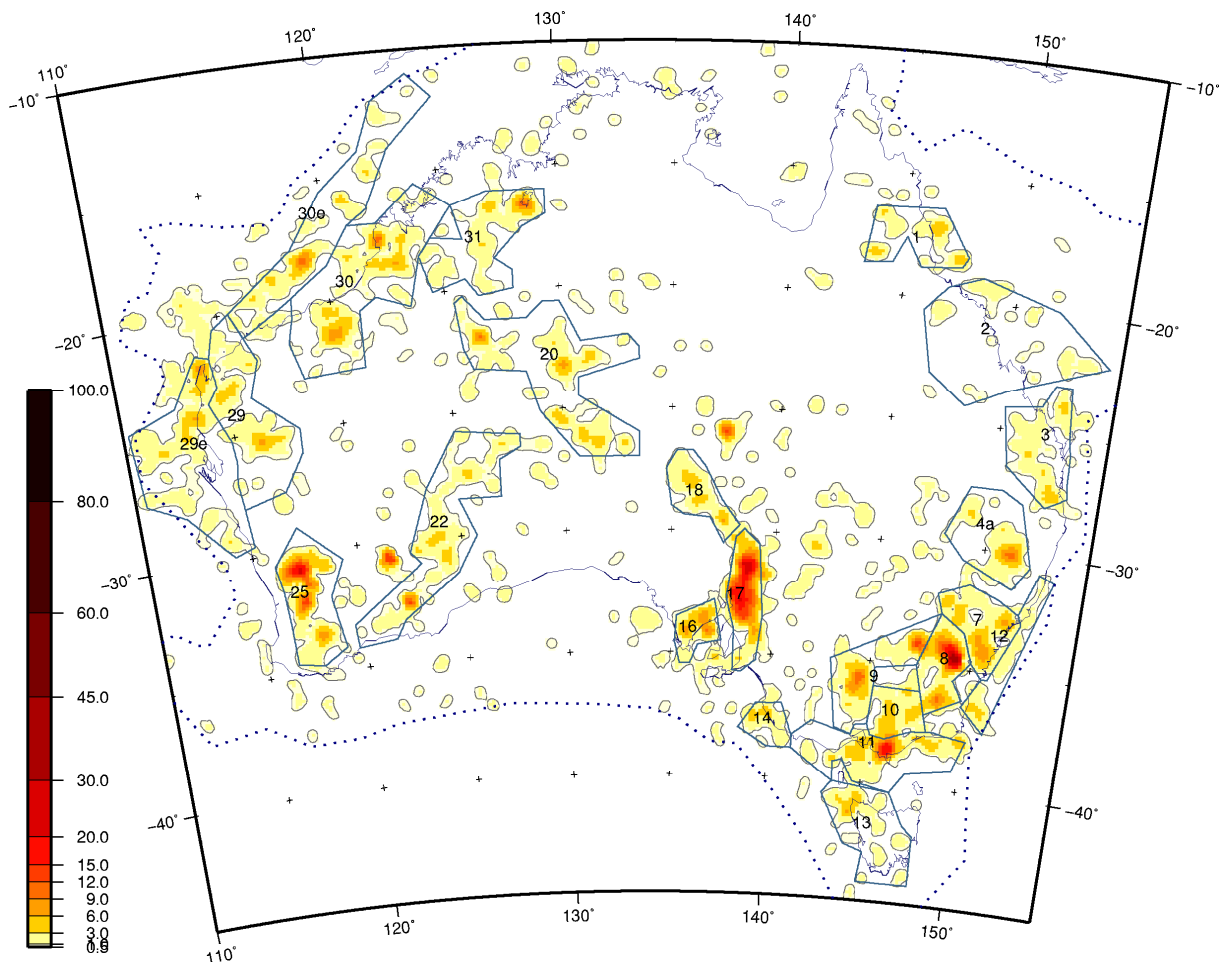


**Figure 12:** The earthquake spatial density of Australia, based on the declustered catalogue with the interpreted Regional zones superimposed. The contour line represents a minimum value of 0.5 earthquakes per cell and the colour scale represents the number of earthquakes per cell. See Table 12 for a description of the numbered source zones.

Figure 12 shows a plot of earthquake density overlain by the selected regional source zones. This is a non-unique selection and a large number of alternative source zones could be selected that also fit the criteria outlined above. Most interpretations would incorporate the areas of more than 1-2 earthquakes per cell. The difference between the interpretations would be around the precise locations of the borders of the zones and which areas of higher occurrence are grouped together as single zones. In the high activity areas (e.g. Flinders Ranges, SW WA and East Gippsland) the borders tend to be well defined and less subject to interpretation. In areas of lower or dispersed activity (e.g. Zones 1 and 2 in Queensland) the selection is highly subjective.

### 3.2.5 Hotspots

As discussed above, if the spatial distribution of earthquakes approximated a Poisson distribution using the declustered and full (non-declustered) catalogue described previously, only 1.6 of the 4,000 cells would contain five or more earthquakes, and none would contain more than five earthquakes. The actual numbers are 91 and 56 respectively. This highly significant deviation from a theoretical Poisson distribution suggests that these areas of anomalously high activity should be treated separately. Consequently, the hotspots are defined as the areas where the spatial density is greater or equal to five earthquakes of magnitude  $M \geq 3.0$  per  $55 \times 55$  km cell. Based on this definition, 58 hotspots were initially identified.

Figure 13 to Figure 17 show the temporal occurrence of earthquakes for five hotspots and provide examples of the analysis that was applied to the 58 hotspots to determine whether they should be

considered in the hotspots layer. The hotspot south of Cowra, NSW (Figure 13), appears to be ongoing and has no obvious correlation to the construction or filling of Wyangala Dam. Similar circumstances relate to the hotspot northeast of Jindabyne, NSW (Figure 14). The apparent decrease in activity around 1990 is likely due to the closure of the Snowy Mountains seismic network and to a lesser extent, the change in magnitude formula used around 1990 (Section 2.3). The hotspot associated with the filling of Talbingo Dam (Figure 15) appears to have tapered off. Figure 16 indicates the earthquake activity near the epicentre of the 1970  $M$  6.0 Cadoux earthquake. This hotspot, which is a region of continuous activity, is a complicated combination of aftershocks and induced earthquakes that lie well outside the Cadoux rupture area. Another type of hotspot tends to be short lived bursts of activity that are not expected to indicate continued activity. The hotspot associated with the 2001-06 Burakin, WA, sequence (Figure 17) is an example of this. In total, nine of the 43 hotspots fall into this category. These hotspots are interpreted as areas of transient activity, being either a short lived aftershock sequence or an episodic swarm.

Through thorough assessment of the 58 areas identified as hotspots, 15 were rejected on the basis that they were not ongoing regions of seismic activity. Consequently, these analyses left a total of 43 hotspots in the hotspot source zone layer.

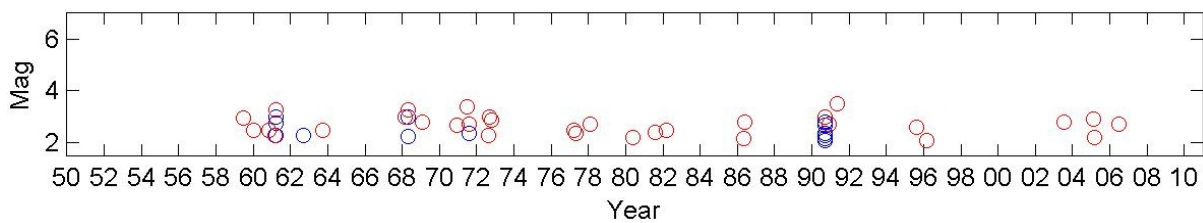


**Figure 13:** Mt Collins hotspot, 23 km south of Cowra and 14 km west of Wyangala Dam with a radius of 14 km. The red circles are mainshocks and the blue circles aftershocks. This region is considered as an ongoing hotspot.

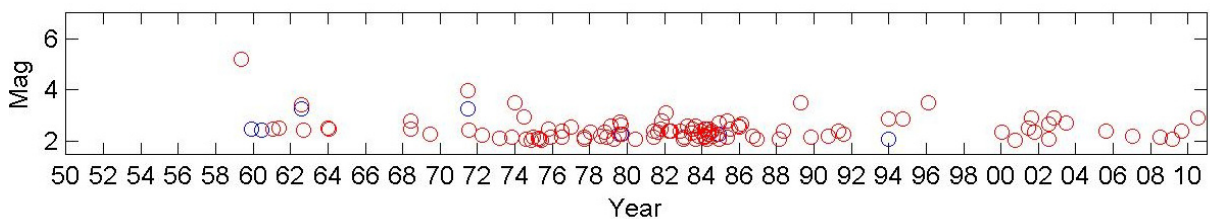


**Figure 14:** The hotspot 15 km northeast of Jindabyne, which includes the Jindabyne and Eucumbene lakes. This region is considered to have ongoing seismicity:

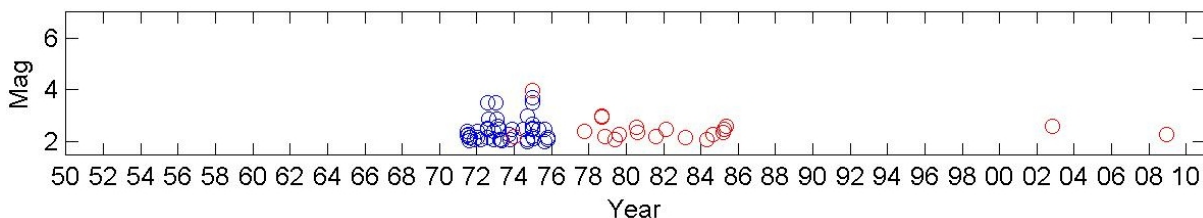


**Figure 15:** Talbingo Lake. This hotspot appears to be a 17 year long sequence associated with the filling of the dam. The dam was completed in 1970 and at the time was the highest in Australia at 161 m. The sequence is now dying out.

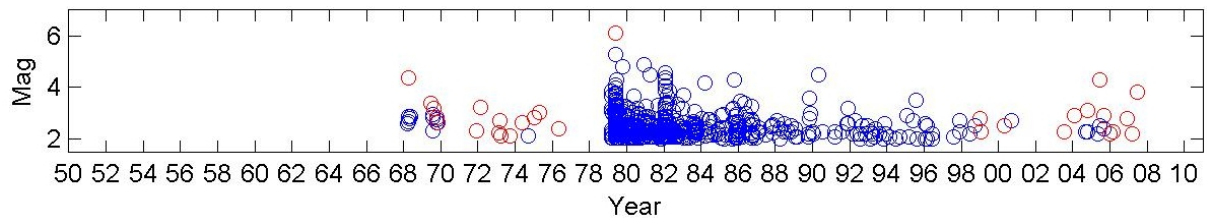


**Figure 16:** This hotspot is centred on the 1979 Cadoux earthquake, radius 40 km. Most of the non Cadoux seismicity is spatially spread over several small clusters. This includes the ten mainshocks  $M > 4.0$  since 2002 where each of the mainshocks is spatially distinct. The many small mainshocks between 1995 and 2002 are due to the declustering algorithm no longer considering the Cadoux earthquake capable of producing aftershocks

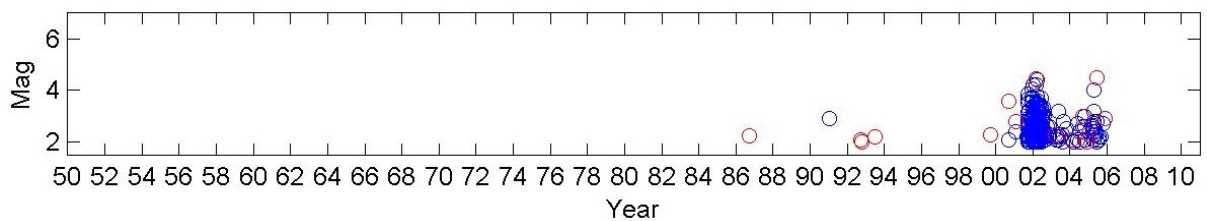


**Figure 17:** The Burakin sequence provides an example of a hotspot that suggests a short-lived burst of activity that is not expected to represent continued activity.

The level of activity is sensitive to the period of time used to calculate the recurrence rate. For example, there is an order of magnitude difference in recurrence frequency when considering post-1988 and post-1992 seismicity for the Tennant Creek hotspot source. Similarly, choosing 1992 as a cut off highly weights recent sequences (e.g. Burakin) but ignores older sequences (e.g. Blue Mountains in 1973). To overcome this problem, two magnitude of completeness models were used. For hotspots associated with transient sequences (e.g. Burakin and Blue Mountains in 1973) an  $M_C$  of  $M$  3.0 since 1902 was used. In contrast, for the hotspots of ongoing activity (e.g. Mt Collins, Tennant Creek and Cadoux), an  $M_C$  of  $M$  3.0 since 1992 was used. The maximum magnitude for each hotspot was the  $M_{max}$  of the region containing the hotspot minus 1.0 magnitude unit. Figure 18 indicates the hotspots determined from the aforementioned analysis. Hotspots that are not considered to be regions of continuous activity are shown in a different colour to the other 34 hotspots in Figure 18.

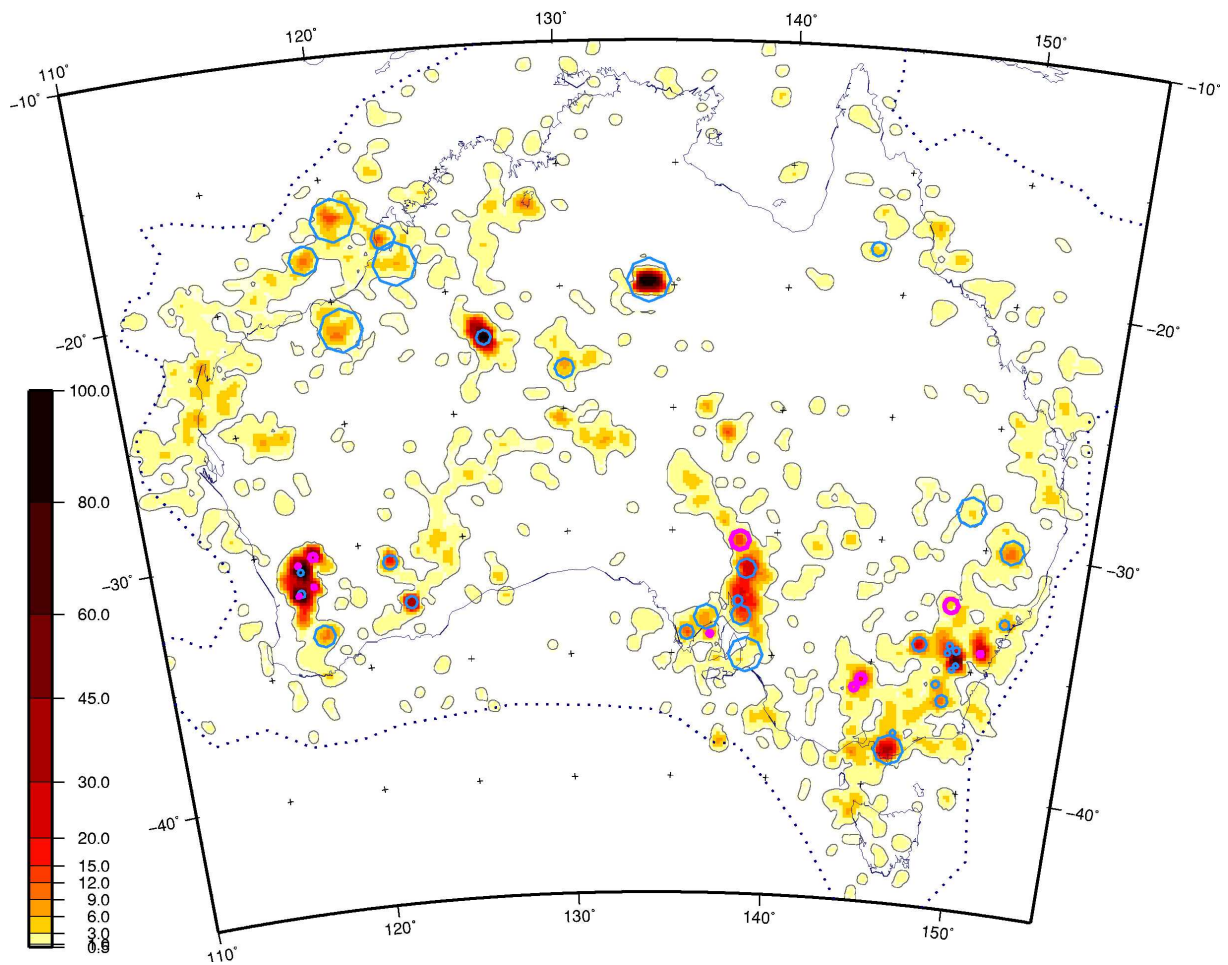


**Figure 18:** The spatial density distribution based on the full catalogue. Hotspots considered continuous are shown in blue circles and hotspots considered to be associated with short lived sequences are shown in magenta circles. The contour line represents a minimum value of 0.5 earthquakes per cell and the colour scale represents the number of earthquakes per cell.

### 3.2.6 Offshore zones

To the north of Australia lie some of the most seismically active areas in the world. Whilst the nearest edge of these zones is more than 400 km from the Australian coast the combination of the high activity rates and the high  $M_{max}$  means that they do impact upon the seismic hazard of Australia. Three zones have been identified. The first encompasses the seismicity in Timor, Lesser Sunda Islands and the eastern Banda Sea. The second encompasses the band of seismicity where the Birds Head micro-plate abuts the Australian plate. The third is the New Guinea region.

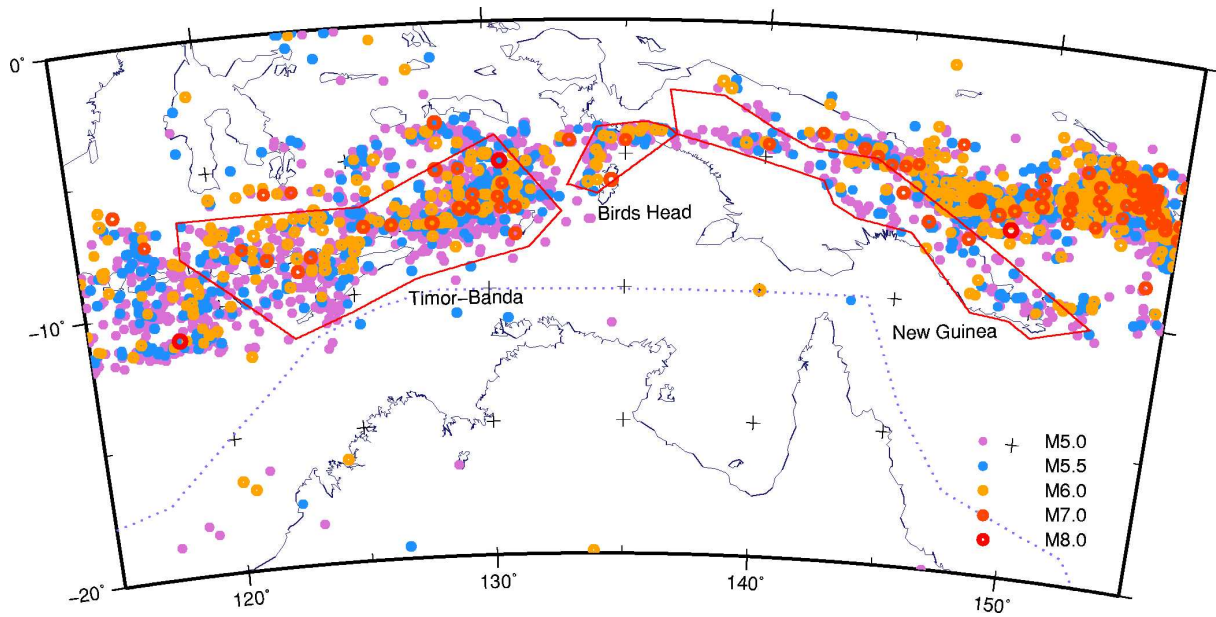


Figure 19: The seismicity to the north of Australia and the three offshore zones used.

### 3.3 SUMMARY OF SOURCE MODEL DEVELOPMENT

To match the observed statistical properties of the seismicity of Australia, multiple Poisson statistical source models are required. In accordance with this result, we have adopted a three layer source zone model: 1) a *Background* layer, with three zones covering 100% of the continent, based on the distribution and characteristics of surface-rupturing palaeo-earthquakes and of crustal properties; 2) a *Regional* layer, of 25 zones covering approximately 50% of the continent, based on the contemporary pattern of earthquake density; and 3) a *Hotspot* layer, of 43 zones covering 2% of the continent, based on the areas of sustained high seismicity.

## 4. Earthquake Recurrence Parameterisation

*M. Leonard*

To forecast the hazard associated with future earthquakes in PSHAs, we must derive statistical models of earthquake occurrence with which to develop stochastic event sets of earthquakes. These statistics are generally governed by the Gutenberg and Richter (1944) magnitude-frequency law, which can be described by the power law relation:

$$\log N = a - bM \quad (3)$$

where  $N$  is the cumulative number of earthquakes having magnitudes larger than  $M$ , and  $a$  and  $b$  are constants that describe the activity rate and relative number of small-to-large earthquakes, respectively (e.g., Wiemer and Wyss, 1997). The parameters required for estimating the seismic recurrence within a given source zone are  $a$  and  $b$  and the maximum magnitude ( $M_{max}$ ) within the source zone. To estimate  $a$  and  $b$  the magnitude of completeness ( $M_C$ ), preferably for multiple dates, is also required. There are various methods for estimating these parameters. In this chapter we provide an overview of these methods and their application to the Australian earthquake catalogue. The methods and models applied in this analysis are outlined and the results presented.

A new algorithm was developed to calculate  $a$  and  $b$ . The algorithm, which is detailed in the following section, is designed to minimise problems with both the Maximum Likelihood method (which is sensitive to the effects of varying magnitude completeness at small magnitudes) and the Least Squares Regression method (which is sensitive to the presence of outlier large magnitude earthquakes). The new algorithm described here overcomes these problems and so allows a fully automated method of calculating  $a$  and  $b$  parameters for all sources zones.

### 4.1 PARAMETERISATION - ESTIMATION OF 'A' AND 'B'

The two primary methods for estimating the Gutenberg-Richter (G-R; Gutenberg and Richter 1944) recurrence parameters  $a$  and  $b$ , are Maximum Likelihood Estimation (Aki 1965) hereafter referred to as ml0 and standard Least Squares Regression (hereafter referred to as ls0). As the ml0 method weights more heavily the more numerous smaller earthquakes, it is generally considered the preferred method for determining earthquake recurrence (Aki 1965). However, the method is sensitive to the assumption that the magnitude of completeness ( $M_C$ ) is known and is constant during the period of the catalogue being analysed. In the well instrumented and higher activity areas of Australia (e.g. the Yilgarn Craton, Flinders Ranges and SE Highlands; Zones 25, 17 and 8 in Figure 12) this assumption holds. However, across much of Australia the assumption fails. The least squares method can be sensitive to the presence of the largest earthquakes in the zone. For example, where there is a gap of 0.3 or more magnitude units in the cumulative number of earthquakes between the largest magnitude in the continuous recurrence data and the largest earthquake(s) in a zone, the largest earthquakes might be considered extreme events. Such events can strongly bias the least squares regressions. When the distribution of the recurrence data has a clear  $M_C$  and no off-trend extreme events, the ml0 and ls0 methods produce effectively identical results. However, many of the 25 regional zones have problems, caused either by the uncertainty of their  $M_C$  and/or the presence of extreme events.

A new algorithm was subsequently developed to minimise sensitivities with both the maximum likelihood and least squares regression techniques, without the need to use expert judgement to determine a preferred  $a$  and  $b$ . For a  $b$ -value of 1.0, each reduction of 0.1 magnitude units (mu) results in an increase in the number of earthquakes by a factor of 1.26. For a reduction of 0.2, 0.3 and 0.4 mu the factor is 1.58, 2.0 and 2.51 respectively. Therefore if a magnitude bin contains one earthquake, the Poisson probability that bins of 0.1, 0.2, 0.3 and 0.4 mu lower will contain one or more earthquakes is 72%, 79%, 86% and 92% respectively. For example, if a catalogue contains one  $M$  5.5 earthquake, there is only a 14% chance that it will not contain a  $M$  5.2 earthquake, and an 8% chance that it will not contain a  $M$  5.1 earthquake.

Similarly, if a region's catalogue contains two  $M$  5.5 earthquakes there is only a 2% chance that there will not be a  $M$  5.2 earthquake and a 1% chance that there will not be a  $M$  5.1 earthquake in the catalogue. This suggests that a gap of either 0.3 or 0.4  $\mu$  would be a reasonable test for identifying extreme events.

We have developed an algorithm that uses a gap of 0.3  $\mu$ , which corresponds to two empty magnitude bins of 0.1  $\mu$  width, to remove extreme events before using ordinary least squares to calculate  $a$  and  $b$ . The first stage takes a subset from  $M_C$  (e.g.  $M$  3.5) until the second empty magnitude bin. The least squares method is then applied to this subset of the data. Hereafter, this method is referred to as ls2. We found, through trial and error, that two gaps for a bin width of 0.1 magnitude units was able replicate the choices an experienced analyst would make. This algorithm has the advantage that it is both automatic and repeatable. We have also developed an algorithm that fixes a line of  $b = 1.0$  at the 1/3 point of the available magnitude-frequency data to calculate  $a$  (referred to as a\_1). A simple logic is then used to select the preferred  $a$  and  $b$  from these four algorithms described (i.e., ls2, ml0, ls0 and a\_1).

Based on global active tectonic data, Schorlemmer *et al.* (2005) demonstrated that the average  $b$  for thrust events is 0.93, with a range of 0.78 to 1.0 depending on rake angle and for strike-slip earthquakes the average  $b$  is 0.98 with a range of 0.95 to 1.1 depending on rake angle. Given that Australian earthquakes are almost exclusively thrust and that declustering a catalogue reduces the  $b$ -value we initially considered the range 0.6 to 1.05 to be an acceptable range of  $b$ -values for the declustered Australian catalogue. After the stakeholder workshop in February 2012, where 0.6 was considered too low, the acceptable range of  $b$ -values was modified to a range of 0.82 to 1.15. As a consequence, the preferred values of  $a$  and  $b$  were selected according to the logical sequence:

- if  $b$  found using ls2 is within the acceptable range, use ls2
- else if the  $b$  value found using ml0 is within the acceptable range, use ml0
- else if the  $b$  value found using ls0 is within the acceptable range, use ls0
- else use method a\_1

Of the 25 regional zones the ls2 method was used for 19, ml0 for one, ls0 for one and a\_1 for four zones.

Figure 20 to Figure 23 show a series of examples where the ls0 (black line) and/or ml0 (red line) methods fail to give reliable estimates of  $b$  because the slope of the curve is affected by either by the uncertainty of their  $M_C$  and/or the presence of extreme events. In contrast, the ls2 (green) method does provide a reliable estimate of G-R recurrence parameters. In Figure 23, none of the three methods (ml0, ls2 and ls0) give a reliable result, so the default value of  $b = 1.0$  is used.

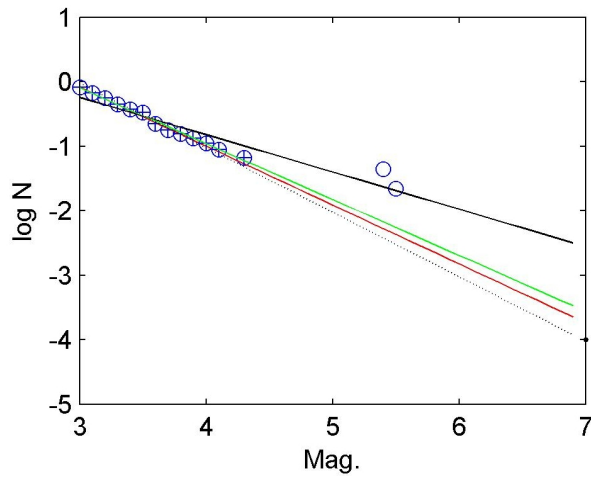


**Figure 20:** Magnitude-frequency statistics of Zone 10 (Victorian North East). The  $b$ -value from  $ls_0$  (black) is biased low by the  $M$  5.4 and 5.5 earthquakes. The  $ml_0$  (red),  $ls_2$  (green) and  $b=1$  (dotted) methods give generally consistent results.

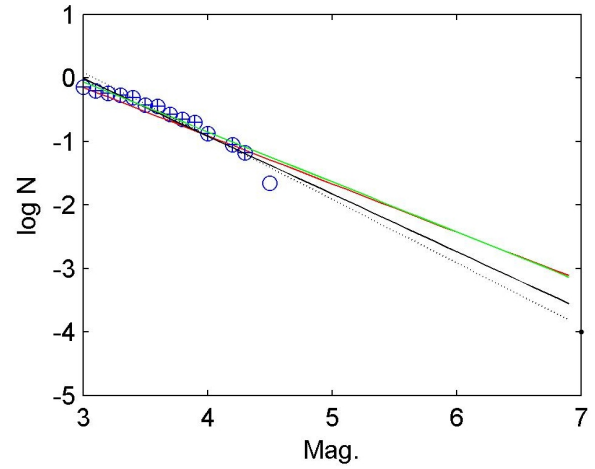


**Figure 21:** Magnitude-frequency statistics for Zone 1 (Chillagoe-Cairns), where the  $b$ -value from  $ls_0$  (black) is biased high but both  $ml_0$  (red) and  $ls_2$  (green) methods give generally consistent results

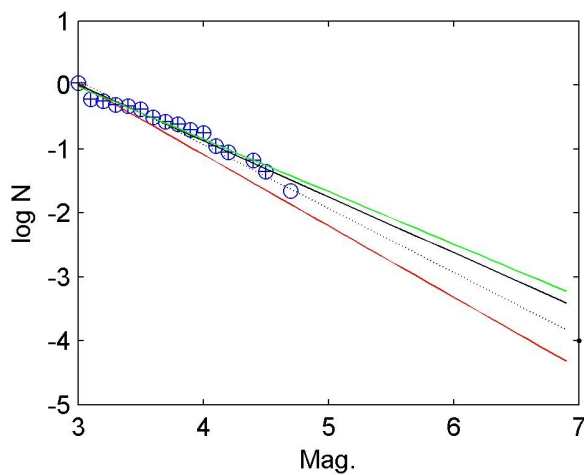


**Figure 22:** Magnitude-frequency statistics for Zone 13 (Western Tasmania and Bass Strait), where the  $b$ -values from  $ml_0$  (red) is biased high but  $ls_0$  (black) and  $ls_2$  (green) both give generally consistent results.

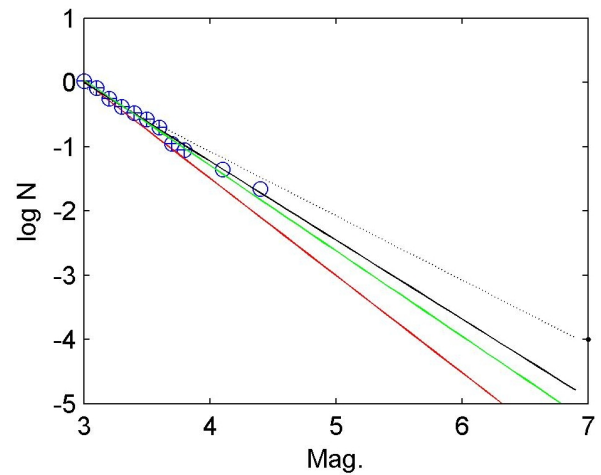


**Figure 23:** Magnitude-frequency statistics for Zone 16 (Eyre Peninsula), where all  $b$ -values, particularly  $ml_0$  (red), are biased high (i.e. greater than 1.15) by the extreme events and a value of  $b=1$  (the dashed line) was assumed.

## 4.2 MAGNITUDE OF COMPLETENESS

The magnitude of completeness ( $M_C$ ) is defined as the lowest magnitude above which all earthquakes in a space-time volume are detected (Wiemer and Wyss, 2000). Single corner magnitude of completeness models assumes that all earthquakes above a specific magnitude occurring after a certain date are detected and that no earthquakes before that date and below that magnitude are available. This gives the completeness model a single magnitude and date “corner”. A multi-corner model uses multiple date and magnitude pairs to allow the catalogue to be extended back in time. The aim of using a multi-step  $M_C$  model is that both large historical earthquakes and small recent earthquakes can be incorporated into the regression for the G-R recurrence parameters ( $a$  and  $b$ ). In theory this could lead to more robust recurrence estimates by minimising the need for extrapolation from the largest earthquake in the catalogue used in

calculating  $a$  and  $b$ , to the largest simulated earthquakes used to calculate the probabilistic hazard. However, the exact location of each corner is highly subjective and this uncertainty adds noise into the cumulative magnitude statistics and as a consequence, into recurrence parameters ( $a$  and  $b$ ). The more uncertain we are in each magnitude/period corner the more potential for noise to be introduced. There is a trade-off between “optimistic”  $M_C$  periods, which whilst including more earthquakes, is more likely to introduce more noise and “pessimistic”  $M_C$  periods which includes less earthquakes but introduces less noise. The single corner model often results in a smaller magnitude range than a multi-corner model. However, because there is only one corner, it is less affected by noise introduced through subjective choices in models with multiple  $M_C$ -period corners.

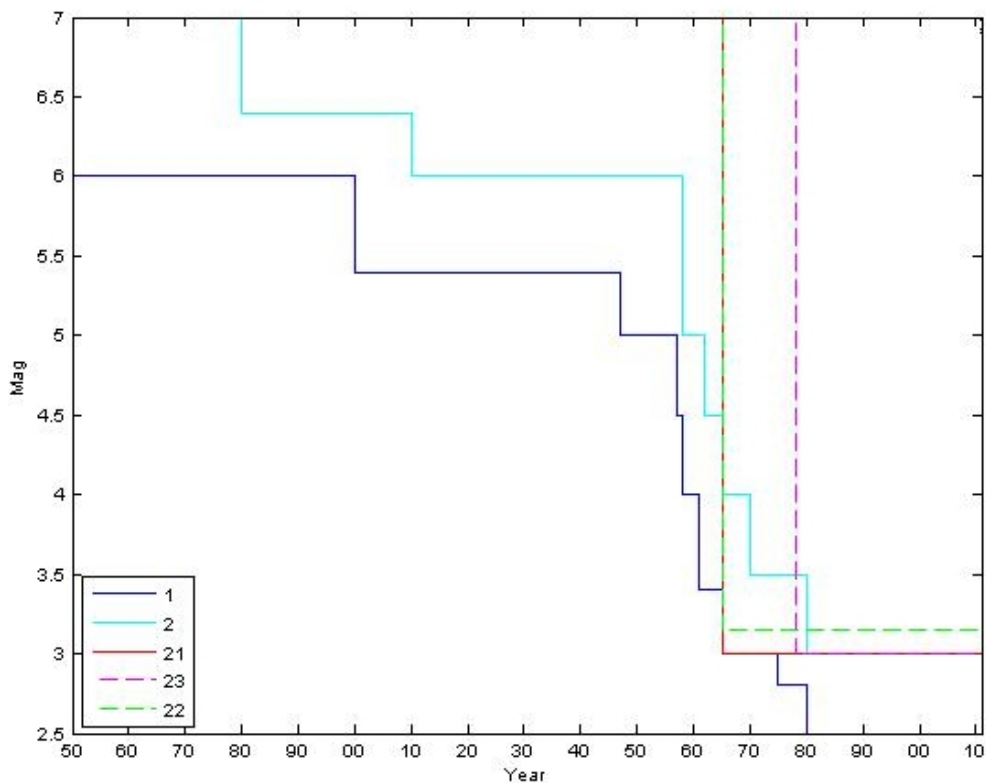


**Figure 24:** The magnitude of completeness models used. Models 1 and 21 applied to most of southern Australia (SW WA, Flinders and Mt Lofty Ranges and SE Australia), with models 2 and 23 applying to northern and central Australia. Model 22 is applied only in SE NSW.

Appendix E provides the details of the method used to calculate and select  $M_C$  models based on that of Leonard (2008). Initially a single corner and a multi corner model was developed for each of the 14 source zones (Leonard *et al.*, 2011) used in the draft hazard map (Burbidge and Leonard, 2011). This updated map utilises 16 multi corner source zone completeness models which fall into two clusters. The first cluster covered most of southern Australia; that is SW WA, Flinders and Mount Lofty Ranges and SE Australia, where felt records provide reasonable coverage of larger earthquakes since the mid 1800s and for which local networks were installed from the early 1960’s. The second cluster includes much of northern and central Australia where the pre-instrumental record is very incomplete and local seismic stations were not installed until the 1970s or even the 1980s. This resulted in two multi corner magnitude of completeness models being defined for these areas. These models are listed in Figure 24 and Table 4 as models 1 and 2 respectively.

Similarly the majority of the 16 single corner models fell into two clusters which were also merged into two  $M_C$  models. A third model was required to cover the Canberra and Snowy Mountains region (Zone 8 in Figure 12). These models are listed in Figure 24 and Table 4 as models 21, 23 and 22 respectively.

For each zone,  $a$  and  $b$  values were calculated using both the single and multi corner model appropriate for that area using both ls2 and ml0. To incorporate the multi corner model, the magnitude-frequency data must be scaled to a single time-magnitude volume. For the ls0 and ls2 methods this was achieved by scaling the number of earthquakes by the appropriate completeness period. For ml0, the method was applied to a synthetic catalogue with a single time-magnitude corner (e.g. 1900 and  $M$  3.0). Finally, each zone was allocated either a single corner or multi corner model as its preferred model based on which one produced the best linearity of the recurrence model, measured by  $R^2$ .

Table 4: Magnitude completeness models shown in Figure 24.

MODEL	1		2		21		22		23	
	YEAR	$M$	YEAR	$M$	YEAR	$M$	YEAR	$M$	YEAR	$M$
	1840	6.0	1880	6.4	1965	3.0	1965	3.15	1978	3.0
	1900	5.4	1910	6.0						
	1947	5.0	1958	5.0						
	1957	4.5	1962	4.5						
	1958	4.0	1965	4.0						
	1961	3.4	1970	3.5						
	1965	3.0	1980	3.0						
	1975	2.8								
	1980	2.5								

### 4.3 MAXIMUM MAGNITUDE

Probabilistic Seismic Hazard Analyses (PSHAs) require an estimate of  $M_{max}$ , the magnitude of the largest earthquake that is thought possible within a specified area. PSHA results are sensitive to the choice of  $M_{max}$ . For example, reducing  $M_{max}$  from 7.5 to 7.0 reduces the 500 year, PGA hazard by about 5% for the simple test case shown in Section 6.4.1.

Earthquake catalogues are usually not long enough to capture the largest possible earthquake for an area, even in very active areas like subduction zones (e.g. both the 2011 Japanese and 2004 Andaman earthquakes were larger than any earthquake observed during the historic or instrumental era). Generally  $M_{max}$  must be estimated indirectly instead. Indirect estimation methods are many, their results vary widely, and opinions differ as to which methods are valid (Wheeler, 2009a,b). Here we use three methods based on some statistical analysis of fault scarps from the handful (7) earthquakes that have produced fault scarps over the last 35 years plus 300 suspected paleoseismology features that have been preserved in the landscape (Clark *et al.* 2011, 2012)."

Clark *et al.* (2011, 2012) propose six 'neotectonic domains' spanning continental Australia based on approximately 300 neotectonic features (mainly Quaternary faults with surface expression). A seventh, entirely offshore domain is proposed based upon analogue studies with the central and eastern USA (Wheeler, 1995, 1996, 2009; Wheeler and Frankel, 2000). Each domain contains 'neotectonic faults' (i.e. those which have hosted deformation under the current Australian crustal stress regime – Clark *et al.* 2011, 2012) which, it is contended, share common recurrence and behavioural characteristics for large earthquakes. The neotectonic domains and known or suspected scarps generated by surface-rupturing earthquakes are shown in Figure 25.

In their analysis Leonard and Clark (2010) utilised the highest quality subset of the scarp data, restricting their analysis to the SW corner of WA where both an excellent DEM was available and the geographic and climatological factors favoured scarp preservation and scarp discoverability. The quality of the data subset they used enabled them to analyse the data in the confidence that the results were not likely to be distorted significantly by catalogue problems. Elsewhere this is not possible. For example, their cratonic source area was the Yilgarn Craton, but this is only one of five areas making up the Clark *et al.* (2011, 2012) neotectonic Domain 1 (Figure 25). The scarp data for Domain 1 includes scarps distant from the Yilgarn, such as Tennant Creek, which encompasses a wide range of surface geology, climatological factors and DEMs. This complicates the analysis of the scarp data not analysed by Leonard and Clark (2010).

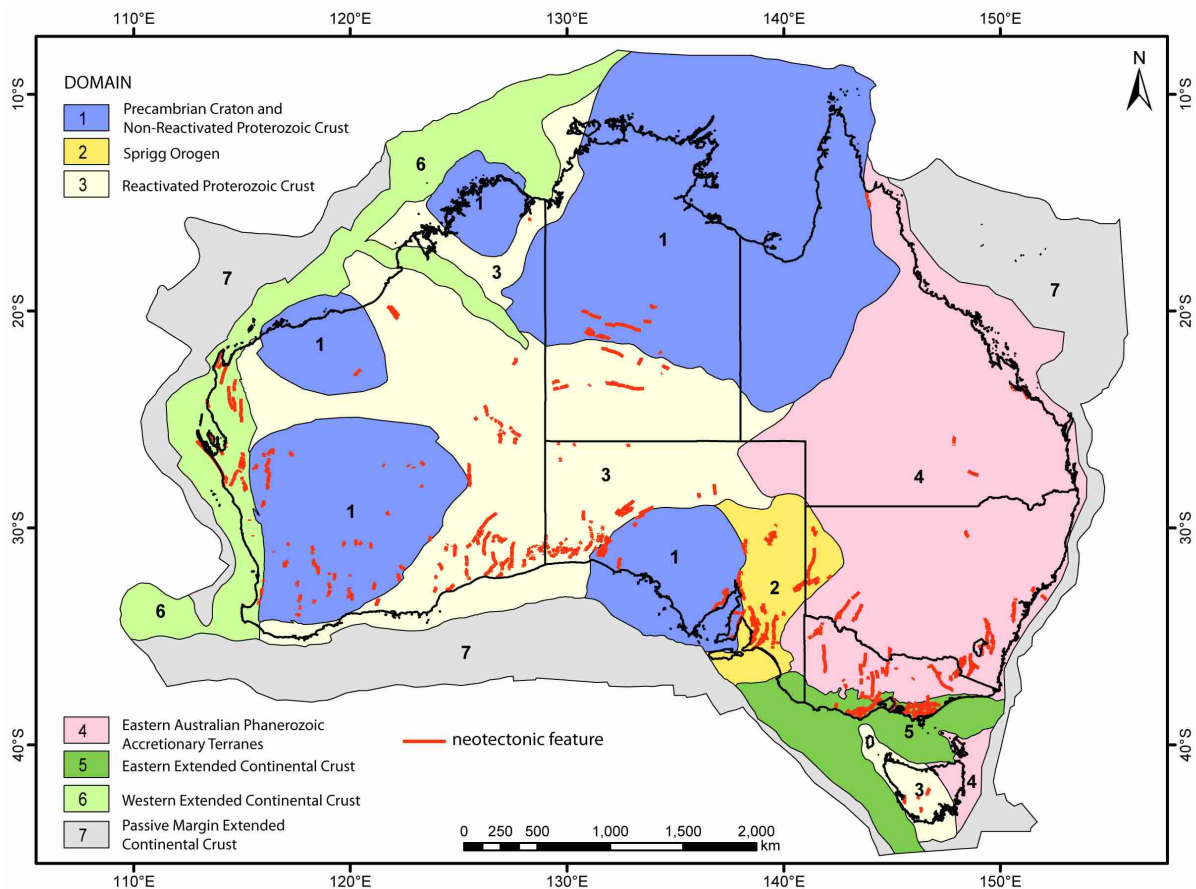


**Figure 25:** Neotectonic domains map of the Australian continent (Clark et al. 2011). Red lines represent suspected or known neotectonic features (primarily fault scarps) recorded in the Geoscience Australia Neotectonic Features Database.

In converting the scarps into an equivalent earthquake catalogue there are four primary problems. Firstly, the small to moderate earthquakes are under represented in the fault scarp data. This lower magnitude cut-off varies between domains, with lengths of 20 to 60 km ( $M$  6.5-7.3) being reasonable minimum lengths (magnitudes) of completeness across the domains. Secondly, longer scarps, as they are both preserved for longer periods and more easily identified, are statistically over-represented. Thirdly, the properties of the earthquakes appear to vary between domains. For example in the Yilgarn Craton, there appear to be many scarps over which the largest earthquakes are evenly spread, whereas in SE Australia there appear to be fewer scarps, but with higher displacements representing the largest earthquakes. This affects both discoverability and the statistics of the resulting database. Finally, all domains show some evidence of a statistical tail of very long scarps, with four of the domains having scarp features with lengths over 165 km. In the absence of field work confirming that these very long scarps have ruptured in a single earthquake we have assumed that these consist of two or more individual scarps and excluded them in our  $M_{max}$  analysis. However, where to draw the cut-off is subjective and varies from domain to domain. There appears to be no simple fixed criteria. Furthermore, the fault length needs to be converted to a magnitude using one or more conversion equations between magnitude and surface rupture length.

In analysing the scarp data to estimate  $M_{max}$ , each of the aforementioned problems requires assumptions to be made, and these assumptions will likely lead to different results. We have analysed the scarp data using three different techniques and in each of these techniques different assumptions are made. Problems one and two are relatively easily accounted for and it was found that the  $M_{max}$  results are not particularly sensitive to the assumptions used to account for them. Problems three and four are the most difficult to account for. The  $M_{max}$  results are most sensitive to solving the fourth problem – identifying the cut-off length for the tail of very long scarps.

All Domains contain very long scarps. The evidence for excluding these large scarps is primarily twofold. Firstly, using the scaling relations of Leonard (2010a), a fault of length 165 km would have a width of 40 km, an average displacement of 6 m and be created by a  $M$  8.0 earthquake. For a fault dipping at  $40^\circ$ , a width of 40 km requires rupture down to at least 26 km which is not consistent with our knowledge of the brittle seismogenic crust (Collins *et al.*, 2003). Secondly, the statistical analysis (see Section 4.3.1) suggests that scarps with lengths 90 km or more are statistically over-represented in many domains, relative to the smaller scarps, in all domains, except perhaps in D5. This over-representation of very long scarps, which are potentially formed by  $M \geq 7.8$  earthquakes, cannot be easily explained by arguments of longer preservation ages or higher discoverability. They are more readily accounted for by being formed by multiple smaller (e.g.  $M \leq 7.3$ ) earthquakes. We have applied three techniques - curve fitting (CF), trough or plateau (TP), and cumulative length statistics (CL) - to derive  $M_{max}$  in each of the six onshore domains.

Whilst the scaling relation to convert surface rupture length to magnitude is inherently uncertain (Leonard, 2010a), the final magnitude is only moderately sensitive to the relation used. Leonard (2010a) developed a set of self consistent relations for both plate boundary and SCR earthquakes, which used the relatively well constrained plate boundary results to guide the SCR relations. Wells and Coppersmith (1994) developed scaling relations for plate boundary areas only. Johnston (1994b) developed scaling relations for SCR areas only, but had only 10 earthquakes to constrain the relations. Despite the differences in base data and/or analysis techniques these relations give reasonably similar results. For example, for a scarp length of 62 km the three relations referred to above give magnitudes of 7.3, 7.2 and 7.1 respectively. In this analysis we use the Leonard (2010a) relations.

#### 4.3.1 Curve Fitting (CF)

This analysis technique requires two stages. The first is a technique for semi-automatically identifying the cut-off between scarps which have ruptured their entire length by a single earthquake and the longer scarps that require multiple earthquakes to rupture their entire length. The second fits a theoretical length-frequency distribution to the fault scarp data.

In Section 4.1 we proposed a set of algorithms that reduced the problems with both the Maximum Likelihood and Least Squares regression methods for calculating the Gutenberg-Richter recurrence parameters ( $a$  and  $b$ ) from an earthquake catalogue. The algorithm extracts a subset of the data which excludes the extreme events, which can significantly bias the recurrence parameters. A similar process is proposed for analysing the scarp data. In this case the length data is binned into 5 km wide bins. Up until lengths close to the length of a  $M_{max}$  fault the number of faults decreases by about 30% for each 5 km increase in length. Therefore after a gap of 15 km between the bin centres (i.e. two bins missing) the expected number of scarps is 1/3 of the number observed before the data gap. Consequently, it would be statistically unlikely that the same underlying process that generated the scarps up to the data gap is the same as the process generating the scarps above the gap. We interpret the scarps above the gap as being formed by multiple rather than single earthquakes. Thus, the length up to the beginning of the second empty bin is considered the upper cut-off length and it is this subset of data, called the capped data that is used in this analysis. For example, in Domain 3 (Figure 26) the technique removes all scarps of length greater than 105 km. As with earthquake recurrence data, the cumulative scarp length data is less sensitive to statistical fluctuation than the incremental scarp length data, so is used in the curve fitting technique.

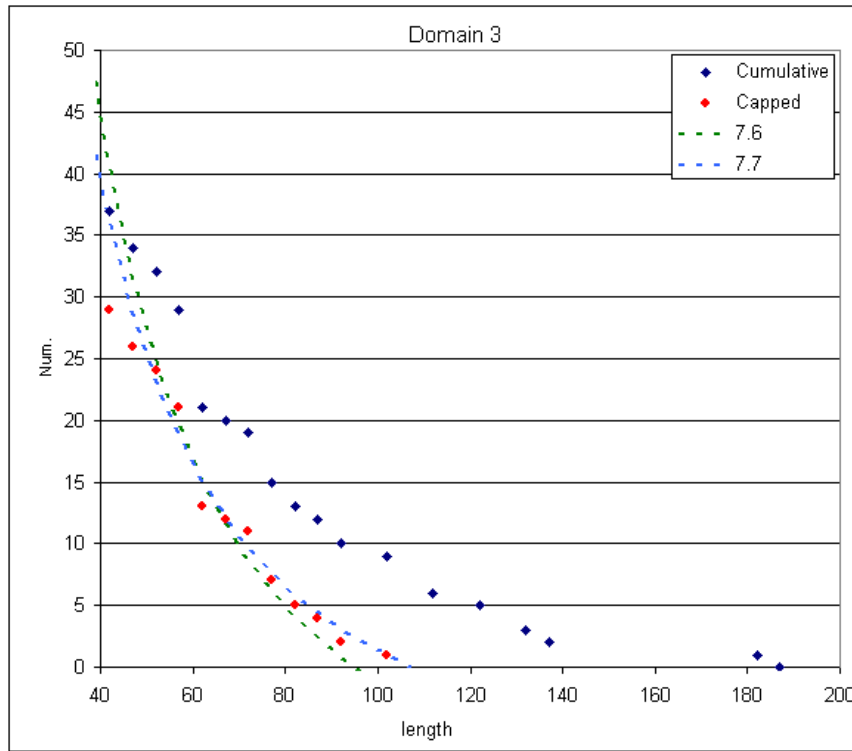


**Figure 26:** Length (km) vs. Cumulative Number data for the scarps in Domain 3. The blue diamonds are the full data set and the red diamonds are the capped data of lengths less than 105 km. The green and blue dashed lines are the theoretical expected distribution (Equation 7), scaled to fit the data between 50 and 80 km.

Equations 3 and 4 are the standard definitions of seismic moment and moment magnitude in SI units.

$$M_0 = \mu DLW \quad 3$$

where  $\mu$  is the rigidity modulus (we use a value of  $3.3 \times 10^{10} \text{ N/m}^2$ ),  $D$  is average fault displacement,  $L$  is average fault length and  $W$  is average fault width. Moment magnitude ( $M_W$ ) is as defined by Hanks and Kanamori (1979):

$$M_W = 2/3 \log M_0 - 6.07 \quad 4$$

Leonard (2010a) proposed the following equations to relate length to seismic moment

$$\log M_0 = 5/2 \log L + 3/2 \log C_1 + \log C_2 \mu \quad 5$$

where  $C_1$  and  $C_2$  are constants to be determined. With the resulting moment magnitude to length scaling relation being:

$$M_W = 1.667 \log L + 4.32 \quad 6$$

The usual Gutenberg-Richter relation, in its normal and exponential forms, is given by:

$$N(m) = 10^{(a-bm)} = N_0 10^{-bm} = N_0 \exp(-\beta m) \quad 7$$

where  $N_0$  is the cumulative number of events of  $m \geq 0$ ,  $a$  is the G-R a-value (i.e.  $a = \log N_0$ ),  $b$  is the G-R b-value (i.e.  $\log N = a - bm$ ) and  $b = \beta / \ln(10)$ . The exponentially truncated form of the Gutenberg-Richter (G-R) relation is given by:

$$N(m) = N_0 \exp(-\beta m) (1 - \exp[-\beta(M_{Max} - m)]) \quad 8$$

Equation 8 is the preferred form for probabilistic seismic hazard analysis and is the form used in this earthquake hazard map (Chapter 6). Substituting Equation 6 into Equation 8 and assuming  $m = M_W$  yields the exponentially truncated Gutenberg-Richter relation as a function of  $\beta$ ,  $M_{max}$  and fault length:

$$N(m) = N_0 \exp(-\beta(1.667 \log L + 4.32))(1 - \exp[-\beta(M_{max} - 1.667 \log L + 4.32)]) \quad 9$$

If all earthquakes above some minimum length produced a surface rupture, all scarps were preserved for an equal time and all scarps were equally discoverable, then the distribution of scarps should follow Equation 9. Clearly all three of these assumptions will not normally hold. However over a range of 0.4 magnitude units these criteria appear to approximately hold. For example the length, displacement and vertical offset for  $M$  7.0 and  $M$  7.4 earthquakes are 41 km, 1.9 m and 1.35 m, and 71 km, 3.0 m and 2.1 m, respectively, with there being 2.5 times as many  $M$  7.0 earthquakes as  $M$  7.4 earthquakes. Therefore, over a range of 0.4 magnitude units the recurrence decreases by a factor of 2.5, length increases by a factor of 1.75 and displacement increases by a factor of 1.56. For a change of 0.3 magnitude units the recurrence, length and displacement values change by factors of 2.0, 1.5 and 1.41 respectively. Over length ranges of this order the three criteria should approximately hold.

The proposed curve fitting (CF) technique attempts to fit Equation 9 to the capped scarp data, in a length range of a factor of at least 1.6 (e.g. 50 to 80 km) and is a direct extension of the technique of Leonard and Clark (2011). The variable  $b$  is set to 0.9 as this is a typical average for Australia (e.g. see Table 11) and multiple curves with varying  $M_{max}$  are calculated. These are fitted to the data by varying  $N_0$ . At shorter lengths the theoretical curve will be above the observed data – scarps do not form, are not preserved and difficult to discover. For the longer lengths the theoretical curve will often be below the observed data – scarps always form, are preserved for longer periods and are easily discovered. The theoretical curve is expected to fit the observed data for a range of lengths immediately below the length corresponding to a  $M_{max}$  earthquake.

The general scientific consensus is that  $M_{max}$  in intra-plate environments is in the range of  $M$ 7.0 to  $M$ 8.0 (Wheeler, 2009), with Leonard and Clark (2011) suggesting that the range is 7.1 to 7.8 for the crustal environments they studied. These magnitude ranges correspond to length ranges of 41 to 164 km and 54 to 123 km respectively. So, for example, in an area with a low  $M_{max}$  ( $M$  7.3) we might expect to fit the data in the range 25-50 km and in an area of high  $M_{max}$  ( $M$  7.6) the range would be 50-80 km.

For Domain 3 the maximum length of the capped data is 105 km. However, because the bins either side of the 105 km-bin are empty, a maximum length of 91 km could also be justified (Figure 26). These correspond to  $M$  7.68 and  $M$  7.59 respectively. Theoretical curves for  $M_{max}$  of  $M$  7.6 and 7.7 fit this data for lengths between 50 and 80 km (Figure 26); both curves having a good fit to the data. The  $M$  7.7 curve over predicts the number of scarps at all lengths greater than 70 km. The  $M$  7.6 curve matches the data between 50 and 80 km and slightly under-predicts the data above 80 km. As this curve is a closer match to the expected pattern,  $M$  7.6 is the preferred  $M_{max}$  for this data.

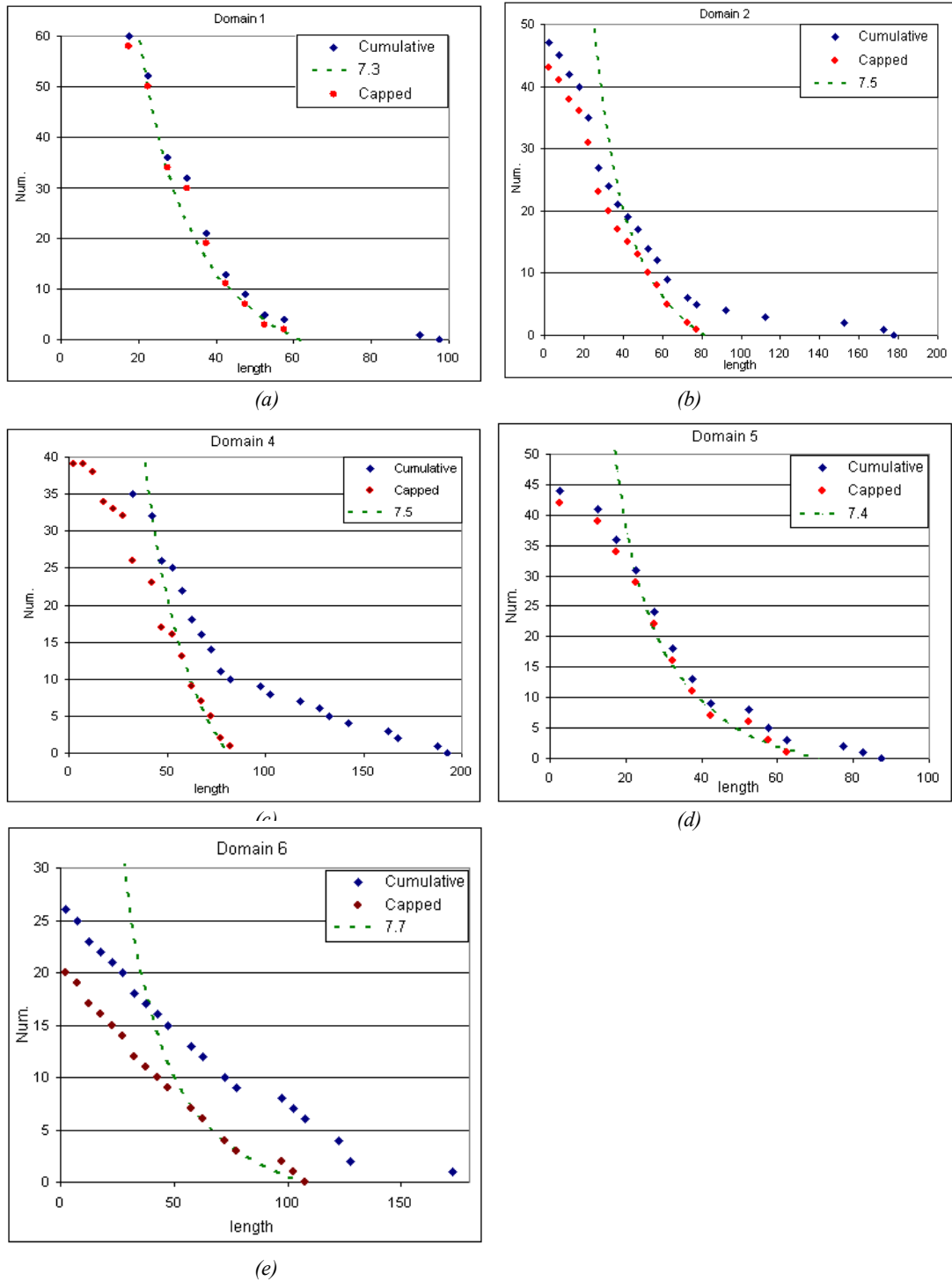


**Figure 27:** Scarp length data (km) versus cumulative number and the fitted curves for Domains 1, 2, 4, 5 and 6. The symbols are the same as in Figure 26.

The other domains have also been analysed using the same approach (Figure 27). For Domain 1 (Figure 27a) a  $M_{max}$  of  $M 7.3$  is a very good fit to the data and consistent with the result of Leonard and Clark (2010) who proposed  $M 7.25$  as  $M_{max}$  for the Yilgarn Craton subset of this data. For Domains 2 and 4, an  $M_{max}$  of  $7.5$  is a good fit to the capped data. Domain 5 is more complicated, with an  $M_{max}$  of  $7.4$  being a reasonable fit to the capped data. There is some geological evidence that there are two sets of faults, longer east-west faults and shorter more north-south oriented faults. Consequently, the  $M 7.4$  might be primarily fitting the north-south fault data. If the longer east-west faults are activated by a single earthquake, an

$M 7.6$  might be a better estimate of  $M_{max}$ . However, the data is inadequate to analyse them separately. For the moment we preserve the  $M 7.4$  value, but as discussed in Section 4.3.4, we round this up to  $M 7.5$  as our preferred  $M_{max}$  in this region. Domain 6 has a small number of scarps with only seven scarps of length greater than 50 km – equivalent to  $M 7.15$  – resulting in poorly constrained data. The curve with a  $M_{max}$  of  $M 7.7$  is a good fit to this limited data and is consistent with the results of Leonard and Clark (2011) who proposed an  $M_{max}$  of 7.65 for the faults in the extended crust in SW Australia. Table 5 summarises the results from this curve fitting technique.

Table 5:  $M_{max}$  estimates for the six domains using the curve fitting technique

	DOMAIN					
	D1	D2	D3	D4	D5	D6
Length (km)	62	81	93	81	71	107
Magnitude	7.30	7.50	7.60	7.50	7.40	7.70

### 4.3.2 Trough and Plateau (T&P)

The second method of estimating  $M_{max}$  discretizes the data into 10 km wide bins and identifies the trough or plateau in the incremental length data bins. The point where the number of scarps either begins to plateau or form a local minima is identified as the maximum length scarp for a single earthquake in the domain. The assumption underlying this method is that this length is a break in the physical characteristics of surface rupture length from a single event and is a likely indicator of  $M_{max}$ . The analysis was repeated twice, once for data starting at 0km and once for bins starting at 5km.

Figure 28 shows the incremental scarp length statistics for Domain 3. In this case the first identified break is at about 100 km, with the 5 km boundary having a break at 95 km. A scarp length of 95 km equates to an earthquake of  $M 7.61$  and this is considered the  $M_{max}$  for this domain. Table 6 summarises the results for the six domains.

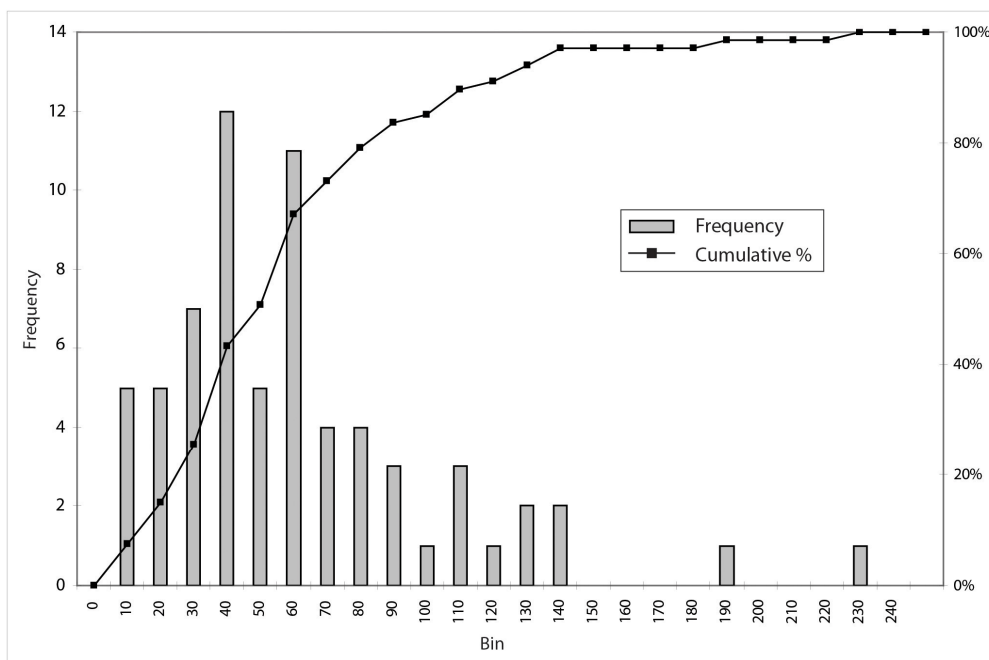


Figure 28: Histogram of the incremental and cumulative fault scarp length statistics for Domain 3 for 10 km bins.

**Table 6:** *M*<sub>max</sub> estimates for the six domains using the trough and plateau technique

	DOMAIN					
	D1	D2	D3	D4	D5	D6
Length (km)	60	80	95	90	80	95
Magnitude	7.28	7.49	7.61	7.57	7.49	7.61

### 4.3.3 Cumulative length statistics (CLS)

Figure 29 presents frequency histograms and cumulative frequency distributions for the fault scarp length data for each neotectonic domain referred to previously. This technique is based on the one described in Clark *et al* (2011). However, in this case data representing scarps less than 20 km in length are excluded in order to account for under-sampling. That is, scarps of 20 km or shorter will be under-represented in the catalogue as a result of reduced discoverability and/or preservation. With respect to the upper end cut-off, the data for most domains are better captured using a 95<sup>th</sup> percentile cut-off (e.g. Figure 29a,b,e,f). However, in regions with a greater spread of fault length values (e.g. Domains 3 and 4 – Figure 29c,d), the 75<sup>th</sup> or 85<sup>th</sup> percentiles values might better constrain the non-outlier data. These plots demonstrate that the arbitrary use of a given percentile cut-off value is not appropriate for all data sets. Accordingly, scarp length values for all three of the percentiles mentioned above are presented in Table 7.

Table 8 presents the weighting used to calculate the weighted average maximum scarp length in each domain. Weightings were chosen by expert judgement. Table 9 presents estimated earthquake magnitudes calculated from the scarp length using the empirical Leonard (2010a) relation. The results range from  $M_W$  7.0-7.8 ± 0.2. For individual domains, the difference in magnitude between the 75<sup>th</sup> and 95<sup>th</sup> percentile estimates is 0.1-0.5 magnitude units.

The 2012 Australian Earthquake Hazard Map

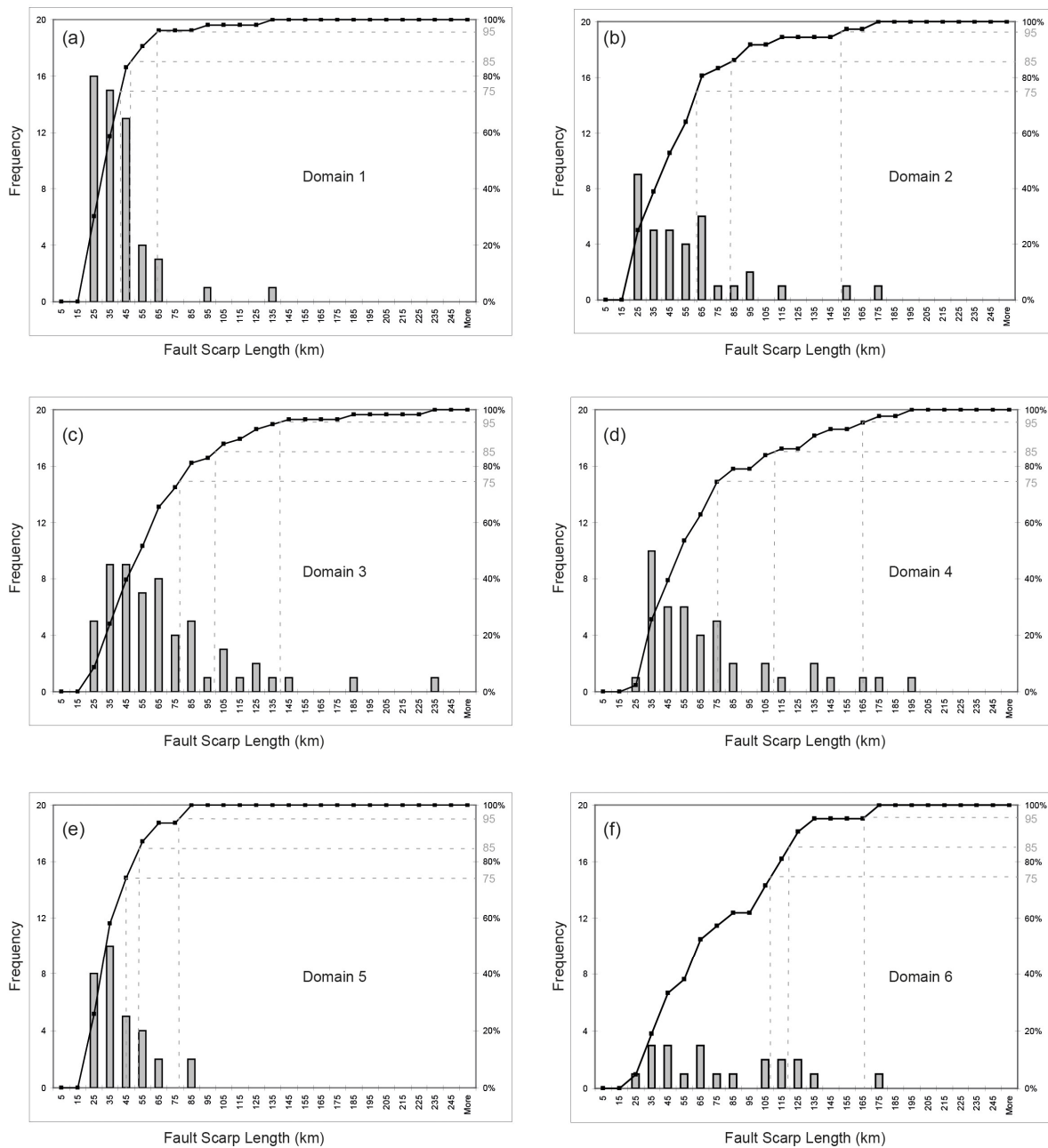


**Figure 29:** Cumulative statistics for fault length data from each of the Neotectonic domains defined by Clark et al. (2011). Data are truncated, so only scarps with lengths of  $\geq 20$  km are included. (a) Domain 1; (b) Domain 2; (c) Domain 3; (d) Domain 4; (e) Domain 5; (f) Domain 6. Refer to Figure 25 for map showing the distribution of the domains. Dashed grey lines assist in visualising the relevant percentile values.

**Table 7:** Maximum scarp length (km) estimates for the six domains using the length statistics technique

	DOMAIN						ALL DATA
	D1	D2	D3	D4	D5	D6	
n	53	36	58	43	31	21	242
median	32.0	44.0	55.0	55.0	32.4	61.5	43.0
75 <sup>th</sup> percentile	42.0	60.5	78.2	75.3	47.1	106.0	63.9
85 <sup>th</sup> percentile	48.2	77.5	103.5	111.4	54.0	123.3	84.5
95 <sup>th</sup> percentile	57.0	120.8	135.8	159.7	70.7	127.0	127.0
Weighted Avg.	55	69	97.	93	67	109.4	

**Table 8:** Weighting applied to each cumulative percentage cut-off maximum magnitude

	DOMAIN					
	D1	D2	D3	D4	D5	D6
75 <sup>th</sup> percentile	0.0	0.5	0.5	0.5	0.0	0.8
85 <sup>th</sup> percentile	0.2	0.5	0.3	0.5	0.2	0.2
95 <sup>th</sup> percentile	0.8	0.0	0.2	0.0	0.8	0.0

**Table 9:** Average characteristic magnitude (proxy  $M_{max}$ ) estimates based upon scarp length

	DOMAIN						ALL DATA
	D1	D2	D3	D4	D5	D6	
75 <sup>th</sup> percentile	7.0	7.3	7.45	7.45	7.1	7.7	7.3
85 <sup>th</sup> percentile	7.1	7.45	7.7	7.75	7.2	7.8	7.55
95 <sup>th</sup> percentile	7.25	7.8	7.85	8.0	7.4	7.8	7.8
Weighted Avg	7.22	7.38	7.63	7.6	7.36	7.72	

#### 4.3.4 Preferred value of $M_{max}$

Table 10 summarises the results for the three analysis methods. In the final weighting, the Curve Fitting method is given a weight of 0.5, the Trough and Plateau method a weight of 0.25 and the Cumulative Length statistics a weight of 0.25 chosen by expert judgement. The CLS  $M_{max}$  value is the weighted average given in Table 9. For Domains 1, 2, 4 and 6 the preferred value is the weighted average of CF, T&P and CLS, rounded to the nearest 0.1 magnitude units. For Domain 5 we have rounded up the value from 7.41 to 7.5. As discussed above, there is some uncertainty as to whether some of the larger faults should have been included in the analysis of this domain. Slightly rounding up the  $M_{max}$  captures some of this uncertainty.

For Domain 3 the weighted average for  $M_{max}$  is 7.6. However we have chosen to allocate an  $M_{max}$  of 7.5 to this domain. We have three reasons to justify this. First, the uncertainty in estimating  $M_{max}$  in most zones is at least  $\pm 0.2$ . Secondly, this simplifies the allocation of an  $M_{max}$  value to a zone as none cross these  $M_{max}$  boundaries. Finally, the difference in hazard between an  $M_{max}$  of 7.6 and 7.5 is insignificant at 10% in 50 years and minor at the 2% in 50 years probabilistic hazard level (Appendix F).

**Table 10:** The  $M_{max}$  values used in the hazard map calculation

	DOMAIN					
	D1	D2	D3	D4	D5	D6
Weighted	7.28	7.47	7.61	7.54	7.41	7.68
Preferred	7.3	7.5	7.5	7.5	7.5	7.7

#### 4.4 SUMMARY OF RECURRENCE ESTIMATION

The most commonly used method (Maximum Likelihood) of estimating  $a$  and  $b$  was found to be unsatisfactory for many zones. This is due primarily to an inadequate knowledge of the variation in  $M_C$ , both spatially and temporally. The least squares method also has well known limitations for estimating  $a$  and  $b$ . A new method, which is a modification of least squares, was developed to overcome the limitation of these methods. This allowed the development of a reliable fully automatic method for calculating earthquake recurrence parameters for areal source zones in Australia.

Five  $M_C$  models, three with a single date-magnitude cut-off and two with multiple date-magnitude cut-offs were developed. With the single cut-off models, an overly optimistic  $M_C$  model results in the data rolling off at low magnitudes. With the multiple cut-off models, an overly optimistic  $M_C$  model results in steps in the magnitude frequency distribution. As both of these affect the estimation of  $a$  and  $b$ , a conservative approach was taken when estimating the cut-offs.

Table 11 to Table 13 provide a summary of the parameters used in the calculation of the seismic hazard for the Background, Regional and Hotspot layers respectively.

**Table 11:** Summary table of the recurrence parameters used for the background zones. Num is the number of earthquakes used in calculating  $a$  and  $b$ ,  $A_{3.5}$  is the number of earthquakes per 1,000 years per 10,000 km<sup>2</sup> of  $M \geq 3.5$ , similarly for  $A_{5.5}$  and  $A_{6.5}$ . Depth is the maximum depth of a rupture plane assumed for that zone, GMPM is a model of the Ground Motion Prediction Equation suite used in each region – see Table 16 for details. Lat and Lon is the centroid of the zone

NUM	NAME	$A_{3.5}$	$b$	$M_{max}$	DEPTH (KM)	GMPM	AREA (KM <sup>2</sup> )	LON	LAT	$A_{5.5}$	$A_{6.5}$
674	Craton	11.60	0.778	7.5	15	WCA	6427672	129	-23	0.3	0.05
24	Non_craton_tas	22.17	0.975	7.5	20	Eastern	160933	146	-41	0.2	0.03
579	Non_craton_main	22.17	0.975	7.5	20	Eastern	2643602	143	-31	0.2	0.03
349	Extended	11.20	0.740	7.7	20	Eastern	3409084	132	-29	0.4	0.07

**Table 12:** Summary table of the recurrence parameter used for the regional zones. Fields and units as per Table 11. For Craton, non-craton and Extended zones the recurrence rates are calculated from the seismicity which is the remainder of the background zone when the regional zones have been excised.

NUM	NAME	$A_{3.5}$	$b$	$M_{max}$	DEPTH (KM)	$M_c$	GMPM	AREA	LON	LAT	$A_{5.5}$	$A_{6.5}$
30	Zone1	21.90	0.955	7.5	20	21	Eastern	96586	145.6	-17.8	0.3	0.03
25	Zone2	10.26	0.781	7.5	20	23	Eastern	307293	149	-21.2	0.3	0.05
32	Zone3	35.69	0.740	7.5	20	23	Eastern	124230	152.3	-25.2	1.2	0.22
41	Zone4a	30.51	1.005	7.5	20	23	Eastern	121832	150.3	-29.1	0.3	0.03
70	Zone7	71.42	0.867	7.5	20	21	Eastern	86975	150.3	-33.1	1.3	0.18
343	Zone8	127.10	0.984	7.5	20	9	Eastern	70585	148.9	-34.8	1.4	0.14
62	Zone9	59.33	1.090	7.5	20	22	Eastern	105371	145.5	-35.8	0.4	0.03
85	Zone10	77.24	0.872	7.5	20	91	Eastern	50350	146.7	-37.1	1.4	0.19
190	Zone11	61.17	0.809	7.5	20	9	Eastern	146047	145.7	-38.5	1.5	0.23
24	Zone12	25.43	1.013	7.7	20	21	Eastern	62644	151.7	-33.6	0.2	0.02
92	Zone13	24.55	1.030	7.5	20	9	Eastern	118387	145.8	-41.8	0.2	0.02
18	Zone14	50.81	1.000	7.5	20	21	Eastern	34168	140.2	-37.8	0.5	0.05
84	Zone16	70.46	0.990	7.3	15	9	WCA	38322	136.3	-34.2	0.7	0.08
146	Zone17	158.76	1.043	7.5	20	7	Eastern	78534	138.6	-32.8	1.3	0.12
28	Zone18	34.59	1.000	7.5	15	23	WCA	67393	136.5	-28.6	0.3	0.03
72	Zone20	31.05	0.763	7.5	15	23	WCA	287922	129.9	-23	0.9	0.16
54	Zone22	35.19	0.731	7.5	15	5	WCA	239050	124.4	-29.6	1.2	0.23
281	Zone25	81.45	0.908	7.3	15	9	WCA	131596	117.4	-31.9	1.2	0.15
56	Zone29	33.89	0.688	7.5	15	7	WCA	189556	115.6	-24.4	1.4	0.29
82	Zone29e	29.48	0.813	7.7	15	7	WCA	267065	113.7	-25.3	0.7	0.11
80	Zone30	32.50	0.773	7.5	15	23	WCA	295995	121.1	-19.5	0.9	0.16
58	Zone30e	25.46	0.915	7.7	15	23	WCA	228003	120.2	-16.6	0.4	0.05
44	Zone31	30.32	0.866	7.5	15	23	WCA	158070	126.8	-18.1	0.6	0.08
192	Timor-Banda	7519	1.014	9.3	50	103	Eastern	599616	125.1	-8.0	72	6.8
188	New Guinea	6953	1.077	9.2	50	102	Eastern	346785	143.4	-6.3	49	4.2
107	Irian Jaya	8390	0.837	8.5	50	102	Eastern	67317	134.7	-4.6	178	26
179	Craton	2.92	0.778	7.5	15	7	WCA	5019767	129	-23	0.2	0.014
	Non craton	3.07	0.975	7.5	20	7	Eastern	1740979	146	-41	0.1	0.004
92	Extended	3.97	0.74	7.7	20	7	Eastern	2574570	143	-31	0.3	0.024

Table 13: Summary table of the recurrence parameter used for the Hotspots. Fields and units as per Table 11.

NUM	NAME	$A_{3.5}$	$b$	$M_{max}$	DEPTH (KM)	$M_c$	GMPM	AREA	LAT	LON	$A_{5.5}$
146	Burakin 4A	0.1972	0.952	5.8	10	26	WCA	1000	117.0	-30.5	24.60
21	Cadoux 4B	0.0964	1.000	6.3	10	25	WCA	1000	117.1	-30.8	9.64
19	Meckering 4C	0.1213	1.000	6.3	10	25	WCA	1000	117.0	-31.7	12.13
58	Bagdin 4Cc	0.0739	1.182	6.3	10	26	WCA	1000	116.9	-31.8	3.20
75	N Kellerberrin 4D	0.0492	1.085	5.8	10	26	WCA	1000	117.7	-31.5	3.33
141	Tampu 4E	0.1637	1.046	5.8	10	26	WCA	1000	117.8	-30.3	13.24
27	Datine 5	0.1560	1.000	6.3	10	25	WCA	7061	117.8	-33.5	2.21
21	S Boulder 6	0.1745	1.000	6.3	10	25	WCA	3135	121.4	-30.8	5.57
11	Dundas 7	0.0964	1.000	6.3	10	25	WCA	2180	122.3	-32.5	4.42
14	Rowlet Shoals 22	0.1386	1.000	6.5	10	25	Eastern	12551	118.9	-18.2	1.10
17	W of Broome 19	0.1963	1.000	6.3	10	25	WCA	28216	120.3	-16.7	0.70
9	NE of Broome 20	0.1648	1.000	6.5	10	25	Eastern	8723	122.4	-17.6	1.89
13	SE of Broome 16	0.2075	1.000	6.3	10	25	WCA	28220	122.8	-18.7	0.74
17	Marble Bar 23	0.1963	1.000	6.3	10	25	WCA	28223	120.2	-21.2	0.70
20	W Lake Mackay 2a	0.4353	1.000	6.3	10	25	WCA	3135	126.5	-21.9	13.89
9	E Lake Mackay 3	0.1213	1.000	6.3	10	25	WCA	5579	130.1	-23.4	2.17
212	Tennant Creek 15	2.5208	1.000	6.3	10	25	WCA	28218	133.8	-19.8	8.93
0	Mt Surprise 8	0.0000	1.000	6.5	10	25	WCA	3134	143.8	-18.2	0.00
6	E Goondiwindi 9	0.0551	1.000	6.5	10	25	Eastern	12547	149.0	-28.5	0.44
13	S Inverell 10	0.1239	1.000	6.5	10	25	Eastern	8717	151.2	-30.0	1.42
15	S Dubbo 24	0.0153	1.162	6.0	10	26	Eastern	3133	148.6	-32.4	0.23
11	S Cessnock 26	0.0765	1.000	6.5	10	25	Eastern	1390	151.3	-32.9	5.50
77	S Blue Mtns 27A	0.0687	1.393	6.0	10	26	Eastern	1000	150.3	-34.2	1.12
4	S Cowra 14b	0.0261	1.000	6.5	10	25	Eastern	1000	148.8	-34.0	2.61
13	S Wyalong 13	0.0765	1.000	6.5	10	25	Eastern	3133	147.3	-34.1	2.44
0	N Crookwell 14d	0.0000	1.000	6.5	10	25	Eastern	1000	149.1	-34.2	0.00
18	Boorowa 14c	0.1514	1.000	6.5	10	25	Eastern	1000	148.7	-34.3	15.14
10	W Gunning 14f	0.1213	1.000	6.5	10	25	Eastern	1000	149.2	-34.8	12.13
3	S Murrumbateman 14g	0.0275	1.000	6.5	10	25	Eastern	1000	149.0	-35.0	2.75
22	Pyramid Hill 11a	0.0324	1.000	6.5	10	26	Eastern	1000	144.2	-36.1	3.24
30	N Echuca 11b	0.0456	1.223	6.5	10	26	Eastern	1390	144.5	-35.7	1.17
1	Talbingo 28b	0.0055	1.000	6.5	10	25	Eastern	1000	148.3	-35.6	0.55
9	N Jindabyne 28a	0.0695	1.000	6.5	10	25	Eastern	2177	148.7	-36.3	3.19
3	Thomson 12a	0.0207	1.000	6.0	10	25	Eastern	1000	146.4	-37.8	2.07
59	S Morwell 12	0.7141	1.000	6.0	10	25	Eastern	12543	146.2	-38.5	5.69
15	Yeelanna 32c	0.1093	1.000	6.5	10	25	Eastern	3136	135.7	-34.2	3.49
12	N Cleve 32a	0.0547	1.000	6.5	10	25	Eastern	8721	136.6	-33.5	0.63
12	Spencer Gulf 32b	0.0257	1.000	6.0	10	26	Eastern	1000	136.9	-34.2	2.57
48	Wilpena 30a	0.2472	1.000	6.5	10	25	Eastern	5579	138.5	-31.5	4.43
44	Lyndhurst 31	0.0338	1.276	6.0	10	26	Eastern	5582	138.2	-30.4	0.17
17	Melrose 30b	0.1386	1.000	6.5	10	25	Eastern	1391	138.2	-32.8	9.96
30	E Crystal Brook 30c	0.1652	1.000	6.5	10	25	Eastern	5578	138.3	-33.4	2.96
9	Crafers 33	0.0437	1.000	6.5	10	25	Eastern	17078	138.6	-35.0	0.26

## 5. Ground-Motion Prediction Equations

*T. I. Allen*

### 5.1 INTRODUCTION

One of the key challenges in assessing earthquake hazard in Australia is in understanding the attenuation of ground-motion through the stable continental crust. There are now a handful of ground-motion prediction equations (GMPEs) that have been developed specifically to estimate ground-motions from Australian earthquakes. These GMPEs, in addition to models developed outside Australia in other regions, are considered here for use for the Australian Earthquake Hazard Map (Table 14).

Since we have little quality strong-motion data recorded within Australia to objectively weight GMPEs based on their performance relative to these data, semi-quantitative weightings were assigned based partially on the performance of the candidate models against recorded small-magnitude earthquake data and partially on professional judgement. Table 14 shows the candidate GMPEs and their specific conditions of use. The initial assessment of candidate models presented herein only uses data for earthquakes of moment magnitude ( $M_W$ ) 4.0 and greater. It should be noted that this minimum magnitude range is less than that prescribed by many of the models (see Table 14). However, it can be argued that GMPEs adequately calibrated at longer periods for large-magnitude earthquakes – periods that determine earthquake magnitude – should also be well-calibrated at lower magnitudes. Consequently, if properly calibrated, any response spectral models should still result in small residuals (observed minus predicted amplitudes) at longer periods for small earthquakes. The performance of GMPEs outside their prescribed magnitude range at short periods may not be expected to be as satisfactory because of source effects that might alter the high-frequency spectrum of the earthquake (e.g. magnitude-dependent stress drop).

The models evaluated are a combination of Australian-specific models and models from other stable continental regions (e.g. eastern North America), in addition to those from active tectonic regions. In the following section we compare candidate GMPEs against recorded data from both Western Australia and eastern Australia. The Australian earthquake loading standards call for ground-motion hazard to be computed on “rock”, which is defined as a site with a time-averaged shear wave velocity greater than 360 m/s (and less than 1,500 m/s) in the upper 30 m (i.e.,  $V_{S30}$ ). In evaluation of the candidate GMPEs, we assume a generic rock site to have a  $V_{S30}$  of 760 m/s, which is similar to average site conditions obtained from geotechnical studies at several seismograph stations across Australia (Collins *et al.*, 2006; Kayen *et al.*, 2010). Consequently, those GMPEs that include  $V_{S30}$  as a predictor variable are set to 760 m/s for the evaluation. The site condition of 760 m/s is often referred to as a “B/C” site based on the National Earthquake Hazard Reduction Program (NEHRP) classification scheme (Wills *et al.*, 2000; Building Seismic Safety Council, 2004). Other GMPEs that do not explicitly include  $V_{S30}$  as a predictor variable use their median prediction. Several of the eastern North American GMPEs (i.e., Atkinson and Boore, 1995; Toro *et al.*, 1997; Campbell, 2003) are developed for “hard rock” conditions with  $V_{S30} \geq 2,000$  m/s. As a consequence, these GMPEs are unlikely to be compatible with the preferred site conditions for the Australian earthquake loading standards (Standards Australia, 2007). The Somerville *et al.* (2009) and Allen (2012) GMPEs are both calibrated to  $V_{S30}$  values of 865 and 820 m/s, respectively. For the purposes of these analyses, we assume these default site conditions are approximately consistent with the “rock” site definition in the earthquake loading standard.

**Table 14:** Candidate GMPEs considered for use in the Australian earthquake hazard map.

REFERENCE	REGION	MAGNITUDE RANGE	DISTANCE RANGE (KM)	SITE CONDITION ( $V_{s30}$ IN M/S)
Gaull <i>et al.</i> (1990)	Southeastern Australia	$4.5 \leq M_L \leq 7.2$	$10 \leq R_{hyp} \leq 500$	-
Gaull <i>et al.</i> (1990)	Western Australia	$4.5 \leq M_L \leq 7.2$	$10 \leq R_{hyp} \leq 500$	-
Atkinson and Boore (1995)	Eastern North America	$4.0 \leq M_W \leq 7.25$	$10 \leq R_{hypo} \leq 500$	2,800
Toro <i>et al.</i> (1997)	Eastern North America (Midcontinent)	$5.0 \leq M_W \leq 8.0$	$1 \leq R_{JB} \leq 500$	2,800
Campbell (2003)	Eastern North America (Hybrid)	$5.0 \leq M_W \leq 8.2$	$1 \leq R_{JB} \leq 1000$	2,800
Atkinson and Boore (2006)	Eastern North America (Rock)	$4.0 \leq M_W \leq 8.0$	$1 \leq R_{rup} \leq 1000$	> 2,000
Atkinson and Boore (2006)	Eastern North America (BC Site)	$4.0 \leq M_W \leq 8.0$	$1 \leq R_{rup} \leq 1000$	760
Chiou and Youngs (2008)	Western North America (California)	$4.0 \leq M_W \leq 8.5$	$1 \leq R_{rup} \leq 200$	760
Liang <i>et al.</i> (2008)	Southwest Western Australia	$4.0 \leq M_L \leq 7.0$	$1 \leq R_{epi} \leq 200$	-
Somerville <i>et al.</i> (2009)	Yilgarn Craton	$5.0 \leq M_W \leq 7.5$	$1 \leq R_{JB} \leq 500$	865
Somerville <i>et al.</i> (2009)	Non-Cratonic Australia	$5.0 \leq M_W \leq 7.5$	$1 \leq R_{JB} \leq 500$	865
Pezeshk <i>et al.</i> (2011)	Eastern North America (Hybrid)	$5.0 \leq M_W \leq 8.0$	$1 \leq R_{rup} \leq 1000$	$\geq 2,000$
Allen (2012)	Southeastern Australia	$4.0 \leq M_W \leq 7.5$	$1 \leq R_{rup} \leq 400$	820

## 5.2 GMPE COMPARISONS WITH WESTERN AUSTRALIAN DATA

A dataset of 38 ground-motion records for earthquakes occurring in the Yilgarn Craton of Western Australia (cf. Zone 25 – Figure 12) were compiled. The records, mostly recorded on strong-motion instruments, are for magnitudes  $M_W$  4.1-4.6 at distances less than 200 km from their respective earthquake sources. The primary source of the data is from the 2001-02 Burakin earthquake sequence. As discussed in Allen *et al.* (2006) it is not certain whether the Burakin earthquake sequence can be considered as typical of earthquakes in the Yilgarn Craton. The swarm-like nature of the sequence and the likelihood that many of the earthquakes would have occurred on recently-ruptured surfaces resulted in anomalously low stress drops for these events relative to published estimates from other stable continental regions. Despite these uncertainties in the Burakin dataset, and in the absence of alternative data, they are still valuable for evaluating candidate GMPEs and should be expected to be characteristic of longer period ground-motions.

Figure 30 shows the median residuals of the geometric mean of the horizontal components ( $\pm 1\sigma$ ) across the full range of response spectral periods for 13 candidate GMPEs evaluated in the present study. The two sets of curves in each subplot represent median residuals for data recorded at hypocentral distances  $R_{hyp} \leq 80$  and  $\leq 200$  km, respectively. In our semi-objective assessment of weightings for the draft hazard map, the former set of curves were considered to be the most instructive, because these distance ranges generally represent the greatest contribution to ground-shaking hazard (e.g., Jones *et al.*, 2005). The distance of 80 km was chosen because it is approximately twice the crustal thickness, and therefore the distance range in which we expect the transition of direct body wave spreading to post-critically reflected waves (e.g., Burger *et al.*, 1987). The data considered herein are generally recorded at sample rates of 100 samples per second. Consequently, we can only compare response spectral periods at one-quarter the sample rate (i.e. 0.04 seconds) with any level of certainty owing to Nyquist frequency and aliasing effects.

As observed in Figure 30, many of the candidate GMPEs overestimate recorded ground-shaking across all periods of interest. The first Australian-specific attenuation models of Gaull *et al.* (1990), on which the present Australian hazard map is based, are compared to the data. Since Gaull *et al.* (1990) only produced

models for peak ground motions (i.e., PGA and PGV), we estimate spectral ordinates by using spectral shape factors from those recommended in Standards Australia (2007) anchored to the Gaull *et al.* (1990) PGA estimates. Of note in the comparison of Western Australian data, the Gaull *et al.* (1990) model for Western Australia appears to work very well at short periods of ground shaking. However, at longer periods, where the model is dependent on the Standards Australia (2007) spectral shape factors, it performs poorly. The Liang *et al.* (2008) GMPE developed for Western Australia also performs quite well at short periods, but appears to overestimate ground shaking at longer periods.

While there is no model that perfectly matches the Western Australian dataset in the near-source distance range, the GMPEs that appear to perform the best across all periods are Atkinson and Boore (2006; BC crust), Allen (2012) and Chiou and Youngs (2008). The general overestimation of ground-motion by commonly used stable continental region GMPEs (e.g. Toro *et al.*, 1997) is of particular concern because previous studies have indicated that the de-aggregated hazard (and risk) is largely due to moderate-magnitude earthquakes at small distance ranges (e.g. Jones *et al.*, 2005). Since the Western Australian earthquakes we evaluate here are within the magnitude range in which the dominant hazard is expressed from previous studies, the results in Figure 30 suggests that previous studies in Western Australia which relied on these GMPEs have overestimated the hazard and risk associated with moderate-magnitude earthquakes. The mean ( $\mu$ ) and standard deviation ( $\sigma$ ) of model residuals against western and central Australian data is given in Table 15.

### 5.3 GMPE COMPARISONS WITH EASTERN AUSTRALIAN DATA

We follow a similar analysis as above for the Eastern Australian dataset (Figure 31). Included in this dataset are ground-motion records that could be classified as occurring in both “non-cratonic” and “extended” crust (see Figure 11). Consequently, when referring to Eastern Australia, we assume that our assessment of candidate GMPEs applies equally across the non-cratonic and extended Australian crust. In total we aggregate 103 records across a range of  $M_w$  4.0-5.3 at distances less than 400 km. As above, we find that many of the GMPEs commonly considered for earthquake hazard analysis in stable continental regions appear to overestimate ground-motions recorded in eastern Australia for these moderate magnitude earthquakes. However, in the present analysis we note that both the hard rock and BC crustal models of Atkinson and Boore (2006) and Allen (2012) appear to have consistently low residuals across all period ranges against the eastern Australian data at distances less than 80 km. Both of these models use similar geometrical attenuation functions in the near source range, suggesting that the attenuation of longer period ground-motion in eastern Australia may be faster than assumed by models that assume theoretical body-wave spreading of  $1/R$ . It should be noted that the Allen (2012) GMPE was largely calibrated using the southeastern Australian dataset used to test the candidate GMPEs for use in the hazard map. The mean ( $\mu$ ) and standard deviation ( $\sigma$ ) of model residuals against eastern Australian data is given in Table 15.

The 2012 Australian Earthquake Hazard Map

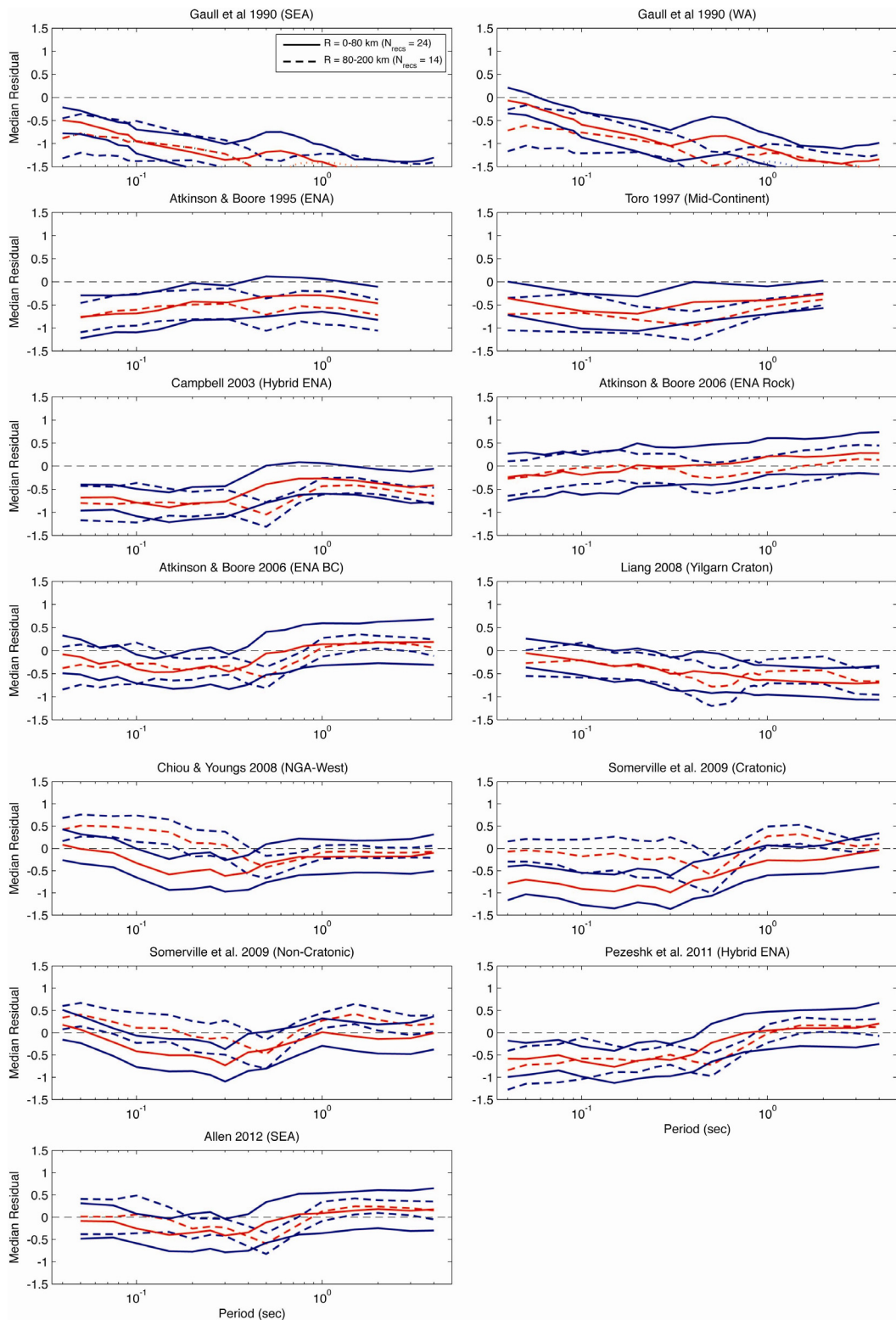


**Figure 30:** Residuals ( $\log_{10}$  observed  $- \log_{10}$  predicted) of 5% damped response spectral accelerations (in  $\text{cm/s}^2$ ) recorded from  $M_w \geq 4.0$  earthquakes in the Yilgarn Craton, Western Australia at distances less than 80 km (solid lines) and between 80 and 200 km (dashed lines), respectively. Median residuals (red lines) are plotted against spectral period with  $\pm 1\sigma$  indicated (blue lines). The response spectra evaluated are the geometric mean of the horizontal components. Earthquake magnitudes are converted back to  $M_L$  using the relations of Allen et al. (2011) for implementation in Gaull et al. (1990) and Liang et al. (2008). The Gaull et al. (1990) PGA models are combined with the spectral shape factors for rock sites as published in AS1170.4-2007 (Standards Australia, 2007).

**Table 15:** Mean ( $\mu$ ) and standard deviation ( $\sigma$ ) of near source ( $R \leq 80$  km) model residuals ( $\log_{10}$  observed –  $\log_{10}$  predicted) for combined periods of ground-motion against western and central, and eastern Australian ground-motion data.

REFERENCE	REGION	WESTERN & CENTRAL $\mu (\pm \sigma)$	EASTERN $\mu (\pm \sigma)$
Gaull <i>et al.</i> (1990)	Southeastern Australia	-1.25±0.34	-1.38±0.49
Gaull <i>et al.</i> (1990)	Western Australia	-0.91±0.32	-1.11±0.51
Atkinson and Boore (1995)	Eastern North America	-0.47±0.31	-0.55±0.49
Toro <i>et al.</i> (1997)	Eastern North America (Midcontinent)	-0.47±0.36	-0.68±0.48
Campbell (2003)	Eastern North America (Hybrid)	-0.55±0.33	-0.58±0.46
Atkinson and Boore (2006)	Eastern North America (Hard Rock)	-0.03±0.43	0.06±0.44
Atkinson and Boore (2006)	Eastern North America (BC Site)	-0.14±0.41	-0.04±0.45
Chiou and Youngs (2008)	Western North America (California/Global)	-0.28±0.37	-0.22±0.45
Liang <i>et al.</i> (2008)	Southwest Western Australia	-0.50±0.36	-0.83±0.47
Somerville <i>et al.</i> (2009)	Yilgarn Craton	-0.60±0.36	-0.68±0.47
Somerville <i>et al.</i> (2009)	Non-Cratonic Australia	-0.25±0.35	-0.39±0.44
Pezeshk <i>et al.</i> (2011)	Eastern North America (Hybrid)	-0.32±0.40	-0.22±0.44
Allen (2012)	Southeastern Australia	-0.07±0.41	0.10±0.45

#### 5.4 TREATMENT OF GROUND-MOTION UNCERTAINTIES

In the present analyses, the uncertainty in ground-motion is treated implicitly within the EQRM software platform used for the development of the 2012 Australian Earthquake Hazard Map. The ground-motion uncertainties captured in the present PSHA can be described through *aleatory variability* and *epistemic uncertainty*. The aleatory variability is considered to be the uncertainty associated with the inherent randomness of future events that cannot be reduced by the collection of additional information (Toro *et al.*, 1997). In practical terms, aleatory variability represents the scatter in data about a median model and is captured in GMPEs as the standard deviation of the logarithmic residuals, which generally conform to a normal distribution, or probability density function (Bommer and Abrahamson, 2006). In the EQRM, the aleatory variability is captured by randomly sampling respective probability density functions (PDFs) of each GMPE as described in Robinson *et al.* (2005).

The epistemic uncertainty is the uncertainty related to the lack of scientific knowledge and is generally captured in PSHA through the use of alternative models (Abrahamson and Bommer, 2005; Bommer and Scherbaum, 2008). In theory, epistemic uncertainty can be reduced to zero through the collection of additional information (Toro *et al.*, 1997; Al Atik *et al.*, 2010). For the development of the 2012 Australian Earthquake Hazard Map, the epistemic uncertainty is captured through logic-tree analysis, where each branch of the logic tree is assigned weights which reflect the relative confidence in the candidate GMPEs. The weights of the candidate models for the present study are discussed below.

The 2012 Australian Earthquake Hazard Map

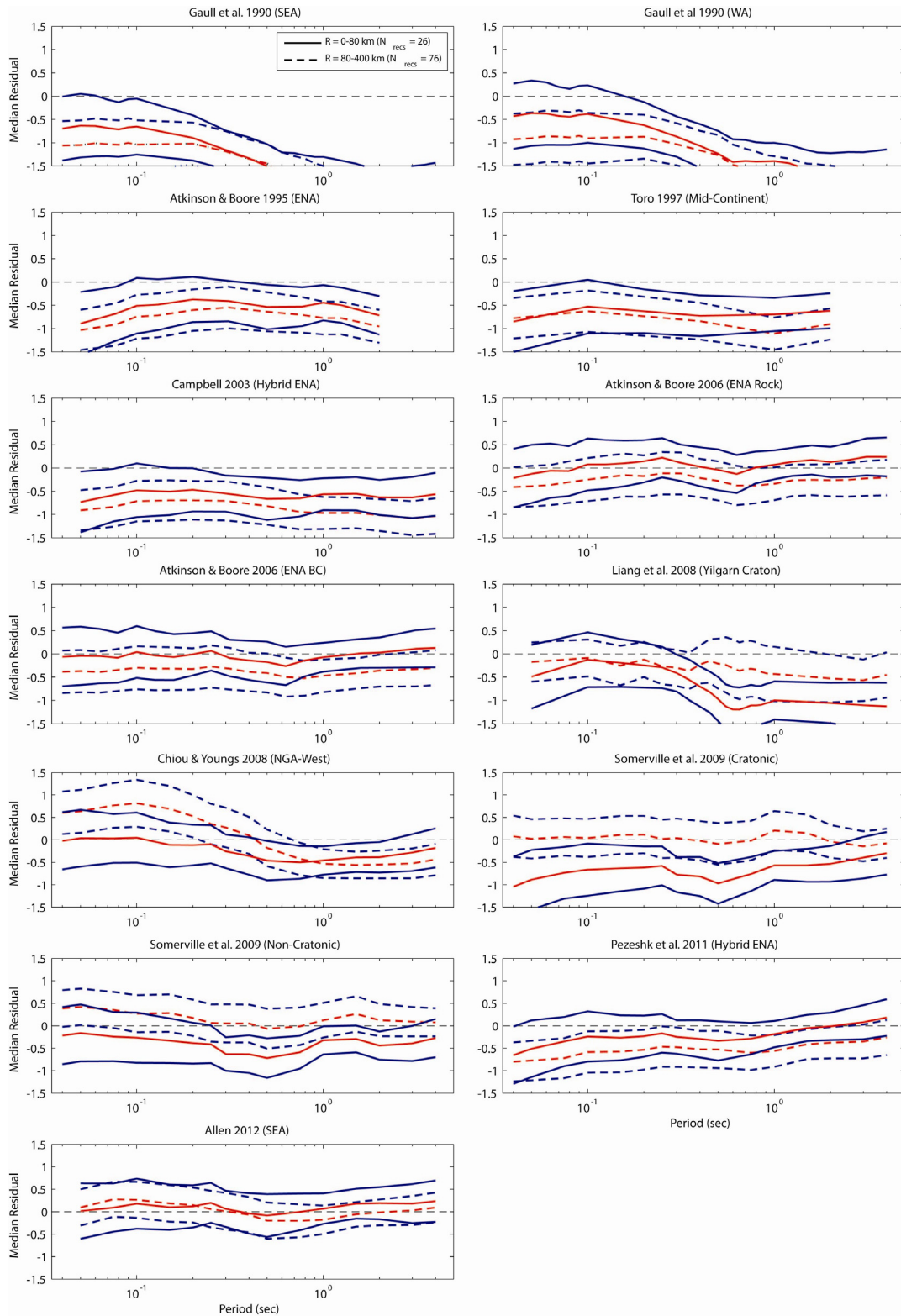


**Figure 31:** Residuals ( $\log_{10}$  observed  $- \log_{10}$  predicted) of 5% damped response spectral accelerations (in  $\text{cm/s}^2$ ) recorded from earthquakes in eastern Australia at distances less than 80 km (solid lines) and between 80 and 400 km (dashed lines), respectively. Median residuals (red lines) are plotted against spectral period with  $\pm 1\sigma$  indicated (blue lines). The response spectra evaluated are the geometric mean of the horizontal components. Earthquake magnitudes are converted back to  $M_L$  using the relations of Allen et al. (2011) for implementation in Gaull et al. (1990) and Liang et al. (2008). The Gaull et al. (1990) PGA models are combined with the spectral shape factors for rock sites as published in AS1170.4-2007 (Standards Australia, 2007).

## 5.5 FINAL GMPE WEIGHTINGS FOR THE 2012 HAZARD MAP

Ground-motion data recorded from earthquakes in Western Australia and eastern Australia have been compared to several candidate GMPEs currently being considered for use in the national hazard model update. As discussed, we assume that our assessment of candidate GMPEs for eastern Australia applies across the simplified non-cratonic and extended domains defined in [Section 3.2.3](#). We provide a semi-quantitative evaluation of various GMPEs based on simple residual analysis. In this analysis many of the models evaluated tend to overestimate ground motions across all periods of shaking. In particular, we find that the spectral shape factors tied to PGA, as recommended by Standards Australia (2007), overestimate ground-motions for moderate-sized earthquakes by over an order of magnitude at some periods. While the current Australian Standard specifies earthquake hazard as PGA, the spectral shape factor used to extend PGA predictions to other response spectral periods may be inappropriate relative to existing PGA hazard models and observed ground-motions.

The absence of ground-motion recordings from large-magnitude Australian earthquakes with which to validate GMPEs inevitably makes model selection subjective. In light of the aforementioned analysis, and following consultation with key stakeholders at the February 2012 hazard map workshop in Canberra, GMPE weightings were recommended by the Geoscience Australia authors and external experts. The GMPE weights used in the 2012 National Australian Earthquake Hazard Map are listed in [Table 16](#). Comparisons of the attenuation characteristics for each of the models listed in [Table 16](#) at pseudo response spectral periods of 0.0 (PGA), 0.2, 0.5 and 1.0 sec are shown for scenario  $M_W$  5.5 ([Figure 32](#)) and  $M_W$  6.5 ([Figure 33](#)) earthquakes, respectively.

**Table 16:** Ground-motion prediction equation weights used in the 2012 Australian Earthquake Hazard Map. The GMPE weights are applied for each region of Australia corresponding to the location of source zones with respect to the simplified domain boundaries outlined in [Figure 11](#): Western and Central Australia weights correspond to the “cratonic” zone; Eastern Australia weights corresponds to the “non-cratonic” zone; and the extended crust weights correspond to the “extended” zones.

REFERENCE	REGION	WESTERN & CENTRAL WEIGHTS	EASTERN WEIGHTS	EXTENDED CRUST WEIGHTS
Atkinson and Boore (2006)	Eastern North America (B/C Site)	0.3	0.25	0.25
Chiou and Youngs (2008)	Western North America California/Global	0.1	0.25	0.25
Somerville <i>et al.</i> (2009)	Yligam Craton	0.3	0.0	0.0
Somerville <i>et al.</i> (2009)	Non-Cratonic Australia	0.0	0.25	0.25
Allen (2012)	Southeastern Australia	0.3	0.25	0.25

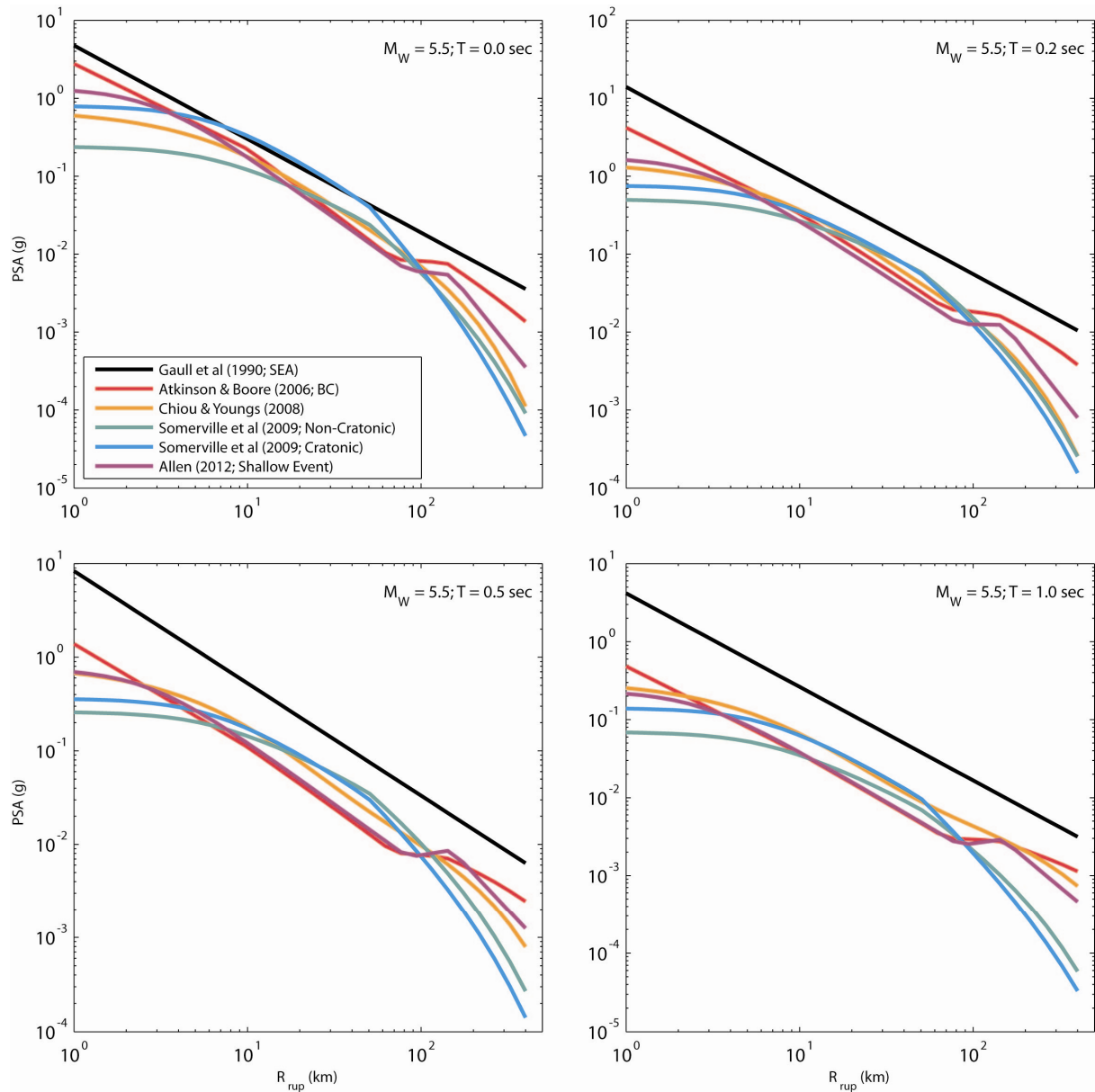


**Figure 32:** Comparison of the median horizontal 5% damped pseudo response spectra (PSA) for GMPEs used in the PSHA for the 2012 Australian Earthquake Hazard Map (see Table 16) for a scenario  $M_W$  5.5 earthquake plotted against  $R_{rup}$  for a series of response spectral periods. The model assumes a vertically dipping surface rupture such that the  $R_{rup}$  is equivalent to the Joyner-Boore distance used by the Somerville et al. (2009) GMPE. The Gaull et al. (1990) PGA attenuation relation for southeastern Australia is shown for comparison. This model is combined with the spectral shape factors for rock sites as published in Standards Australia (2007). The time-averaged shear-wave velocity in the upper 30 m ( $V_{S30}$ ) is set to 760 m/s for those models which explicitly use  $V_{S30}$  as an input parameter. The spectral values are represented as the geometric mean of horizontal component ground-motion.

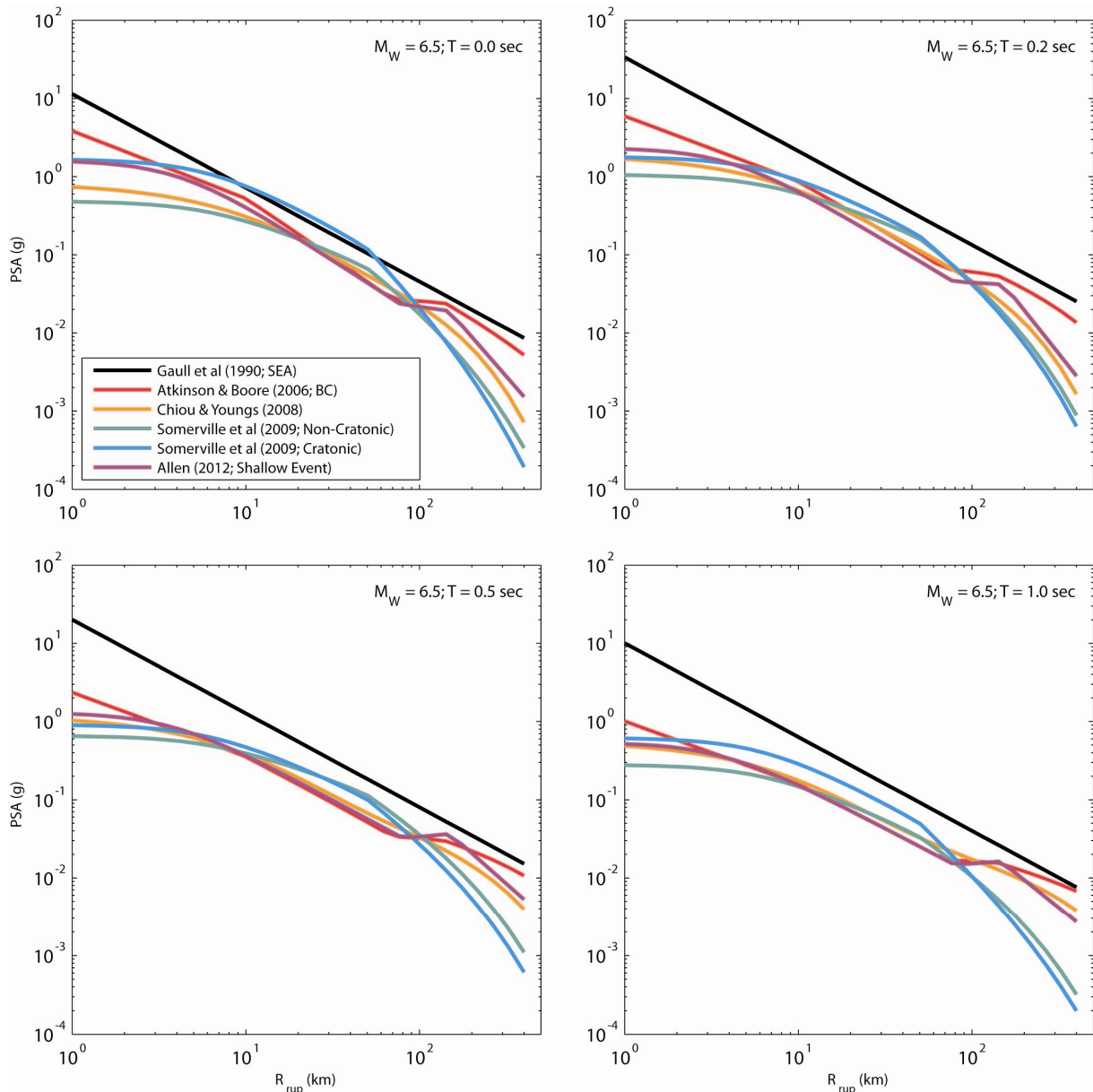


**Figure 33:** Comparison of the median horizontal 5% damped pseudo response spectra (PSA) for GMPEs used in the PSHA for the 2012 Australian Earthquake Hazard Map (see Table 16) for a scenario  $M_W$  6.5 earthquake plotted against  $R_{rup}$  for a series of response spectral periods. Please see Figure 32 caption for more detailed discussion on this figure. The spectral values are represented as the geometric mean of horizontal component ground-motion. See Figure 32 caption for a more detailed description of figure.

## 5.6 GMPEs FOR OFFSHORE ZONES

Despite the large distances between Australia and the active subduction zones near Timor-Leste and the Banda Sea, earthquakes from these sources are felt frequently across the northern extent of Australia (e.g. Hearn and Webb, 1984; Gaull and Kelsey, 1999). Consequently, it is prudent to consider the contribution for these earthquake sources in the national hazard model (Figure 19). Because the attenuation properties within the continental crust that separates the Australian mainland from the active subduction zone to the north is not well known, we must make several assumptions. Firstly, we assume that the attenuation behaviour of ground-motion between Australia and the areal offshore source zones is similar to that of eastern (non-cratonic) Australia. However, we expect that the contribution of hazard from these zones would be dominated by large-magnitude earthquakes (approximately  $M_W > 7.0$ ). These magnitudes

represent the upper threshold of those that are appropriate for the suite of GMPEs used for non-cratonic Australia (Table 14). It is expected that the magnitude-scaling function of the SCR-specific GMPEs (e.g. Atkinson and Boore, 2006; Somerville *et al.*, 2009; Allen, 2012) will perform poorly when extrapolated beyond defined magnitude range of a given GMPE. Comparing GMPEs developed for subduction zone earthquakes (e.g. Youngs *et al.*, 1997; Zhao *et al.*, 2006) for a theoretical  $M_w$  8.5 earthquake, we note that there is considerable variability in the magnitude scaling among these models (Figure 34). Indeed the variability of near source PGA values estimated by the non-cratonic suite of GMPEs (Table 16) do not appear to be considerably different to those from the subduction zone relations. Because of the apparent similarities at near-source distances and the assumption that the ground motion propagates through continental crust towards the Australian mainland, we preserve the use of the non-cratonic suite of GMPEs for the offshore source zones of Timor-Leste, Banda Sea and New Guinea. We note at distances around 500 km that there is considerable variability among the non-cratonic GMPEs. However, given the uncertainty surrounding the attenuation of ground-motion in this region, it is felt that this variability is necessary to capture the full epistemic uncertainty of hazard in northern Australia.

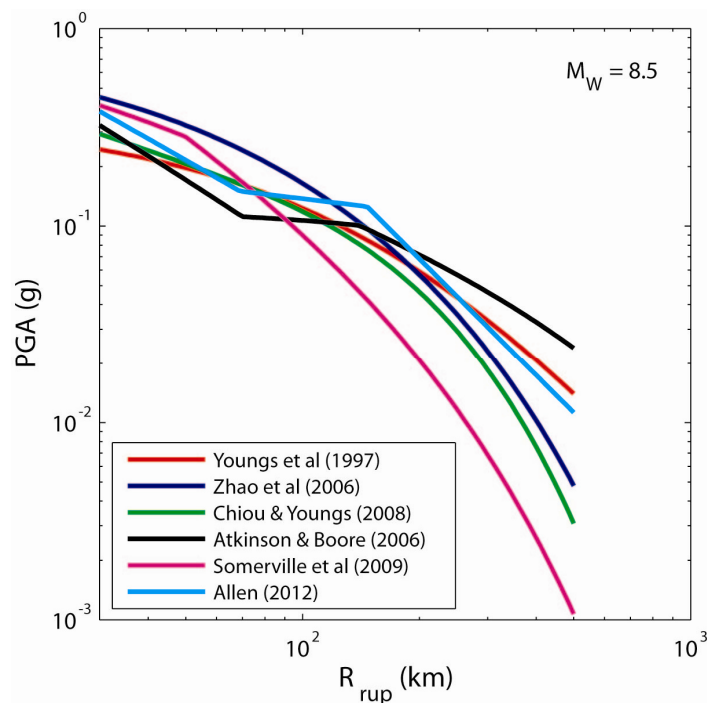


**Figure 34:** Comparison of the attenuation from subduction zone GMPEs (Youngs *et al.*, 1997; Zhao *et al.*, 2006) and those models used for eastern (non-cratonic) Australia (Table 16). The figure indicates the attenuation of peak ground acceleration for a  $M_w$  8.5 earthquake with a depth of 30 km. It is noted that ground-motions for several of the GMPEs here are extrapolated beyond the magnitude and distance ranges defined by their respective authors.

## 6. The 2012 Australian Earthquake Hazard Maps

*D. R. Burbidge, M. Leonard, D. Robinson and D. Gray*

The Australian earthquake hazard maps have been created using GA's open-source earthquake hazard and risk model, EQRM, which is available as a free download from <http://eqrm.sourceforge.net/>. The EQRM is an event-based hazard and risk code in which a "synthetic catalogue" of events is generated across the region of interest to calculate the hazard or risk (Robinson *et al.* 2006). This event-based approach differs from that of a traditional probabilistic seismic hazard assessment (PSHA), which integrates over all magnitude and distance combinations to obtain the hazard. The event-based approach has the advantage of being easy to extend to risk (i.e. loss) maps, but is much more computationally intensive. Further details regarding EQRM can be found in Robinson *et al.* (2005, 2006) or the documentation which accompanies the latest version of EQRM.

### 6.1 METHOD

The following steps are required in order to calculate a seismic hazard map from a synthetic catalogue of earthquakes (Robinson *et al.* 2006)

1. A synthetic earthquake catalogue is generated from an earthquake source (location and recurrence) model;
2. The level of ground shaking from each earthquake is propagated to the sites of interest using one or more attenuation models (also known as ground motion prediction equations - GMPEs);
3. The local regolith and its effect on ground shaking is then included using a site response model (if needed); and
4. The hazard is estimated by summing the probabilities of all events that exceed a particular ground motion for all the sites of interest.

Source location, magnitude and ground-motion variability are taken into consideration by randomly sampling their respective probability density functions (PDFs) as described in Robinson *et al.* (2005). The GMPEs used, and their respective weightings applied to represent the epistemic uncertainty in the choice of ground-motion model, are described in [Chapter 5](#).

Before conducting the assessment, a range of validation and model sensitivity tests were applied. These tests investigated the sensitivity of the results to, for example, the number of events in a source zone, and compared the EQRM results to two of the test cases of Thomas *et al.* (2011). The results of this validation study are described in [Appendix F](#).

For the hazard maps presented herein the following parameters/models were applied:

1. Finite rupture planes were formed for each earthquake with a dip restricted to 35° but with a free strike (i.e. they can be orientated in any direction). Between 1 and 17 million earthquakes were distributed randomly across all the zones of each map layer depending on the size of the area covered by the zones.
2. Dimensions of the rupture (i.e. length and width) for a given magnitude were taken from the Stable Continental Regions relations equations in Leonard (2010a).
3. The top edge of the rupture must be equal to, or deeper than, 0 km. The bottom edge of the rupture is limited to 15-20 km, depending on the zone (see [Table 11](#) and [Table 12](#)). The maximum rupture depth in the hotspots was limited to 10km ([Table 13](#)).
4. The minimum magnitude considered for each zone is 4.5. The maximum magnitude and recurrence model for each zone is described in [Section 4.3](#) and is given for each zone in the tables shown in [Section 4.4](#).

5. Revised magnitude ( $M$ ) values (Section 2.3; cf. Allen *et al.* 2011) were used to calculate the Gutenberg-Richter (G-R) values shown in this paper. The G-R values for the unrevised and moment magnitude versions of the catalogue were also calculated for comparison purposes but are not discussed here.
6. Ground motions were calculated out to a distance of 400-500 km for each earthquake depending on the map.
7. The hazard is represented as the geometric mean of horizontal component ground-motion.
8. The resulting probabilistic hazard maps were created at nineteen different return periods ranging from 100 to 10,000 years. The hazard values in these maps correspond to ground motions with (respectively) a 1/100 to 1/10,000 chance of being exceeded each year.
9. For each return period, the hazard values are calculated at response spectral accelerations (RSA) at periods of 0.0 to 1.0 s at intervals of 0.1s (a total of eleven different RSA periods). The 0.0 s map is also known as the “peak ground acceleration” hazard map.
10. No site amplification due to local site conditions was applied to ensure it is consistent with the current map in AS1170.4. Similarly, the resulting seismic risk (i.e. the losses) from the hazard has not been calculated.

The Extensible Markup Language (xml) files used by EQRM for each of the layers can be provided by the authors on request. These contain the detailed polygons, Gutenberg-Richter  $a$  and  $b$  values and other hazard parameters used in creating event sets and hazard maps. The event sets created by EQRM for the layers are also available on request but is a much larger dataset.

To calculate the hazard, up to 17 million earthquakes (depending on the layer) are generated synthetically and the ground motions are calculated for a set of 48,000 regularly spaced points across the continent of Australia for each earthquake. The points are arranged in a grid with a 0.15 degree spacing. The ground motions at each point are then used to calculate the hazard at the various RSA periods required. Thus, for each of the 48,000 locations across Australia, we generate hundreds of different hazard values corresponding to different combinations of RSA period and return period for each layer. Other return period and RSA period combinations could also be calculated in the future without great difficulty if required. Due to limited space, not all these combinations of RSA and return period hazard maps can be presented in this document. Instead, a limited selection is presented here and additional maps can be provided on request.

The hazard data is saved as a series of GMT (Generic Mapping Tools - <http://gmt.soest.hawaii.edu/>) compatible NetCDF files. Standard GMT tools can then be used for post-processing. For example, the maximum of the various layers can be found using “grdmath” and the data was smoothed with “grdfilter”. The data for the hazard curves was found by interpolating the NetCDF files using “grdtrack” to the longitude and latitude of the centre of the specified city. GMT tools (“grdimage”, “grdview” and “grdcontour”) were also used to generate maps to visualise the hazard values shown in the next section. The exact bash scripts used with the specific GMT commands chosen can be provided by sending a request to the authors.

## 6.2 RESULTS

As described in Section 3.2 (cf. Leonard *et al.* 2011), this hazard assessment consists of a number of layers. In this section we present a range of different hazard maps for different layers, return periods and RSA periods, and show how these could be combined into a final hazard map. Each hazard map can also be convolved with a 2D Gaussian function with a specified width. This has two effects:

1. The small detail in the maps which are smaller than the Gaussian width are removed. This reduces numerical noise, produces a smoother final map and reduces the level of detail;

2. The Gaussian function can be interpreted as approximately representing the spatial uncertainty in the hazard (e.g. due to the imprecise location of the zone boundaries). The Gaussian width is six times the standard deviation. This means that convolving the hazard map with a 240 km width Gaussian function also implies that aspects such as the zone boundaries have an effective spatial uncertainty of +/- 40 km at one standard deviation.

The smoothing has the effect of softening the hard edges produced by source zone based hazard maps. The effect is similar to weighting a large number of alternative zonation hazard maps where the boundary location and weights vary spatially ([Appendix F, Section 12.7](#)). The AS1170.4 map was also smoothed for similar reasons (i.e. to represent the spatial uncertainty to zone boundaries) as documented by McCue (1993).

The final map can also be smoothed with a Gaussian function or other shaped filter, but in this case this is purely to reduce the complexity of the final map (e.g. to reduce the number of steep contours or very complicated contours). There is no “correct” or “incorrect” amount of this type of smoothing. It depends purely on how smooth the final map should be for a particular application. For some applications, such as use in a building code, reasonably strong smoothing is appropriate since this eases implementation in a national code. For other uses, such as possible use in the insurance industry, no smoothing may be more appropriate (*K. Campbell, pers comm*).

### 6.2.1 Background Source Zones Only

[Figure 35](#) shows the 500 year, PGA (i.e. 0.0 s RSA period) hazard for the background zones only. The parameters of each source zone are summarised in [Section 4.4](#). A 240 km wide Gaussian spatial filter was used to smooth the map. The 500 year map shows the ground motions which have about a 10% chance of being exceeded in 50 years. All the main shocks in the Australian part of the earthquake catalogue have been used to generate this hazard. In other words, this is the hazard from the entire catalogue if the earthquakes were spread evenly over the cratonic, non-cratonic and extended geologic domains of Australia instead of being concentrated in a few areas.

The 0.0 s RSA period (PGA) hazard in this map is everywhere low (i.e.  $< 0.02$  g), but is very slightly higher in the cratonic (e.g. 0.017 g) and extended (e.g. 0.015 g) parts of Australia (approximately west of the Tasman Line) than in the non-cratonic (eastern and extended) areas (e.g. 0.014 g) of Australia. This is due to a combination of higher rate of earthquake occurrence and lower attenuation in the cratonic parts of Australia (see [Chapter 5](#); cf. Allen *et al.* 2011). However, this difference is very small and only a small change in the input parameters can make the hazard in the zones identical. Hazard in the extended regions happens to be about the same as in the Eastern non-Cratonic regions for this particular RSA and return period (for the boundaries of these regions see [Figure 11](#)). Again, it would be very sensitive to minor changes in the input parameters.

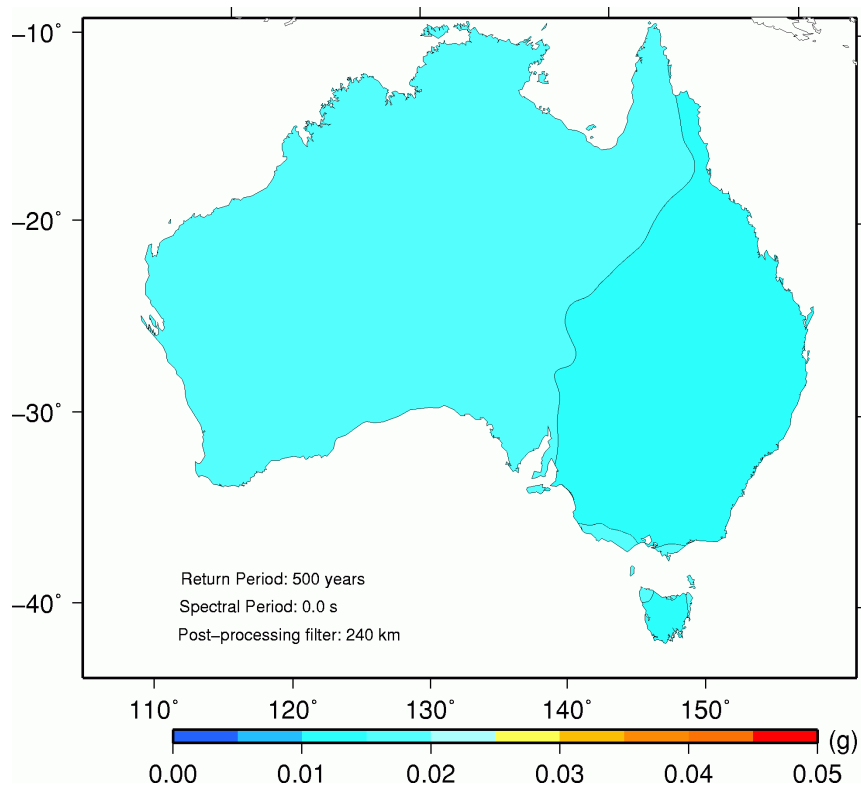


**Figure 35:** The 500 year return period Background zone PGA (0.0 s RSA period) hazard map smoothed with a 300 km Gaussian spatial filter. The recurrence parameters are those described in [Table 11](#). Note different scale than used in most figures below.

### 6.2.2 Regional Source Zones Only

[Figure 36](#) shows the 500 year, 0.0 s RSA (PGA) hazard for the Regional zones only, smoothed with a 60 km width Gaussian filter. The parameters of each source zone are also summarised in [Section 4.4](#) and [Table 12](#). The zones in Timor and PNG were not included, nor were earthquakes outside the Regional zones in the Background areas. The filter chosen here is narrow (60km) to allow comparison with the wider filters used below. Hazard in the Regional zones is generally similar, although those in Western Australia are slightly higher than those in the east of Australia.

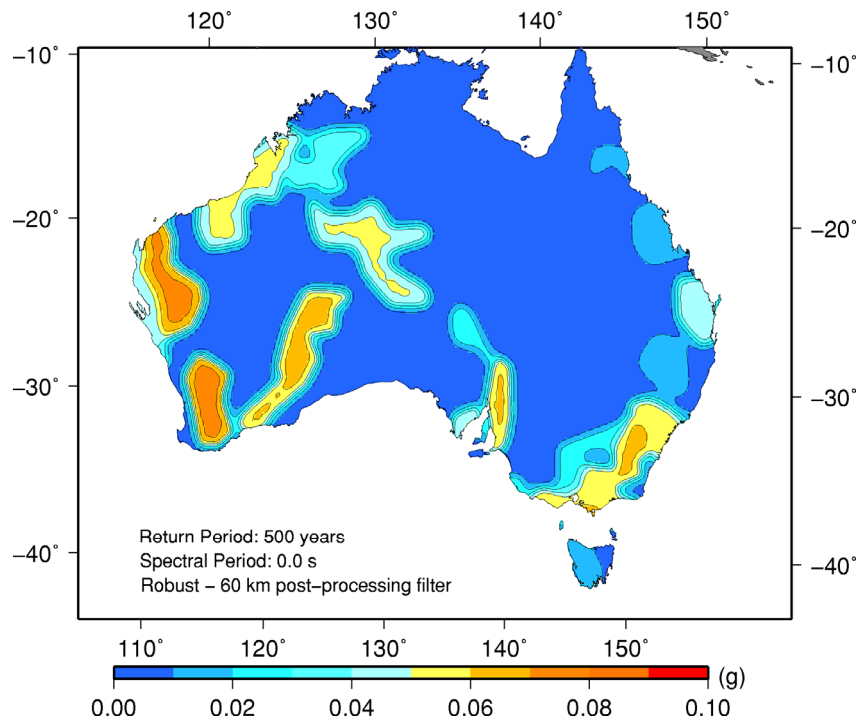


**Figure 36:** The 500 year return period Regional zone PGA (0.0 s RSA period) hazard map with a 60 km Gaussian spatial filter. The recurrence parameters are those described in Table 12 but with the activity rate in the offshore (e.g. Timor and PNG) and background zones set to zero.

### 6.2.3 Hotspot Source Zones Only

Figure 37 shows the 500 year, 0.0 s RSA (PGA) hazard for the Hotspot zones only, smoothed again with a 60 km width Gaussian filter. The parameters of each source zone can also be found in Section 4.4. As described in Section 3.2.5 (cf. Leonard *et al.* 2011), the full catalogue was used (i.e. no declustering and with all the main shocks included) to calculate the hazard in each hotspot zone. As one might expect, hazard values here are basically spikes centred on each hotspot.

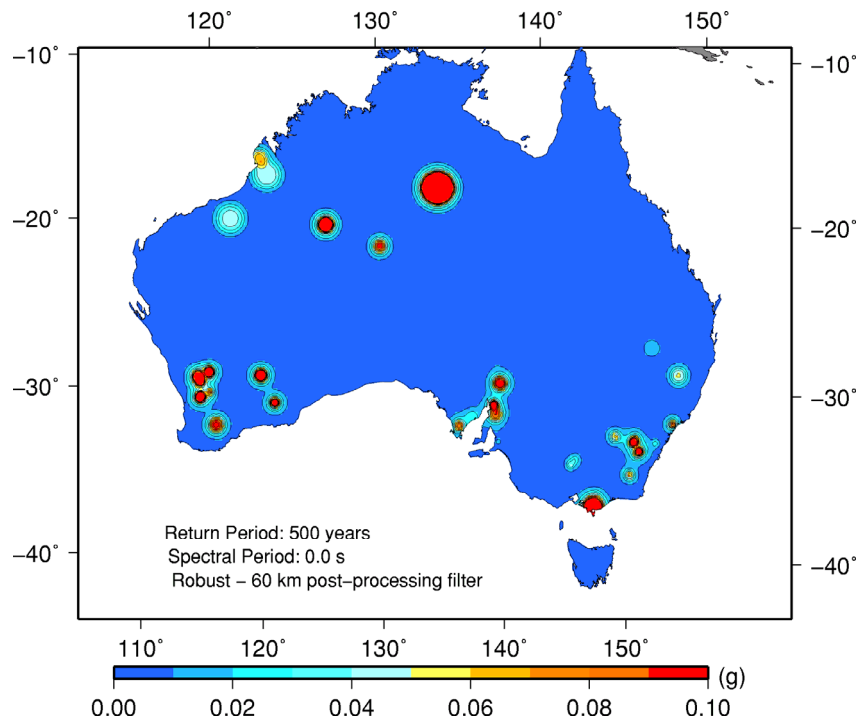


**Figure 37:** The 500 year return period Hotspot zone PGA (0.0 s RSA period) hazard map with a 60 km Gaussian spatial filter.

#### 6.2.4 Combined Regional and Background Zones

The individual hazard layers can be combined in a variety of ways. One possibility is to calculate the recurrence rate for the remainder of the earthquakes outside the Regional zones, whilst still using the Background zone boundaries. [Figure 38](#) shows the hazard for this model with the recurrence rates given in [Table 12](#). The additional zones in Timor, Banda Sea and West Papua have also been added and the distance out to which the ground motions were calculated for each synthetic event was increased from 400 km to 500 km. These zones are included in all the remaining maps in this section. The cumulative effect of these changes is to raise the hazard values across the continent slightly. The cratonic Background zone has a higher hazard than the non-cratonic Background zone but this difference is not visible in [Figure 38](#) because of the particular choice of contouring. As mentioned in [Section 6.2.1](#), the presence or absence of this particular contour is sensitive to minor changes in the input parameters and/or choice of contouring level. Note that, as the earthquakes in the background zones which are within 500 km of a regional zone contribute to the hazard in the regional zone, the hazard levels within the regional zones is slightly higher than those in [Figure 36](#). This map/grid is henceforth referred to as the Regional\_prob map.

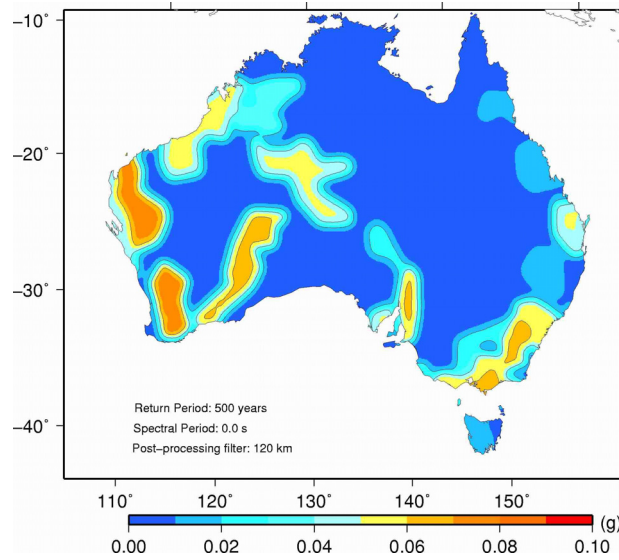


**Figure 38:** The 500 year return period PGA (0.0 s RSA period) hazard map for the map with regional zones surrounded by background zones combined with some offshore zones to the north of Australia. A 240 km Gaussian spatial filter has been applied. The recurrence parameters are those described in Table 12. This map is henceforth referred to as the *Regional\_prob*.

Another possibility is to combine the Regional and Background layers in a weighted average. The result of giving the Regional layer a weight of 0.67 and the Background layer a weight of 0.33 is shown in Figure 39. As expected, within the regional source zones the hazard has decreased slightly (about 0.015g) and the hazard in the background areas has increased slightly. As the background hazard remains low it is not obvious, from Figure 39, that there has been an increase in hazard for all background areas. This map/grid is henceforth referred to as the *Regional\_weight* map.

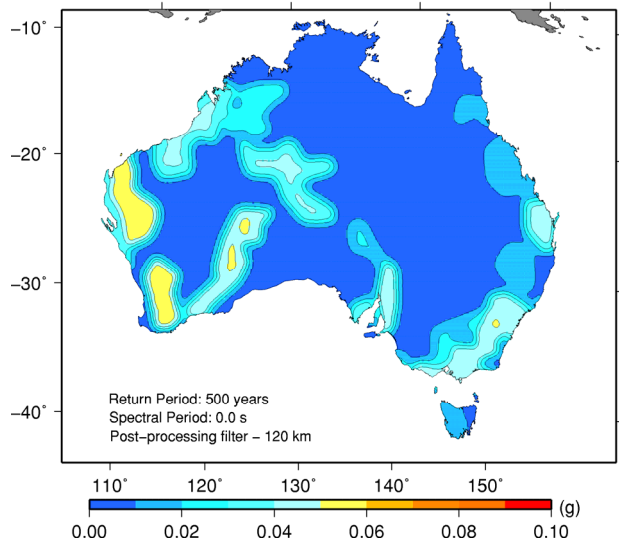


**Figure 39:** The 500 year return period PGA (0.0 s RSA period) hazard map for the map with regional layer weighted 0.67 and the background layer weighted 0.33. This map is henceforth referred to as the *Regional\_weight*.

Another combination is to use the maximum of the Regional and Background recurrence rates for each source zone. The rates for the Background zones are given in Table 11 and those for the Regional zones in Table 12. This is a conservative method of calculating the hazard giving the maximum or worst case of the two models of seismic hazard. It may not be the most appropriate for some applications (e.g. in the insurance industry - K. Campbell, pers. comm.) Taking the maximum of two layers means that the total

integrated seismic moment across Australia is not conserved, but it allows the hazard in the areas of low seismic activity to be increased without decreasing the hazard in areas of high seismic activity. In other words, the Background layer's hazard values are acting as a floor to the Regional maps. Figure 40 shows the 500 year, 0.0 s hazard for the Background and Regional layers combined in this way. Each layer has been Gaussian filtered with the widths specified in the previous sections. This map/grid is henceforth referred to as the Regional\_robust map

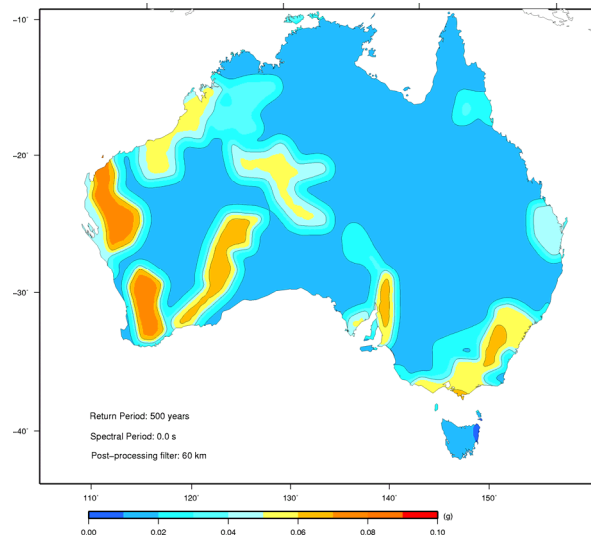


**Figure 40:** The 500 year return period, PGA (RSA 0.0 s period) hazard map calculated using the maximum recurrence rate for the Regional and Background layers. This map is henceforth referred to as the Regional\_robust.

### 6.2.5 Combining the Regional, Background and Hotspot Zones

The Regional and Background zones were combined into a single source model for input into the modelling software (i.e. EQRM), by using various weighted combinations of the recurrence parameters given in Table 11 and Table 12. It was not practical to do this for the Hotspots. Each of the models shown in Figures 37 to 39 took approximately 2 days on a 42 node 1 terabyte parallel computer. Due to the higher earthquake density required adding in the hotspots would further increase this. Also the input parameter file would become very complicated. Therefore we combine the Hotspot layer with the combined Regional and Background layer by post-processing the two hazard grids/maps.

The layers are combined using two methods. The first is taking the maximum of the two grids/maps. The second takes the average where the hazard level of a Hotspot is greater than that of the combined Regional and Background value, and the combined Regional and Background value elsewhere. The resulting grid is then smoothed with a 90km wide Gaussian filter. The maximum hazard approach for the Regional\_robust map is shown in Figure 41a and b for the 500 year, PGA (0.0 s RSA period) hazard maps. Figure 41b shows the same map in 3D perspective to better illustrate the hazard values at the Hotspots.

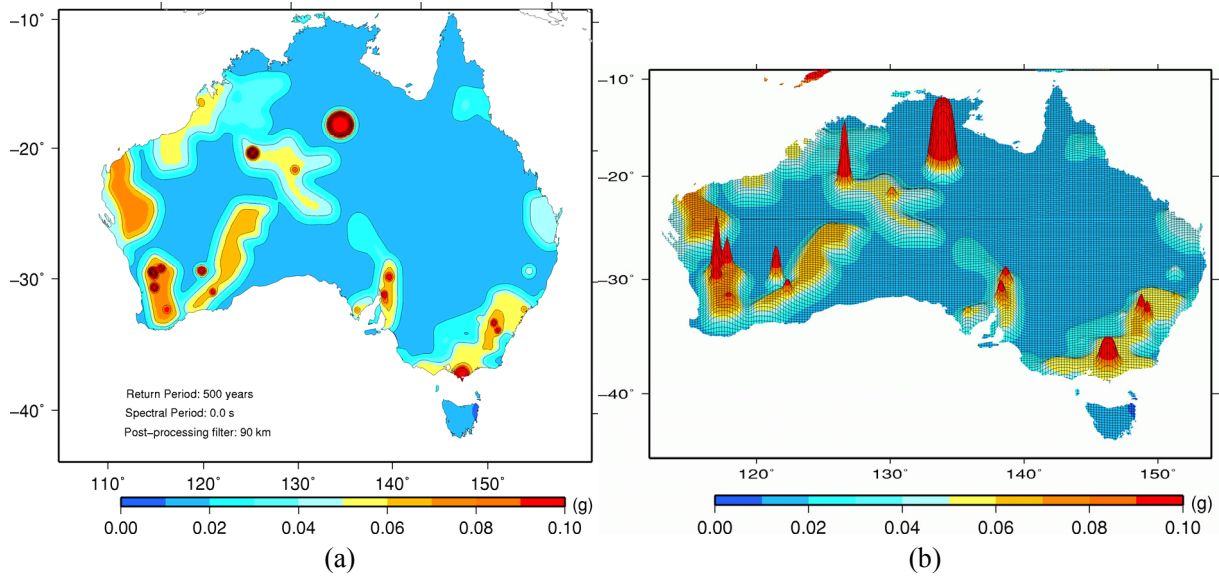


**Figure 41:** The 500 year return period PGA (0.0 s RSA period) hazard map calculated using the maximum hazard value of the combined Regional and Background hazard map (Regional\_robust) and the Hotspot hazard map in (a) 2D and (b) 3D.

One alternative method is to take the average of the combined Regional and Background grid/map and the Hotspot only grid/map in regions where the Hotspot hazard is higher. In the example shown below we combine the Regional\_prob map (Figure 38) and the Hotspot map (Figure 37) in this way. This is, in effect, a less conservative (i.e. lower) method of incorporating the hazard from the Hotspots into the building code map. The result of this particular weighting and smoothing is shown in Figure 42.

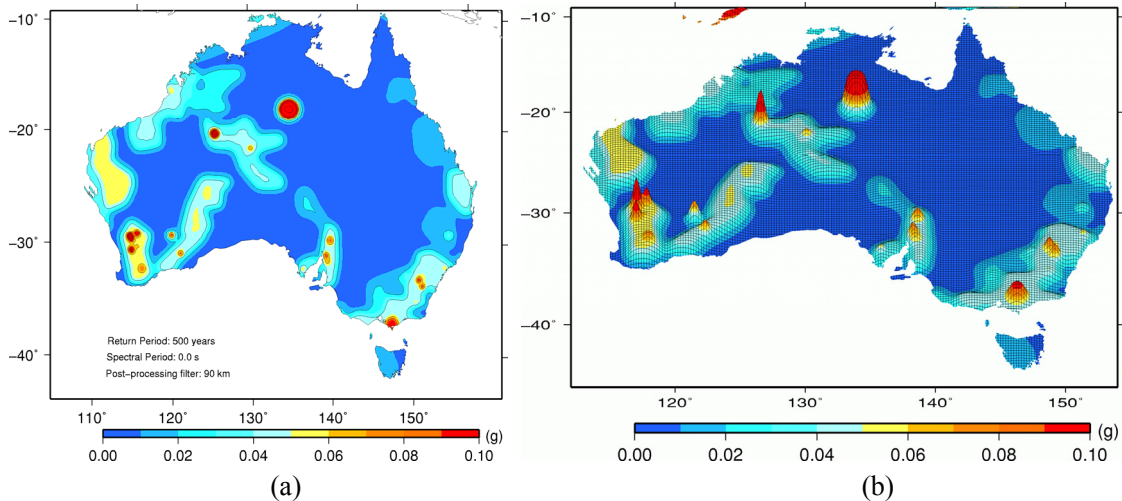


**Figure 42:** The 500 year return period PGA hazard map calculated with a 50/50 weighting in the regions where the Hotspot exceeds the combined Regional and Background layer (Regional\_weight) and after smoothing with a 90km wide Gaussian filter. The map is shown in 2D in (a) and in 3D perspective in (b).

### 6.3 THE PREFERRED AUSTRALIAN EARTHQUAKE HAZARD MAP

The final alternative presented here is to combine the Regional\_robust model shown in Figure 40 (with zones from the Regional, Background and offshore zones combined) with the hotspot layer (Figure 37). In the areas with the Hotspots, the hazard is the average of these two models. Outside of the Hotspots the hazard is identical to the Regional\_robust model. This map was then further smoothed with a 90 km wide Gaussian filter in post-processing. This is our preferred method of combining the maps to be considered for the Australian earthquake loading standards. The resulting hazard map is shown in 2D and 3D in Figure 43.

## The 2012 Australian Earthquake Hazard Map

The capital cities are labelled in the 2D map (Figure 43a). This map has the advantage of including the ground motion generated by the Background zones inside the Regional zones in a probabilistic way and also includes the elevated hazard generated by the Hotspots.

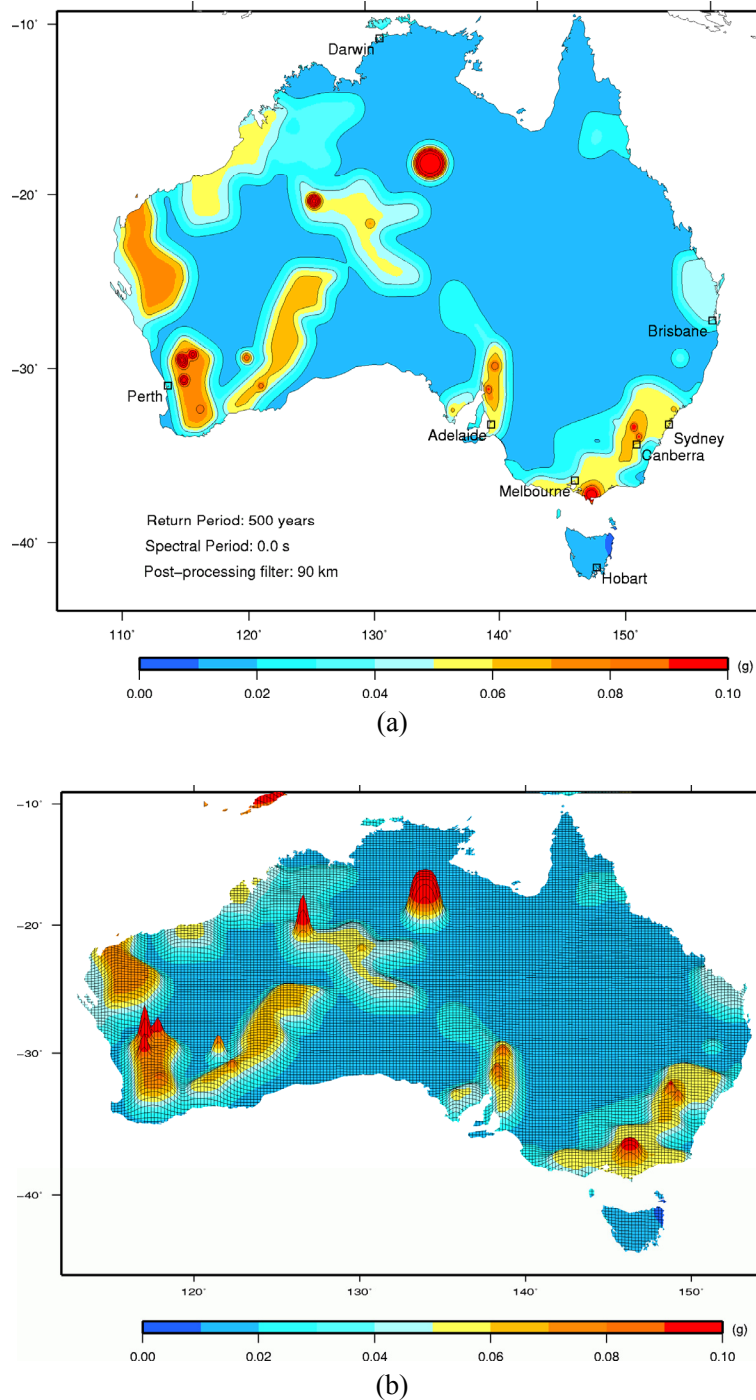


**Figure 43:** The 500 year return period PGA hazard map calculated with a 50/50 weighting in the regions where the hotspot exceeds the hazard shown in Figure 40. The model was then smoothed with a 90 km wide Gaussian filter. The map is shown in 2D in (a) and in 3D perspective in (b). The State and Territories capital cities are labelled in (a). This map is the authors' preferred weighting and smoothing.

### 6.3.1 Effect of the Gaussian width

The effect of using a 300 km Gaussian filter on the hotspot layer on the final hazard map is shown in [Figure 44a,b](#). Most of the hot spot zones in [Figure 44](#) produce hazard values less than the regional or background zones and thus do not appear in the maximum hazard map. Those that do appear (e.g. Tennant Creek) are smaller in amplitude but cover a slightly larger area. The edges of the Tennant Creek Hotspot are also more tapered when the larger width filter is used.

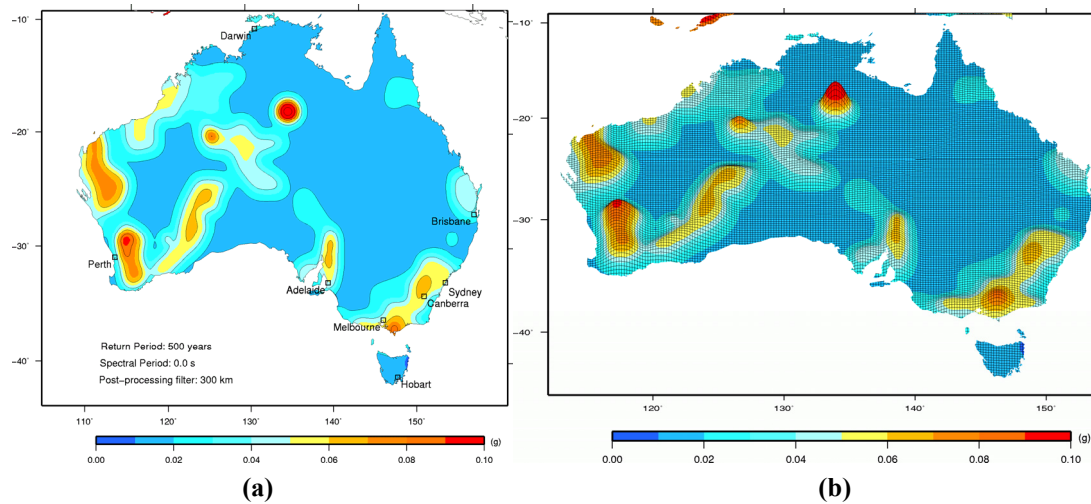


**Figure 44:** The maximum hazard value for the preferred combination of layers ([Figure 43](#)) but with the spatial filter width increased to 300 km for all layers in (a) 2D and (b) 3D.

### 6.3.2 Effect of return period

[Figure 45](#) shows the national 0.0s RSA (PGA) hazard maps for a return period of (a) 2,475 years and (b) 10,000 years. The 2,475 year map corresponds to ground motions with 2% chance of being exceeded in 50 years. Naturally the level of hazard goes up as the return period increases. However, note that the rate of increase is slower for the Hotspot zones (e.g. Tennant Creek) than it is for the Regional zones. This is mostly due to the lower  $M_{max}$  values used in the Hotspot layer zones ([Section 4.3](#); cf. Leonard *et al.* 2011).

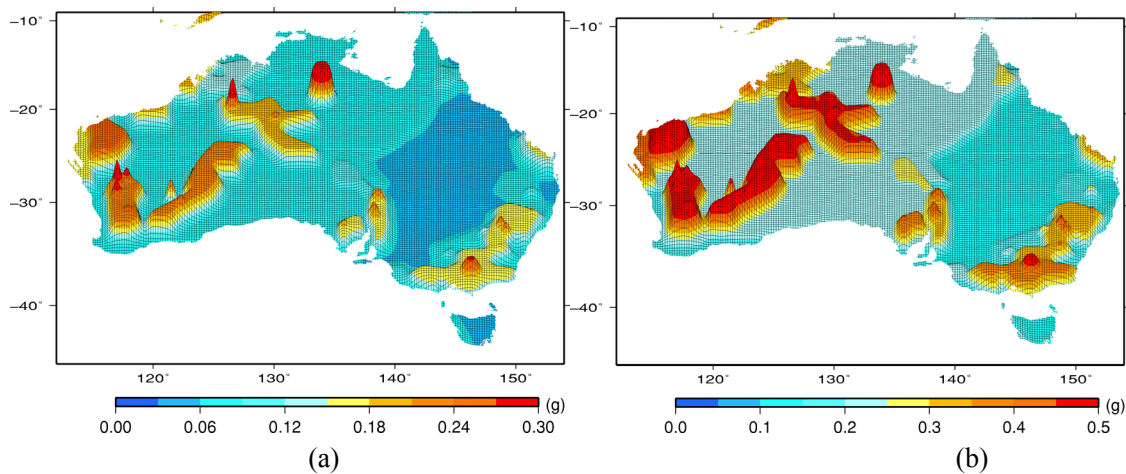


**Figure 45:** The 0.0s hazard value for all three source zone layers for return periods of (a) 2,500 years and (b) 10,000 years. The three layers are combined in the same way as that shown in [Figure 43](#). Note that the colour scale and the vertical exaggeration in both (a) and (b) differs from the previous figures to prevent saturation.

### 6.3.3 Effect of spectral response period

Figure 46 shows the 500 year hazard map for two other spectral response periods (0.2 and 1.0 s) across the country. Hazard values for the 0.1 s map are consistently higher and, for the 1.0 s period map, lower than the 0.0 s period map right all across Australia (compare Figure 43 to Figure 46).

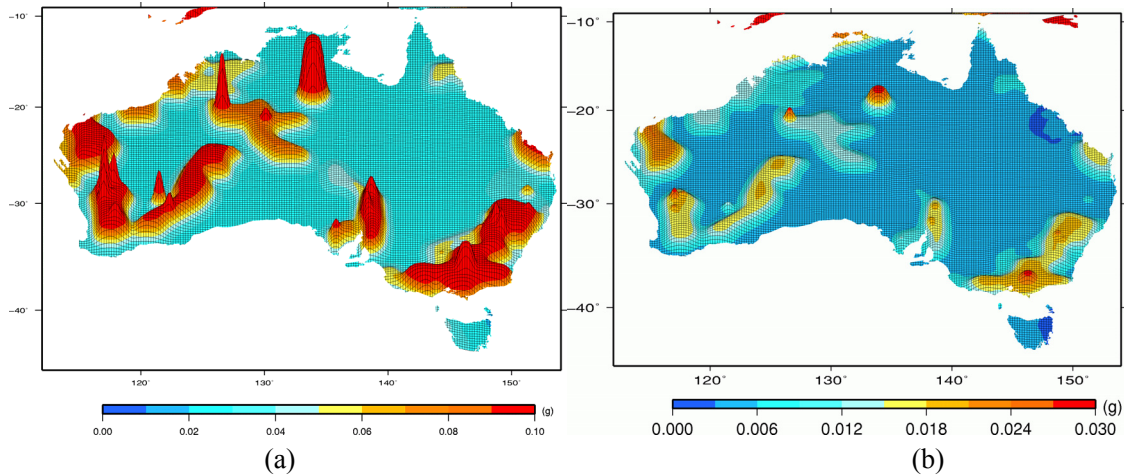
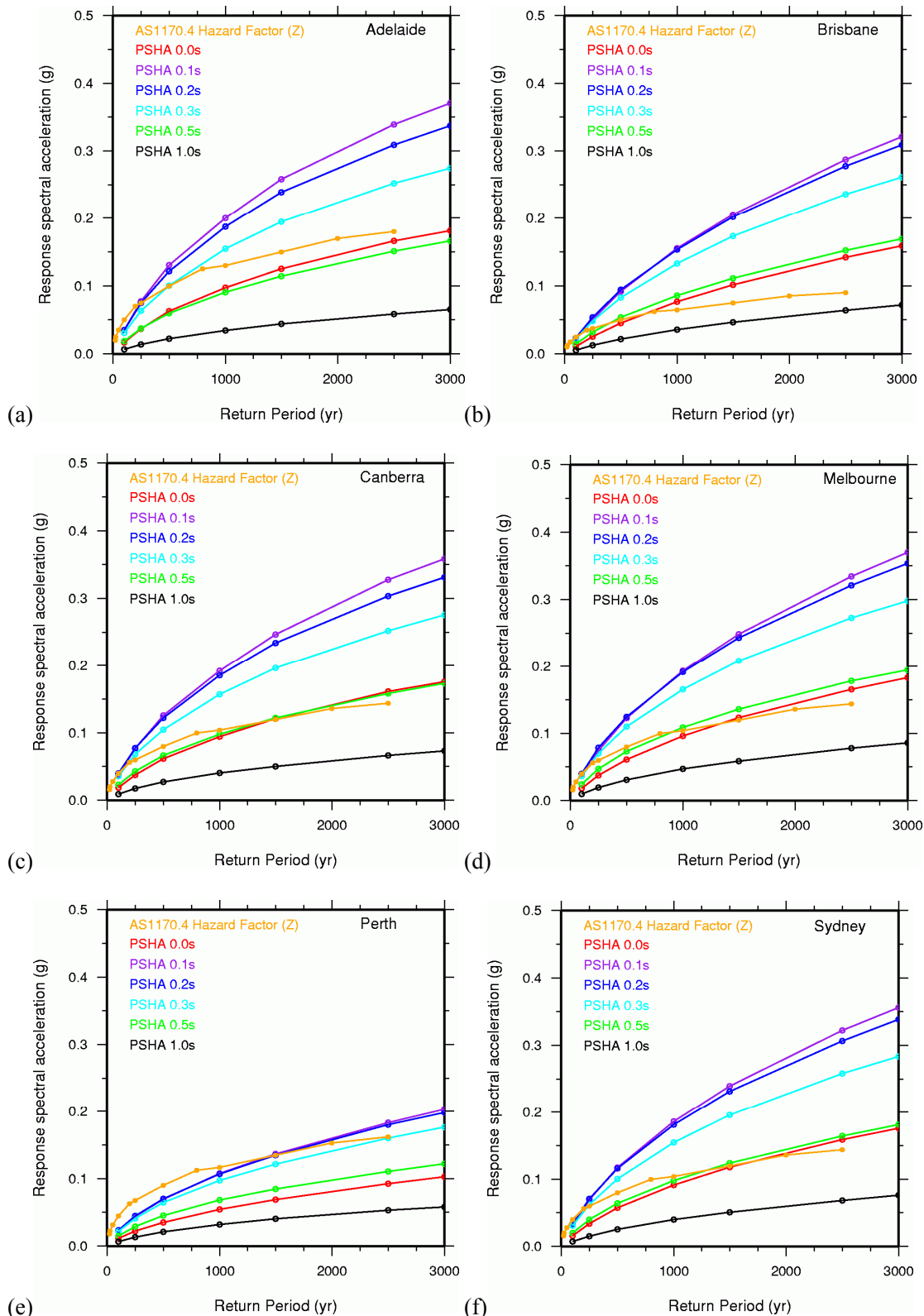


Figure 46: The 500 year hazard value for all three source zone layers for (a) 0.1s RSA period and (b) 1.0 s RSA period. The three layers are combined in the same way as those shown in Figure 43.

### 6.3.4 Selected Hazard Curves

Figure 47f shows hazard at a specific point in Sydney as a function of return period for the four different response periods (the four solid lines). Analogous figures for points in Adelaide, Brisbane, Canberra, Hobart, Melbourne and Perth are shown in Figure 47a-e. Also shown in Figure 47 are the AS1170.4 hazard Z factor curves for rock calculated from Tables 3.1 and 3.2 in AS1170.4-2007 (the dashed orange curve).

As can be seen for all the locations shown in Figure 47, the hazard at 0.1, 0.2 and 0.3 s RSA periods in the PSHA are higher than that for the 0.0 s RSA period hazard (solid red curve); the 0.5 s RSA period curve is similar to the 0.0 s RSA curve and the 1.0 s hazard is always lower. This is a direct result of the response spectral shape given by the GMPEs used to develop the map (see Chapter 5). Naturally the hazard also increases as the return period increases, but starts to roll off at the higher return periods.



**Figure 47:** Response spectral acceleration as a function of return period at six different spectral periods for locations in (a) Adelaide, (b) Brisbane, (c) Canberra (d) Melbourne, (e) Perth, and (f) Sydney for the preferred model shown in Figure 43. The red, cyan, blue, light blue, green curves and black are the RSA values for 0.0 s, 0.1 s, 0.2 s, 0.3 s, 0.5 s and 1.0 s from the relevant earthquake hazard map. The orange curve is the hazard factor, Z, calculated using the appropriate tables in AS1170.4-2007.

For most of the points considered here, the hazard factor ( $Z$ ) in the current code (orange dashed curve) is closest to either the 0.0 s (PGA) and 0.5 s or the 0.3 s PSHA values (solid red, green and cyan curves), depending on the location and return period. The exception is Perth where the hazard in this assessment is lower than the  $Z$  factor values given in the Table. However, it should be noted that the hazard increases rapidly the further from the coast the site is located (e.g. Figure 44), so the hazard for “Perth” is highly sensitive to the longitude of the point selected to represent the hazard for the city. The difference between  $Z$  and the PSHA with RSA periods in the range of 0.0 to 0.3s values are typically  $<0.05$  g for these particular locations. The hazard value for the point near Melbourne (Figure 47d) at 0.0 s, 500 years (0.05g) is similar to the PGA hazard value determined for the general Melbourne area by Brown and Gibson (2004). However, like Perth, the hazard changes rapidly near Melbourne (Figure 43).

## 6.4 DISCUSSION

### 6.4.1 Uncertainties and limitations

The uncertainties in estimating the G-R recurrence parameters ( $a$ ,  $b$ ,  $M_{max}$ ) are not explicitly included in these maps (e.g. by using multiple recurrence models). In the case of the  $M_{max}$ , this parameter this will not significantly affect the 500 year return period map since all plausible values of  $M_{max}$  are above  $M$  7.0. Figure 48 shows the impact of changing  $M_{max}$  from 5.0 to 7.5 for Zone 11. As seen in the figure, increasing  $M_{max}$  from 5.0 to 7.0 nearly doubles the hazard, but changing it from 7.0 to 7.5 changes it by only about 5%. This would be typical for most locations across Australia.

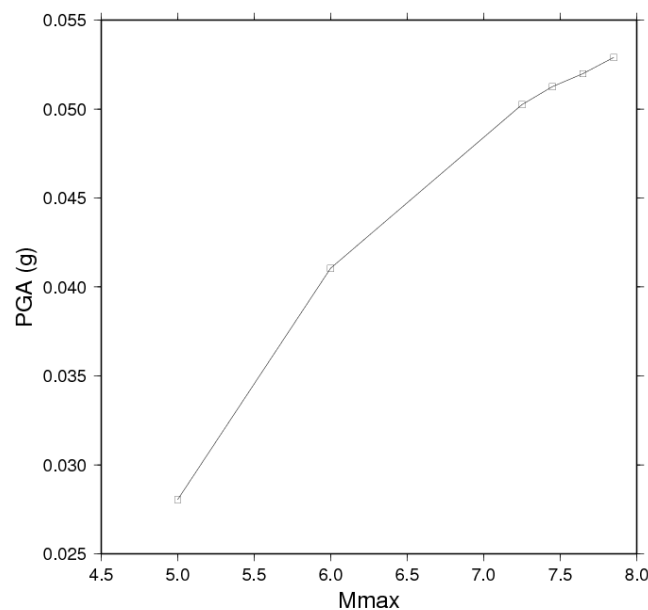


**Figure 48:** The effect of changing the  $M_{max}$  variable on the hazard at a single location in Zone 11 (Victoria) at a return period of 500 years.

We have also assumed that there are no basin effects. In the multi-hazard assessment of Perth, Sinadinovski *et al.* (2005) considered the attenuation of short-period seismic waves from the Yilgarn Craton to the east that pass through the Perth Basin. This was based on very limited data. In the absence of sufficient new data to test this effect, we find it difficult to justify the application of this or any similar relation. Similarly, faults are not included as the data available to constrain the rates of fault motion are currently very limited. Furthermore, the effect on the hazard values from faults would generally be quite localised, and would most likely be removed by the smoothing required for a building code map.

#### 6.4.2 Choice of map for AS1170.4

One of the key problems with the previous maps from the perspective of producing a map appropriate for a loading code was that the hazard in areas with few earthquakes (e.g. Central Queensland) was low or zero. In the current AS1170.4-2007 map this was worked around by an expert committee smoothing previous hazard maps out into these areas using expert judgement. Here we extend the hazard out to these regions by using the Background zones based on a simplified geological interpretation of Australia. This has the advantage that the hazard for the whole of Australia is now calculated probabilistically. It is also easy to update these Background zones by simply including earthquakes as they happen and by modifying the zone boundaries over time, as required.

The Regional scale earthquake source zones have the advantage of more closely representing the observed distribution of seismicity without going into a high level of detail. This minimises the number of rapidly changing hazard values (i.e. steep contours) while still providing a more accurate representation of the distribution of seismicity at the regional scale relative to the Background maps. The only areas where the hazard pattern (i.e. areas of high and low hazard) may change rapidly from version to version are near the edges of the zones. The advantage of this map over that currently utilised in AS1170.4-2007 is that the hazard is calculated probabilistically across a range of return and RSA periods, and can be updated in a straightforward manner as new information becomes available.

The Hotspot zones represent small scale, often transient, variations in hazard across the continent much more accurately than the previous two layers. However, on a time scale of a decade or more many of these hotspots can be expected to change, with new ones needing to be added and inactive ones requiring removal. Accordingly, the Hotspot layer will not necessarily remain stable from one edition of the map (and hence building code) to the next. In addition, the Hotspot zones always produce very steep contours in the maps as they are quite small in area. Note that this would be an issue for any map with multiple small zones (e.g. Brown and Gibson 2004). Large amounts of smoothing can remove these steep contours, either by smoothing the initial seismicity (e.g. Hall *et al.* 2007) or by smoothing the final map (see for example Figure 44). However, in both cases the effect of this would be to increase the hazard over a larger area than that indicated by the distribution of seismicity.

The authors consider that the maps shown in Figure 43 offer a rational balance between detail and smoothness for an application like a hazard map for a building code. In these maps the hazard in the Hotspot regions is the average of the Hotspot layer and the combined (regional, offshore and background zones) layer in that area. The final map is smoothed with a 90 km wide Gaussian filter. This map is fairly smooth, but still retains the major active Hotspots. While this is our preferred model, many other combinations of smoothing and weighting are also possible and easy to create if more or less detail is required for a particular application. This could include the possibility of absolutely no smoothing, if that was desired.

It has been identified by one reviewer that maps produced by finding the maximum (or average) of two separate hazard models are not strictly the probabilistic seismic hazard at a constant probability level across all of Australia (K. Campbell, pers. comm.). However, we consider that using the maximum of two source models and including the Hotspots by averaging the hazard into the final map is a reasonable compromise between a strict fully probabilistic map and one designed to fulfil the goal of “life safety” that is stipulated in the Australia Standard and most building codes worldwide. A strict application of PSHA to central Queensland, for example, would reduce the hazard in that area to zero since no earthquakes have been recorded there. This would mean that there would be no need for earthquakes to be considered in designing structures in this area, which we consider would be inappropriate for the building code. It should also be pointed out that it is very unlikely that the “true” hazard calculated with a very long earthquake catalogue (e.g. 10,000 years) for this area would actually be zero. The lack of earthquakes in this, and other remote areas of Australia, is an artefact of the short length of the existing earthquake catalogue, and not a sign that earthquakes in those areas cannot occur in the future. Thus for building code hazard maps a floor of some kind is essential.

Finally, there also remains the choice of which RSA and return period would be most suitable for the base map in the loading code. The simplest option would be to use a similar return period as that used in the current AS1170.4 map. This will keep changes in the hazard factor ( $Z$ ) in AS1170.4 to  $<0.05$  g for the majority of the continent, outside of the hotspots. The choice of the RSA period depends on which period best represents the structure(s) of interest in the code. As discussed in McPherson *et al.* (2011), the hazard factor,  $Z$ , does not have a well defined physical value (i.e. a response spectral period) but appears to be equivalent to the hazard with a RSA period in the range of 0.0 to 0.3 s for most locations (cf. Figure 47).

### 6.4.3 Other Applications of the Seismic Hazard Maps

While the main goal of these hazard maps is for engineering application under the Australian earthquake loading code (AS1170.4), they have a range of other potential uses, such as selecting scenarios for detailed hazard or risk assessments. A scenario seismic hazard or risk map shows the level of ground shaking or the impact from a specific earthquake. Many of the inputs to a scenario hazard/risk map are the same as for a probabilistic map, thus developments in one help the other. As previously mentioned, the EQRMs produce a list of events as part of the process of calculating the hazard. Therefore, doing an assessment in this way makes it straight forward to disaggregate the hazard and select an event or events for a scenario hazard/risk assessment. Such maps are not used in the current standard, but have particular utility in scenario development to assist emergency managers with disaster response planning.

Some applications (e.g. risk modelling for the insurance industry) tend to require a more strict adherence to PSHA than that of our preferred map (Figure 43). With the exception of the smoothing the Regional\_weighted map is strict PSHA and, as demonstrated in Appendix F, Gaussian smoothing could be replaced by multiple weighted models with spatially offset source zones. The weighted inclusion of the Hotspots does not adhere to strict PSHA but the impact on risk is minor. We note that at most 2% of the Australian population, and possibly as little as 1%, live in the Background zones sufficiently distant from a regional source zone that the seismic hazard is entirely derived from the hazard in the Background. As such the difference between impact models (e.g. insured loss) based on our preferred map (Figure 43), the Regional\_weighted (Figure 39) or the Regional\_weighted with weighted Hotspots (Figure 42) would be small.

### 6.4.4 Summary

In this chapter we have presented the results of a full probabilistic seismic hazard assessment (PSHA) for Australia. As with most PSHAs, a range of results are possible depending on how the available earthquake data is defined. These cover different choices of seismic source zones, response spectral acceleration periods, return periods and earthquake recurrence models (from one with a high level of spatial detail which includes “Hotspots” to one with a very low level of spatial detail). The results presented here are based on the best available data for Australia, while the methods developed and/or applied have been designed to be flexible and straightforward to update. These models provide an effective basis for future revisions of the hazard map underpinning the Australian earthquake loading code AS1170.4. For the next revision of the Standard, the authors recommend the weighting and smoothing shown in Figure 43 (and Figure 1) would be appropriate, although the final decision of which particular map should be included is ultimately a decision for Standards Australia and the relevant committee.

## Acknowledgements

The authors would like to acknowledge Ben Cooper and Vanessa Newey for their help with modifying EQRM so that it could be used for this project.. We would also like to thank Gary Gibson for his initial work on the national earthquake catalogue and to thank J. Rynn and D. Weatherly for providing us with their Queensland catalogue of earthquakes. The authors would also like to acknowledge Ken Campbell, Paul Thenhaus, Paul Somerville and Kevin McCue for their reviews of the original manuscript. Finally, we would also like to thank Russell Cuthbertson, Gary Gibson, David Love, Paul Somerville and Felipe Dimer de Oliveira for attending a feedback workshop on the draft hazard map in February 2012. Many of the plots and maps in this manuscript were made using the Generic Mapping Tools (Wessel and Smith, 1998). This report is published with the permission of the CEO of Geoscience Australia.

## References

- Abrahamson, N. A., and J. J. Bommer (2005). Opinion Paper: Probability and uncertainty in seismic hazard analysis, *Earthquake Spectra* **21**, 603-607.
- Aki K., 1965. Maximum likelihood estimation of b in the formula  $\log N = a - bM$  and its confidence limits *Bull. Earthquake Res. Inst. Tokyo Univ.*, 43 (1965), pp.237-239.
- Al Atik, L., N. Abrahamson, J. J. Bommer, F. Scherbaum, F. Cotton, and N. Kuehn (2010). The variability of ground-motion prediction models and its components, *Seism. Res. Lett.* **81**, 794-801.
- Allen T. I. 2010. *The influence of attenuation in earthquake ground-motion and magnitude estimation: implications for Australian earthquake hazard*. Proceedings of the Australian Earthquake Engineering Society Conference, 26-28 November 2010, Perth. Paper No. 1.
- Allen, T.I., 2012. *Stochastic ground-motion prediction equations for southeastern Australian earthquakes using updated source and attenuation parameters*, GA record 2012/XX (in press).
- Allen T. I., Burbidge D. R., Clark D. J., McPherson A. A., Collins C. D. N. and Leonard M. 2011. *Development of the next generation Australian National Earthquake Hazard Map*. Proceedings of the 9<sup>th</sup> Pacific Conference on Earthquake Engineering, 14-16 April 2011, Auckland, New Zealand.
- Allen T. I., Dhu T., Cummins P. R. and Schneider, J. F. 2006. Empirical attenuation of ground-motion spectral amplitudes in southwestern Western Australia, *Bulletin of the Seismological Society of America* **96**, 572–585.
- Allen, T., G. Gibson, and C. Hill (2000). *The Thomson Reservoir triggered earthquakes*. Proceedings of the Australian Earthquake Engineering Society Conference, 2000, Hobart.
- Atkinson G. M. and Boore D. M. 1995. Ground-motion relations for eastern North America, *Bulletin of the Seismological Society of America* **85**, 17-30.
- Atkinson G. M. and Boore D. M. 2006. Earthquake ground-motion predictions for eastern North America, *Bulletin of the Seismological Society of America* **96**, 2181-2205.
- Bakun, W. H. and Joyner, W. B. 1984. The  $M_L$  scale in central California, *Bulletin of the Seismological Society of America* **74**, 1827-43.
- Bommer, J. J., and N. A. Abrahamson (2006). Why do modern probabilistic seismic-hazard analyses often lead to increased hazard estimates?, *Bull. Seism. Soc. Am.* **96**, 1967–1977.
- Bommer, J. J., and F. Scherbaum (2008). The use and misuse of logic-trees in probabilistic seismic hazard analysis, *Earthq. Spectra* **24**, 997-1009.
- Brown A. and Gibson G. 2004. A multi-tiered earthquake hazard model for Australia, *Tectonophysics*, **390**, 25-43.
- Building Seismic Safety Council. 2004. *NEHRP recommended provisions for seismic regulations for new buildings and other structures (FEMA 450), 2003 edition*. Building Seismic Safety Council, National Institute of Building Sciences, Washington DC.
- Building Seismic Safety Council. 2009. *NEHRP (National Earthquake Hazards Reduction Program) Recommended Seismic Provisions for New Buildings and Other Structures (FEMA P-750), 2009 edition*. Building Seismic Safety Council, National Institute of Building Sciences, Washington DC.
- Burbidge D. and Leonard M., 2011. *The 2012 Australian Seismic Hazard Map – Draft maps*. Proceedings of the Australian Earthquake Engineering Society Conference, 18-20 November 2011, Barossa Valley.
- Burbidge D., Allen T. Collins C., McPherson A., Drummond B., Leonard M., Clark D., Cummins P., Cuthbertson R., Dentith M., Gaull B., Gibson G., Leiba M., Love D., McCue K., Somerville P., Rynn J. and Wilson J. 2010. Future Directions for the National Earthquake Hazard Map. *Geoscience Australia Record* **2010/04**. 25 p.
- Burger R. W., Somerville P. G., Barker J. S., Herrmann R. B. and Helmberger D. V. 1987. The effect of crustal structure on strong ground motion attenuation relations in eastern North America. *Bulletin of the Seismological Society of America* **77**, 420-439.

- Campbell K. W. 2003. Prediction of strong ground motion using the hybrid empirical method and its use in the development of ground-motion (attenuation) relations in eastern North America. *Bulletin of the Seismological Society of America* **93**, 1012–1033.
- CEUS-SSC (2012). Technical Report: Central and Eastern United States Seismic Source Characterization for Nuclear Facilities, EPRI, Palo Alto, CA, U.S. DOE, and U.S. NRC.
- Chiou B. S.-J. and Youngs R. R. 2008. An NGA model for the average horizontal component of peak ground motion and response spectra. *Earthquake Spectra* **24**, 173–215.
- Clark, D., McPherson, A. and Collins, C. D. N. 2011. Australia's seismogenic neotectonic record: a case for heterogeneous intraplate deformation. *Geoscience Australia Record* 2011/11, 95 pp.
- Clark, D., McPherson, A. and Van Dissen, R. in press. Long-term behaviour of Australian Stable Continental Region (SCR) faults. *Tectonophysics*.
- Collins, C.D.N., Drummond, B.J. and Nicoll, M.G., 2003. Crustal thickness patterns in the Australian Continent. *Geological Society of Australia, Special Publication* 22, 121-128.
- Collins, C., R. Kayen, B. Carkin, T. Allen, P. Cummins, and A. McPherson (2006). Shear wave velocity measurement at Australian ground motion seismometer sites by the spectral analysis of surface waves (SASW) method, *Earthquake Engineering in Australia, Canberra, ACT, November 24-26, 2006, Proceedings: Australian Earthquake Engineering Society*.
- Cuthbertson R. 2006. *Automatic calculation of seismicity rates in eastern Queensland*. Proceedings of the Australian Earthquake Engineering Society Conference, 24-26 November 2006, Canberra. Paper No. 137.
- Cuthbertson R. 2007. *Automatic calculation of seismicity rates in eastern Queensland*. Proceedings of the Australian Earthquake Engineering Society Conference, 23-25 November 2007, Wollongong. Paper No. 19.
- Dent V. F. 2009. *Seismic network capability and magnitude completeness maps, 1960-2005 for Western Australia, South Australia and the Northern Territory*. Proceedings of the Australian Earthquake Engineering Society Conference, 11-13 November 2009, Newcastle.
- Denham D. 1982. Proceedings of the workshop on Australian earthquake magnitude scales, *Australian Bureau of Mineral Resources Record* **1982/29**. 36 p.
- Eiby, G. A. and Muir, M. G. 1961. Tables to Facilitate the study of near earthquakes, *New Zealand Department of Scientific and Industrial Research, Seismological Observatory Bulletin*, S-109.
- Gardner J. K. and Knopoff L. 1974. Is the sequence of earthquakes in southern California, with aftershocks removed, Poissonian? *Bulletin of the Seismological Society of America* **64**, 1363-1367.
- Gaull, B.A. and Gregson, P.J. 1991, A new local magnitude scale for Western Australian earthquakes, *Australian Journal of Earth Sciences*, **38**:3, 3251-260.
- Gaull, B. A., and P. Kelsey (1999). Historical felt intensities as a guide to earthquake hazard, *Aust. J. Earth. Sci.* **46**, 365-376.
- Gaull, B. A., Michael-Leiba M. O. and Rynn J. M. W. 1990. Probabilistic earthquake risk maps of Australia. *Australian Journal of Earth Sciences* **37**, 169-187.
- Goertz-Allmann, B. P., B. Edwards, F. Bethmann, N. Deichmann, J. Clinton, D. Fäh, and D. Giardini (2011). A new empirical magnitude scaling relation for Switzerland, *Bull. Seism. Soc. Am.* **101**, 3088–3095.
- Greenhalgh, S. A. and Singh, R. 1986. The seismicity of the Adelaide Geosyncline, South Australia, *Bulletin of the Seismological Society of America* **78**, 243-263.
- Grünthal, G., R. Wahlström, and D. Stromeyer (2009). The unified catalogue of earthquakes in central, northern, and northwestern Europe (CENEC)—updated and expanded to the last millennium, *J. Seismol.* **13**, 517–541.
- Gupta, H. K. (2002). A review of recent studies of triggered earthquakes by artificial water reservoirs with special emphasis on earthquakes in Koyna, India, *Earth-Sci. Rev.* **58**, 279–310.
- Gutenberg, B. and Richter, C.F. 1944. Frequency of earthquakes in California, *Bulletin of the Seismological Society of America*, 185-188.

- Hall L., Dimer F. and Somerville P. 2007. *A spatially distributed earthquake source model for Australia*. Proceedings of the 2007 Australian Earthquake Engineering Society Conference, 23-25 November 2007, Wollongong.
- Hearn, S. J., and J. P. Webb (1984). Continental-scale felt effects of the large Banda Sea earthquake of 4 November 1963, *Bull. Seism. Soc. Am.* **74**, 349-351.
- Johnston, A. C. 1994a. Appendix C-summary tables, SCR seismicity database. In: A. C. Johnston, K. J. Coppersmith, L. R. Kanter and C. A. Cornell (eds.), *The earthquakes of stable continental regions-v. 2*, pp. C-1-C-46. Electric Power Research Institute, Palo Alto, California.
- Johnston, A. C. 1994b. Seismotectonic interpretations and conclusions from the stable continental region seismicity database. In: A. C. Johnston, K. J. Coppersmith, L. R. Kanter and C. A. Cornell (eds.), *The earthquakes of stable continental regions-v. 1, Assessment of large earthquake potential*, pp. 4-1-4-103. Electric Power Research Institute, Palo Alto, California.
- Johnston, A. C. 1994c. The stable continental region database. In: A. C. Johnston, K. J. Coppersmith, L. R. Kanter and C. A. Cornell (eds.), *The earthquakes of stable continental regions-v. 1, Assessment of large-earthquake potential*, pp. 3-1-3-80. Electric Power Research Institute, Palo Alto, California.
- Johnston, A. C. (1996). Seismic moment assessment of earthquakes in stable continental regions—I. Instrumental seismicity, *Geophys. J. Int.* **124**, 381-414.
- Jones T., Middelman M. and Corby N. 2005. *Natural hazard risk in Perth, Western Australia*. Geoscience Australia, Canberra. 352 p.
- Kayen, R., B. Carkin, and D. Minasian (2010). Shear wave velocity of Australian strong motion seismometer sites by the Spectral Analysis of Surface Waves method (SASW): 2010 Survey, U.S. Geological Survey, Menlo Park, CA 33.
- Leonard M. 2008. One hundred years of earthquake recording in Australia. *Bulletin of the Seismological Society of America* **98**, 1458-1470.
- Leonard M. 2010a. Earthquake fault scaling; self-consistent relating of rupture length, width, average displacement and moment release. *Bulletin of the Seismological Society of America* **100**, 1971-1988.
- Leonard M. 2010b. *Analysis of the spatial statistical properties of continental seismicity*. Proceedings of the Australian Earthquake Engineering Society Conference, 26-28 November 2010, Perth.
- Leonard M. and Clark D. 2011. A record of stable continental region earthquakes from Western Australia spanning the late Pleistocene: Insights for contemporary seismicity. *Earth and Planetary Science Letters* DOI:10.1016/j.espl.2011.06.035.
- Leonard M., Clark D., Collins C. and McPherson A. 2011. *The 2012 Australian Seismic Hazard Map – Source Zones and Parameterisation*. Proceedings of the Australian Earthquake Engineering Society Conference, 18-20 November 2011, Barossa Valley. Paper No. 30.
- Li Q., Liu M., and Stein S. 2009, Spatio-temporal complexity of continental intraplate seismicity: insights from geodynamic modeling and implications for seismic hazard estimation. *Bulletin of the Seismological Society of America* **99**, 52–60.
- Liang J. Z., Hao H., Gaull B. A. and Sinadinovski C. 2008. Estimation of strong ground motions in southwest Western Australia with a combined Green's function and stochastic approach. *Journal of Earthquake Engineering* **12**, 382–405.
- McCue K., Gibson G., Michael-Leiba M., Love D., Cuthbertson R. and Horoschun G. 1993. *Earthquake hazard map of Australia, 1991*. Australian Geological Survey Organisation, Canberra. [map]
- McCue, K. F. 1993. *The revised Australian hazard map, 1991*. Proceedings of the Australian Earthquake Engineering Society Conference, 25 September 1992, Sydney. pp. 21-25.
- McGregor P. M. and Ripper I. D. 1976. Notes of earthquake magnitude scales. *Bureau of Mineral Resources Record* **1976/56**.
- McPherson A., Leonard M., Collins C., Clark D. Burbidge D. and Allen T. 2011. *The 2012 Earthquake Hazard Map of Australia - Introduction and Approach*. Proceedings of the Australian Earthquake Engineering Society Conference, 18-20 November 2011, Barossa Valley. Paper No. 37.

- Michael-Leiba M. and Malafant, K. 1992. A new local magnitude scale for southeastern Australia, *BMR Journal of Australian Geology and Geophysics*, **13**, 201-205.
- Parsons T. 2002 Global Omori-law decay of triggered earthquakes: large aftershocks outside the classical aftershock zone. *Journal of Geophysical Research* **107**, doi:10.1029/2001JB000646.
- Pezeshk S., Zandieh a. and Tavakoli B. 2011. Hybrid empirical ground-motion equations for Eastern North America using NGA models and updated seismological parameters. *Bulletin of the Seismological Society of America*, 101 (4), 1859-1870.
- Richter C. F. 1935. An instrumental magnitude scale, *Bulletin of the Seismological Society of America* **25**, 1-32.
- Richter C. F. 1958. *Elementary Seismology*. W. H. Freeman and Co., San Francisco.
- Robinson, D., Fulford, G. and Dhu, T. 2005. EQRM: Geoscience Australia's earthquake risk model, technical manual version 3.0. *Geoscience Australia Record* **2005/1**.
- Robinson, D., Dhu, T. and Schneider, J. 2006. Practical probabilistic seismic risk analysis: a demonstration of capability. *Seismological Research Letters* **77(4)**, 453-459.
- Sagar S. and Leonard M. 2007. *Automatic calculation of seismicity rates in eastern Queensland*. Proceedings of the Australian Earthquake Engineering Society Conference, 23-25 November 2007, Wollongong. Paper No. 46.
- Schorlemmer D., Weimer S. and Wyss M., 2005. Variations in earthquake size distribution across different stress regimes, *Nature*, 437, 539–542.
- Scordilis, E. M. (2006). Empirical global relations converting  $M_S$  and  $m_b$  to moment magnitude, *J. Seismol.* **10**, 225–236.
- Sinadinovski C., Edwards M., Corby N., Milne, M., Dale K., Dhu T., Jones A., McPherson A., Jones T., Gray D., Robinson, D. and White, J. 2005. Earthquake Risk. In: T. Jones, Middelmann M. and Corby N. (ed.), *Natural hazard risk in Perth, Western Australia - Cities Project Perth Report*, Geoscience Australia, Canberra. [https://www.ga.gov.au/image\\_cache/GA6529.pdf](https://www.ga.gov.au/image_cache/GA6529.pdf)
- Somerville P. G., Graves R. W., Collins N. F., Song S. G. and Ni S. 2009a. *Ground motion models for Australian earthquakes*. Report to Geoscience Australia, 29 June 2009.
- Somerville P., Graves R., Collins N., Song S. G., Ni S. and Cummins P. 2009b. *Source and ground motion models for Australian earthquakes*. Proceedings of the 2009 Australian Earthquake Engineering Society Conference, 11-13 December 2009, Newcastle.
- Standards Australia. 2007a. *Minimum design loads on structures (known as the SSA Loading Code), AS1170.4-2007 Part 4: Earthquake loads (2nd edition)*. Standards Australia (Standards Association of Australia), Homebush, NSW.
- Standards Australia. 2007b. *Minimum design loads on structures (known as the SSA Loading Code), AS1170.4 Supp 1-2007 Part 4: Earthquake loads - Commentary*. Standards Australia (Standards Association of Australia), Homebush, NSW.
- Stein S. and Liu, M. 2009. Long aftershock sequences within continents and implications for earthquake hazard assessment. *Nature* **462**, 87-89.
- Stepp J. C. 1972. *Analysis of completeness of the earthquake sample in the Puget Sound area and its effect on statistical estimates of earthquake hazard*. First Microzonation Conference, Seattle. pp. 897-909.
- Thomas, P., Wong, I. and Abrahamson, N., 2010. *Verification of Probabilistic Seismic Hazard Analysis Computer Programs*, PEER Report 2010/106.
- Toda S., Stein R. S., Reasenberp P. A., Dieterich J. H. and Yoshida A. 1998 Stress transferred by the 1995  $M_w$ 6.9 Kobe, Japan shock: effect of aftershocks and future earthquake probabilities. *Journal of Geophysical Research* **103**, 24543–24565.
- Toro G. R., Abrahamson N. A. and Schneider J. F. 1997. Model of strong ground motions from earthquakes in central and eastern North America: best estimates and uncertainties. *Seismological Research Letters* **68**, 41-57.

- Wells D. L. and Coppersmith K. J. 1994. New empirical relationships among magnitude, rupture length, rupture width, rupture area, and surface displacement. *Bulletin of the Seismological Society of America* **84**, 974-1002
- Wessel, P., and Smith, W. H. F., 1998. New, improved version of the Generic Mapping Tools Released, *Eos Trans. AGU* **79**, 579.
- Wheeler, R. L. 1995. Earthquakes and the cratonward limit of Iapetan faulting in eastern North America. *Geology* **23**, 105-108.
- Wheeler, R. L. 1996. Earthquakes and the southeastern boundary of the intact Iapetan margin in Eastern North America. *Seismological Research Letters* **67**, 77-83.
- Wheeler, R. L. 2009. Sizes of the largest possible earthquakes in the Central and Eastern United States- Summary of a workshop, September 8-9, 2008, Golden, Colorado. United States Geological Survey Open-File Report 2009-1263.
- Wheeler, R. L., and Frankel, A. 2000. Geology in the 1996 USGS Seismic Hazard Maps, Central and eastern United States. *Seismological Research Letters* **71**, 273-282.
- White R. E. 1968. A local magnitude scale for South Australian earthquakes. *Bulletin of the Seismological Society of America* **58**, 1041-1057.
- Wiemer, S., and M. Wyss (1997). Mapping the frequency-magnitude distribution in asperities: An improved technique to calculate recurrence times?, *J. Geophys. Res.* **102**, 15,115-15,128.
- Wiemer S. and Wyss M. 2000. Minimum magnitude of complete reporting in earthquake catalogs: examples from Alaska, the Western United States, and Japan. *Bulletin of the Seismological Society of America* **90**, 859-869.
- Wilkie J. R. 1996. Earthquake source parameters, Victoria, Australia, La Trobe University, Melbourne. PhD, 218.
- Wilkie, J., Gibson, G., Wesson, V. 1994. Richter magnitudes and site corrections using vertical component seismograms, *Australian Journal of Earth Sciences*, **41:3**, 221-228.
- Wills, C. J., M. Petersen, W. A. Bryant, M. Reichle, G. J. Saucedo, S. Tan, G. Taylor, and J. Treiman (2000). A site-conditions map for California based on geology and shear-wave velocity, *Bull. Seism. Soc. Am.* **90**, S187-S208.
- Wheeler R. L. 2009a. Methods of  $M_{\max}$  Estimation East of the Rocky Mountains. *US Geological Survey Open-File Report 2009-1018*. 48 p.
- Wheeler R. L. 2009b. Sizes of the largest possible earthquakes in the Central and Eastern United States - Summary of a workshop, September 8-9, 2008, Golden, Colorado. *US Geological Survey Open-File Report 2009-1263*. 308 p.
- Youngs, R. R., S.-J. Chiou, W. J. Silva, and J. R. Humphrey (1997). Strong ground motion attenuation relationships for subduction zone earthquakes, *Seism. Res. Lett.* **68**, 58-73.
- Zhao, J. X., J. Zhang, A. Asano, Y. Ohno, T. Oouchi, T. Takahashi, H. Ogawa, K. Irikura, H. K. Thio, P. G. Somerville, Y. Fukushima, and Y. Fukushima (2006). Attenuation relations of strong ground motion in Japan using site classification based on predominant period, *Bull. Seism. Soc. Am.* **96**, 898-913.

## 7. Appendix A: Logic Used for the Development of the Earthquake Catalogue

*T. I. Allen*

### 7.1 INTRODUCTION

This appendix describes the development of the earthquake database that will form the basis of the 2012 Australian Earthquake Hazard Map (AUSTCAT).

The catalogue is a composite catalogue and draws on information from the existing catalogues listed below. The format of the spatial area covered is: longitude1/longitude2/latitude1/latitude2.

- 1) GG-Cat: An earthquake catalogue compiled by Gary Gibson.
  - a. Covers the area 110/156/-48/-10 from 1788-06-22 to 2010-05-26
- 2) QUAKES: GA's catalogue of Australian and regional events.
  - a. Covers the area 110/155/-45/-9 from 1902-05-07 to 2010-08-26
- 3) ISC AUST: All earthquakes in the International Seismological Centre's catalogue attributed to the network AUST. This catalogue was primarily included to assist with the validation of catalogue magnitudes to determine the stations used to locate each event.
  - a. Covers the areas 111.856/155.235/-44.920/-10.350 from 1967-01-31 to 2008-04-30
- 4) ISC Timor/Banda Sea: Additional earthquakes not captured in GG-Cat. These data were added to calibrate recurrence for offshore seismic sources that may affect northern Australia. Covers the area (from 1906-06-14 to 2011-04-17):
  - a. West: 108/110/-50/-10
  - b. North: 108/160/-10/-4
  - c. East: 156/160/-50/-10
- 5) QEDB: Queensland earthquake catalogue compiled by J. Rynn and D. Weatherly. Covers state of Queensland and adjacent regions from 1866-12-29 to 2009-12-31

### 7.2 STEPS TO CREATE MASTER CATALOGUE (MDAT):

- Parse each of the individual catalogues into Matlab mat files using m-code scripts. When parsing ISC locations with multiple location solutions, use the following logic to select preferred location:
  - if available, use EHB location
  - select solution with lowest error with gap angle less than 180 degrees
  - if no solution applicable, select solution with maximum ISC solution ID assuming it is the most recent and robust
  - IDC preferred locations are removed for events of ISC median magnitude LT 5.0
- Append GG-Cat to ISC (offshore) catalogue
- Merge ISC AUST to mdat.
- Merge QUAKES to mdat
- Merge QEDB to mdat

- Create preferred catalogue parameters using the following order for finding preferred source for each magnitude type:
  - $M_W$ : GG-Cat, HRVD, NEIC, AUST, Allen (2006, 2007), QEDB, Other
  - $M_S$ : GG-Cat, ISC, PAS, AUST, QEDB, Other
  - $m_b$ : GG-Cat, ISC, AUST, NEIC, IDC, QEDB, Other
  - $M_L$ : GG-Cat (MEL for lat  $\leq -36$  & lon  $\geq 141$  or lat  $\leq -29$  & lon  $\geq 149$  [from 1993 SCA network]), AUST, ISC, GG-Cat (MEL other), QEDB, Other
  - Other  $M$ : GG-Cat, QEDB
- Preferred magnitude types as listed in order above (larger of  $m_b / M_S$  chosen). Earthquakes with unknown magnitude types are assumed to be equivalent to  $M_L$

### 7.3 STEPS TO REVISE LOCAL MAGNITUDES, $M_L$

- Get approximate seismic station open and close times
- Assign zone for correcting magnitudes from the following polygons (see Fig. 5 in main text):
  - walon = [129 110. 110. 135.0 135.0 138.3 138.3 129];
  - walat = [-10 -18.5 -45 -45 -29 -29 -10 -10];
  - ealon = [138.3 138.3 141.0 141.0 155.5 155.5 145.5 138.3];
  - ealat = [-10 -29 -29 -45 -45 -18 -10 -10];
  - salon = [135 135 141 141 135];
  - salat = [-29 -40 -40 -29 -29];
- Get station list that recorded each earthquake, either from:
  - ISC catalogue directly
  - Lookup table of active Australian seismograph stations within 1,500 km of the epicentre assuming documented open and close dates
    - If stations open from mid-2007, assume they are currently open
- With station distribution, undertake  $M_L$  correction assuming the methodology of Allen *et al* (2010) under the following criteria
  - Zone 1: Central and Western Australia
    - Correct pre-1990 events to Gaull and Gregson (1991) assuming Richter (not ADE solutions)
    - Correct pre-1968 ADE events to Gaull and Gregson (1991) assuming Richter
    - Correct events with unknown magnitude types (inc  $M_P$ ,  $M_D$ ,  $MLI$ ) to Gaull and Gregson (1991) assuming Richter
  - Zone 2: Eastern Australia
    - Correct pre-1990 events to Michael-Leiba and Malafant (1992) assuming Richter (not MEL solutions)
    - Correct pre-1994 MEL events to Michael-Leiba and Malafant (1992) assuming Richter
    - Correct post-2002 MEL events to Michael-Leiba and Malafant (1992) assuming Richter
    - Correct 1994-2002 MEL events to Michael-Leiba and Malafant (1992) assuming Wilkie (1996)
    - Correct events with unknown magnitude types (inc  $M_P$ ,  $M_D$ ,  $MLI$ ) to Michael-Leiba and Malafant (1992) assuming Richter

- Zone 3: Mt Lofty and Flinders Ranges
  - Correct pre-1968 ADE events to Greenhalgh and Singh (1986) assuming Richter
  - Correct pre-1986 non-ADE events to Greenhalgh and Singh (1986) assuming Richter
  - Correct events with unknown magnitude types (inc  $M_P$ ,  $M_D$ ,  $MLI$ ) to Greenhalgh and Singh (1986) assuming Richter
- Apply generic magnitude correction for those earthquakes where no station information was available, specifically:

$$M_{L,rev} = 0.93 * M_L \text{ (Richter)} + 0.02. \quad (9.1)$$

Table A.1: List of the 50 largest earthquakes documented to have occurred on the Australian continent. The table indicates original and revised local magnitude estimates, in addition to the preferred magnitude used in these hazard analyses. NSW = New South Wales; NT = Northern Territory, Qld = Queensland; SA = South Australia, Vic = Victoria; WA = Western Australia in this table, ML is local magnitude, MLR is revised local magnitude, mb is body-wave magnitude, MS is surface-wave magnitude, MP is intensity-based magnitude, and M is the preferred magnitude. Note that M may not necessarily be derived from ML.

DATE	LON	LAT	PREF ML	REV ML	PREF M	M TYPE	LOCATION
1941-04-29 01:35:00	116.197	-26.791			6.8	MS	Meeberrie, WA
1968-10-14 02:58:00	116.98	-31.62	6.9	6.9	6.7	MW	Meckering, WA
1929-08-16 21:28:00	120.66	-16.99			6.6	MS	Off Broome, WA
1988-01-22 12:04:00	133.855	-19.896	6.7		6.6	MW	Tennant Creek, NT
1885-01-05 12:20:00	114	-29			6.5	MS	Off Geraldton, WA
1892-01-26 16:48:00	149.5	-40.4	6.9 (MP)	6.4	6.4	MLR	E of Flinders Is, Tasman Sea
1941-06-27 07:55:00	137.34	-25.95	6.0	5.6	6.4	MW	Simpson Desert, NT
1885-05-12 23:37:00	148.9	-39.9	6.8 (MP)	6.3	6.3	MLR	E of Flinders Is, Tasman Sea
1988-01-22 00:35:00	133.795	-19.866	6.3		6.3	MW	Tennant Creek, NT
1988-01-22 03:57:00	133.839	-19.878	6.4		6.3	MW	Tennant Creek, NT
1897-05-10 05:26:00	139.75	-37.3	6.6 (MP)	6.2	6.2	MLR	Kingston-Beachport, SA
1979-04-23 05:45:00	120.164	-16.616	6.6	5.9	6.2	MW	Rowley Shoals, WA
1997-08-10 09:20:00	124.333	-16.159	6.0		6.2	MW	Collier Bay, WA
1970-03-24 10:35:00	126.673	-22.059	6.7	5.8	6.1	mb	Tobin Lake, WA
1979-06-02 09:47:00	117.104	-30.821	6.2	6.2	6.1	MW	Cadoux, WA

The 2012 Australian Earthquake Hazard Map

DATE	LON	LAT	PREF ML	REV ML	PREF M	M TYPE	LOCATION
1873-12-15 04:00:00	127.5	-26.25			6.0	MS	E of Warburton, WA
1884-07-13 03:55:00	148.5	-40.5	6.4 (MP)	6	6.0	MLR	Cape Barren Island, Tas
1884-09-19 10:27:00	149.5	-40.8	6.4	6	6.0	MLR	E of Flinders Is, Tasman Sea
1910-01-13 00:15:00	155.2	-44.5			6.0	MS	Tasman Sea
1920-02-08 05:24:00	111	-35			6.0	MS	Off Cape Leeuwin, WA
1938-04-17 08:56:00	137.2	-25.5	5.6	5.2	5.9	MW	Simpson Desert, SA
1970-03-10 17:15:00	116.512	-31.093	5.9	5.9	5.9	MLR	Calingiri, WA
1941-05-04 22:07:00	136.9	-26.3	5.2	4.3	5.8	MW	Simpson Desert, SA
1986-03-30 08:53:00	132.734	-26.31	6.0	5.6	5.7	MW	Marryat Creek, SA
1988-01-22 04:18:00	133.569	-20.09	5.7		5.7	ML	Tennant Creek, NT
1988-01-22 12:39:00	133.788	-19.971	5.7		5.7	ML	Tennant Creek, NT
1988-09-30 20:43:00	134.038	-19.89	5.7		5.7	ML	Tennant Creek, NT
2000-12-25 13:24:00	120.052	-42.509			5.7	MW	South of Australia, Southern Ocean
1885-01-30 15:05:00	148.83	-39.81	6.0 (MP)	5.6	5.6	MLR	E of Flinders Is, Tasman Sea
1922-04-10 10:46:00	144.85	-39.14	5.7	5.6	5.6	MLR	King Island, Tas
1931-03-13 21:11:00	144.5	-39.5	5.7 (MP)	5.6	5.6	MLR	NE of King Island, Bass Strait
1946-09-14 19:48:00	149.35	-39.97			5.6	MS	E of Flinders Is, Tasman Sea
1961-05-21 21:40:00	150.606	-34.564	5.6	5.6	5.6	MLR	Robertson, NSW
1975-01-10 08:20:00	126.11	-27.74			5.6	mb	Great Victoria Desert, WA
1976-02-19 02:32:00	114.3	-19.41			5.6	mb	Off Onslow, WA
1989-05-28 02:55:00	130.745	-25.137	5.6		5.6	ML	Mt Olga, NT
1883-08-28 16:55:00	151.7	-25.5	5.9 (MP)	5.5	5.5	MLR	Gayndah, Qld
1884-03-28 13:12:00	148.9	-41.2	5.9 (MP)	5.5	5.5	MLR	Tasman Sea
1884-05-10 21:30:00	148.9	-41.2	5.9 (MP)	5.5	5.5	MLR	Tasman Sea

DATE	LON	LAT	PREF ML	REV ML	PREF M	M TYPE	LOCATION
1885-03-20 23:03:00	149.5	-40.5	5.9 (MP)	5.5	5.5	MLR	E of Flinders Is, Tasman Sea
1902-09-19 10:35:00	138	-35	6.0	5.5	5.5	MLR	Warooka, SA
1903-07-14 10:28:00	142.533	-38.433	5.6 (MP)	5.5	5.5	MLR	Warrnambool, Vic
1907-01-31 07:50:00	148.5	-39.5	5.9 (MP)	5.5	5.5	MLR	E of Flinders Is, Tasman Sea
1922-02-28 15:00:00	145	-39	5.5 (MP)	5.5	5.5	MLR	Bass Strait, Vic
1934-11-18 21:58:00	149.2	-34.8	5.6 (MP)	5.5	5.5	MLR	Gunning, NSW
1937-12-20 22:35:00	136.5	-25.5	5.6	5.2	5.5	MW	Simpson Desert, NT
1941-05-04 23:24:00	136.9	-25.3			5.5	MS	Simpson Desert, NT
1963-02-26 14:10:00	121.2	-22.2			5.5	mb	E of Nullagine, WA
1966-05-03 19:07:00	147.168	-37.042	5.5	5.5	5.5	MLR	Mt Hotham, Vic
1970-02-16 21:20:00	111.65	-20.07			5.5	mb	Off North West Cape, WA
1973-03-09 19:09:00	150.34	-34.187	5.5	5.5	5.5	MLR	Burratorang, NSW
1978-05-06 19:52:00	126.56	-19.55	6.2	5.5	5.5	MLR	Christmas Creek, WA
1979-06-07 06:45:00	117.308	-30.761	5.5	5.5	5.5	MLR	Cadoux, WA
1988-01-27 11:27:00	133.918	-19.759	5.5		5.5	ML	Tennant Creek, NT
1988-01-29 10:19:00	133.956	-19.771			5.5	mb	Tennant Creek, NT
1989-10-13 09:59:00	122.407	-17.666	5.4		5.5	MW	NE of Broome, WA
1990-01-17 06:38:00	116.99	-31.72	5.5		5.5	ML	S of Meckering, WA
1997-05-09 06:31:00	118.009	-44.29	4.3		5.5	MW	South of WA, Southern Ocean

#### 7.4 $M_B$ TO $M_W$ CONVERSION FACTORS

The conversion of most magnitude types in the Australian earthquake catalogue to  $M_W$  was largely possible through the application of published conversion factors. However, through the present analyses, it was found that existing  $m_b$  to  $M_W$  conversion equations were not necessarily appropriate for the Australian earthquake catalogue. Consequently, an Australian-specific conversion was developed. Body-wave magnitude for those earthquakes that also possess a  $M_W$  value within continental Australia were extracted from the earthquake catalogue for earthquakes of magnitude  $3.5 \leq m_b \leq 6.5$ . Similarly to the relationships developed for  $M_L$ , a bi-linear relationship was found to be the most appropriate for Australian earthquakes.

$$\begin{aligned}
 M_W &= 0.77m_b + 0.81 && \text{for } m_b \leq 5.1 \\
 M_W &= 0.77m_b + 0.69(m_b - 5.1) + 0.81 && \text{for } m_b > 5.1
 \end{aligned}
 \tag{9.2}$$

Equation 9.2 is applicable for  $3.5 \leq m_b \leq 6.5$  and the relationship has a standard deviation of 0.34 magnitude units.

## 7.5 AUSTCAT FIELDS

DATESTR:	Date string of earthquake
DATENUM:	Number of days since 1 Jan 0000 (used in matlab)
TYPE:	Event type manually classified by Gary Gibson (e.g. local event, blast, coal blast, teleseismic)
DEPENDENCE:	Describes dependence of event as classified by Gary Gibson (e.g. mainshock, aftershock, foreshock)
LON:	Preferred event longitude
LAT:	Preferred event latitude
DEP:	Preferred event depth
LOCSRC:	Preferred location source
PREFMW:	Preferred observed MW
PREFMWSRC:	Preferred source of MW
PREFMS:	Preferred observed MS
PREFMSSRC:	Preferred source of MS
PREFmb:	Preferred observed mb
PREFmbSRC:	Preferred source of mb
PREFML:	Preferred observed ML
PREFMLSRC:	Preferred source of ML
REVML:	Revised ML using OBSML corrected using logic described above
OTHERM:	Other magnitude type not captured above
OTHERMTYPE:	Type of other magnitude (e.g. MD, MP)
OTHERMSRC:	Source of other magnitude type
MX_ORIGML:	Takes preferred magnitude type and preserves original ML (PREFML) if ML preferred type. Field also merges other magnitude types assumed to be equivalent to ML (e.g. MP, M?)
MX_REVML:	Same as MX_ORIGML, but applies ML corrections to original ML (PREFML)
MX_ORIGMLSRC:	Source of MX_ORIGML
MS2MW:	MS converted to MW using relations of Scordilis (2006) where applicable
mb2MW:	mb converted to MW using relations of presented above
ML2MW:	ML converted to MW using relations of Allen <i>et al.</i> (2011) for Australian events (CWA, EA and MLFR)
ML2MWG:	ML converted to MW using relations of Grünthal <i>et al.</i> (2009) for all events
PREFMW:	Preferred MW using logic above
PREFMWSRC:	Source of preferred MW
COMM:	Any comments from GG-Cat or ISC associated with event - usually location

## 7.6 REFERENCES

- Allen, T. I., D. R. Burbidge, D. Clark, A. A. McPherson, C. D. N. Collins, and M. Leonard (2011). Development of the next generation Australian National Earthquake Hazard Map, Proceedings of the 9th Pacific Conference on Earthquake Engineering, Auckland, New Zealand.
- Allen, T. I., P. R. Cummins, T. Dhu, and J. F. Schneider (2007). Attenuation of ground-motion spectral amplitudes in southeastern Australia, *Bull. Seism. Soc. Am.* 97, 1279–1292.
- Allen, T. I., T. Dhu, P. R. Cummins, and J. F. Schneider (2006). Empirical attenuation of ground-motion spectral amplitudes in southwestern Western Australia, *Bull. Seism. Soc. Am.* 96, 572–585.

- Gaull, B. A., and P. J. Gregson (1991). A new local magnitude scale for Western Australian earthquakes, *Aust. J. Earth. Sci.* 38, 251-260.
- Greenhalgh, S. A., and R. Singh (1986). A revised magnitude scale for South Australian earthquakes, *Bull. Seism. Soc. Am.* 76, 757-769.
- Grünthal, G., R. Wahlström, and D. Stromeyer (2009). The unified catalogue of earthquakes in central, northern, and northwestern Europe (CENEC)—updated and expanded to the last millennium, *J. Seismol.* 13, 517–541.
- Michael-Leiba, M., and K. Malafant (1992). A new local magnitude scale for southeastern Australia, *BMR J. Aust. Geol. Geophys.* 13, 201-205.
- Scordilis, E. M. (2006). Empirical global relations converting MS and mb to moment magnitude, *J. Seismol.* 10, 225–236.
- Wilkie, J. R. (1996). Earthquake source parameters, Victoria, Australia, La Trobe University, Melbourne. PhD, 218.

## 8. Appendix B: Sources of earthquake solutions in the catalogue

*C. D. N. Collins*

The primary source of data for the earthquake catalogue developed for the 2012 National Earthquake Hazard Map was GG-Cat. The earthquake solutions in GG-Cat (2010 version) are attributed to 62 sources. Some of these reflect changes in the names of the agencies responsible (e.g. BMR, AGSO, AUST refer to what is now Geoscience Australia) or changes in the source name used for the same agency (e.g. MUN, MGO).

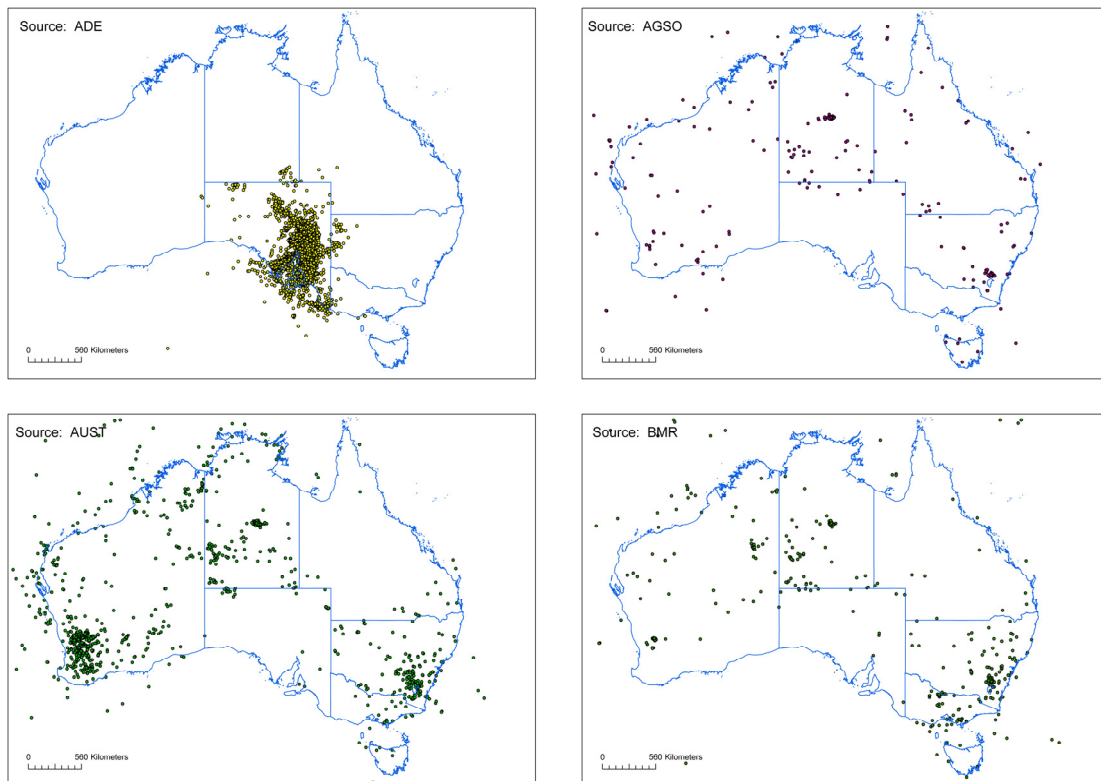
### 8.1 SOURCES IN GG-CAT 2010

ABE	Abe (1981, 1982, 1984) Catalog of Large Earthquakes, 1897-1980.
ADE	Adelaide (University of Adelaide, Flinders University, PIRSA, DMITRE)
AGSO	Australian Geological Survey Organisation
AUST	Australian Geological Survey Organisation Geoscience Australia
BCIS	Bureau Central International Seismologique
BJI	Beijing, China Earthquake Administration
BMR	Bureau of Mineral Resources
BRS	University of Queensland, Brisbane
BurkeG	Burke-Gaffney, Riverview Observatory, Sydney
CAN	Australian National University, Canberra
Cotton	L. A. Cotton, University of New South Wales
CQU	Central Queensland University, Rockhampton
Denham	David Denham
DES	Doyle, Everingham and Sutton, 1968, Jnl GSA, 15, pt2, 295-312
DJA	Lembaga Meteorologi dan Geofisika, Jakarta, Indonesia
Doyle	Hugh Doyle
Drake	Laurie Drake, Riverview Observatory, Sydney
E.T.	Everingham and Tilbury, 1972, Jnl Royal Soc of WA, 55, 3, 90-96
EHB	Centennial Catalogue (Engdahl-Hilst-Buland)
EIDC	Experimental International Data Center
ERL	Earthquake Research Lab, San Francisco, California
G&R	Gutenberg and Richter (1954) catalogue, 1904-1952.
Garran	
GG	Gary Gibson, Environmental Systems and Services
Gliddon	
GSQ	Geological Survey of Queensland
HDR	unknown agency code, Indonesia 1993
Holmes	Holmes, W.M., 1933, Trans Royal Soc Vic, 45, 2, 150-151
IDC	International Data Center
ISC	International Seismological Centre
ISM	Unknown source quoted by BMR, 1972 February and March (NOT ISC)
ISS	The International Seismological Summary, 1918-1963
JMA	Japan Meteorological Agency, Tokyo, 1926-present
Joklik	Gunning NSW earthquakes, Joklik and Casey 1952
Jones	Unknown source, Queensland, 1950-1957
KMcC	Kevin McCue, Canberra
Leiba	Marion Leiba, Canberra
LEM	Lembang, Indonesia, 1959-1961, see DJA

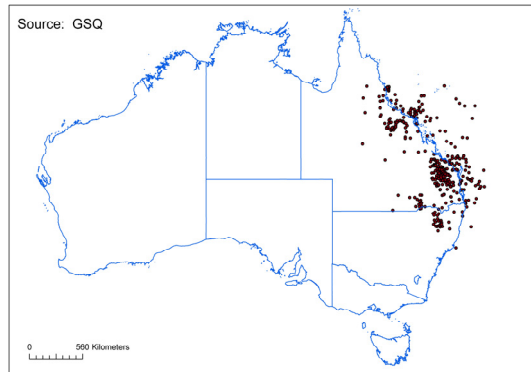
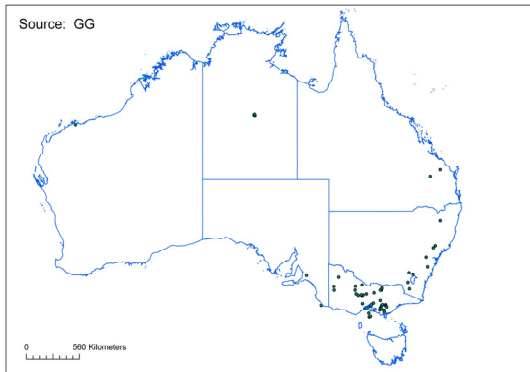
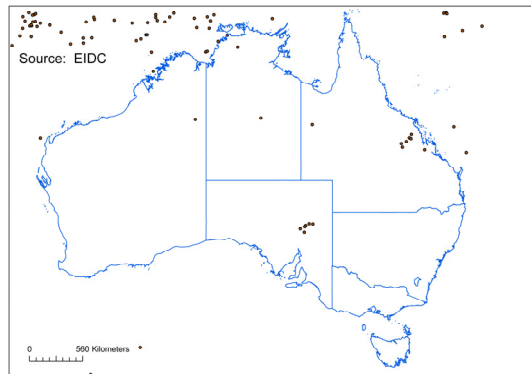
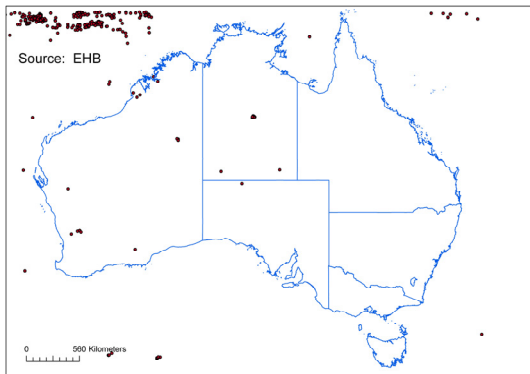
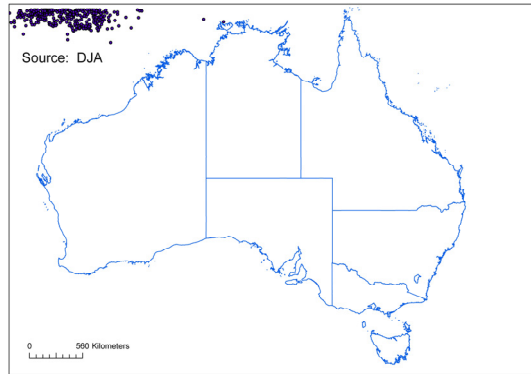
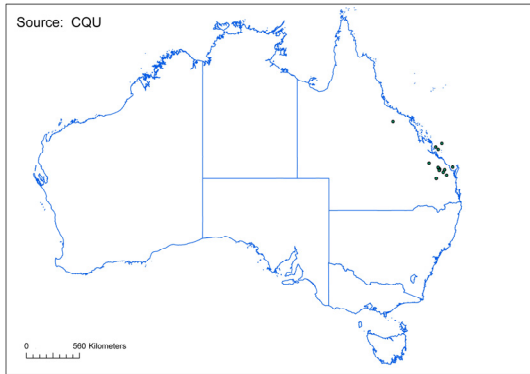
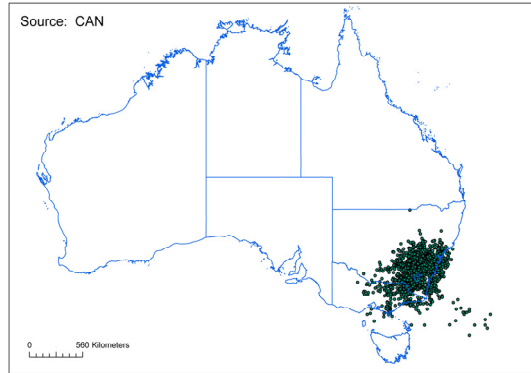
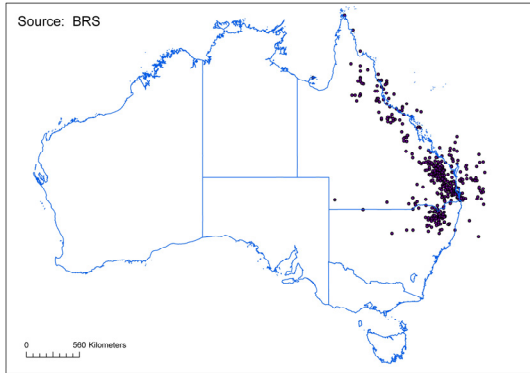
**The 2012 Australian Earthquake Hazard Map**

Malpas	Katherine Malpas, Adelaide
McArdle	Alison McArdle, Adelaide
MEL	Seismological Research Centre, Melbourne, Victoria
MELOBS	Melbourne Observatory
MGO	Mundaring Geophysical Observatory, Western Australia
MOS	Institute of Physics of the Earth, Moscow, Russia
MUN	Mundaring Geophysical Observatory, Western Australia
NEIC	National Earthquake Information Center
NEIS	National Earthquake Information Service
Osburne	Unknown source, Warrnambool earthquake, 1848
PEK	Peking, until 1987-12-31, recoded as BJI, Beijing, from 1988-01-01
Qld Met	Meteorological Bureau, Queensland, 1866-1912
RC	Russell Cuthbertson, Environmental Systems and Services, Brisbane
RobUnd	Rob Underwood
Rynn	Jack Rynn, Centre for Earthquake Research in Australia, Brisbane
SEQW	South East Queensland Water, Brisbane
Spennemann	Dirk Spennemann, Charles Sturt University, New South Wales
Sykes	Catalogue of SCR earthquakes, 1900-1989, Pacheco and Sykes (1992)
TAU	University of Tasmania, Australia
Underwood	Rob Underwood
UQ	University of Queensland (Now deleted, references re-coded as BRS)
USCGS	US Coast and Geodetic Survey
USGS	US Geological Survey

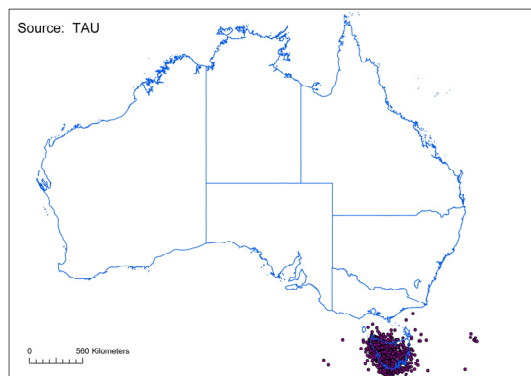
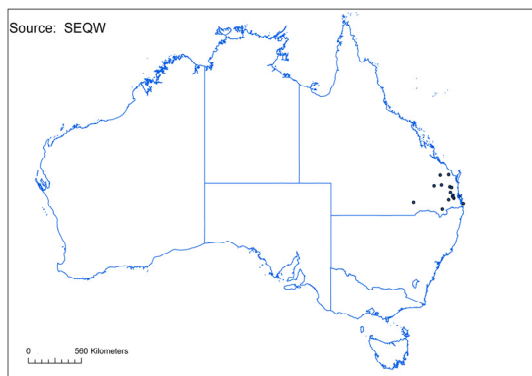
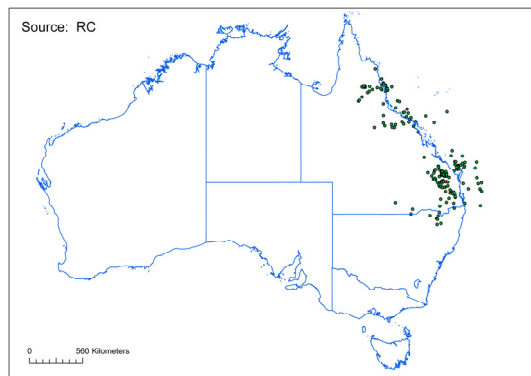
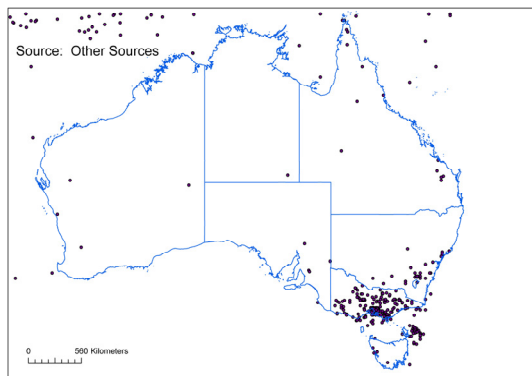
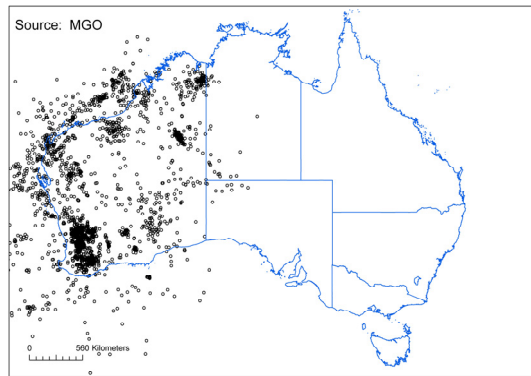
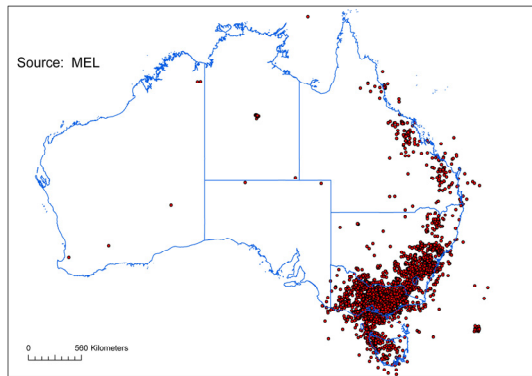
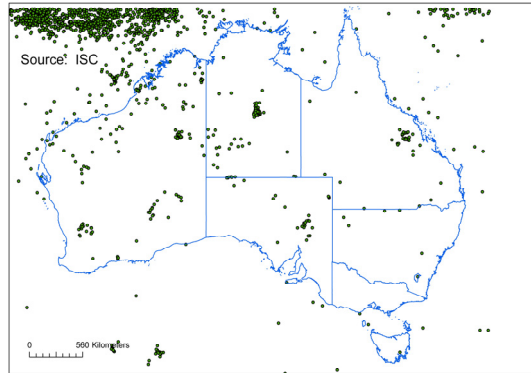
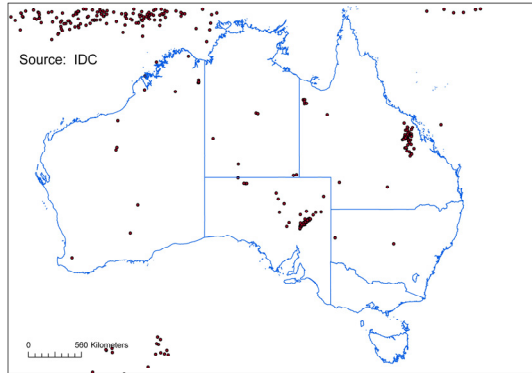
The distributions of earthquakes which are attributed to the above sources in the catalogue are shown in the maps in [Figure B 1](#).



# The 2012 Australian Earthquake Hazard Map



# The 2012 Australian Earthquake Hazard Map



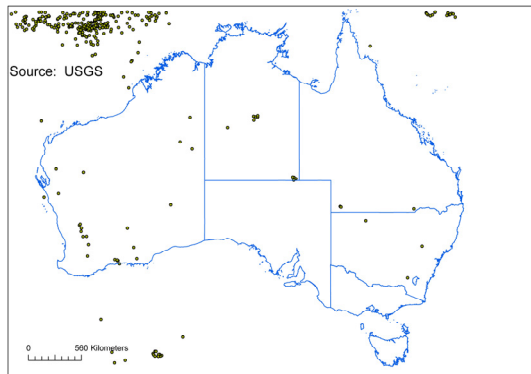


Figure B 1 Distribution of earthquakes by Source in GG-Cat (2010).

## 8.2 REFERENCES

- Abe, K., 1981, Magnitudes of large shallow earthquakes from 1904 to 1980: *Physics of the Earth and Planetary Interiors*, v. 27, p. 72-92.
- Abe, K., 1982, Magnitude, seismic moment and apparent stress for major deep earthquakes, *Journal of the Physics of the Earth*, v. 30, p. 321-330.
- Abe, K., 1984, Complements to "magnitudes of large shallow earthquakes from 1904 to 1983". *Physics of the Earth and Planetary Interiors*, v. 34, p. 17-23.
- Doyle, H.A., Everingham, I.B., and Sutton, S.J., 1968, Seismicity of the Australian Continent: *Journal of the Geological Society of Australia*, 15 (2), 295-312.
- Everingham, I.B. and Tilbury, L. (1972) Information on Western Australian earthquakes 1849-1960. *Royal Society of Western Australia. Journal* 55, 90-96.
- Gutenberg, B., and Richter, C.F., 1954, *Seismicity of the earth and associated phenomena*; Princeton University Press, Princeton, N.J.
- Holmes, W.M., 1933. *Transactions of the Royal Society of Victoria*, 45, 2, 150-151.
- Joklik G.F. and Casey N. J., 1952. Gunning-District, N.S.W. Earth Tremors, November, 1952. Bureau of Mineral Resources Record, 1952/91.
- Pacheco J. F. and Sykes L. R. 1992. Seismic moment catalog of large shallow earthquakes, 1900 to 1989: *Bulletin of the Seismological Society of America*, v. 82, no. 3, p. 1306 - 1349.

## 9. Appendix C: Effectiveness of the catalogue declustering

*M. Leonard*

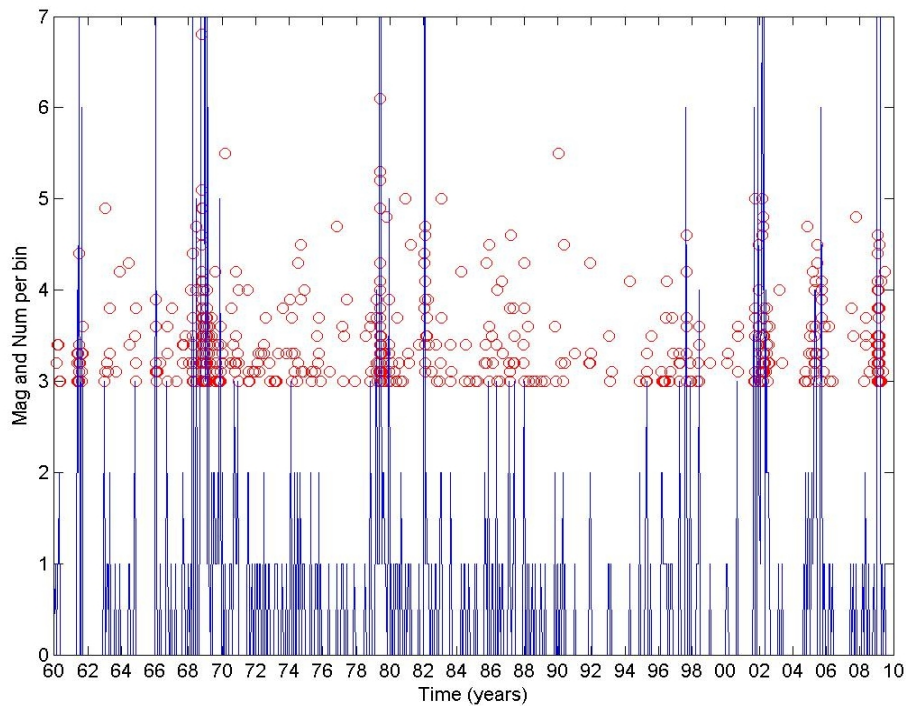
### 9.1 INTRODUCTION

A declustered earthquake catalogue should be approximately Poissonian in time (e.g., Gardner and Knopoff, 1974). Consequently, an ideal declustering algorithm should produce an approximately Poisson distribution. The initial algorithm (hereafter referred to as Method 2) from Leonard (2008) was found to not be effective in removing all dependent (foreshocks and aftershocks) events. As discussed in [Section 2.5](#) this algorithm was modified using the findings of Stein and Liu (2009) – called Method 3. This was combined with Method 2 in reverse time to remove foreshocks (Method 4) and the expert judgement of Gary Gibson (Method 1) to give a three step removal process. To test the effectiveness of this declustering process the clustered and declustered catalogues were compared to the theoretical Poisson distributions.

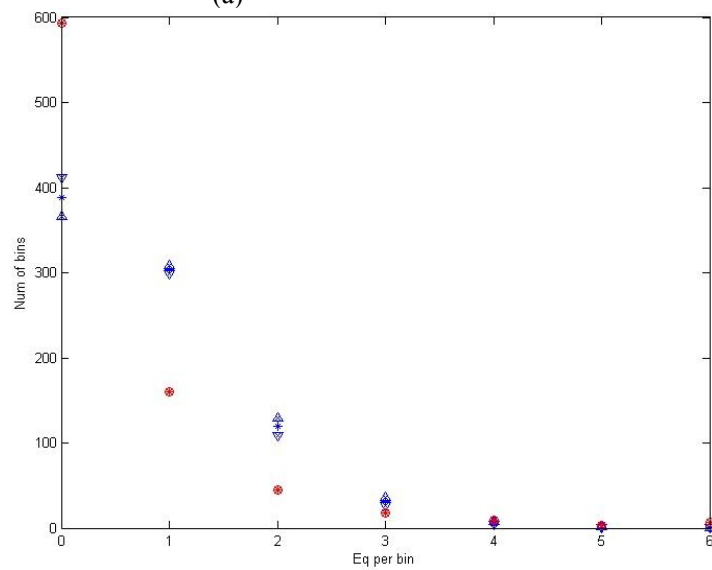
### 9.2 YILGARN (ZONE 25)

The Yilgarn region of Western Australia (Zone 25 in [Figure 12](#)). This area tends to have very active aftershock sequences, earthquake swarms and clusters of related earthquakes. Due to major changes to the seismic network the catalogue also has a high degree of variability in its epicentral accuracy. These factors make declustering the catalogue from this region challenging.

The distribution of earthquakes in time and their Poisson statistics are shown in [Figure C 1](#). The number of bins over the time period was chosen to be approximately 1.33 times the number of earthquakes, giving an average probability of 0.75 for an earthquake to occur in a cell. This gives a theoretical Poisson probability of six or more earthquakes occurring in a single bin of 0.0001. Consequently, in a catalogue of 640 earthquakes in 850 cells the probability of six or more earthquakes occurring in a bin is 0.1. As can be seen from [Figure C 1a](#), there are numerous bins with six or more earthquakes. This is reflected in the Poisson distribution ([Figure C 1b](#)) where there are more bins than expected with zero earthquakes, less bins than expected with one and two earthquakes, and more bins than expected with five or more earthquakes.



(a)



(b)

Figure C 1 (a) The occurrence of all earthquakes  $M$  greater than or equal to 3.0 in the Yilgarn region of Western Australia between 1960 and 2010. The red circles are the individual earthquakes and the blue data are the number of earthquakes in each 21 day bin. (b) the Poisson statistics of the earthquake catalogue The blue diamonds are the theoretical Poisson distribution for 640 temporally random earthquakes in 850 bins, with the blue triangles being the 1 sigma uncertainties. The red circles are the actual count of the number of bins containing zero to 6 earthquakes – effectively a horizontal summation of the data in (a). Note that the very many bins with more than 6 earthquakes are not shown, but are all inconsistent with a Poisson distribution.

Performing the same analyses using the declustered catalogue, almost all the peaks observed in the original catalogue are removed except for the spike in activity in late 2004 and 2005 (Figure C 2a). This spike was the second biggest burst of activity in the Yilgarn since 1980. It consisted of eight earthquakes of  $M$  4.0 or greater. Unlike the localised 2002 Burakin and 2009 Beacon sequences, the events in this spike consisted of five clusters spread over a  $50 \times 80$  km area. As such they were not identified as aftershocks by the combined method described in the previous section. Apart from this burst of activity, the proposed

sequence of algorithms has effectively declustered the catalogue. The final declustered data between 1960 and 2003, shown in [Figure C 3](#), is consistent with a model of temporal Poisson earthquake occurrence.

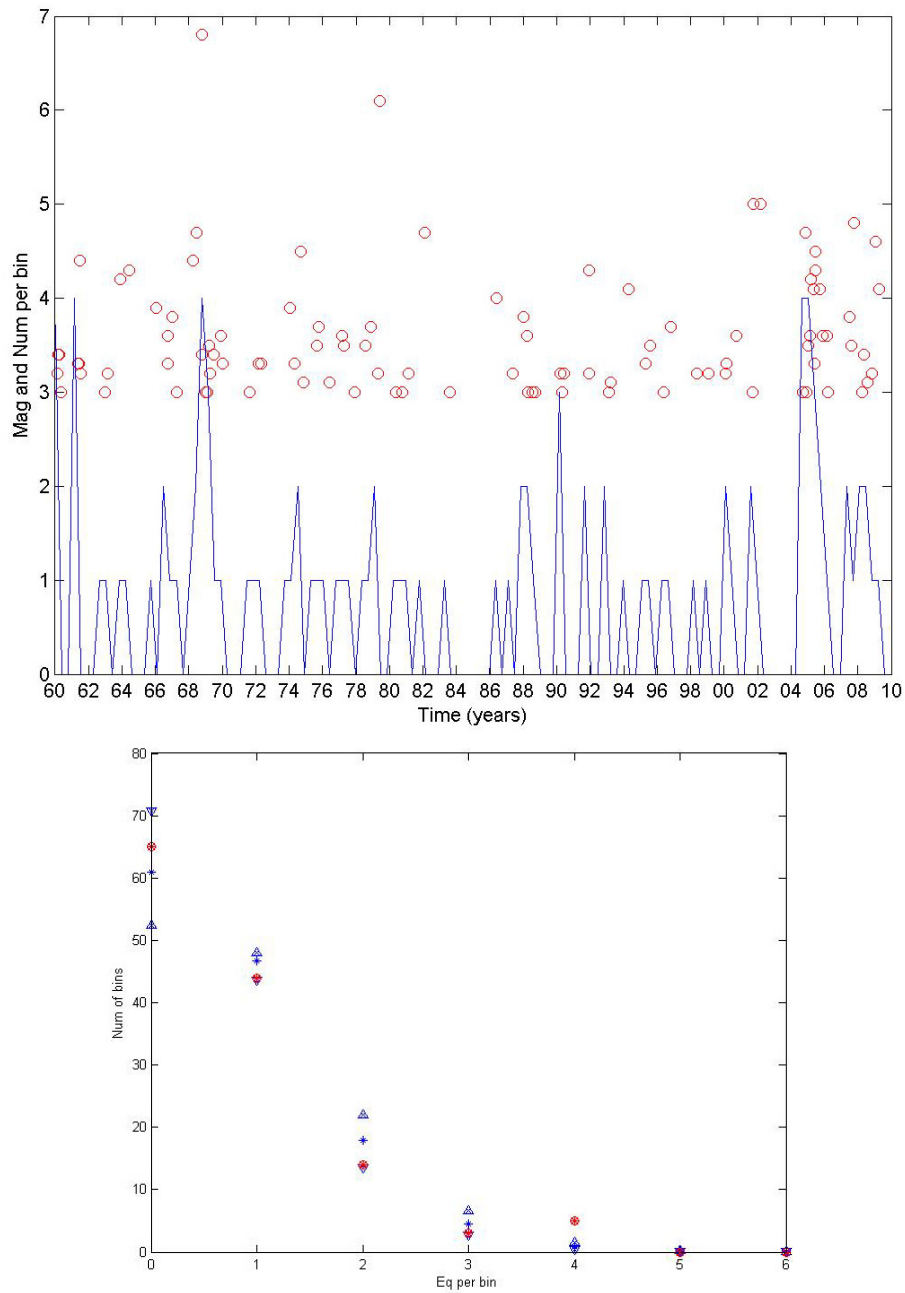


Figure C 2: (a) The declustered catalogue of earthquakes with a magnitude greater than or equal to 3.0 in the Yilgarn region of Western Australia between 1960 and 2010 and (b) the Poisson statistics of the earthquake catalogue.

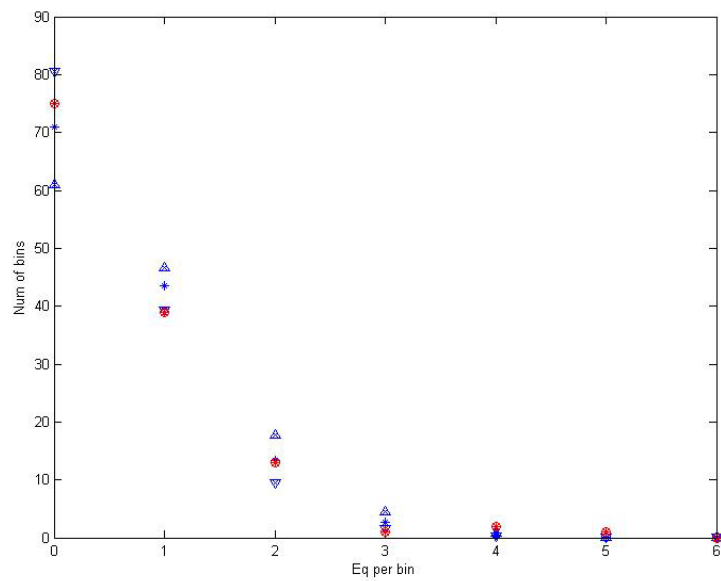


Figure C 3: Poisson statistics for the Yilgarn 1960 to 2002. This data is consistent with the assumption of earthquake occurrence being a Poisson process.

### 9.3 MT LOFTY AND FLINDERS RANGES (ZONE 17)

A similar analysis was undertaken in the Flinders Ranges and Mt Lofty ranges region. The results show that the original catalogue suggests that the temporal distribution of the earthquakes is approximately Poissonian even without declustering (Figure C 4b). The declustered catalogue had temporal distribution of the earthquakes close to a Poisson distribution but with a handful of anomalous periods. Further investigation identified that these anomalies were caused by mining blasts incorrectly identified as earthquakes. When these were removed from the catalogue, the statistics of earthquake occurrence became identical to the theoretical Poisson distribution (Figure C 4 c and d). This raises the possibility that some of the other peaks in activity identified in other areas are unidentified mine blasts.

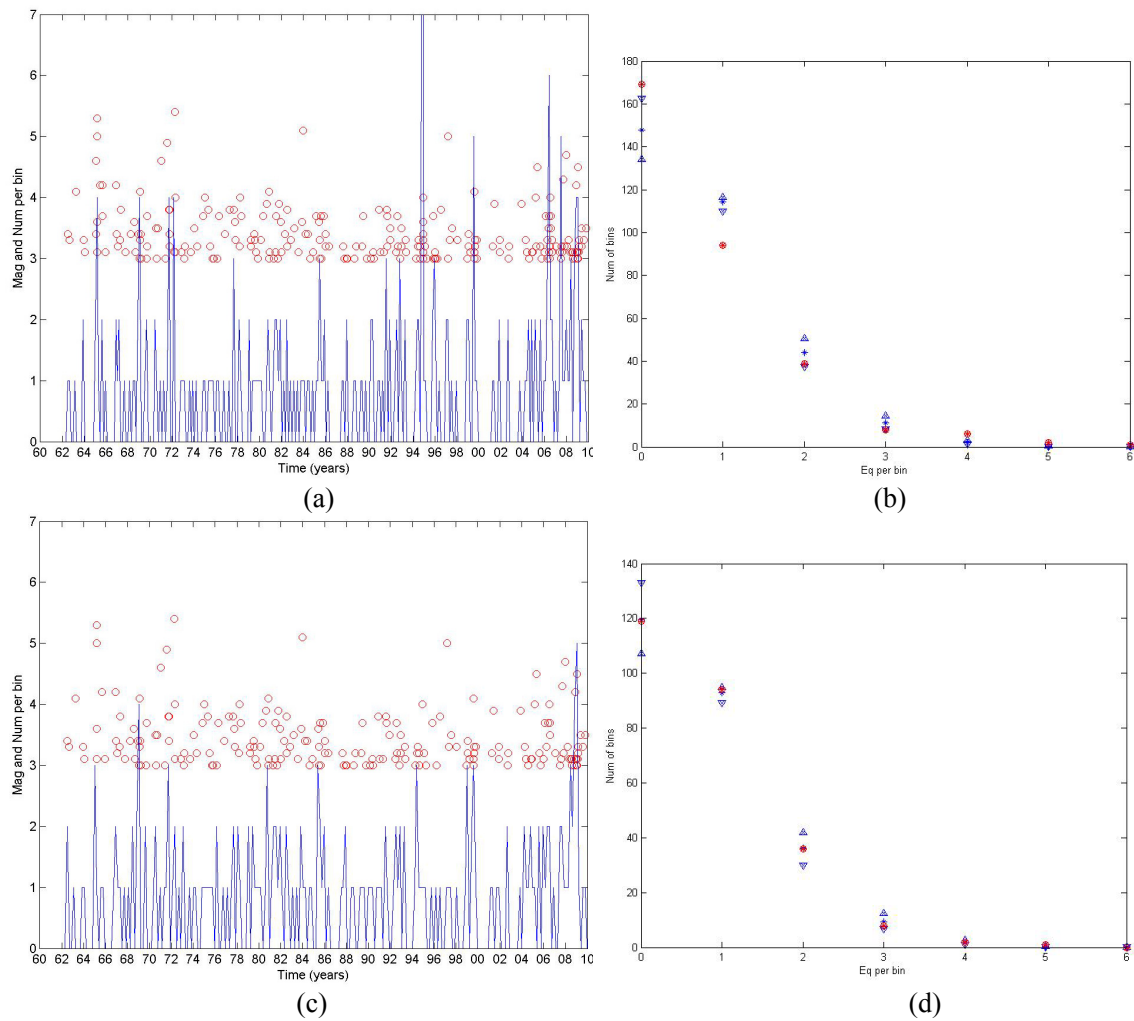


Figure C 4 Occurrence and Poisson data for the Mt Lofty and Flinders Ranges, top row (a and b) are the full catalogue, and the bottom row (c and d) are the declustered and demined catalogue.

## 9.4 SUMMARY

Similar analyses were undertaken for several other regions as well as the entire continent, and information about them is available from the authors on request. In all cases the declustered data closely matched a theoretical Poisson distribution. As such we are confident that the catalogue has been effectively declustered.

# 10. Appendix D: Summary of neotectonic domains model simplification for ground-motion modelling as part of the new Australian National Hazard Map

*D. Clark and A. McPherson*

## 10.1 INTRODUCTION

Herein we present a summary of the generalisation of the Neotectonic Domains Model, as presented in Clark *et al.* (2011, 2012), for the purposes of ground-motion modelling contributing to the development of the new Australian Earthquake Hazard Map. The Clark *et al.* (2011, 2012) model as presented includes crustal types for which no robust ground-motion models are available at the national scale. In order to validly apply existing ground-motion models an aggregation of the seven neotectonic domains by crustal type into three superdomains – ‘cratonic’, ‘non-cratonic’ and ‘extended’ was desirable. This required several simplifications which are not necessarily consistent with the domains model methodology, and so are documented in detail. In particular, domain regions of small areal extent have, in some cases, been incorporated into nearby larger domains. An estimate of  $M_{max}$  for each new superdomain is presented, based solely on 75<sup>th</sup> percentile fault scarp length values.

## 10.2 DOMAIN SIMPLIFICATION

Ground-motion models used in seismic hazard assessment (e.g. Somerville *et al.*, 2009) distinguish between cratonic and non-cratonic crust. In Australia, cratonic crust includes the Archaean and Proterozoic shield areas, and Proterozoic mobile belts, which have not been subject to significant tectonic modification during the Phanerozoic Eon. Non-cratonic crust includes crust that has formed, assembled, or been significantly tectonically modified during the Phanerozoic Eon. The cratonic crustal type is thought to exhibit ground-motion and seismic attenuation characteristics roughly similar to eastern North America (e.g. Somerville, 2001) and non-cratonic similar to western North America (e.g. Somerville *et al.*, 1999). Crust that has been significantly extended during the Mesozoic might be distinguished in terms of its seismic wave attenuation properties from other non-cratonic crust (e.g. Toro *et al.*, 1997). [Table D 1](#) (modified after Clark, 2010) documents the proposed grouping of the neotectonic domains according to this broad crustal type schema. Illustrations of the Clark *et al.* (2011, 2012) domains model, and the revised model are presented in [Figure D 1](#) for comparison.

*Table D 1 Grouping of neotectonic domains (cf. Clark et al., 2011, 2012) by crustal type.*

Domain	Crustal Type		
	cratonic	non-cratonic	extended
1	X		
2		X	
3	X		
4		X	
5			X
6			X
7			X

The 2012 Australian Earthquake Hazard Map

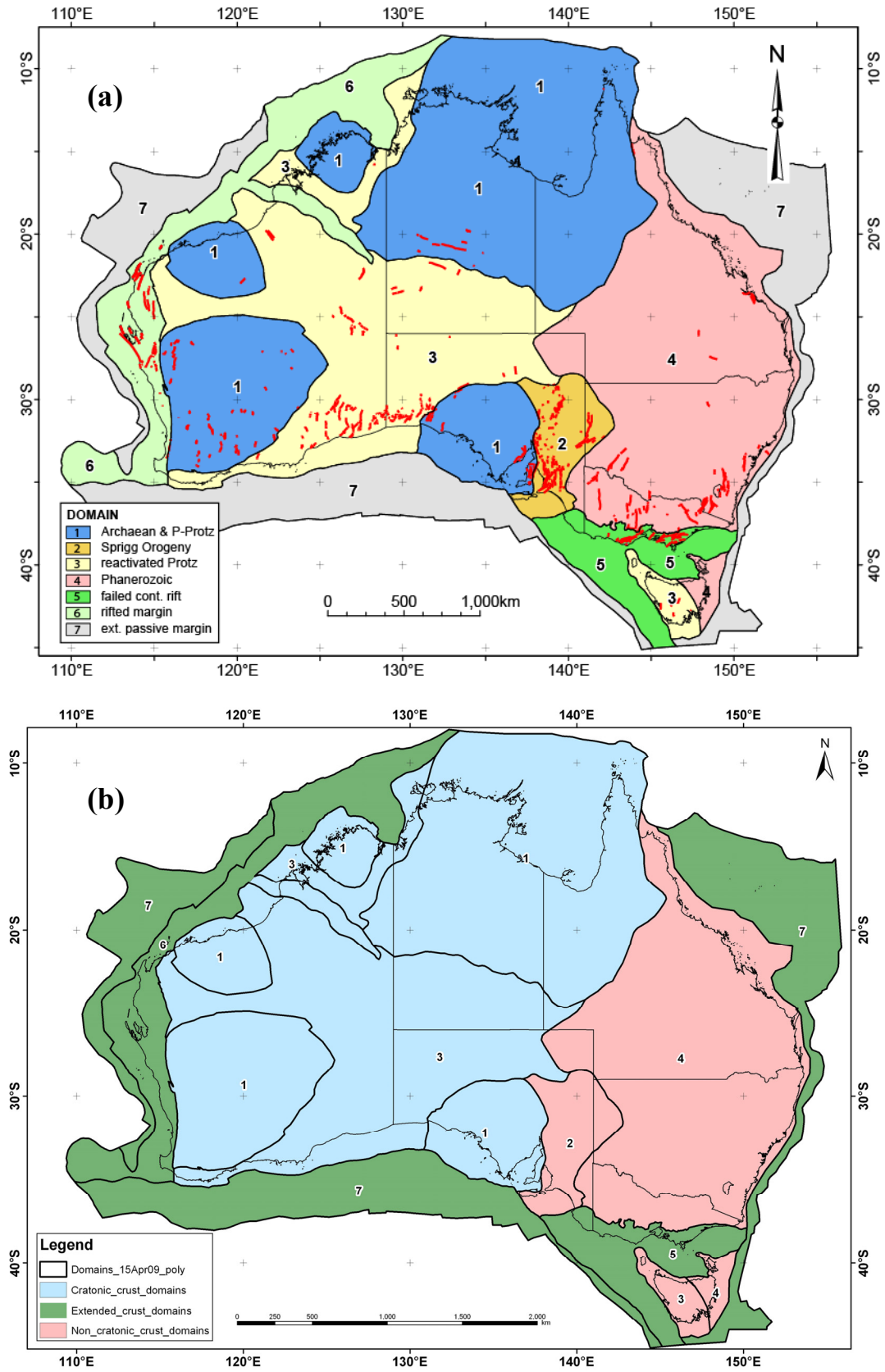


Figure D 1 (a) the neotectonic domains model of Clark et al. (2011, 2012), and (b) domain aggregation into superdomains based upon broad crustal type, as discussed herein.

The separation between cratonic and non-cratonic crust roughly follows the Tasman Line (Glen, 2005) (Figure D-1b). Domain 2 (the Sprigg Orogen) has been assigned to the non-cratonic superdomain. Seismic reflection profiling indicates that a reverse faulting architecture at the surface, which formed largely in the early Palaeozoic Delamerian Orogeny, relates to late Proterozoic asymmetric rift architecture at depth (Flöttmann & Cockshell, 1996). It has been proposed that this rift architecture in some way explains for the concentration of Neogene tectonism within the domain (Clark *et al.*, 2011, 2012), similar to other inverting rift settings in Australia (e.g. the Gippsland, Otway and Carnarvon basins). While this may justify inclusion of the domain in the Extended crust superdomain, the Phanerozoic history of extensive inversion of rift structures near to the surface during the Delamerian Orogeny, leading to the development of a fold and thrust belt architecture (Preiss, 1987; Marshak & Flöttmann, 1996; Paul *et al.*, 1999), has strong affinities with the adjacent Tasmanides (e.g. Glen, 2005). For this reason, Domain 2 has been included in the non-cratonic crust superdomain for the purposes of this analysis.

Simplifications made that are in detail inconsistent with the neotectonic domains model (Clark *et al.*, 2011, 2012) involve the Fitzroy Trough (WA) in the cratonic crust superdomain, and western Tasmania, in the non-cratonic crust superdomain. The Fitzroy Trough is the deepest Palaeozoic depocentre of the Canning Basin, and has the most fully developed extensional architecture of the basin (Yeates *et al.*, 1984). Limited reactivation of the marginal structures of the trough during the Mesozoic (Drummond *et al.*, 1987, 1991) and Tertiary (Keep *et al.*, 2007) has been documented, similar to the eastern margins of the northern Perth and southern Carnarvon basins (Hocking *et al.*, 1987). However, it is thought that at the scale of the national seismic hazard map the ground-motion attenuation properties of the trough could not be resolved from the enclosing cratonic crust due to the narrow width of the trough (David Burbidge, Geoscience Australia, personal communication, 2011). Therefore, the trough has been incorporated into the cratonic crust superdomain (Figure D-1b).

Western Tasmania was placed within Domain 3 (Clark *et al.*, 2011, 2012) (Figure D 1a) based upon the widespread exposure of Neoproterozoic rocks, metamorphism and deformation fabrics (e.g. Berry *et al.*, 2008), and its pre-Delamerian Orogeny correlation with crust west of the Tasman Line (Glen, 2005). Despite a long Palaeozoic deformation history, and the proposal that analogous Proterozoic basement floors the Selwyn Block in the Lachlan Fold belt to the north (Cayley *et al.*, 2002), it was maintained that the character of the scarps are more akin to those in Domain 3 (cf. Domain 4). In contrast, the historic seismicity characteristics of this region are similar to the eastern highlands in Domain 4 (Clark *et al.*, 2011 - their Figure 34). This observation, together with its small spatial extent and isolation from the rest of Domain 3, justifies its amalgamation into the adjacent non-cratonic crust superdomain for the purpose of ground-motion modelling.

### 10.3 FAULT LENGTH ANALYSIS

Population distributions for fault length data extracted from neotectonic features falling within the superdomains (cf. Figure D-1b) are presented in Figure D 2, D-3 and D-4. Summary statistics for the fault length data are presented in the inset tables in each figure. Data from all three superdomains show a strong positive skew (skewness 1.51-2.18). Pronounced breaks in slope in each cumulative percentage curve above 40-70 km in length suggest that this character might be in part related to segmented fault behaviour, with longer scarps representing several partially or non-overlapping ruptures. There is a suggestion of bimodality in the distributions for the cratonic and non-cratonic domains, with potential secondary peaks at ~60-70 km and 50-60 km, respectively. The distribution for the extended is more heterogeneous, perhaps reflecting the diversity in geologic setting of the data (i.e. failed intracontinental rift vs. extended passive margin). Median values for each domain fall in the length range of 30-40 km, consistent with the length of ruptures consequent of the 1968 Ms6.8 Meckering, and the 1988 Ms6.9 Tennant Creek earthquakes (Gordon & Lewis, 1980; Crone *et al.*, 1997).

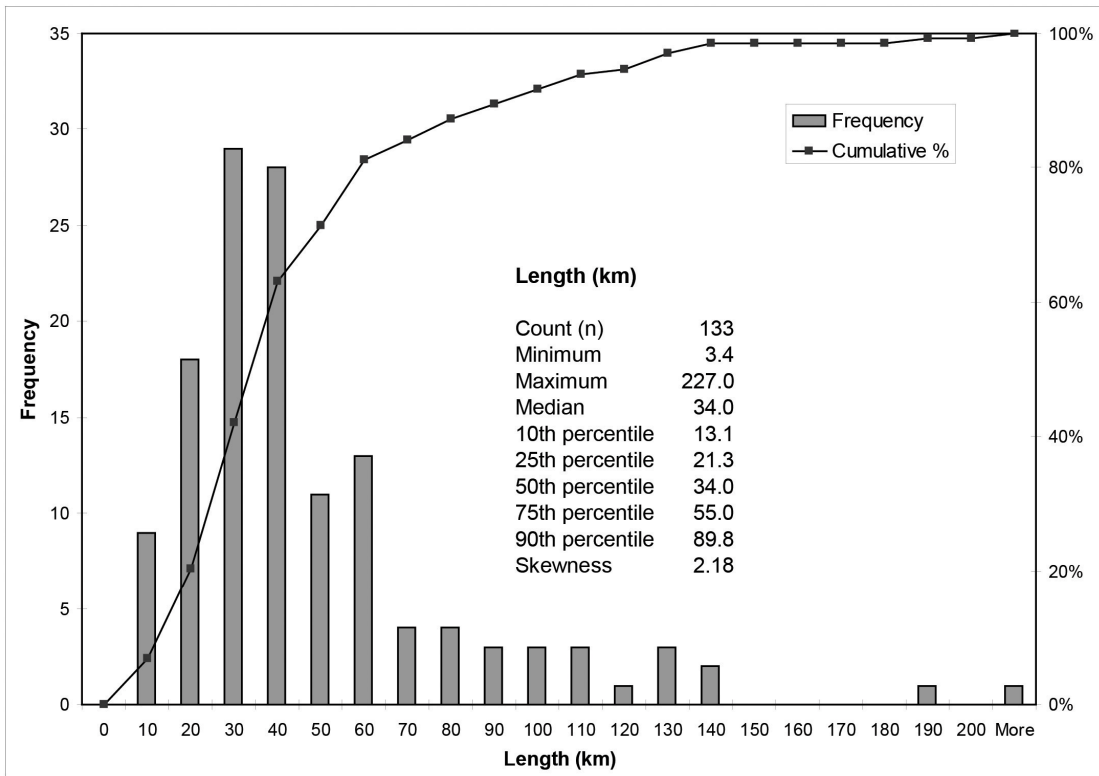


Figure D 2. Neotectonic fault length data for the aggregated 'cratonic' superdomain.

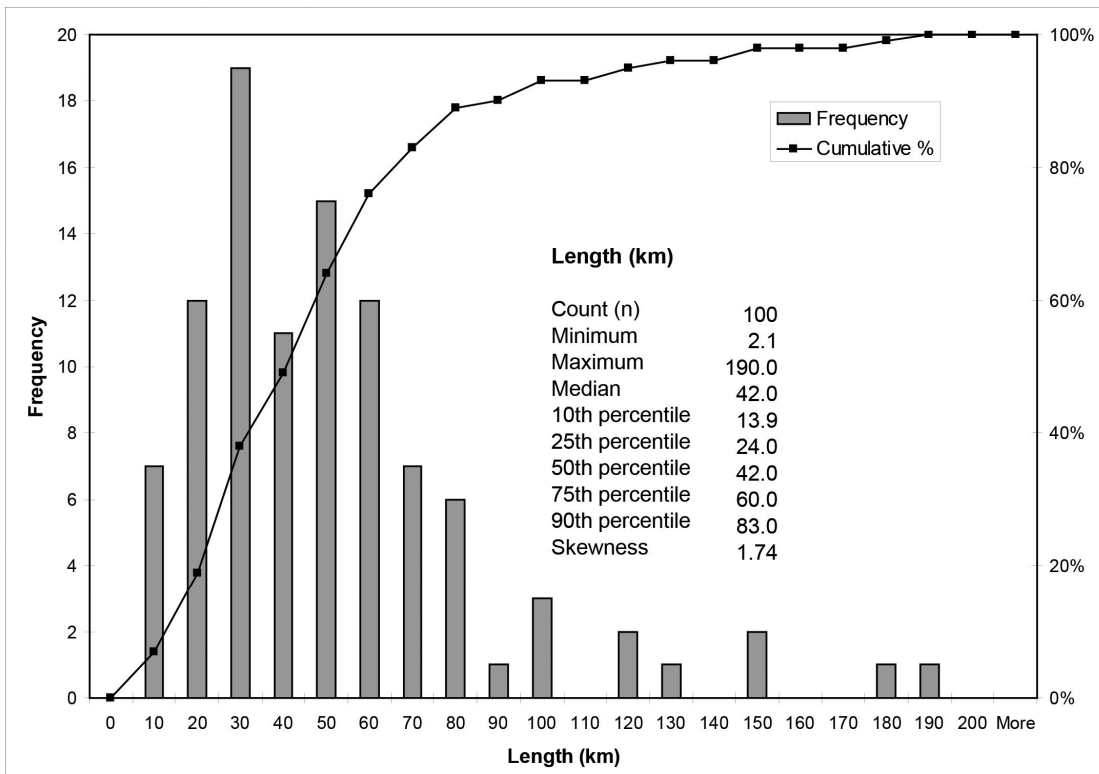


Figure D 3 Neotectonic fault length data for the aggregated 'non-cratonic' superdomain.

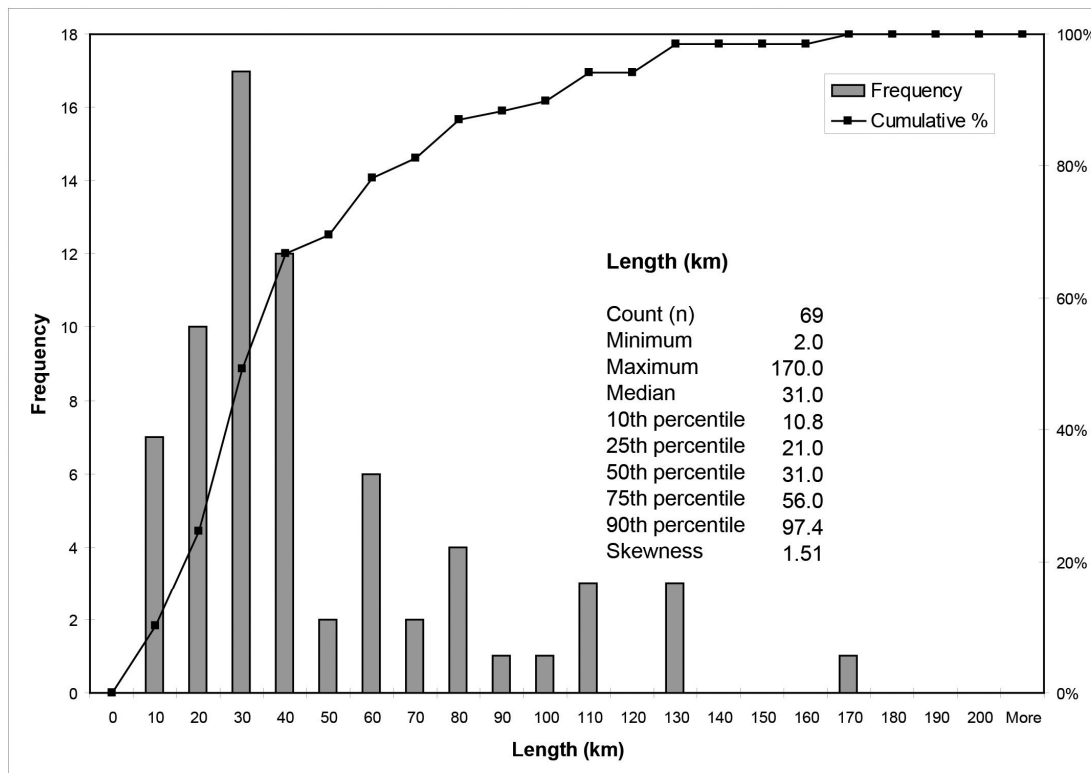


Figure D 4 Neotectonic fault length data for the aggregated 'extended' superdomain.

The summary statistics for each superdomain are remarkably similar (Figure D 5b). A range of variability of less than ~10 km is evident in 10th and 90th percentiles and 1st and 3rd quartiles. The median values have a range of 11 km. The source of this homogeneity is apparent when the summary statistics for the component domains comprising the superdomains is considered (Figure D 5a). Each superdomain essentially combines a domain containing generally low length values with a domain dominated by high length values (i.e. D1 + D3 = cratonic, D2 + D4 = non-cratonic, D5 + D6 = extended). The variability that distinguished the Clark *et al.* (2011, 2012) domains, and implied spatial variation in maximum magnitude earthquake, is therefore largely 'averaged' out.

#### 10.4 CONSIDERATIONS FOR MAXIMUM MAGNITUDE EARTHQUAKE ( $M_{MAX}$ ) FOR BACKGROUND ZONES

Maximum magnitude earthquake estimates were made using the rationale of Clark *et al.* (2011, 2012). Because single event displacements are not known for the majority of features in the neotectonics database,  $M_{max}$  was necessarily derived from fault scarp length assuming entire scarp-length rupture, and by averaging the magnitudes predicted from a range of different published earthquake scaling relations (Somerville *et al.*, 1999; Somerville, 2001; Somerville *et al.*, 2009; Leonard, 2010) (Table D 2). As a simple basis for comparison, the calculations of  $M_{max}$  below are based on the 75th percentile fault length aggregated from all faults within a superdomain (cf. Section 4.3). In contrast to section 4.3, the entire dataset is used here, rather than only scarps above 20 km in length. This has the effect of lowering the 75th percentile estimate of  $M_{max}$  by 0.1-0.2 magnitude units.

As implied by Figure D 5, the aggregation of domains into superdomains results in an effective averaging of  $M_{max}$  estimates. While the  $M_{max}$  estimates for the superdomains are within error of the component neotectonic domains (Table D 2), there is a potential to significantly underestimate  $M_{max}$  in inverting passive margin crust settings (e.g. D6). This is particularly the case if the results of Leonard & Clark (2011) are considered, which indicate  $M_{max}$  as high as  $M_w$  7.7 in this crustal setting. It is therefore conservative to assign  $M_{max}$  estimates to each superdomain according to the highest  $M_{max}$  value from its constituent domains (see Tables 10 and 11).

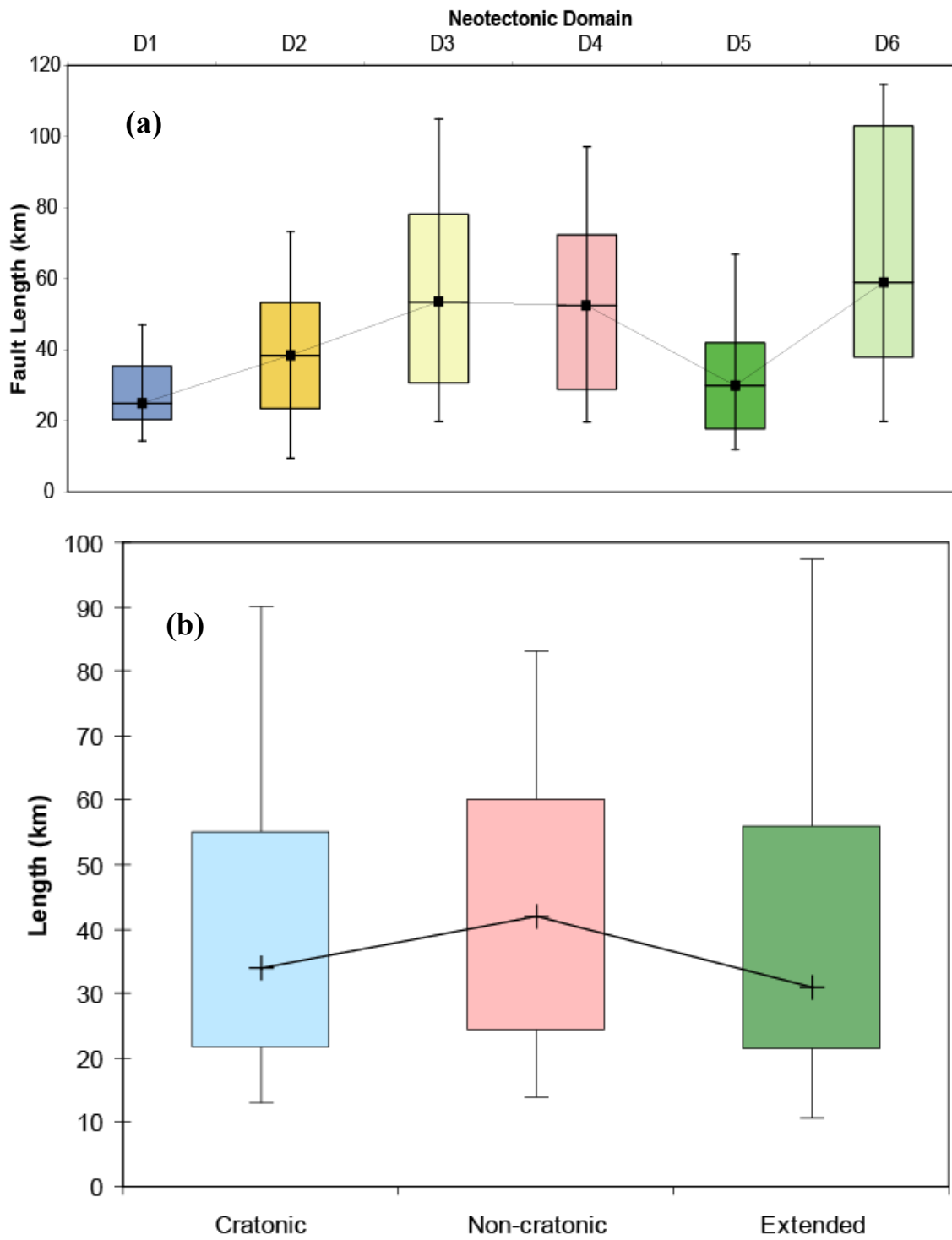


Figure D 5. Summary of Neotectonic fault length statistics for (a) the six onshore neotectonic domains (after Clark et al., 2011) and (b) the three superdomains presented herein. Whiskers are 10<sup>th</sup> and 90<sup>th</sup> percentiles, and bottom and top of boxes are 1<sup>st</sup> and 3<sup>rd</sup> quartiles respectively. Median values are represented by crosses.

Table D 2 Comparison of Mmax estimates from Clark et al. (2011) and the present study. See Clark et al. (2011) for calculation method.

DOMAIN	DESCRIPTION	N	FAULT LENGTH (KM) [75TH PERCENTILE VALUE] 50 DEG DIP; 15 KM DEPTH	MEAN MMAX (PROXY)	SD
1	Archaean & P-Proterozoic	64	35.4	6.9	0.2
2	Sprigg Orogeny	40	53.3	7.2	0.1
3	Proterozoic Mobile Belt	50	78.2	7.4	0.1
4	Phanerozoic terrances	38	72.4	7.3	0.1
5	Failed continental rift	21	42.0	7.0	0.2
6	Inverting passive margin	17	103.0	7.5	0.1
<b>SUPERDOMAIN</b>					
Cratonic	D1+D3	133	55.0	7.2	0.2
Non-cratonic	D2+D4	100	60.0	7.3	0.2
Extended	D5+D6	69	56.0	7.2	0.2

## 10.5 REFERENCES

- Berry R. F., Steele D. A. & Meffre S. J. M. 2008. Proterozoic metamorphism in Tasmania: Implications for tectonic reconstructions. *Precambrian Research* 166, 387-396.
- Cayley R. A., Taylor D. H., VandenBerg A. H. M. & Moore D. H. 2002. Proterozoic – Early Palaeozoic rocks and the Tyennan Orogeny in central Victoria: the Selwyn Block and its tectonic implications *Australian Journal of Earth Sciences* 49, 225-254.
- Clark D., McPherson A. & Collins C. D. N. 2011. Australia's seismogenic neotectonic record: a case for heterogeneous intraplate deformation. *Geoscience Australia Record* 2011/11, 95 p.
- Clark D., McPherson A. & Van Dissen R. 2012. Long-term behaviour of Australian stable continental region (SCR) faults. *Tectonophysics* 566-567, 1-30.
- Crone A. J., Machette M. N. & Bowman J. R. 1997. Episodic nature of earthquake activity in stable continental regions revealed by palaeoseismicity studies of Australian and North American Quaternary faults. *Australian Journal of Earth Sciences* 44, 203-214.
- Drummond B. J., Etheridge M. A. & Middleton M. F. 1987. The geometry of extensional structures in the Fitzroy Trough, Canning Basin, Western Australia. *Bureau of Mineral Resources, Geology and Geophysics. Record* 1987/51.
- Drummond B. J., Sexton M. J., Barton T. J. & Shaw R. D. 1991. The nature of faulting along the margins of the Fitzroy Trough, Canning Basin, and implications for the tectonic development of the Trough. *Exploration Geophysics* 22(1), 111-115.
- Flottmann T. & Cockshell C. D. 1996. Palaeozoic basins of southern South Australia: New insights into their structural history from regional seismic data. *Australian Journal of Earth Sciences* 43, 45-55.
- Glen R. A. 2005. The Tasmanides of Eastern Australia. In: Vaughan A. P. M., Leat P. T. & Pankhurst R. J. (eds.), *Terrane Processes at the Margins of Gondwana*. Geological Society of London Special Publication 246, pp. 23-96.
- Gordon F. R. & Lewis J. D. 1980. The Meckering and Calingiri earthquakes October 1968 and March 1970. *Western Australia Geological Survey Bulletin* 126, 229 p.
- Hocking R. M., Moors H. T. & van de Graaff W. J. E. 1987. Geology of the Carnarvon Basin, Western Australia. *Geological Survey of Western Australia Bulletin* 133, 307 p.
- Keep M., Harrowfield M. & Crowe W. 2007. The Neogene tectonic history of the North West Shelf, Australia. *Exploration Geophysics* 38, 151-174.
- Leonard M. 2010. Earthquake Fault Scaling: Relating Rupture Length, Width, Average Displacement, and Moment Release. *Bulletin of the Seismological Society of America* 100, 1971-1988.

- Marshak S. & Flöttmann T. 1996. Structure and origin of the Fleurieu and Nackara Arcs in the Adelaide fold-thrust belt, South Australia: Salient and recess development in the Delamerian Orogen. *Journal of Structural Geology* 18, 891-908.
- Paul E., Flöttmann T. & Sandiford M. 1999. Structural geometry and controls on basement-involved deformation in the northern Flinders Ranges, Adelaide Fold Belt, South Australia. *Australian Journal of Earth Sciences* 46, 343-354.
- Preiss W. V. 1987. The Adelaide Geosyncline - late Proterozoic stratigraphy, sedimentation, palaeontology and tectonics. *Geological Survey of South Australia Bulletin* 53.
- Somerville P. G. 2001. Earthquake source scaling and ground motion attenuation relations for the central and eastern United States Final Report to the U.S. Geological Survey Contract No. 99HQGR0098.
- Somerville P. G., Irikura K., Graves R., Sawada S., Wald D., Abrahamson N., Iwasaki Y., Kagawa T., Smith N. & Kowada A. 1999. Characterizing earthquake slip models for the prediction of strong ground motion. *Seismological Research Letters* 70, 59-80.
- Somerville P., Graves R. W., Collins N. F., Song S. G. & Ni S. 2009. Ground motion models for Australian earthquakes. Report to Geoscience Australia 29 June 2009.
- Toro G. R., Abrahamson N. A. & Schneider J. F. 1997. Model of strong ground motions from earthquakes in central and eastern North America: best estimates and uncertainties. *Bulletin of the Seismological Society of America* 68, 41-57.
- Yeates A. N., Gibson D. L., Towner R. & Crowe R. W. A. 1984. Regional Geology of the Onshore Canning Basin, W.A. In: Purcell, P.G. (Editor). *The Canning Basin, WA. Proceedings of the Geological Society of Australia/Petroleum Exploration Society of Australia Symposium, Perth, 1984*, 23-55.

# 11. Appendix E Calculation of $M_C$ and the sensitivity of recurrence rates on $M_C$

*M. Leonard*

## 11.1 INTRODUCTION

The magnitude of completeness ( $M_C$ ) is defined as the lowest magnitude above which all earthquakes in a space-time volume are detected (Weimer and Wyss 2000). A single corner magnitude of completeness models assumes that all earthquakes after a certain date above a specific magnitude are detected and that no earthquakes before that date and below that magnitude are available. This gives the completeness model a single magnitude and date “corner”. A multi-corner model uses multiple date and magnitude pairs to allow the catalogue to be extended back in time. The aim of using a multi-step  $M_C$  model is that both large older earthquakes and small recent earthquakes can be incorporated into the regression for the recurrence parameters ( $a$  and  $b$ ). In theory this could lead to more robust estimates of  $a$  and  $b$  and allow less extrapolation from the largest earthquake used in calculating  $a$  and  $b$ , to the largest earthquakes used to calculate the probabilistic hazard. However, the exact location of each corner is highly subjective and this uncertainty adds noise into the recurrence data. This introduces noise into the cumulative magnitude statistics and so into recurrence parameters ( $a$  and  $b$ ). The more uncertain we are in each magnitude/period corner the more potential for noise to be introduced. There is a trade-off between “optimistic”  $M_C$  periods which whilst including more earthquakes is more likely to introduce more noise and a “pessimistic”  $M_C$  periods which includes less earthquakes but introduces less noise. While the single corner model often results in a smaller magnitude range than a multi-corner model, since there is only one corner it is less affected by this subjectivity.

In recent years there have been numerous attempts at quantifying  $M_C$  across Australia (Cuthbertson 2006, 2007; Sagar and Leonard 2007, 2008; and Dent 2009). All have encountered difficulties due to the combination of Australia’s low level of seismicity, distribution and history of seismic stations, and heterogeneous properties of the Australian crust. The most commonly utilised methods were developed overseas for areas of both high seismicity and high network density and their application to Australia has proved problematic.

Sagar and Leonard (2007) applied the ZMAP software (Wiemer and Wyss 2000) to the Australian catalogue but the results were overly complicated. As Dent (2009) states “In a low seismicity region like Australia, a seismograph may run for a long time and unequivocally indicate that no earthquake occurred in the region of the seismograph over a relatively long period. However, the ZMAP program would interpret the lack of events as indicating the catalogue for that region and time was incomplete and therefore did not include that time-space in its calculation of seismicity rates.” In areas of high network density (i.e. Victoria and SE NSW) the method produced credible results.

To estimate  $M_C$ , Cuthbertson (2006) found the Stepp Test (Stepp 1972) excessively sensitive to changes in the catalogue, difficult to automate, and time consuming if done manually. Alternatively, Cuthbertson (2006) developed a method that calculated the network detection magnitude from the network configuration in space and time. Quality factors were subjectively assigned to each station based on expected sensitivity. In addition to calculating for a particular zone, Cuthbertson (2006) extended the method to a  $\sim 50 \times 50$  km grid. This had the advantage of measuring variability across a larger zone, but the disadvantage that each individual square has a high error. These errors were subsequently minimised by averaging. They used weighting based on the period of time above the detection threshold. For the study area, where there were both high quality earthquake catalogue and station database, the technique proved very robust. Cuthbertson (2007) applied the above method to all of eastern Australia. Unfortunately they do not give a time space breakdown of  $M_C$  across eastern Australia.

Leonard (2008) compared the magnitude-frequency statistics ( $\log N = a - bM$ ) for 10 years of data in five year increments. This allowed  $M_C$  to be estimated in increments of five years for each of the four zones of

enhanced seismic activity they analysed. Leonard (2008) subsequently used the historical catalogue to estimate  $M_C$  for the pre-instrumental period.

Dent (2009) took the method of Cuthbertson (2006, 2007) and applied it to western and central Australia. Dent (2009) noted that most stations in WA, SA and NT are generally more sensitive than stations considered highly sensitive in Queensland. This is likely due to the lower attenuation in western and central Australia (Section 5). As such the program probably gives a slightly higher  $M_C$  than is actually the case. Dent (2009) produced a series of maps estimating the network detectability for the years 1960, 1970, 1980 and 2005. They suggest that the  $M_C$  values proposed by Leonard (2008) are too low and their values probably reflect the best monitored portion of the zone and not the average, with the worst monitored portion being higher by as much as 1.0 magnitude unit.

None of the aforementioned authors had access to the earthquake catalogue (GG\_Cat) now being used as the basis for this update of the national hazard map. Sagar and Leonard (2007) and Leonard (2008) used the catalogue described by Leonard (2008), which in eastern and southern Australia is less complete than GG\_Cat. Cuthbertson (2006) used a local Queensland catalogue which is probably of similar completeness to GG\_Cat, although possibly more complete for the region. Cuthbertson (2007) used the ESandS catalogue, which is probably very similar to GG\_Cat in eastern Australia. Generally these differences only apply to earthquakes of magnitude less than 3.0. Dent (2009) calculated theoretical  $M_C$  using a database of seismic stations and did not use an earthquake catalogue.

Initially the models proposed by Leonard (2008) were used to calculate the recurrence parameters (a and b) for each zone. However, these gave anomalous results. So new  $M_C$  models, both a single and multi corner, were developed for 16 regions using the latest version of GGCat. Here we will discuss the method used to generate the time varying  $M_C$  model and the results are compared for several source zones. Conclusions drawn on the trade-off between the benefit including older large earthquakes in the regression of G-R a and b parameters against the disadvantage that, since the various corners are rarely accurately known, noise is introduced into the earthquake statistics. The final preferred  $M_C$  model for each source zone is then presented.

## 11.2 METHOD

A method similar to that of Leonard (2008) was initially used to reassess  $M_C$  for various regions of Australia. This involved producing magnitude versus number plots for multiple overlapping time windows and then, for each time window, assessing the magnitude of completeness. As a guide for estimating the completeness magnitude, the rate for an extended period (e.g. 1965-2010) was overlaid onto all other recurrence plots. The models were then incorporated into the software used to estimate the recurrence parameters and then iteratively modified.

The initial  $M_C$  models were estimated from plots such as shown in Figure E 1. The dashed black line is the recurrence rate calculated for a single period (eg. 1965-2010) using the data coloured red in Figure E 1's sub-plots. In subsequent plots the point where the cumulative data drops below this line is considered to be the magnitude of completeness for this period. So for 1880-1905  $M_C$  for the data shown in Figure E 1 is considered to be M4.0. Similarly 1920-1945  $M_C$  is M 5.0, 1960-1985  $M_C$  is M 2.8 and 1980 – 2005  $M_C$  is M 2.0. This analysis was repeated with varying start dates (i.e. 1880 and 1950) analysis periods (i.e. 25 or 10 years) and magnitude min widths (i.e. 0.3 or 0.1). Generally this analysis allowed a time resolution of about  $\pm 15$  and  $\pm 5$  years for the two analysis periods, with the typical magnitude uncertainties of about  $\pm 0.25$  magnitude units. Such analyses were undertaken for 16 local areas of Australia.

A similar method was used to estimate a single corner  $M_C$  model. In order to maximise the number of earthquakes a lower magnitude at a later cut-off date was generally preferred. For example in the MLFR a catalogue of M3.0 and above since 1965 has about triple the number of earthquakes than that for M3.5 and above since 1960. These single cut-offs were then used in the method described above to modify the average recurrence rate (the dashed line in Figure E 1) and used to iteratively modify the initial multi-corner  $M_C$  models.

The 16 individual multi-corner  $M_C$  models were found to cluster into two groups, with for example SE Australia, SW WA and the MLFR all having very similar  $M_C$  models. Two general models were constructed, that roughly correspond to the populated and rural/remote areas of Australia. Whilst reducing from 16 to two  $M_C$  models resulted in the loss of some data in most regions the impact was very minor. Two regional models have the significant advantage that it simplified the process of allocating an  $M_C$  model as zone boundaries were refined, zones split and zones merged.

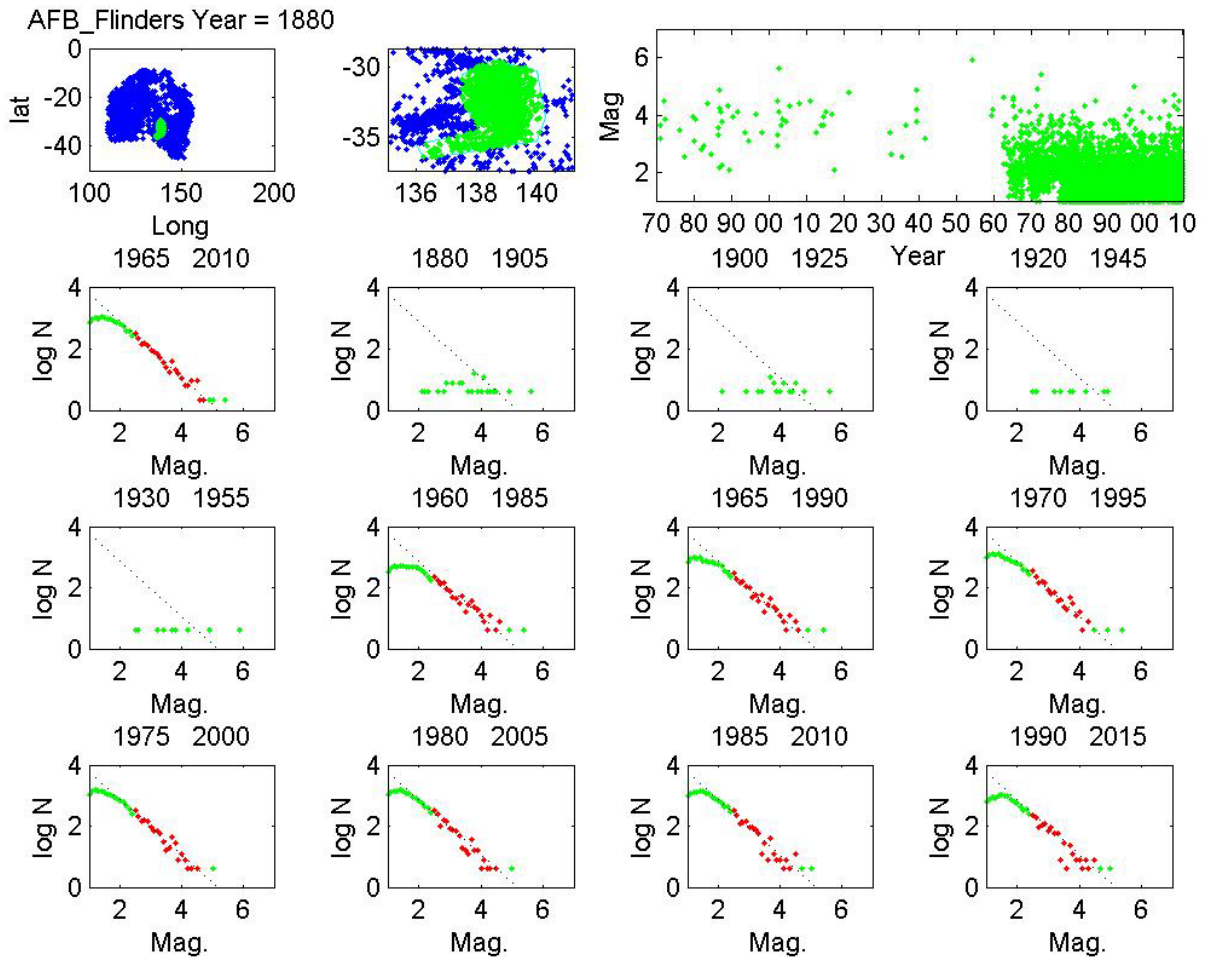


Figure E 1 Earthquake recurrence analysis of the Adelaide Fold Belt region. Points in green are all the earthquakes in the region. The points in red are those between magnitude 2.5 and the magnitude where continuity of the data breaks down. The black dashed line is the recurrence rate calculated from the data from 1965 to 2010 and is used in the other figure to guide for the magnitude of completeness.

Figure E 2 shows the area covered by the 16 regions and the estimated completeness dates for earthquakes of magnitude 3.5 or greater. In the populated southern regions M3.5 completeness was obtained in the early 1960's. But in the remote NW areas this was not achieved until the 1970's and in the Gulf of Carpentaria not until the 1990's. The 16 models, whilst covering most of the area covered by the regional source zone layer, does not cover the whole of the continent. To fill in the gaps Voronoi polygons were formed around the centroid of each of the 16 zones and the completeness date applied to the entire polygon (Figure E 3). This was used as a guide when estimating  $M_C$  for the background zones.

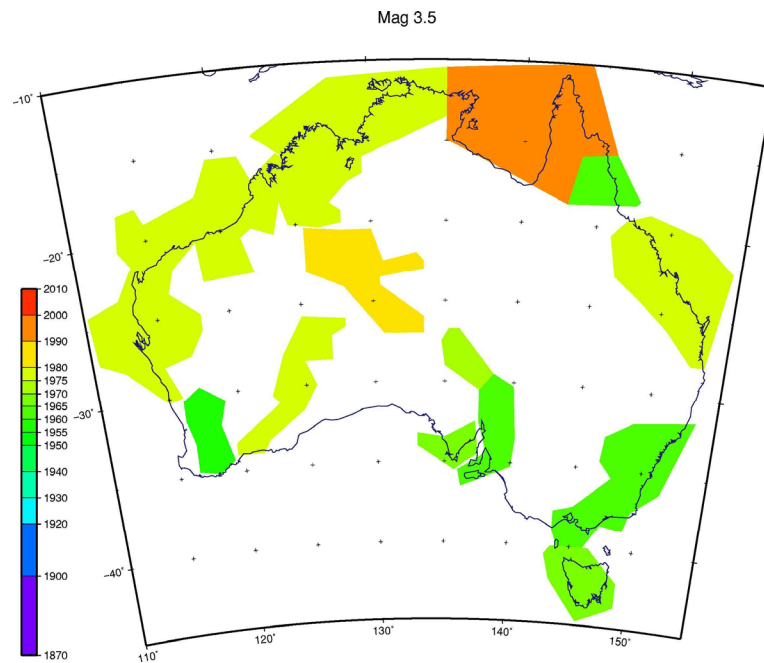


Figure E 2 Dates from which the catalogue is complete in each region for M3.5 and above.

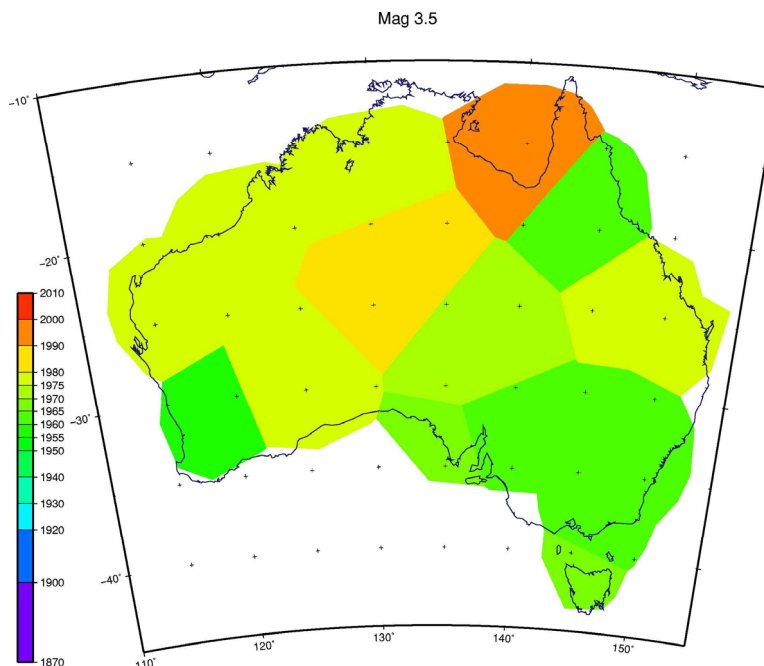


Figure E 3 As per Figure E 2 but the areas have been extrapolated using Voronoi polygons based on the centroid of each zone in Figure 2.

Figure E 4 shows the effect of the different  $M_C$  models on recurrence rates for the Mount Lofty and Flinders Ranges (MLFR). The single  $M_C$  model (1965, M3.0) gives a recurrence rate for M6.5 or larger earthquakes of 0.0017 per year. The corresponding rates for the generic populated and MLFR specific  $M_C$  models are 0.0016 and 0.0013 per year respectively. In this case all rates are within the each others 1 standard deviation and have almost identical correlation coefficients. Either the standard deviation or the correlation coefficient ( $R^2$ ) is the basis of most statistically robust tools used to rank models, such as the Akaike Information Criteria (AIC). In this case there is no statistically significant difference between the two multi-corner  $M_C$  models - the standard deviations, correlation coefficients, number of earthquakes

included, and the recurrence rates are all very similar. As such the generic multi-corner model is chosen over the local multi-corner model.

In choosing between the single and multi-corner models we balance the possible increase in the standard deviation (and/or decrease in  $R^2$ ) against the value of including the infrequent larger magnitude earthquakes. For the MLFR area the regional multi-corner  $M_C$  (Figure E 4b) is chosen as it has both a slightly smaller standard deviation than the single corner  $M_C$  (Figure E 4a) and includes two more larger earthquakes.

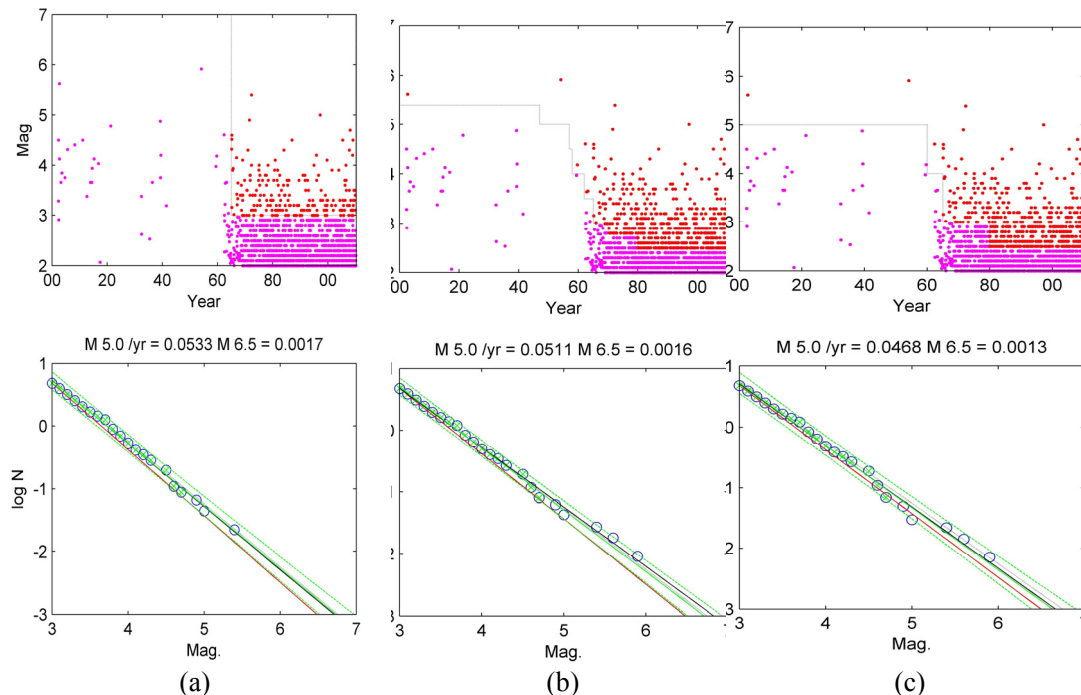


Figure E 4 MLFR recurrence rates for (a) single (b), regional multi corner, and (c) local multi corner  $M_C$  models. The green line is the modified least squares fit, which uses the data points marked with a green X, with the  $\pm 2\sigma$  range shown with dashed green lines. The black line is the least square result for all data and the red is the Maximum Likelihood estimate.

Other areas with similarly complete catalogues, such as Eastern Victoria, and SE NSW, have very similar characteristics to the MLFR data, with the recurrence rates and  $R^2$  being relatively insensitive to the  $M_C$  model used. As the standard deviations are the same or slightly smaller, and the multi-corner  $M_C$  model increases the number of larger earthquakes in these regions, the multi-corner  $M_C$  model has been selected. In other areas the single corner  $M_C$  has a smaller standard deviation and/or there are few larger earthquakes included by the multi-corner  $M_C$ . In these cases the single corner  $M_C$  model was selected.

In SW WA the recurrence rates for the single and multi corner models are different. We propose two possible explanations for this. As suggested by several authors, the seismicity in this region did “switch on” in the 1950’s so having completeness periods for large earthquakes prior to then is distorting the post 1960 data. Alternatively the seismicity was ongoing but the magnitude of completeness was around M6.0. Either way, we consider a single corner  $M_C$  of M3.0 since 1965 the most robust choice.

In areas with relatively poor catalogues both estimating  $M_C$  models and selecting between  $M_C$  models is difficult. Even in areas of relatively high seismicity, such as the north-western area of WA, the catalogues can be relatively poor. Due to the low population there is no historic catalogue for this area. Due to the low network density, even to this day, the lower magnitude cut-off is sensitive to the absence of just one station. As shown in Figure E 5 earthquakes of magnitude 4.0 and greater have been observed since 1960 and earthquakes down to M2.5 since 1980. However detection at these levels has not been consistent. As well as a single corner model (M3.0 since 1980) three other multi-corner models were tested. All multi-corner

models appear to over estimate the number of magnitude 4.5 - 5.0 earthquakes. As such, in this case, the single corner  $M_C$  model was adopted.

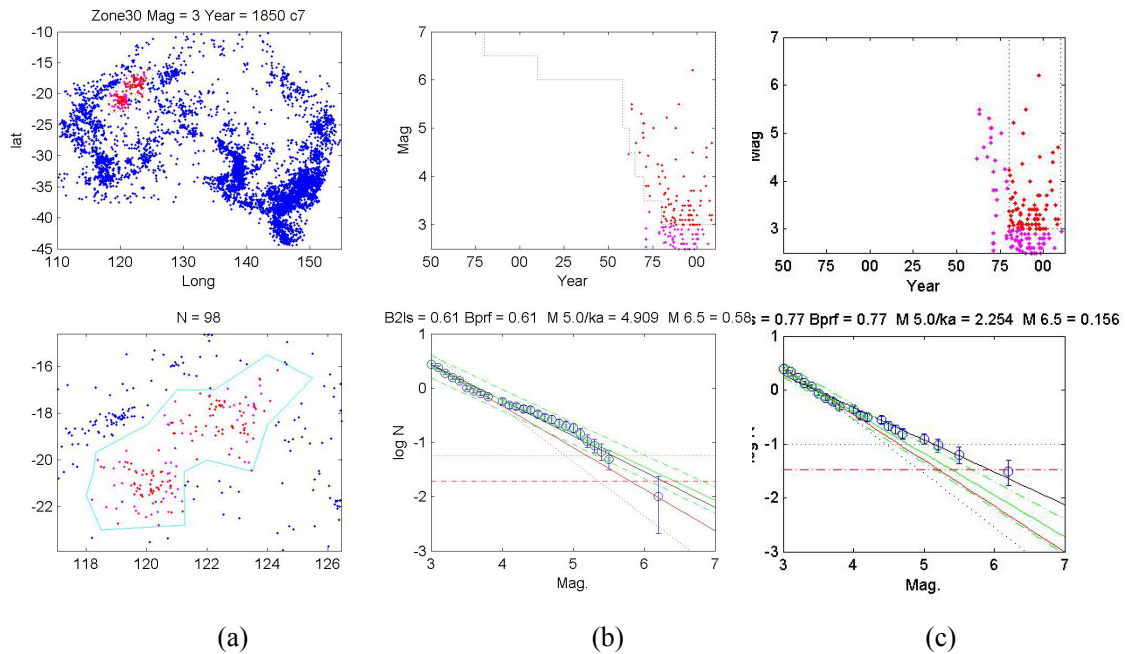


Figure E 5 (a) seismicity, (b)  $M_C$  and (c) recurrence for northeast Western Australia.

In some areas the catalogue appears to be variable. For example in SE Queensland (Fraser Island to the Gold coast and 250 km inland) the catalogue contains “bursts” of earthquakes in the mid-1950’s and between 1978 and 1982, with very few earthquakes recorded between 1960 and 1977, and no earthquakes between 1967 and 1977. See Figure E 6. As such, a single corner  $M_C$  prior to 1978 cannot be justified. Single corner  $M_C$  models with corners of 1978, 1980 and 1982 for  $M \geq 3.0$  give highly varying results. The multi corner  $M_C$  model is similarly variable, being sensitive to the three  $M_{4.5-4.9}$  earthquakes in the 1950’s and 1960’s and the  $M_{5.6}$  in 1918. Given these sensitivities a conservative  $M_C$  model of  $M \geq 3.0$  since 1982 has been adopted.

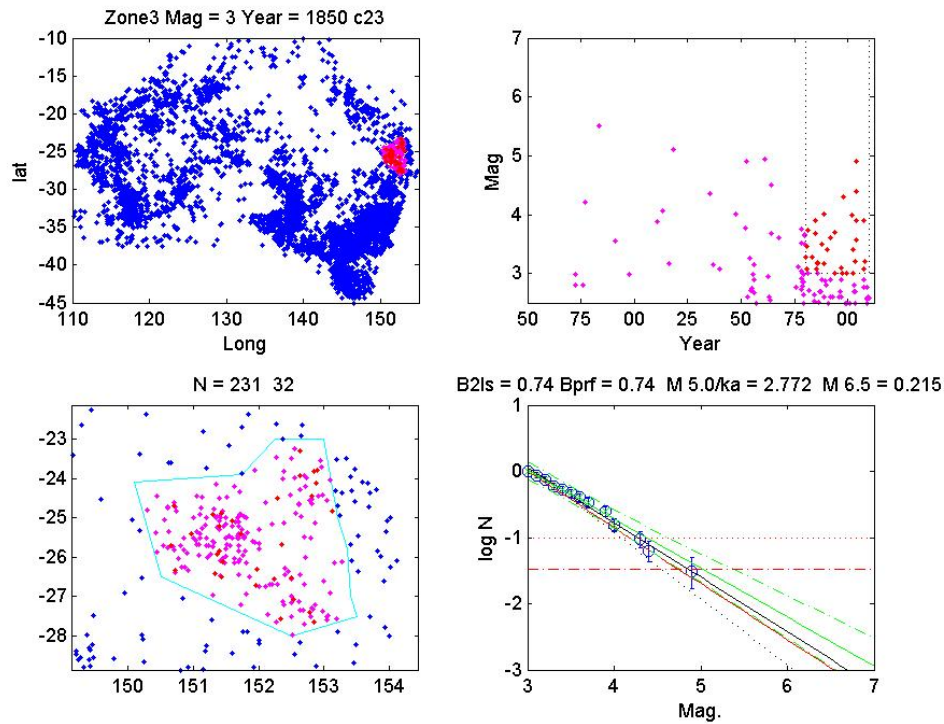


Figure E 6 Seismicity,  $M_C$  and recurrence for southeast Queensland.

### 11.3 CONCLUSION

Both single and multi corner  $M_C$  models were calculated for each of the 16 test regions. Due to similarity of models these could be reduced to three single corner and two multi-corner models. The preferred model was selected on the basis of the log-linearity of the recurrence data, standard deviation and correlation coefficient ( $R^2$ ). Of the 23 source zones in the Regional layer the preferred  $M_C$  model was multi-cornered for 10 and single cornered for 13 zones. The three Background layers all used a multi-corner  $M_C$  model. [Table 4](#) summarises the  $M_C$  model used in each zone.

## 12. Appendix F Sensitivity and Validation Testing of EQRM

*D. R. Burbidge*

### 12.1 INTRODUCTION

In addition to the earthquake source model and ground motion model, a number of numerical parameters controlling the calculation also need to be set in EQRM. Here we discuss how these other numerical parameters were chosen for the national map. The first part of this appendix discusses some sensitivity tests, the latter part discuss some validation tests done using the tests described by Thomas *et al.* (2010).

### 12.2 NUMBER OF EVENTS

To calculate the hazard, EQRM generates a synthetic catalogue of earthquakes between the minimum and maximum magnitude at a rate controlled by the earthquake recurrence model (the truncated Gutenberg-Richter equation). If the number of events is too small, then the range of possible ground motions at a specific site may be insufficiently sampled. This would mean that changing the number of events, or random seed used to generate them, could significantly change the hazard at a given point. Since this is a purely numerical parameter, the hazard values should be insensitive to the number of events chosen.

To test this, a purely hypothetical hazard scenario was created. The scenario consisted of a single square source zone  $11^\circ$  by  $11^\circ$  surrounding a square target area of  $1^\circ$  by  $1^\circ$ . Since the hypothetical source zone is symmetrically distributed around the target zone, the hazard across the target zone should be uniform. To check this the hazard was measured at  $0.01^\circ$  interval across the target zone and the minimum and maximum values were found using synthetic catalogues ranging from 1,000 events to 1,000,000 events. The hazard was calculated by spawning event sets across the GMPE's Probability Density Function (PDF). For a detailed discussion of spawning see Robinson *et al.* (2006). The models shown here both used the Toro *et al.* (1990) GMPE PDF. The minimum and maximum hazard values in the test area are shown in [Figure F 1](#).

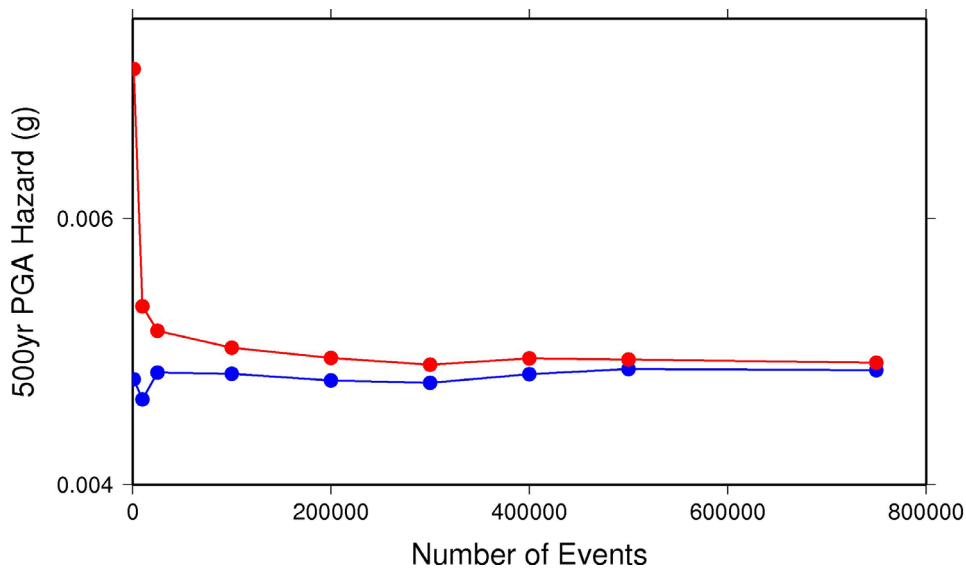


Figure F 1 The minimum (blue curve) and maximum (red curve) PGA hazard at 500 years across a square target zone as a function of the number of events in the synthetic catalogue.

Several features are noticeable, firstly as the number of earthquakes in the synthetic catalogue is increased, the difference between the minimum and maximum hazard in the target zone decreases (i.e. the hazard becomes more uniform). Once the number of events exceeds  $\sim 100,000$ , the rate of change of the hazard as a function of the number of events decreases dramatically. Also it can be seen that using spawning causes the hazard to decrease more rapidly than random sampling, suggesting that the choice of the random seed is biasing the sampling. Therefore, the conclusion from this simple test is that the synthetic earthquake density needs to be at least 0.1 events per  $\text{km}^2$ . For the maps in Chapter 6 the number of events was set to produce greater than 0.3 events per  $\text{km}^2$ , depending on the layer, and used spawning to sample the GMPE Probability Density Functions (PDFs). For example, for the regional plus background zone layer (Figure 38) 17 million events were used to cover the whole of Australia plus the offshore zones, and 1.3 million for the Hotspot layer which covered a much smaller area.

### 12.3 MAXIMUM MAGNITUDE

Although this is not a numerical parameter, here we show the effect on the hazard of the choice of maximum magnitude on this synthetic test. All tests here used 500,000 events in the outer source zone and random sampling from the GMPE PDF. The PSHA curves for the maximum and minimum hazard in the test area are shown in Figure F 2 for two different seismicity rates (the number of earthquakes in the large source zone above  $M_w 3.0$  per annum).

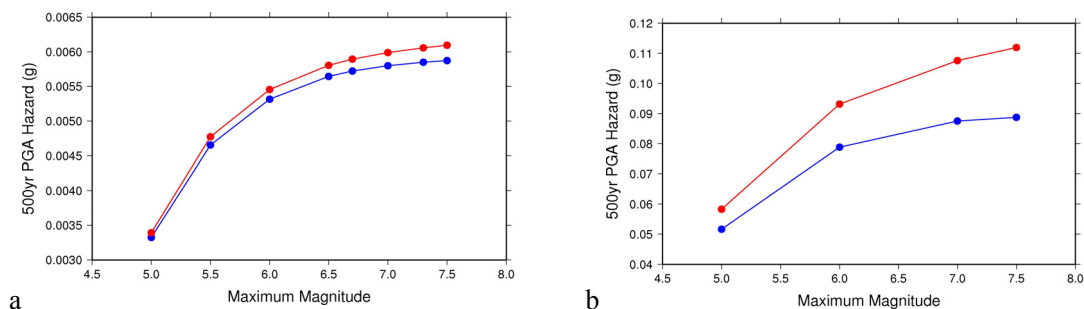


Figure F 2: The minimum (blue) and maximum (red) 500 year PGA hazard in the test hazard map as a function of maximum magnitude for two different earthquakes rates (a) 1 earthquake above  $M_w 3.0$  per annum, and (b) 50 earthquakes above  $M_w 3.0$  per annum.

As one might expect, increasing the maximum magnitude increases the hazard, although the effect reduces above  $M_{max}$  7.0 at this return period where the models become much less sensitive to this parameter. The other effect is that the difference between the maximum and minimum hazard curves is reduced as  $M_{max}$  becomes smaller. This is because the same number of events will sample the smaller PDF with the lower  $M_{max}$  values more effectively as  $M_{max}$  becomes smaller. The other effect is that this difference also becomes larger as the rate,  $A$ , increases (compare Figure F 2b with Figure F 2a). The conclusion from this study is that the earthquake density must be higher as either  $M_{max}$  or  $A$  increases, but the effect on the final hazard values at the 500 year return periods when  $M_{max}$  is greater than 7.0 is relatively small.

#### 12.4 MINIMUM MAGNITUDE

The other factor, a numerical one, which affects the magnitude PDF, is the minimum, or cut-off, magnitude.

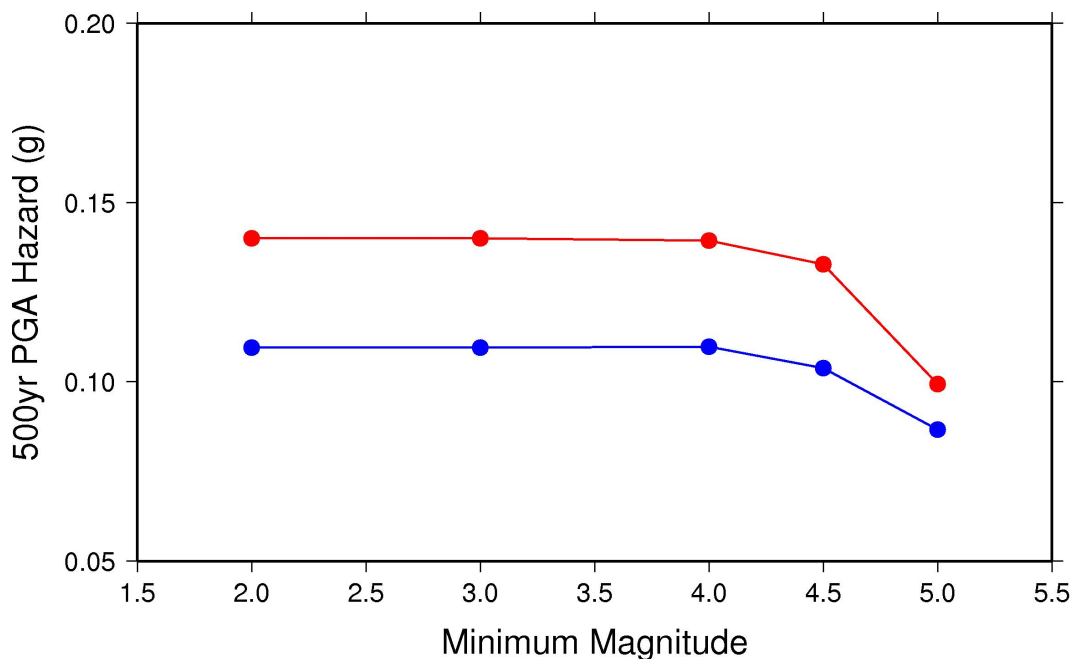


Figure F 3: The effect on the minimum (blue) and maximum (red) hazard in the test area when the minimum magnitude of the earthquakes included in the synthetic catalogue is changed.

Figure F 3 shows the effect on the hazard of changing this parameter. All other parameters are the same as before ( $M_{max}$  7.5, 500,000 events). As can be seen, increasing the cut-off magnitude starts to decrease the hazard once earthquakes which can produce shaking at this level (in this case around 0.1 g) start to be removed from the synthetic catalogue. The only advantage is that it improves the level of uniformity slightly by sampling the PDF more thoroughly. The conclusion from this test is that the minimum cut-off magnitude should be between 4.0 and 4.5. The other factor to note when selecting the minimum magnitude is that only ground motions from earthquakes large enough to cause damage to buildings should be considered in hazard maps for building code purpose. Large ground motions at 0.0s from small (<4.5) magnitude earthquakes are possible but are probably not long enough in duration to usually cause damage to well constructed buildings. However, it is impossible to be certain as there is little damage data from earthquakes in Australia. Other comparable studies have used minimum magnitudes between 4.0 and 5.0; Brown and Gibson (2004) used 4.0 for their hazard map of Victoria, Stucchi *et al.* (2011) used 4.8 for their hazard map of Italy, Bozzoni *et al.* (2011) used 4.5 for their map of the East Caribbean and Petersen *et al.* (2008) use 5.0 for their map of the US. In the absence of any further Australian specific information for this parameter, the minimum magnitude used in this

assessment was chosen to be 4.5 as a reasonable estimate of a “typical” minimum magnitude used by other similar studies in the past.

## 12.5 NUMBER OF MAGNITUDE BINS

In addition to the minimum and maximum magnitudes, the earthquake recurrence is split into a number of magnitude bins. The effect of the number of bins is shown in Figure F 4 (the other parameters in the hazard map are held constant).

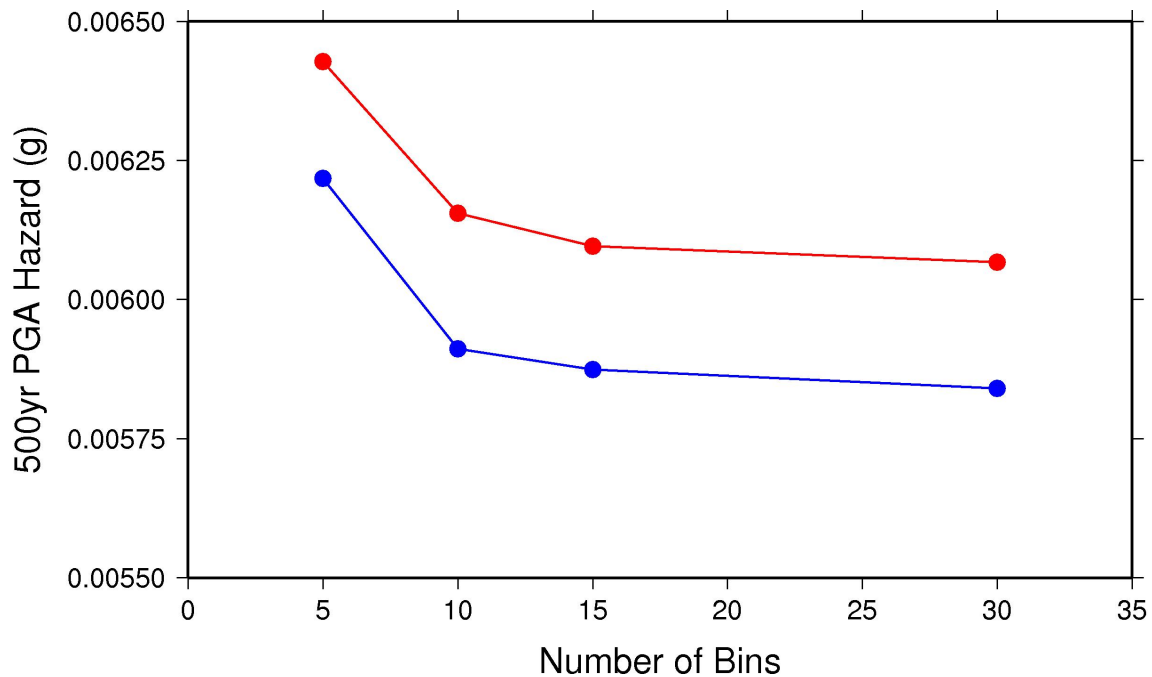


Figure F 4: The effect of the number of magnitude bins on the hazard on the minimum (blue) and maximum (red) hazard in the test area.

As one might expect, not having enough bins increases the hazard slightly because the PDF is not as accurately sampled. Above 15 bins there appears to be no significant effect. Therefore the number of bins chosen for the national hazard map was selected to be 15.

## 12.6 VALIDATION TESTS

No test can ever prove definitively that a model will always be valid, particular when that model is producing probabilistic results. However we can test to see if the model produces similar results to other probabilistic or scenario models for certain test cases. Until recently, there have not been any published studies which have compared the results of one hazard model code to other codes with a well specified set of test cases. This changed with the publication of the Pacific Earthquake Engineering Research (PEER) study in 2010 which compared the results from numerous hazard models with a series of well specified problems. Even though the problems are well specified, differences between the models are expected due to differences in the underlying assumptions, modelling methods and numerical error. However, one does expect the results to at least approximately agree.

Since most of the tests use the original Sadigh *et al.* (1997) GMPE, this was added to EQRN suite of GMPEs. EQRN originally was intended to implement the Campbell (2003) version of the Sadigh *et al.* (1997). This validation study showed that the original implementation of this GMPE in EQRN gave different ground motions to the original Sadigh *et al.* (1997) equations for

reasons that were not fully determined. As a result, the subroutines designed to implement Sadigh *et al.* (1997) were completely rewritten.

Due to limited time, only the PEER Set 1 Case 1 and Case 11 studies were tested against the results from EQRM for this study.

### 12.6.1 PEER Set 1 Case 1

This test compares the ground motions predicted by various hazards codes at points surrounding a vertical rupture plane for a magnitude 6.5 earthquake. For further details about this particular test case, see Thomas *et al.* (2010). Figure F 5 shows the ground motions predicted by EQRM (black curve) and those predicted by the models tested by PEER (red curve). To within numerical error they are the same.

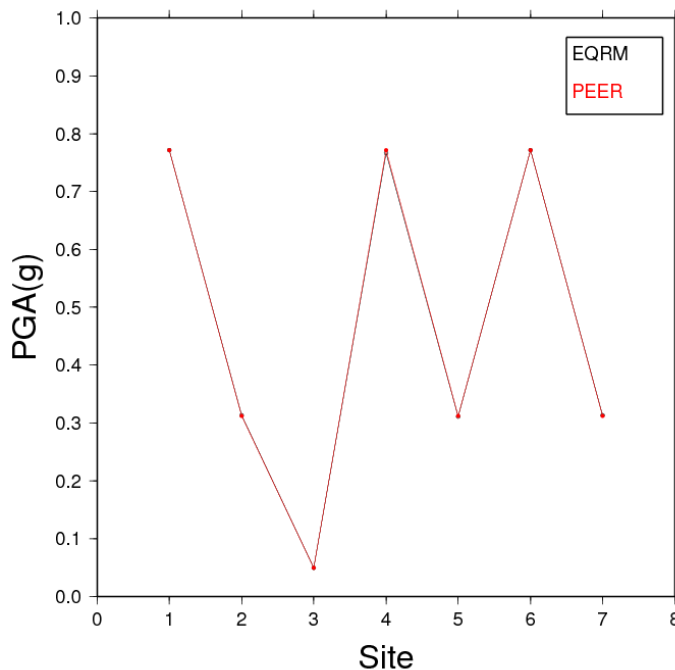


Figure F 5: This figure compares the ground motions predicted by EQRM (black curve) to the ground motions calculated by PEER (red curve) for seven sites surrounding a strike-slip fault (PEER Test Case 1). The two curves at this scale are identical.

### 12.6.2 PEER Set 1 Case 11

This test compares the probabilistic seismic hazard predicted by various codes for points within and outside a specific earthquake source zone. For further details about this particular test case, see Thomas *et al.* (2010). Figure F 6 shows the annual probability of exceedence (PoE) of specific peak ground accelerations (PGAs) predicted by EQRM (black curve) and the average PoEs for all the models tested by PEER for this problem (red curve). To within numerical error they are the same.

Although these are only two validation tests, the fact that they are identical gives us greater confidence that the hazard values produced by EQRM when a large number of events are modelled are the same as what would be calculated using other models. This was reinforced when the draft hazard maps presented in Burbidge and Leonard (2011) were broadly consistent with those produced using OpenSHA (K. Campbell, pers. comm.).

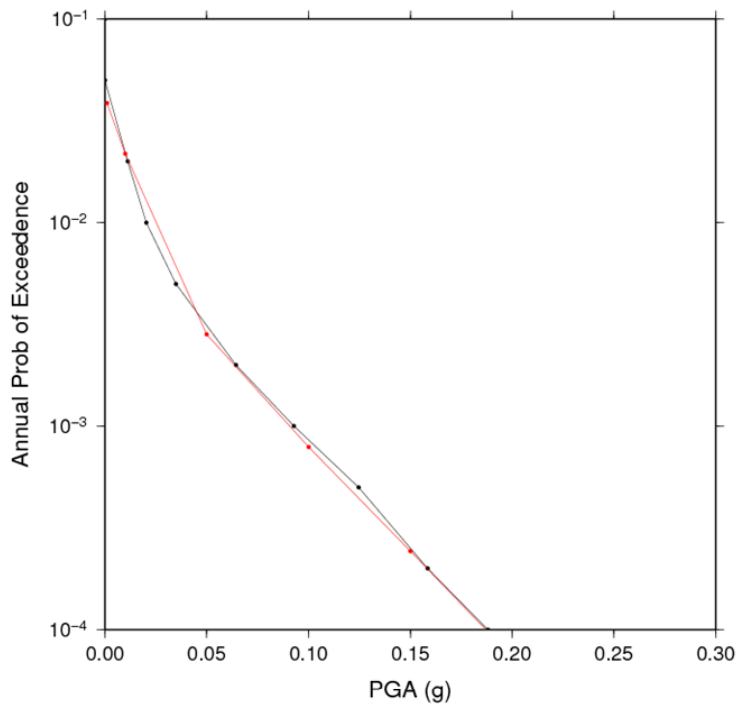


Figure F 6: This figure compares the annual probability of exceedence for different Peak Ground Accelerations (PGA) predicted by EQRМ (black curve) and those calculated by the PEER for a site above an earthquake source zone (PEER Test Case 11)

## 12.7 EFFECT OF SMOOTHING

This subsection discusses the effect of running a post-processing Gaussian filter over a hazard map in order to reproduce the spatial uncertainty in the location of source zone boundaries and reduce numerical noise. Figure F 7 shows a cross section through a PGA, 500 year hazard map produced by a single square source zone (green points). In longitude the zone goes from 125.9 degrees to 130.9 degrees and has a recurrence rate of 1.0 earthquake above magnitude 3.0 per annum. The hazard values reach a plateau in the across the zone and roll off outside the zone. The hazard across the plateau appears to have some “noise” because the number of events in the zone is too small to produce a completely flat plateau.

The red curve shows the hazard across the same cross-section after applying a Gaussian filter with a width of 1,500 km to the map. The width of the filter much larger than the width of the zone at this latitude and so produces a lot of smoothing. The effect of a strong filter like this is to reduce the peak of the hazard inside the zone and increase the hazard outside of it. One additional effect is to reduce the variability in the hazard values caused by not having enough events in the zone.

The black curve in Figure F 7 shows the hazard from a different set of eleven source zones chosen to mimic the effect of smoothing. These zones were also square zones of the same size as the one which produced the hazard shown in the green and red curves in Figure F 7. However each zone was displaced by 1 degree in longitude from the next and causing each zone to overlap the next. The set of zones went from 120.0 degrees (the left edge of the leftmost zone) to 135 degrees (right edge of the right most zone). The recurrence rate of each zone was changed so that the two outermost zones had a recurrence rate of 0.0277 earthquakes above magnitude 3.0, while the innermost zone had a recurrence rate of 0.16667 earthquakes. The recurrence rate of the zones between the innermost zone and the outermost zones was found by linear interpolation between these two rates so that the rate peaked in the middle and decreased as one moved out to

the outermost zones. The reason for selecting this particularly set of zones is that it represents a complex logic tree with eleven branches to the extent EQRM can do this in the current version of the code. Each zone represents a different branch and the change in the rate represents the weight given for that branch. In this case the innermost zone is given the highest weight, and the outermost zones the least.

The hazard this particular set of zones creates is shown by the black curve in Figure F 7. It peaks above the location of highest activity zone and reduces outside of it. Compared to the hazard after smoothing (red curve in Figure F 7), this curve has the same shape but is displaced and slightly higher. The cause of the displacement is the particular longitudes used for this set of eleven zones. The cause of the difference in height is the particular weighting (i.e. recurrence rates) given to the eleven zones. However, the important aspect to notice is that the shape of the black and red curves is very similar. In other words, the effect of smoothing the final map with a Gaussian in post-processing is analogous to using a very large (technically infinite) number of multiple zones where the innermost zones are given the greatest weight and the outermost zones the least. The latter is closer to the more traditional method of treating the spatial uncertainty in source zone locations by using multiple models. However it is much more computational intensive, particularly with an event based model like EQRM. When using an event-based PSHA model, the effect of having multiple weighted zones to represent some spatial uncertainty in the zone boundaries can be much more easily reproduced by using a post-processing filter of a specific shape.

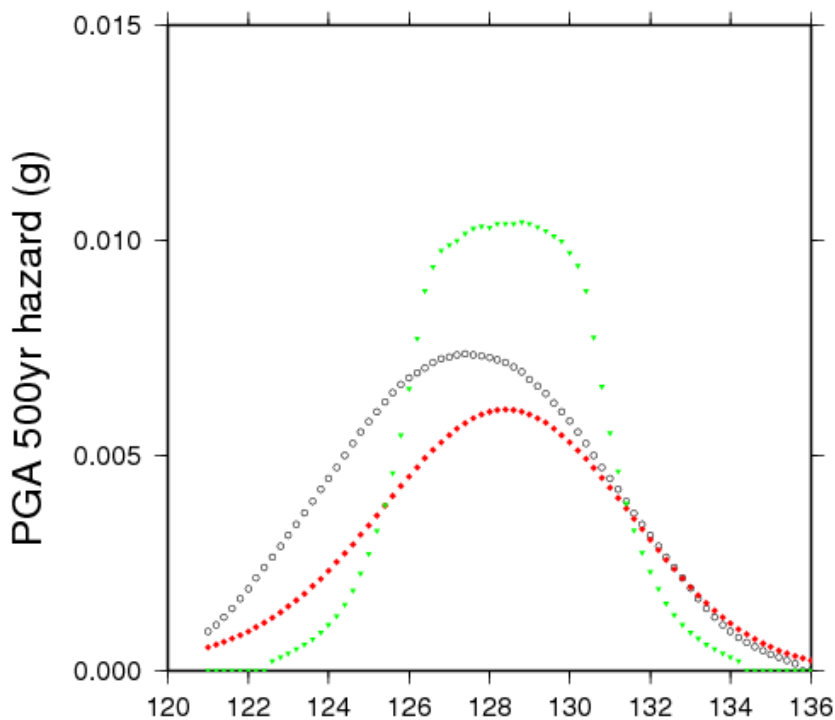


Figure F 7: Three cross sections through three 500yr, PGA hazard maps to show the effect of smoothing. The green points show the hazard as a function of longitude before smoothing. The red points show the hazard after smoothing with a Gaussian filter along the same cross section. The black points show a cross-section through a set of eleven source zones chosen to mimic the effect of smoothing the hazard in post-processing. For further details of the three models, see the text

### 12.7.1 Effect of Smoothing on a Hazard Map

Figure F 8 shows the effect of changing the width of the Gaussian filter on the preferred hazard map shown in Figure 43. In Figure F 8a the Gaussian width has been reduced to 60km from the preferred map's 90km filter. Figure F 8b shows the map when the width was increased to 300km. The effect is fairly small for both maps. When the filter is reduced there is an increase in fine details of the map (compare Figure 36 with Figure F 8a). In particular, the Hotspots become more pronounced. In other words, there are more contours around each hot spot indicating that the slope has become steeper. In Figure F 8b, where the smoothing has been increased, the Hotspots are more subdued and some of the contours have joined up. For example, the outermost Tennant creek contours has joined the one further to the south. The reason that the effect of smoothing is most pronounced on the Hotspots is because they are spatial features about the same size as the Gaussian widths demonstrated here. If the width was increased still further, the regional features would then start to merge until eventually the hazard map become completely flat (similar to the background only hazard map shown in Figure 35).

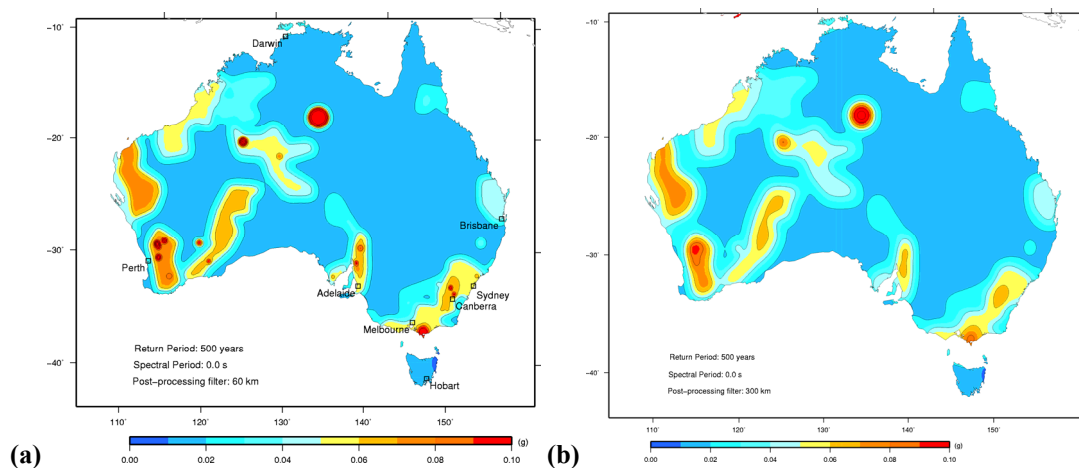


Figure F 8: The 500 year return period PGA hazard map for (a) the Regional source zones with a 150 km Gaussian filter, and (b) the Hotspot zones and a 300 km Gaussian filter.

## 12.8 SUMMARY

In summary, the parameters chosen for the national earthquake hazard map are shown in Table F 1.

The fault dip was chosen to be 35 degrees in the absence of significant data for that parameter. This dip was chosen as this is the theoretical dip of a thrust fault according to the Mohr-Coulomb failure criterion when maximum principal stress is horizontal and angle of internal friction is 30 degrees. Thrust faults were chosen since the majority of focal mechanisms that have been analysed in Australia are thrust (Leonard *et al.* 2002).

The azimuth of the faults was allowed to sample the full range of values, again due to a lack of data on that parameter. Only a handful of focal mechanisms are available for Australia and very few are for large earthquakes. The depth of the earthquakes was allowed to vary anywhere between 0 km and 15-20 km depending on the zone, consistent with the typical range of events in Australia (Leonard 2008).

Table F 1 Summary of the main parameters used in the hazard calculations

PARAMETER	VALUE
Minimum magnitude	4.5
Maximum magnitude	7.3-7.7 (Section 4.3)
GMPE	Variable (Chap 5)
GMPE sampling	Spawning
Event density	>0.3 quakes/km <sup>2</sup> for all zones
Number of magnitude bins	15
Dip	35°
Azimuth	180+/-180°
Depth to the base of the seismogenic zone	Normally 15km, 20km in zones with a high <i>Mmax</i>
Minimum depth at top of the rupture plane	0 km
<i>a</i> , <i>b</i> -value	Variable, see Chap 4

## 12.9 REFERENCES

- Bozzoni, F., Corigliano, M., Lai, C. G., Salazar, W. Scandella, L., Zuccolo, E., Latchman, J., Lynch, L., Robertson, R. 2011, Probabilistic Seismic Hazard Assessment at the Eastern Caribbean Islands, *Bull Seism. Soc. Am.* 101, 5, 2499-2521.
- Brown A. and Gibson G. 2004. A multi-tiered earthquake hazard model for Australia, *Tectonophysics*, 390, 25-43.
- Burbidge, D. and Leonard, M., The 2012 Australian Seismic Hazard Map – Draft Maps, 2011, *The Australian Earthquake Engineering Society 2011 Conference Proceedings*, 18-20 November, Barossa Valley, South Australia.
- Campbell, K.W, 2003. A Contemporary Guide to Strong-Motion Attenuation Relations, in *International Handbook of Earthquake and Engineering Seismology* (W.H.K. Lee, H. Kanamori, P.C. Jennings, and C. Kisslinger, Eds.), Supplement to Chapter 60, Vol. 2, Part B, Handbook CD, Academic Press, London.
- Leonard, M. Ripper, D. and Yue, L., Australian earthquake fault plane solutions, GA record 2002/19, 2002.
- Petersen, M.D., Frankel, A.D., Harmsen, S.C., Mueller, C.S., Haller, K.M., Wheeler, R.L., Wesson, R.L., Zeng, Y., Boyd, O.S, Perkins, D.M., Luco, N., Field, E.H., Wills, C.J. and Rukstales, K.S., 2008, Documentation for the 2008 Update of the United States National Seismic Hazard Maps, USGS Open-File Report 2008–1128.
- Sadigh, K., Chang, C.-Y., Egan, J.A., Makdisi, F., and Youngs, R.R. 1997. Attenuation relationships for shallow crustal earthquakes based on California strong motion data. *Seism. Res. Lett.* 68, 180–189.
- Stucchi, M., Meletti, C., Montaldo, V., Crowley, H., Calvi, G. M., Boschi, E., Seismic Hazard Assessment (2003-2009) for the Italian Building Code, 2011. *Bull.Seis. Soc. Am.* **101**, 4, 1885-1911.